

Jeremy Charles Ely  
Department of Geography  
University of Sheffield

# Flow Signatures on the Bed and the Surface of Ice Sheets

PhD Thesis  
Submitted in accordance with the requirements  
for the degree of Doctor of Philosophy

October, 2015



# Table of Contents

Tables and Figures .....	IV
Abstract	VII
Acknowledgements .....	VIII
Chapter 1 Introduction .....	1
1.1 Ice Sheets .....	1
1.2 Ice Sheet Flow Signatures .....	2
1.2.1 Basal Flow Signatures .....	4
1.2.2 Surface Flow Signatures .....	10
1.2.3 Connecting the Surface and the Bed of an Ice Sheet .....	17
1.2.4 Summary of Ice Sheet Flow Signatures .....	19
1.3 Thesis Aim and Objectives .....	19
1.4 Structure and Outline of this Thesis .....	20
1.5 Publications .....	20
Section A: Insights into the Characteristics and Formation of Subglacial Bedforms .....	22
Chapter 2 Patterning and Growth of Subglacial Bedforms .....	23
2.1 Introduction .....	23
2.2 Previous Work .....	25
2.2.1 Pattern Formation and Interactions within Bedform Fields .....	25
2.2.2 Patterning and Subglacial Bedforms .....	26
2.3 Dataset .....	33
2.4 Are Drumlins Regularly Positioned? .....	35
2.4.1 Methods: Spatial Statistics .....	35
2.4.2 Results: Spatial statistics .....	42
2.4.3 Interpretation: Regular, Random or Clustered? .....	54
2.5 Secondary Patterning Interactions .....	60
2.5.1 Methods: Drumlin Size and Spacing Metrics .....	60
2.5.2 Results: Drumlin Spacing and Size Metrics .....	66
2.5.3 Interpretation: Are Drumlins “Printed”? .....	73
2.5.4 Interpretation: Simple Stabilisation .....	78
2.5.5 Interpretation: Drumlin Growth .....	78
2.5.6 Interpretation: Static or Migratory? .....	79
2.6 Discussion and Implications .....	80
2.6.1 Subglacial Bedforms as Patterns .....	80
2.6.2 Implications for Drumlin Formation Theories .....	82
2.6.3 Implications for the subglacial environment .....	84
2.7 Summary and Conclusions .....	86
Chapter 3 A Size and Shape Continuum of Subglacial Bedforms? Implications for their Genesis	87
3.1 Introduction .....	87
3.2 Previous Work .....	89
3.3 Methods .....	95
3.4 Results .....	102
3.4.1 Cluster Analysis .....	102
3.4.2 Nomenclature Based Results .....	107
3.4.3 Location Based Results .....	110
3.5 Interpretation .....	112
3.5.1 Flutes .....	112

3.5.2	Drumlins and MSGL.....	112
3.5.3	Flow-transverse Bedforms .....	114
3.5.4	Quasi-Circular Bedforms .....	115
3.5.5	Subglacial bedform continua. ....	118
3.6	Discussion and Implications .....	119
3.6.1	Implications for Formation Hypotheses.....	119
3.6.2	Controls on the Size and Shape of Subglacial Bedforms .....	127
3.6.3	Comparison to the Instability Hypothesis .....	129
3.7	Summary and Conclusions.....	132
<b>Section B: Insights into the Characteristics and Formation of Ice Sheet Surface Flow Signatures. 133</b>		
<b>Chapter 4 Antarctic Surface LSSs: Insights into their formation arising from analysis of their morphology and glaciological context ..... 134</b>		
4.1	Introduction.....	134
4.2	Background.....	134
4.3	Methods.....	140
4.3.1	Mapping .....	140
4.3.2	The Spatial, Morphological and Glaciological Characteristics of LSSs .....	146
4.3.3	Testing Formation Hypotheses .....	149
4.4	Results.....	152
4.4.1	Mapping .....	152
4.4.2	LSS Morphological and Glaciological Characteristics .....	154
4.4.3	Testing Formation Hypotheses .....	159
4.4.4	Summary of Results .....	172
4.5	Discussion .....	173
4.5.1	Implications for LSS Formation Hypotheses.....	173
4.5.2	Hybrid Model of LSS Formation .....	178
4.5.3	Flow Stripes or Foliations? .....	180
4.5.4	Implications for Reconstructing Palaeo-Ice Flow .....	183
4.6	Summary and Conclusions.....	184
<b>Plate 1 185</b>		
<b>Chapter 5 Transverse Surface Structures on the Antarctic Ice Sheet ..... 187</b>		
5.1	Introduction.....	187
5.2	Previous Work.....	189
5.3	Methods.....	195
5.3.1	Mapping .....	195
5.3.2	TSS Morphological and Glaciological variables.....	199
5.4	Results.....	204
5.4.1	Static Mapping .....	204
5.4.2	Multi-Temporal Mapping .....	204
5.4.3	TSS Morphology.....	206
5.4.4	Glaciological Characteristics .....	210
5.5	Discussion .....	212
5.6	Summary and Conclusions.....	215
<b>Section C: Comparing Basal and Surficial Ice Sheet Flow Signatures..... 217</b>		
<b>Chapter 6 Discussion: Connections between flow signatures on the base and the surface of an ice sheet. .... 218</b>		
6.1	Introduction.....	218
6.2	Background .....	218
6.3	Morphological Comparison Between Basal and Surficial Flow Signatures .....	222



6.4	The Bed and the Surface of the Rutford Ice Stream.....	226
6.5	Airborne Radar.....	232
6.6	Modelling of the Flow of Ice Over Subglacial Bedforms .....	247
6.7	Discussion.....	252
6.8	Summary and Conclusions.....	256
<b>Chapter 7 Summary and Conclusions.....</b>		<b>258</b>
7.1	Aims and Objectives .....	258
7.2	Future Work .....	262
7.3	Concluding remark.....	264
<b>Bibliography</b>		<b>265</b>

# Tables and Figures

## Tables

Table 1: Ice sheet surface flow signatures.....	12
Table 2: Compilation of previous studies on the regularity of drumlin spatial distribution.....	28
Table 3: Senistivity analysis results of the functions $L_{inhom}(r)$ and $g_{inhom}(r)$ .....	51
Table 4: Correlation coefficients and best-fit line equations for all studied bivariate relationships.....	70
Table 5: Location and reference of collated mapping of subglacial bedforms.....	99
Table 6: Data type and source for mapping.....	99
Table 7: Summary statistics of subglacial bedform categories.....	110
Table 8: Tested expectations of the compression hypothesis and the basal transfer hypothesis.....	152
Table 9: Descriptive statistics of measured LSS variables.....	155
Table 10: Expectations of the two main LSS formation hypotheses and comparision to results.....	174
Table 11: Location and date of imagery studied.....	198
Table 12: Descriptive statistics of TSS variables.....	207

## Figures

Figure 1.1: Contemporary and palaeo ice streams.....	2
Figure 1.2: The bed and the surface of an ice stream.....	3
Figure 1.3: Subglacial bedforms.....	6
Figure 1.4: Types of drumlin internal structure.....	7
Figure 1.5: Overview of the Shaw-mega flood hypothesis.....	9
Figure 1.6: Examples of longitudinal surface structures.....	14
Figure 1.7: Transverse surface structures on the surface of MacAyeal Ice Stream.....	16
Figure 1.8: Bed to surface transfer model.....	18
Section A: Hill-shaded elevation model of Dodge County, Wisconsin, USA.....	22
Figure 2.1: Subglacial bedform patterns.....	24
Figure 2.2: Summary of patterning behaviour for dunes.....	26
Figure 2.3: Histograms of spacing measurements of subglacial bedforms.....	29
Figure 2.4: Frequency of drumlin width, plotted with a logarithmic scale.....	32
Figure 2.5: Representation of drumlins within the dataset.....	34
Figure 2.6: Flowsets of the last British-Irish Ice Sheet.....	35
Figure 2.7: The problem of defining a study area or bounding box.....	39
Figure 2.8: Summary of the Ripley K function and pair correlation function procedures.....	41
Figure 2.9: Histogram of Clark and Evans statistic value.....	42
Figure 2.10: Typical output from the $L(r)$ test.....	44
Figure 2.11: Typical output of the $g(r)$ test.....	45
Figure 2.12: The inhomogenous pair correlation function for all studied flowsets.....	53
Figure 2.13: Boxplot of the number of drumlins in a flowset and whether the drumlins are regular.....	54
Figure 2.14: The $L(r)$ statistic of the Leitrim drumlin field.....	56
Figure 2.15: Drumlins as either discrete bumps (“blisters”) or as continuous waveforms.....	57
Figure 2.16: Results of $L(r)_{inhom}$ compared to a Matern hard-core point process.....	58
Figure 2.17: Testing a clustered, regular grid of points.....	59
Figure 2.18: Illustration of derived distribution metrics.....	62
Figure 2.19: Expected drumlin metrics due to patterning interactions.....	63-66
Figure 2.20: Comparative boxplots of drumlin side spacing measurements.....	67
Figure 2.21: Comparative boxplots of durmlin along flow spacing measurements.....	68
Figure 2.22: Scatter plot matrix of the shape of the distribution for all variables studied.....	69
Figure 2.23: The relationships between $\phi$ and $\lambda$ .....	72
Figure 2.24: The relationships between $\phi$ and $\Lambda$ .....	72
Figure 2.25: The relationships between $\lambda$ and $\Lambda$ .....	73
Figure 2.26: Schematic summary of the shape of probability distribution functions.....	73
Figure 2.27: Cross cutting drumlins in NE Scotland, near Thurso.....	75
Figure 2.28: Cone shaped drumlin distributions.....	77
Figure 2.29: Hypothetical interplay between drumlin growth and drag.....	85

Figure 3.1: Different types of subglacial bedform and their orientation to ice flow direction .....	88
Figure 3.2: A schematic representation of bedform transitions .....	92
Figure 3.3: Subglacial bedforms not considered within the transition-based continuum hypothesis .....	93
Figure 3.4: Schematic representations of different continuum hypotheses .....	94
Figure 3.5: Thought experiment for testing light as a continuum .....	96
Figure 3.6: Location of mapped subglacial bedforms .....	97
Figure 3.7: Schematic of derived bedform axes .....	100
Figure 3.8: Schematic of how a continuum or different populations may be detected.....	101
Figure 3.9: The size and shape of subglacial bedforms.....	104
Figure 3.10: DBSCAN sensitivity analysis .....	105-106
Figure 3.11: DBSCAN results.....	107
Figure 3.12: Contour plots to assess the degree of overlap between labelled bedform types .....	109
Figure 3.13: Outlines of the <i>a</i> -axis and <i>b</i> -axis of bedform scatter plots grouped by location .....	111
Figure 3.14: Drumlin and MSGL metrics .....	113
Figure 3.15: Metrics of subglacial ribs.....	115
Figure 3.16: Examples of spatial transitions between ribbed moraines and drumlins.....	117
Figure 3.17: How different types of bedform hypotheses may account for subglacial bedform continua .	121
Figure 3.18: Satellite images of quasi-circular sand dunes .....	124
Figure 3.19: The relationship between sedimentology and bedform shaping processes .....	126
Figure 3.20: Predicted growth rates of bedforms by the instability hypothesis.....	131
Section B: The surface of Byrd Glacier .....	133
Figure 4.1: LSSs at the mouth of the Bindschaller and MacAyeal ice streams .....	135
Figure 4.2: Longitudinal foliations on the surface of Comfortlessbreen, Svalbard.....	137
Figure 4.3: The compression hypothesis of LSS formation .....	138
Figure 4.4: Development of a LSS at the confluence of two ice masses.....	139
Figure 4.5: The basal transmission hypothesis of LSS formation .....	140
Figure 4.6: Comparison of the three sources of data used for mapping .....	142
Figure 4.7: Examples of disrupted longitudinal surface structures .....	143
Figure 4.8: Comparison of LSSs mapped on different data sources .....	145
Figure 4.9: Location of transects for measuring LSS spacing.....	148
Figure 4.10: Expected outcomes of polynomial fitting to spacing measurements .....	150
Figure 4.11: Hypothetical relationship between LSS spacing and flow unit width.....	151
Figure 4.12: Examples of mapped LSSs .....	154
Figure 4.13: The length of mapped LSS polylines.....	155
Figure 4.14: The spacing of mapped LSS polylines.....	156
Figure 4.15: The velocity of LSS start point .....	157
Figure 4.16: The correspondence between ice velocity and LSSs .....	158
Figure 4.17: LSS start point ice thickness .....	159
Figure 4.18: Histogram of the coefficient <i>a</i> .....	160
Figure 4.19: Qualitative observations of pronounced LSSs at flow unit boundaries .....	161
Figure 4.20: The relationship between flow unit width and mean LSS spacing .....	163
Figure 4.21: Regression lines between flow unit width and mean LSS spacing per flow unit.....	165
Figure 4.22: The relationship between ice thickness and LSS spacing .....	166
Figure 4.23: The relationship between ice velocity and LSS spacing .....	167
Figure 4.24: Histograms of the ratio between LSS spacing and ice thickness .....	168
Figure 4.25: Examples of basal roughness indices compared to LSS mapping .....	170
Figure 4.26: LSSs observed to begin at ice rumples .....	171
Figure 4.27: LSS emanating from possible sticky spots .....	172
Figure 4.28: Examples of LSSs formed in low ice velocities .....	175
Figure 4.29: Examples of LSSs formed in convergent ice .....	178
Figure 4.30: A hybrid model of LSS formation .....	180
Figure 4.31: Examples of regularly spaced LSSs.....	181
Figure 4.32: The relationship between LSSs and isochrone folding .....	182
Plate 1: Maps of Antarctic LSSs .....	185-186
Figure 5.1: Ice stream surface texture .....	188
Figure 5.2: Modelling of flow over bumps in the bed of an ice stream.....	191
Figure 5.3: Whillans and Johnsens' (1983) model for the formation of TSSs .....	192
Figure 5.4: Basal shear stress inversion compared to surface morphology for Bindschadler ice stream .	193
Figure 5.5: TSS mapping locations and sources of data.....	196-197
Figure 5.6: TSSs on the ice stream studied at multiple time slices.....	198
Figure 5.7: Location of TSS spacing measurement transects.....	201
Figure 5.8: Definition of velocity anomaly across TSSs.....	202-203

Figure 5.9: Examples of mapped TSSs .....	205
Figure 5.10: Maps of TSSs from satellite images at different time periods .....	206
Figure 5.11: The length of TSSs .....	207
Figure 5.12: Boxplot of TSS length grouped by location.....	208
Figure 5.13: Histograms of TSS spacing.....	209
Figure 5.14: Boxplot of TSS spacing grouped per ice stream.....	209
Figure 5.15: Mean velocity across the crest-line of TSSs .....	211
Figure 5.16: Velocity anomaly across TSSs.....	211
Figure 5.17: Ice thickness across the crestline of TSSs.....	211
Figure 5.18: The ratio between TSS spacing and ice thickness .....	212
Figure 5.19: Bed and surface topography profiles across prominent TSSs .....	215
Section C: The bed and the surface of Rutford Ice Stream .....	217
Figure 6.1: Schoofs model of ice flow over a drumlin .....	219
Figure 6.2: Simulations of subglacial bedforms caused by a groove-ploughing mechanism.....	220
Figure 6.3: The effect of LSSs and TSSs on hydraulic gradients, and thus deformation rates .....	221
Figure 6.4: Comparison between subglacial lineation and LSS length .....	223
Figure 6.5: Comparison between the spacing of subglacial lineations and LSSs.....	223
Figure 6.6: Comparison of the across-flow length of transverse flow signatures .....	225
Figure 6.7: Comparison between the spacing of transverse flow signatures.....	225
Figure 6.8: Summary of surficial and basal flow signatures of Rutford Ice Stream .....	227
Figure 6.9: Landsat images of the surface of Rutford Ice Stream .....	228
Figure 6.10: Comparison between surficial and basal flow signatures of the Rutford Ice Stream.....	230
Figure 6.11: Along flow transect of the bed of the Rutford Ice Stream .....	231
Figure 6.12: Comparison between surface and bed for across-flow transect B .....	232
Figure 6.13: Comparison between the bed and the surface across transect C .....	232
Figure 6.14: Locations of studied across-flow radar profiles .....	234
Figure 6.15: Radargram and interpretation of line PI1 .....	235
Figure 6.16: Radargram and interpretation of line FO2 .....	236
Figure 6.17: Radargram and interpretation of line RC2 .....	237
Figure 6.18: Location of bed bumps and LSSs along flightlines on Pine Island Glacier .....	238
Figure 6.19: Location of bumps and LSSs along flightlines on Foundation Ice Stream .....	238
Figure 6.20: Location of bumps and LSSs along flightlines on Recovery Glacier .....	239
Figure 6.21: Location of studied along-flow radar lines .....	241
Figure 6.22: Radargram and interpretation of line AC1 .....	242
Figure 6.23: Radargram and interpretation of line RC2 .....	243
Figure 6.24: Radargram and interpretation of line SL1 .....	244
Figure 6.25: Radargram and interpretation of line TW2 .....	245
Figure 6.26: Location of TSSs and bed bumps across flightlines over Academy and Support Force .....	246
Figure 6.27: Location of TSSs and bed bumps across flightlines over Recovery and Slessor glaciers....	246
Figure 6.28: Location of TSSs and bed bumps across flightlines over Thwaites glacier .....	247
Figure 6.29: Bed and ice surface output from the model of Chapwanya et al. (2010) .....	249
Figure 6.30: Initial results of full-stokes modelling of ice flow over subglacial bedforms .....	251
Figure 6.31: Hypothetical arrangement of the bed and internal isochrones .....	253
Figure 6.31: Proposed hybrid model of TSS formation .....	255

# Abstract

Ice flow produces morphological features at the bed and on the surface of ice sheets. These ‘flow signatures’ provide us with an insight into the mechanisms, history and characteristics of ice sheet flow. In this thesis I examine the characteristics of basal and surficial ice sheet flow signatures, as well as possible links between them. The first chapter introduces ice sheet flow signatures. At the bed, a suite of landforms known as subglacial bedforms are found. The surface of an ice sheet is home to longitudinal surface structures (LSSs) and transverse surface structures (TSSs). Whilst the two environments are mostly considered in isolation, links between the sets of flow signatures found at each have been suggested.

Section A deals with basal flow signatures. Chapter 2 asks whether subglacial bedforms are patterned. Drumlins are found to be regularly placed within the landscape, and likely grow or shrink over time. Chapter 3 examines whether subglacial bedforms conform to a size and shape continuum. By collating and analysing a dataset of 96,900 measurements of size and shape it is found that 3 continua of subglacial bedforms exist: flutes, lineations and ribs. The latter two are joined by an understudied class of quasi-circular bedforms.

Section B deals with surficial flow signatures. In Chapter 4 I present and analyse a map of the LSSs of the Antarctic Ice Sheet. The morphology, spatial distribution and glaciological context of LSSs leads to the proposal of a model for their formation. Chapter 5 presents the first systematic study of TSSs. Mapping and analysis reveals that TSSs are regularly spaced, differ little in their morphology between ice streams and are most likely stationary.

Section C compares basal and surficial ice sheet flow signatures. In Chapter 6, morphological comparisons, a case study of the Rutford Ice Stream, analysis of ice penetrating radar and examination of ice flow modelling lead to the conclusion that the majority of basal and surficial flow signatures are separate entities. Chapter 7 concludes the thesis and provides suggestions for future research.

## Acknowledgements

Firstly, I would like to thank my supervisor Chris Clark. This thesis would not have been possible without his generously provided ideas, continual support and inspirational enthusiasm for science. Countless hours spent pondering maps, satellite images and graphs together have shaped this thesis. “Nature has an answer.”

I would also like to thank my second supervisor Matteo Spagnolo for his input and comments. The discussions we had whilst measuring fabric in muddy pits, dragging radar equipment over drumlins, flying hexacopters over flutes, and in his office have greatly improved this thesis.

Many of the ideas in this thesis were presented and discussed at meetings of ‘the bedformers.’ I would therefore like to thank Chris Stokes, Andrew Fowler, Richard Hindmarsh and Paul Dunlop for fruitful discussions.

I am very grateful to Chris and Kathy Denison, not only for the financial support they provided through a University of Sheffield Alumni Scholarship, but also their encouragement throughout my time as a Ph.D. student. I enjoyed their visits to Sheffield and the discussions we had, both on ice sheets and dairy farming. I also acknowledge the support of a University of Sheffield Alumni Department L.R. Moore Studentship.

The Ph.D. students, post-docs and staff in the department have made the time taken to complete this thesis enjoyable. Most notably I would like to thank Jonathan Kingslake, Richard Hayes, Stephen Livingstone, Darrel Swift and Felix Ng.

Thank you to my family and friends for your enduring support. Please continue to point and ask “so is that a drumlin?”

Finally, this thesis is dedicated to my Mum, who would have loved to have read it.

# Chapter 1 Introduction

*“Nature uses only the longest threads to weave her patterns, so that each small piece of her fabric reveals the organisation of the entire tapestry”*

Richard P. Feynman, 1964.

## 1.1 Ice Sheets.

Patterns can be observed in numerous natural systems (Ball, 1999). Some of the most striking examples are ‘woven’ by geomorphic systems (Murray et al., 2014). This thesis is about the patterns that are produced by ice sheets. Two sets of ‘tapestries’ where patterns can be observed are studied; ice sheet beds and ice sheet surfaces. Furthermore, possible links between the two are examined.

Ice sheets, such as the Antarctic and Greenland ice sheets, can be defined as masses of ice with an aerial extent greater than 50,000 km<sup>2</sup>, the flow of which is largely undetermined by basal topography (Benn and Evans, 2010, p.6). Their importance to society derives mainly from the vast volumes of water that they contain. Complete melting of the Greenland and Antarctic ice sheets would lead to approximately 70 m of sea level rise (Church et al., 2001). During the Quaternary, the total amount of water stored in ice sheets has repeatedly fluctuated in regular cycles known as ice ages (Shackleton, 1987; Ehlers and Gibbard, 2004). The palaeo-ice sheets which existed during these ice ages serve as useful analogues for existing ice sheets. Determining the processes and dynamics of palaeo-ice sheets and contemporary ice sheets is thus vital for predicting future ice sheet behaviour and potential contribution to sea level rise (e.g. Alley et al., 2005; Kleman et al., 2006; Pollard and DeConto, 2009).

Ice flux is inhomogeneous across an ice sheet, as most ice discharge is concentrated into narrow corridors of fast flow, termed ice streams (Swithinbank, 1954; Rignot et al., 2011; Figure 1.1). Likened to the arteries of ice sheets (Bennet, 2003), these regions of rapid ice flow account for approximately 90% of the discharge of the Antarctic Ice Sheet (Morgan et al., 1982). Palaeo-ice streams have also been inferred from the geomorphological record they leave behind (e.g. Stokes and Clark, 1999; Figure 1.1). Thus, understanding the behaviour of ice streams is pertinent to understanding the dynamics of both palaeo and contemporary ice sheets. The rapid motion of ice streams is thought to be a product of basal processes (Alley et al., 1986;

Engelhardt and Kamb, 1997; Tulaczyk et al., 2001). Direct access to the bed of an ice stream is logistically difficult to achieve, with high resolution geophysical techniques restricted to small areas (Smith et al., 2007; King et al., 2009), limiting our understanding of their spatio-temporally complex behaviour. Research has focused either on the exposed beds of palaeo-ice sheets (e.g. Kleman and Borgström, 1996; Piotrowski and Tulaczyk, 1999; Stokes and Clark, 2001; Ross et al., 2009; Ó Cofaigh et al., 2010), or deriving basal boundary conditions from ice surface measurements (e.g. Joughin et al., 2004; 2009; MacAyeal, 1992; Sergienko and Hindmarsh, 2013). Both the bed and the surface of an ice sheet display numerous features, or *flow signatures* (Section 1.2), the formation of which may hold insights into ice stream operation.

Figure 1.1. Contemporary and palaeo ice streams. Left: Ice velocity of the Antarctic Ice Sheet derived from InSAR data (from Rignot et al., 2011). Right: Location of hypothesised palaeo-ice streams as predicted by Denton and Hughes (1981) (from Stokes and Clark, 2001).

## 1.2 Ice Sheet Flow Signatures

When viewing either the bed or the surface of an ice sheet at the scale of an ice stream, it is apparent that neither is flat (Figure 1.2). Ice sheet beds are covered with subglacial bedforms, formed at the interface between ice and its substrate (Boulton and Clark, 1990b; Hughes et al., 2010); undulating landforms which have been studied for over a century (e.g. Chamberlin, 1883). Satellite images of the surface of ice streams record subtle changes in ice reflectance, often interpreted to be the manifestation of topographic undulations (Merry and Whillans, 1993; Raup et al., 2005). Thus, both the upper and lower surfaces of ice sheets undulate. These undulations record information pertaining to ice flow conditions, and for the purpose of this thesis, are collectively referred to as *flow signatures*.



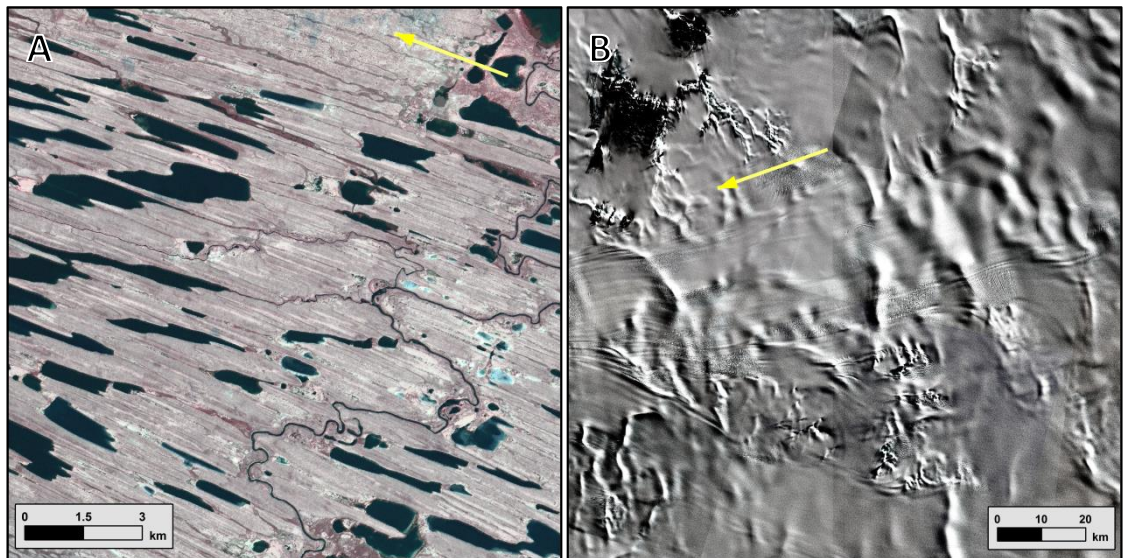


Figure 1.2. The bed (A) and surface (B) of an ice stream. Yellow arrows denote approximate flow direction. A) Landsat false colour composite with SPOT pan-chromatic drape of the bed of the Haldane palaeo-ice Stream, North-West Territories, Canada. Note the many flow parallel landforms, mega-scale glacial lineations (MSGGL). Data sourced from [www.geobase.ca](http://www.geobase.ca) B) Pan-chromatic Landsat ETM+ image of the surface of David Glacier, Antarctica. Note the flow parallel lineations (flow stripes) going approximately right to left across the image and the much larger sinuous bands transverse to flow upstream.

The flow signatures observed on both the bed and the surface of ice sheets often have a remarkable repetitive arrangement within the landscape or upon the ice sheet surface (Figure 1.2). This repetition means that, rather than being isolated forms, flow signatures commonly belong to a larger pattern. Despite this, basal and surficial flow signatures have rarely been considered under the framework of pattern formation developed through observing other natural systems (e.g. Ball, 1999; Werner, 1999). Natural patterns are often the result of self-organisation and interactions within a complex system (Baas, 2007; Murray et al., 2014). The spatial, morphological and glaciological context of flow signatures are yet to be fully quantified. Therefore, key patterning characteristics, such as the regularity of flow signatures (Murray et al., 2014), are yet to be verified. Furthermore, little is known about interactions between flow signatures. Do they grow, migrate, collide or coarsen? This hinders their consideration as patterned phenomena (reviewed in Section 2.2.1), a framework which may help to shed light upon their genesis. Below I briefly review ideas regarding flow signature formation (Sections 1.2.1 and 1.2.2) before reviewing ways in which the two may be connected (Section 1.2.3).

### 1.2.1 Basal Flow Signatures

The flow of ice over unconsolidated sediment produces gently undulating topography. The landforms found at these terrains are referred to as subglacial bedforms (Rose and Letzer, 1977; Menzies and Rose, 1987). Since conditions at the ice-bed interface exert an important control on ice dynamics (e.g. Kleman and Glasser, 2007), the genesis of subglacial bedforms is pertinent to fully understanding ice sheet dynamics. Additionally, subglacial bedforms provide us with information for palaeo-ice sheet reconstruction (e.g. Boulton and Clark, 1990a, b; Kleman and Borgström, 1996; Evans et al., 2005). Scientific interest in subglacial bedforms first flourished at the end of the 19<sup>th</sup> Century (e.g. Chamberlin, 1883; Davis, 1884; Tarr, 1894; Upham, 1894). However, their presence underneath contemporary ice sheets has only recently been confirmed, and is limited to small surveyed areas (e.g. Smith et al., 2007; King et al., 2009; Figure 1.3.B). Hence, much of our current understanding of subglacial bedforms is formulated from studying the beds of palaeo-ice sheets (e.g. Clark, 1993; Graham et al., 2009; Greenwood and Clark, 2010).

Classically, subglacial bedforms are separated into different types. The most frequently studied are drumlins (Figure 1.3.A), which are hills, typically between 250 to 1000 m long, 120 to 300 m wide, and 0.5 to 40 m in relief, that are streamlined in the direction of ice flow (Clark et al., 2009; Spagnolo et al., 2012). Mega-scale glacial lineations (MSGs) are also streamlined in the direction of ice flow, but are perceived to be of a scale much larger than that of drumlins (Clark, 1993). This enhanced length has been attributed to their formation under fast flowing ice (Clark, 1994; Hart, 1999; Stokes and Clark, 2002), a hypothesis confirmed by their presence and rapid migration underneath the Rutford Ice Stream, Antarctica (King et al., 2009; Figure 1.3.B). The term ‘flute’ is generally reserved for subglacial bedforms found in glacial forelands (Boulton, 1976). Flutes are elongate ridges typically associated with a stoss-side boulder (Figure 1.3.C), extending some tens to hundreds of meters parallel to ice flow.

Subglacial ribs (often confusingly referred to as ribbed or Rogen moraine) are found transverse to flow direction (Figure 1.3.D). They display a great range of morphology, stretching from 45-16,214 m long, 17-1,116 m wide, 1-64 m high and spaced 12-5,800 m apart (Dunlop and Clark, 2006b). Less often, even larger mega-scale subglacial ribs have been observed (Greenwood and Kleman, 2010; Klages et al., 2013; Figure 1.3.E). Additionally, a number of bedforms which are quasi-circular have been noted (Hill, 1973; Markgren and Lassila, 1980; Greenwood and Clark, 2010). These are

often classified as drumlins (Davis, 1884) or referred to mammillary or elliptical hills (Chamberlin, 1883). Thus, ice sheet beds contain a variety of landforms which have been collated under the term subglacial bedforms.



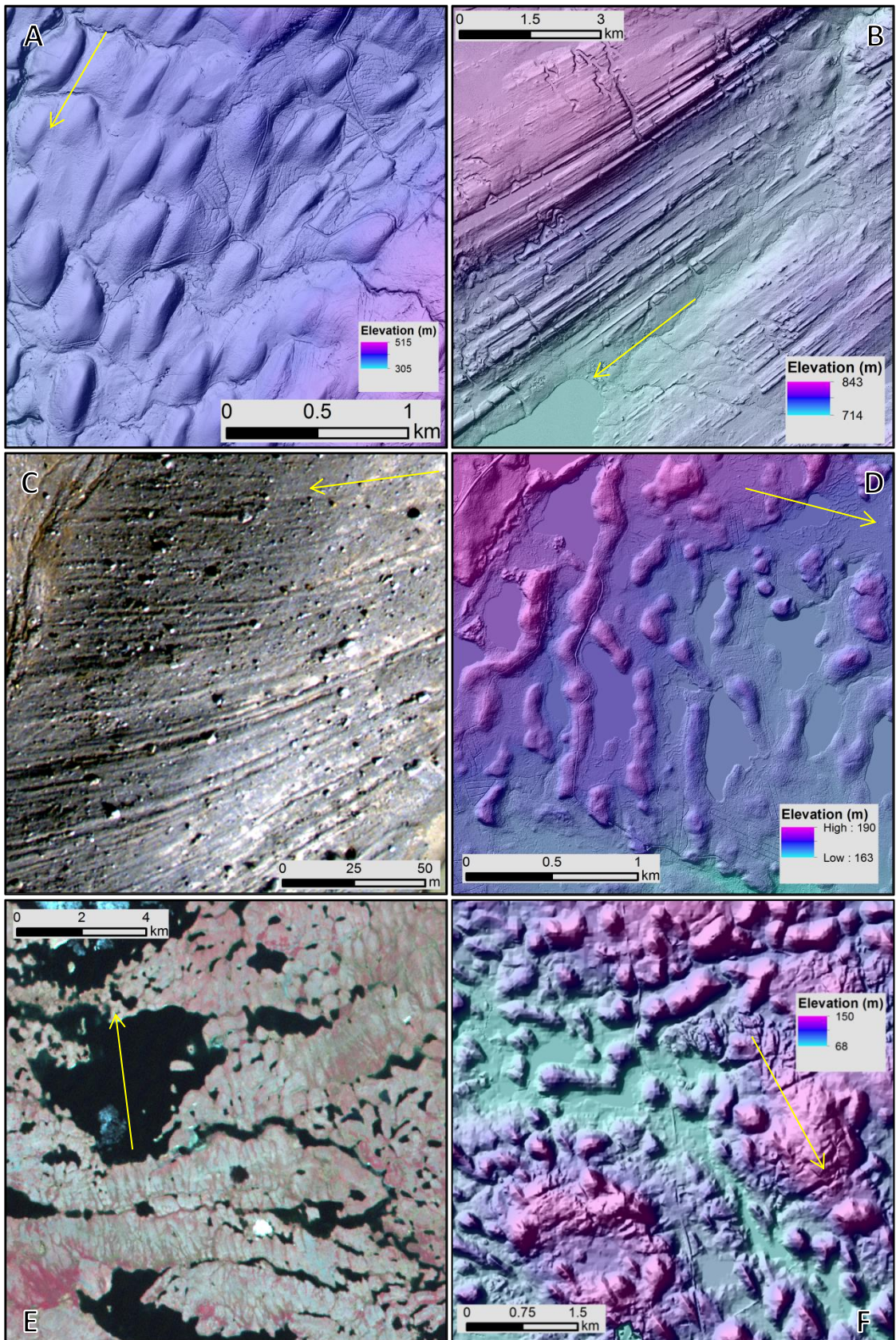


Figure 1.3. Caption overleaf.

Figure 1.3. Subglacial bedforms. Yellow arrows denote inferred palaeo-ice flow direction. A) Hill-shaded LiDAR derived DEM of drumlins, in the Yorkshire Dales, England. Source: Environment Agency Geomatics Group. B) Hill-shaded LiDAR derived DEM of MSGL in Alberta, Canada. Source: Alberta Geological Survey. C) Aerial photograph of flutes at the forefront of Conwaybreen, Svalbard. Source: NERC ARSF. D) Hill-shaded LiDAR derived DEM of subglacial ribs in Finland. Source: National Land Survey of Finland. E) Landsat ETM+ false colour composite of mega-subglacial ribs, Nunavut, Canada. Source: [www.geobase.ca](http://www.geobase.ca) F) Hill-shaded DEM of a transition between subglacial ribs and drumlins, where many quasi-circular bedforms occur. Source: OSNI.

A lack of observations of subglacial bedform formation beneath contemporary ice masses has influenced the proliferation of numerous formation hypotheses. Indeed, Shaw (1983, p.476) remarks that “there are almost as many theories of drumlin formation as there are drumlins.” Thus, it is beyond the scope of this thesis to review each of these individually, instead reviews can be found elsewhere (e.g. Menzies, 1979; Clark, 2010; Shaw, 2010). However, many of the hypotheses share similar characteristics, enabling generalisations to be made.

The internal sedimentary composition of subglacial bedforms is diverse (Figure 1.4), varying between and within fields of bedforms (Stokes et al., 2011). This has led to the development of numerous hypotheses seeking to explain sediment structures within bedforms (e.g. Dardis et al., 1984; Möller, 1987). Such diversity has led to the argument that subglacial bedforms are polygenetic, formed by different process histories (Lindén et al., 2008; Möller, 2010). However, others have argued that formation hypotheses based purely upon sedimentology, ignore the observation that subglacial bedforms occur within fields of many (up to hundreds) associated individuals (Clark, 2010). Thus, numerous hypotheses for the formation of whole bedform fields have been developed (e.g. Smalley and Unwin, 1968; Boyce and Eyles, 1991; Smalley and Warburton, 1994; Hättestrand and Kleman, 1999). Under this view, much of the sediment record may be irrelevant to answering the question of how the bed evolves from a presumably initially flat plane (Clark, 2010).

Figure 1.4. Types of drumlin internal structure, compiled from the literature by Stokes et al. (2011). Composition and amount of sediment contained within a drumlin varies considerably between and within drumlin fields.

The morphometric properties of subglacial bedforms, such as drumlins or MSGL, often reveal commonality between bedforms found in disparate settings (e.g. Spagnolo et al., 2014a). The morphometry of bedforms given a specific geomorphological label are often considered in isolation (e.g. Dunlop and Clark, 2006b; Clark et al., 2009; Spagnolo et al., 2014a), often revealing unimodal histograms of size and shape metrics (c.f. Hillier et al., 2013). This has led to the development of further formational hypotheses which attempt to explain separate bedform ‘types’ regardless of local factors (e.g. Gordon et al., 1992; Hättestrand and Kleman, 1999; Clark et al., 2003; Hooke and Medford, 2013). The bedform-specific view therefore requires separate theories to account for drumlins and MSGL for example. This is counter to previous suggestions that subglacial bedforms actually belong to a much larger morphological continuum (Aario, 1977; Rose, 1987). This morphological continuum has been interpreted to be genetic, forming the basis of ‘unifying’ theories of subglacial bedform formation (e.g. Clark, 2010; Shaw, 2010). Briefly, only two competing theories attempt to explain the subglacial bedforms as a single phenomenon within a continuum. These are the mega-flood hypothesis (Shaw, 2010) and the deforming till instability hypothesis (e.g. Hindmarsh, 1998a; Fowler, 2010b). The development of these theories may be premature, because the continuum hypothesis remains as an untested conjecture. For example, do drumlins grade into MSGL or are they actually distinct landforms?

The Shaw (2010) mega-flood hypothesis relies upon subglacial floods of a high enough magnitude to detach an ice sheet from its bed. This is argued to produce



bedforms via two mechanisms: erosion and transportation of sediment in a manner analogous to fluvial bedforms, and by eroding cavities into the overlying ice which then fill with wet sediment upon flood subsidence and recoupling (Figure 1.5; Shaw and Sharpe, 1987; Shaw et al., 1989; Shaw, 1994, 2002; Fisher and Taylor, 2002). However, the mega-flood hypothesis has been heavily criticised, primarily due to the vast quantity of water required to generate entire fields of bedforms spanning for several tens of square kilometres (Clarke et al., 2005; Livingstone et al., 2013). Additionally, subglacial bedforms appear to have migrated beneath the Antarctic Ice Sheet, without the occurrence of a mega-flood (King et al., 2009).

Figure 1.5. Overview of the Shaw mega-flood hypothesis for the formation of subglacial bedforms. From Shaw (2002). Large subglacial flood events detach the overlying ice from the bed. Vortices within the flood water carve out erosional subglacial bedforms. Vortices also erode into the overlying ice, forming cavities which fill with saturated sediment (producing bedforms) after the flood has subsided.

The Hindmarsh-Fowler deforming till instability hypothesis is based upon the non-linear flow of three substances at the ice-bed interface: ice, water and sediment. Deformable subglacial sediment was first invoked for the formation of subglacial bedforms by Smalley and Unwin (1968), before observational verification of its presence beneath ice (Boulton and Jones, 1979; Alley et al., 1989). Their ideas were expanded on by Boulton (1987), who proposed that deforming subglacial sediment can

either accumulate around an obstacle (either pre-existing, or formed within the layer itself), or stream around it acting as an erosional agent. The instability hypothesis expands on the proposed erosional and depositional nature of subglacial sediment. However, instead of requiring a pre-existing obstacle to form the core of each bedform, the coupled flow of ice, subglacial sediment and water is thought to be inherently unstable (Hindmarsh, 1998a, b; Fowler, 2010a, b). An unstable system is one that acts to amplify small perturbations or random forcings to any of its components (e.g. subglacial water pressure or sediment thickness), such that a positive feedback occurs and this disturbance grows. Often, such disturbances tend to a preferred wavelength of maximum growth. One characteristic of instabilities is that they produce regular patterns, determined by the preferred wavelength of the system. Thus, the instability hypotheses views subglacial bedforms as the consequence of an unstable system of coupled ice, water and sediment flow. Therefore, under the instability theory subglacial bedforms are seen as patterned phenomena (see Section 2.2.1). Currently, numerical models of the instability hypothesis are unable to produce truly three-dimensional bedforms (Chapwanya et al., 2011), and invoke separate instabilities to account for different types of subglacial bedform (e.g. Fowler, 2010a, b). However, some of the proponents of this theory are now suggesting that a newly developed numerical model can account for all subglacial bedform variants, arising from the combination of instabilities acting under an ice sheet (Fowler and Chapwanya, 2014).

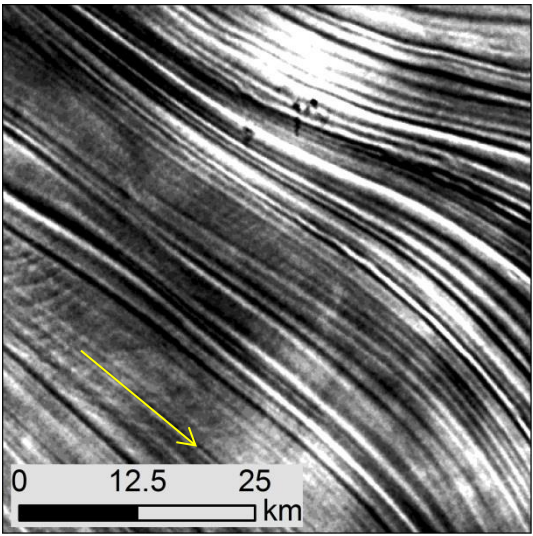
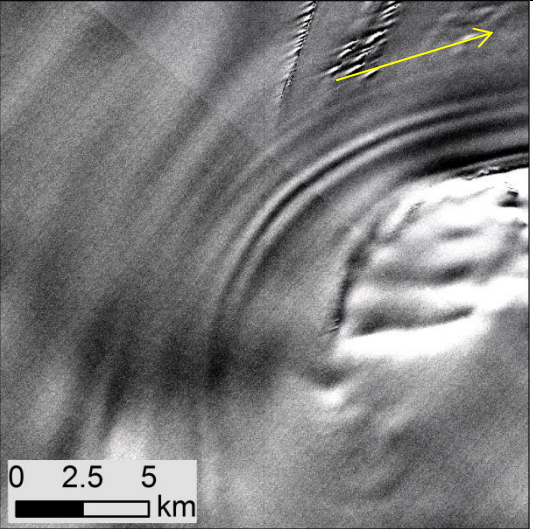
Overall, it is clear that a spectrum of subglacial bedform formation hypotheses exist, ranging in their scale of explanation from individual landforms to attempting to explain the formation of all subglacial bedforms, sometimes focussing on sediment structures, other times on bedform or flowset morphometries. Indeed, the challenge for any theory of subglacial bedform formation is to account for both the morphological and sedimentological properties of subglacial bedforms. Whether this requires a plethora of formation theories, under the view that all bedforms are the product of a geomorphological equifinality, or a single theory which is able to explain all subglacial bedforms via the same mechanism is still a contentious issue.

### 1.2.2 Surface Flow Signatures

Like the bed, the surface of an ice sheet also gently undulates, forming numerous identifiable flow signatures. Merry and Whillans (1993) noticed a variety of structures visible on Ice Stream B, which they gave informal names such as flowstripes, mottles,



warps, lumps and horsetails. Examples can be seen in table 1. These flow signatures are either transverse to, or aligned with flow direction. The edges of an ice stream, where fast flow borders slow, also have numerous features, including elevated ridges and heavily crevassed topography (Merry and Whillans, 1993; Raymond, 1996). Indeed, crevasses themselves can be useful indicators of ice sheet dynamics (Vornberger and Whillans, 1990; Price and Whillans, 2001; Smith et al., 2002). The origin of crevasses and shear margin features is relatively well understood (Meier, 1958; Vaughan, 1993; Jacobel et al., 2000; Smith et al., 2002; Pralong and Funk, 2005), and thus will not be covered in this thesis. Instead the more enigmatic signatures of flow apparent on the ice surface are explored (Table 1).

Feature	Description	Image
Flowstripes	Elongated furrows and ridges, 1-2 m in amplitude, 1 km apart and up to 100's of km long (Raup et al., 2005). Modis image of flowstripes on the Ross-Ice Shelf, emanating from Ice Stream A.	
Horsetails	Curved flow stripes found at the onset of ice streaming. Landsat image of horsetails at the onset to the Rutford Ice Stream.	

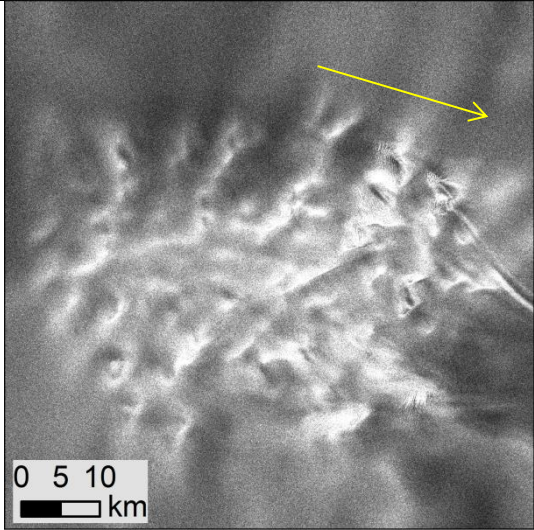
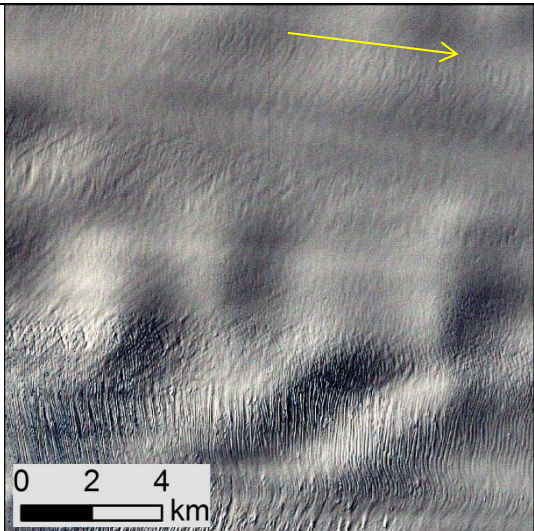
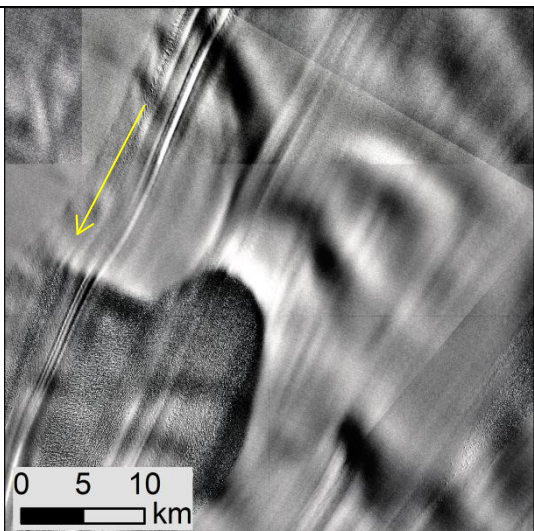
Lumps	Small topographic highs, approximately 1500 m long, 300 m wide, 600 m apart and aligned transverse to flow. Radarsat image of lumps at the onset to Denman Glacier.	
Warps	Larger versions of lumps, 4 km long, 1.5 km wide, 8 km apart. Aligned at right angles to ice flow. Landsat image of warps on the surface of Ice Stream E.	
Mottles	Undulations which appear as alternating dark and bright patches, around 10km apart. Landsat image of Mottles on the surface of Slessor Ice Stream.	

Table 1. Ice sheet surface flow signatures as defined by Merry and Whillans (1993). Descriptions from Merry and Whillans (1993) unless stated otherwise. Yellow arrows denote approximate ice flow direction.

Subtle flow-parallel features are generally found on the outlet glaciers, ice streams and ice shelves of ice sheets (Figure, 1.6). These are collectively referred to as longitudinal surface structures (LSSs; Glasser and Gudmundsson, 2012) and are commonly subdivided into two categories. The term flowstripe (or alternatively ‘flow-band’, ‘flow-line’ or ‘streakline’) is usually retained for features which occur on top of fast flowing ice streams of Antarctica (Figure 1.6A) and that continue onto ice shelves (Figure 1.6B), sustaining themselves for large distances (100’s of km; Crabtree and Doake, 1980; Merry and Whillans, 1993). Alternatively, the term longitudinal foliation is usually applied to features which are found on the surface of smaller glaciers (Figure 1.6C), with numerous examples occurring worldwide (Hambrey, 1975; Hooke and Hudleston, 1978; Jennings et al., 2014). The two sets of nomenclature are occasionally used interchangeably (Glasser and Gudmundsson, 2012). Arguably, a key distinguishing feature between flow stripes and foliations is that foliations have been shown to be three-dimensional in nature (Hambrey and Glasser, 2003), whereas flow stripes may represent variations in surface reflectance of the ice which are non-topographic (Hulbe and Whillans, 1997). However, LSSs are very subtle, generally achieving less than 2 m in amplitude across a distance of over 1 km (Raup et al., 2005). Additionally, reflectance changes in the ice caused by ice crystal fabric alignment differences may also be topographic (Hulbe and Whillans, 1997). Thus, it is difficult to distinguish between purely 2-D and 3-D features, and the distinction may be arbitrary. Hence, I will consider the two together here, grouping them under the term longitudinal surface structures (LSSs).



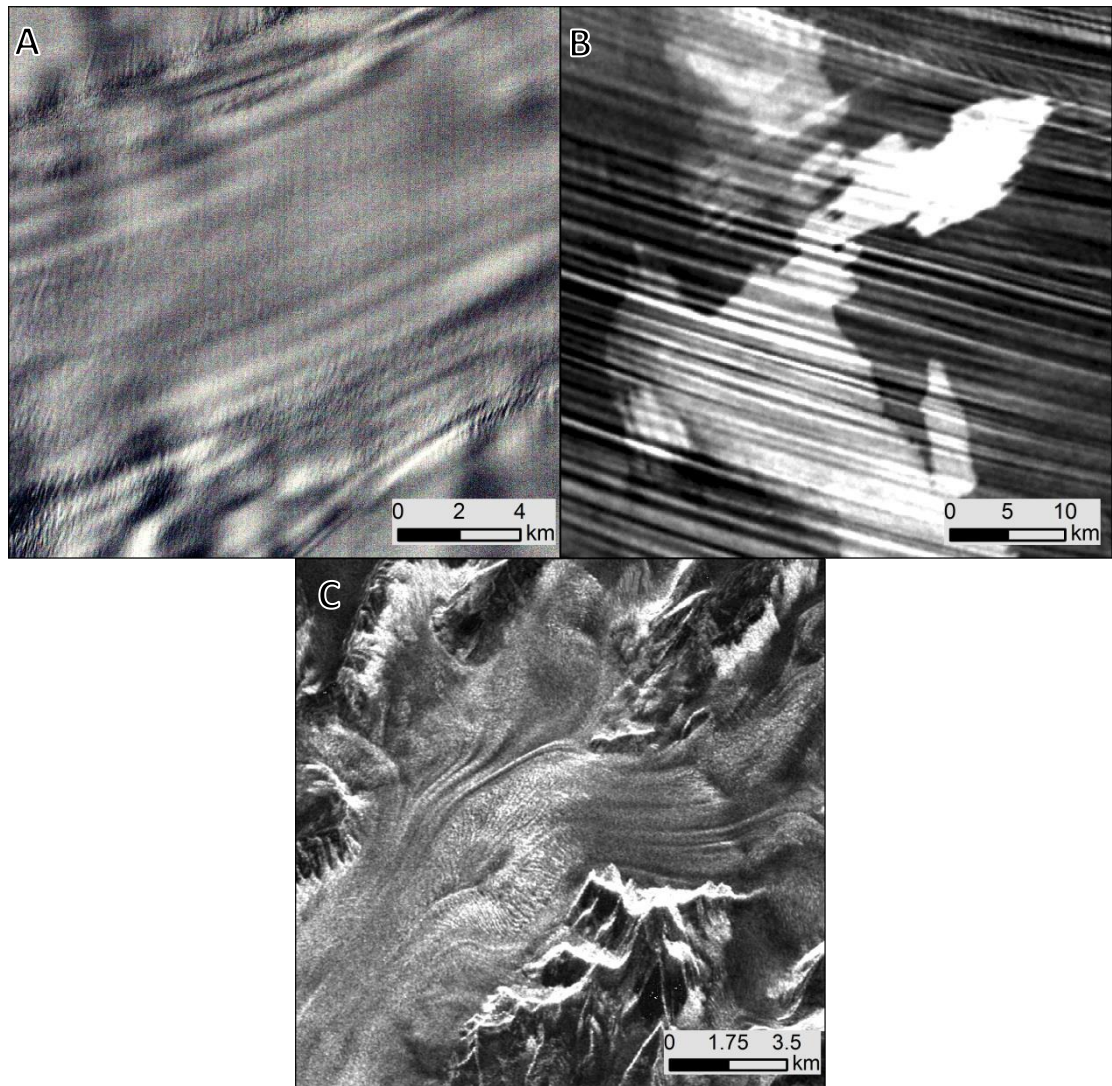


Figure 1.6. Examples of longitudinal surface structures in different glaciological settings. A) Landsat ETM+ image of flow-stripes on the surface of Ice Stream E. B) MODIS image of flow-stripes on the Ross Ice Shelf. C) RADARSAT image of foliations on Erskine Glacier, Antarctic Peninsula.

Despite their subtle nature, LSSs can be informative of current and past ice sheet flow conditions. Occasionally, LSSs are preserved on the surface of previously active ice streams or tributaries (Conway et al., 2002), recording palaeo-ice flow in the interior of an ice sheet (e.g. Siegert et al., 2013). LSSs continue from grounded ice onto ice shelves. The distortion and distribution of LSSs on ice shelves can also provide information into previous ice flow regimes (e.g. Casassa et al., 1991; Casassa and Whillans, 1994; Wuite and Jezek, 2009; Catania et al., 2012). However, the amount of information that can be extracted from the study of LSSs is limited by a lack of understanding of their formation.

Multiple hypotheses have been proposed for the formation of LSSs (see Glasser and Gudmundsson, 2012, for a comprehensive review). A leading hypothesis for their formation sees them as the transmission and attenuation of changes in basal friction (bumps or regions of high friction) to the ice surface; occurring where the rate of basal sliding is high compared to internal deformation (Gudmundsson et al., 1998). Hence, LSSs may be informative of ice sheet basal conditions. Conversely, foliations are hypothesised to form when pre-existing inhomogeneities in the ice (i.e. crevassing, stratification) are deformed and stretched down ice flow (Hambrey, 1977), occurring where ice flow is laterally compressive and longitudinally extensional (Hooke and Hudleston, 1978; Glasser and Scambos, 2008). Longitudinal surface structures also form as the consequence of shear between converging tributaries (Glasser and Gudmundsson, 2012). These models view longitudinal surface structures as a response to ice stresses, as opposed to a response to properties of the bed. A further subtype of LSS was proposed by Glasser and Gudmundsson (2012), occurring due to lateral compression where two tributaries meet. These features are distinguishable as they are narrower and more clearly defined than other LSSs (Glasser and Gudmundsson, 2012). Despite their near ubiquitous abundance on top of glaciers and ice streams, little is known about their scale, patterns and geography.

Transverse surface structures (TSSs) have received comparatively little scientific attention, and are even more poorly defined. Merry and Whillans (1993) described three types of TSS (Table 1), suggesting different modes for their origin. They distinguished their three types, lumps, warps and mottles, primarily on the basis of scale. Many of these features have been attributed to flow around subglacial obstacles (e.g. Figure 1.7; Whillans and Johnsen, 1983; Stokes et al., 2007). However, such a relationship with subglacial topography is not always apparent (Whillans and van der Veen, 1993). Thus, others have invoked variations in basal lubrication (Hindmarsh, 1998c) or ice strength (Whillans and van der Veen, 1993) to account for their genesis. Additionally, some TSSs form standing waves on the ice stream surface, whilst others migrate in the direction of ice flow (Hulbe and Whillans, 1994; Price et al., 2001). Inversions of basal shear stress often reveal similar wave-like patterns (e.g. Sergienko and Hindmarsh, 2013). As Joughin et al. (2009) note for Pine Island and Thwaites Glaciers, West Antarctica, these variations in basal shear stress tend to correspond to variations in ice surface reflectance recorded by satellite images. However, the ubiquity and significance of TSSs is unknown, and their scale is poorly defined within the literature.

Figure 1.7. Transverse surface structures on the surface of MacAyeal Ice Stream. From Stokes et al. (2007). Labelled feature has been found to correspond to a subglacial bedrock ridge. However, note the occurrence of numerous other features forming transverse to flow direction.

Although not as numerous as subglacial bedforms, both LSSs and TSSs also have multiple hypotheses for their origin. Interestingly, both have been linked to variations in subglacial conditions. A morphometric dataset of both types of surficial flow signatures may shed light upon their genesis, providing constraints on spacing, distribution and regularity. Such an approach is akin to that taken for studying subglacial bedforms (e.g. Spagnolo et al., 2014a). However, the availability of information regarding ice parameters such as velocity and ice thickness (Rignot et al., 2011; Fretwell et al., 2013), could provide further constraints upon models of their formation.

### 1.2.3 Connecting the Surface and the Bed of an Ice Sheet

Despite being spatially separated by a layer of ice, often kilometres thick, the bed and surface expressions of an ice sheet are linked, allowing for inversions of basal conditions from surface measurements (e.g. MacAyeal, 1992; Joughin et al., 2006). Flow disturbances at the bed can cause fluctuations in both surface topography and velocity. The transmission of such disturbances occurs through a diffusive process, with the ice selectively transmitting bumps of a specific scale and thus acting as a band-pass filter (Gudmundsson, 2003). Examining the effect of a bedrock perturbation and an area of high friction, Gudmundsson (2003) found that, for moderate ratios between internal deformation and basal sliding, basal variability is easily transmitted toward the surface (Figure 1.8). This is especially the case where the wavelength of the bumps is approximately 3-10 ice thicknesses, although this is dependent upon the slip ratio. However, the transmission of basal variability is sensitive to its amplitude and the temperature gradient of the ice (Gudmundsson and Raymond, 2008). Thus, whilst the surface may transmit information about the properties of the bed, it is not a perfect mirror.

Figure 1.8. Modelled effect of a bedrock bump (left) and a perturbation in basal slipperiness (right) upon ice flow. General ice flow direction is from left to right. The top plane depicts surface strain anomalies, with red showing compression and blue extension. Below this, surface velocity anomalies are depicted, red for downward velocity, blue for upward. The third plane from top shows the shaded ice surface shape, with green contours indicating the magnitude of the bedrock bump or basal drag perturbation. Finally, the bottom plane depicts horizontal and vertical velocities, with dashed lines showing vertical velocity and solid horizontal velocity.

Some have furthered the connection between the bed and the surface of ice, suggesting that flow signatures are linked. Schoof (2002) examined the flow of ice over a drumlin, and the effect this has upon the surface of an ice sheet. His work suggests that a drumlin can produce enough form drag to induce a perturbation of the ice surface, using a model similar to that used to account for the formation of LSSs (Gudmundsson et al. 1998). A further relationship between subglacial bedforms and LSSs is proposed by the groove-ploughing hypothesis for the formation of MSGL's (Clark et al., 2003). Here, MSGL are proposed to be the consequence of basal 'keels' of ice which erode the underlying sediment. The groove-ploughing model invokes the presence of LSSs in order to prolong the attenuation of these keels, suggesting that MSGL's and LSSs are linked. Sergienko and Hindmarsh (2013) found regular variations in basal drag which



they linked to mega-scale subglacial ribs (e.g. Greenwood and Kleman, 2010). Such variations in drag would produce surface undulations. However, their work did not consider any correspondence these variations in drag may have to surface features. Therefore, little work has been done to compare ice basal and surficial flow signatures, despite the proposed links between basal and surficial ice properties (e.g. Clark et al., 2003; Gudmundsson, 2003).

#### 1.2.4 Summary of Ice Sheet Flow Signatures

Both basal and surficial ice sheet flow signatures record information pertaining to ice flow dynamics (e.g. Stokes and Clark, 2002; Kleman and Glasser, 2007; Catania et al., 2012). However, both have numerous hypotheses for their formation (e.g. Menzies, 1979; Glasser and Gudmundsson, 2012). The distribution and morphological properties of subglacial bedforms has proven to be a useful tool in their study (e.g. Dunlop and Clark, 2006b; Clark et al., 2009; Spagnolo et al., 2012). Further work of this nature may help solve the key question of whether they should be considered as individual features or as a single phenomenon. Little morphometric analysis has been conducted upon surface flow signatures (n.b. Raup et al., 2005), despite an abundance of data regarding the glaciological conditions under which they form (e.g. Fretwell et al., 2013); such data is unavailable for subglacial bedforms. Infrequently, the two are considered together (e.g. Schoof, 2002; Clark et al., 2003). However, systematic comparison of basal and surficial flow signatures has yet to be achieved.

### 1.3 Thesis Aim and Objectives

The aim of this thesis is to further our understanding of ice flow by elucidating the characteristics of, and possible links between, ice sheet flow signatures. This will be achieved through the following objectives:

***Objective 1:** Examine the morphological and spatial properties of subglacial bedforms, in order to shed light onto their genesis.*

Objective 1 will be achieved by collating a large dataset of subglacial bedforms and analysing their morphometric and spatial properties. This will focus on two pertinent research questions (See Section 1.2.1 for outline):

- Do subglacial bedforms display characteristics of patterning?
- Do subglacial bedforms form a size and shape continuum?

*Objective 2: Examine the morphological, spatial and glaciological properties of ice sheet surface flow signatures.*

Objective 2 will be achieved by mapping surface flow signatures on the surface of the Antarctic ice sheet. Their distribution and morphometric properties will be defined and theories for their formation tested (See Section 1.2.2 for outline), utilising available datasets of glaciological parameters (e.g. Rignot et al., 2011; Fretwell et al., 2013).

*Objective 3: Compare and contrast the properties of basal and surficial ice sheet flow signatures, in order to determine the extent to which they are linked.*

Objective 3 will be achieved through a morphometric comparison of surficial and basal ice sheet flow signatures, analysis of ice penetrating radar lines in Antarctica, and a consideration of bed to surface transfer (e.g. Gudmundsson, 2003).

Further details on the methods used, rationale for each objective and hypotheses tested are provided within each chapter.

## **1.4 Structure and Outline of this Thesis**

There are many unresolved questions regarding ice sheet flow signatures. Study of either in isolation can provide insight into their own formation. However, the two are rarely considered together despite both being formed by ice sheet processes. Therefore, this thesis is split into three sections. In Section A (Chapters 2 and 3) I focus on ice sheet and glacier beds, examining the characteristics of subglacial bedforms in order to gain understanding of the subglacial environment. In Section B (Chapters 4 and 5), I focus on the surface of an ice sheet. Here I examine their morphological characteristics, and examine the consequences for their formation. Basal and surficial flow signatures are reunited in Section C (Chapter 6), where I discuss the similarities and differences between the two. Chapter 7 then provides a summary of results and future work that is required.

## **1.5 Publications**

Several papers related to this thesis have been published prior to its acceptance. The following list documents these papers and documents which portion of the thesis has been adapted for publication. Further publications are planned.

Spagnolo, M., Clark, C.D., Ely, J.C., Stokes, C.R., Anderson, J.B., Andreassen, K., Graham, A.G. and King, E.C., 2014. Size, shape and spatial arrangement of mega-

scale glacial lineations from a large and diverse dataset. *Earth Surface Processes and Landforms*, 39(11), pp.1432-1448.

This paper uses some of the mapped data from Chapter 3 in order to analyse the morphological and spatial properties of MSGL. Although data is used, no writing from this paper is incorporated into the thesis.

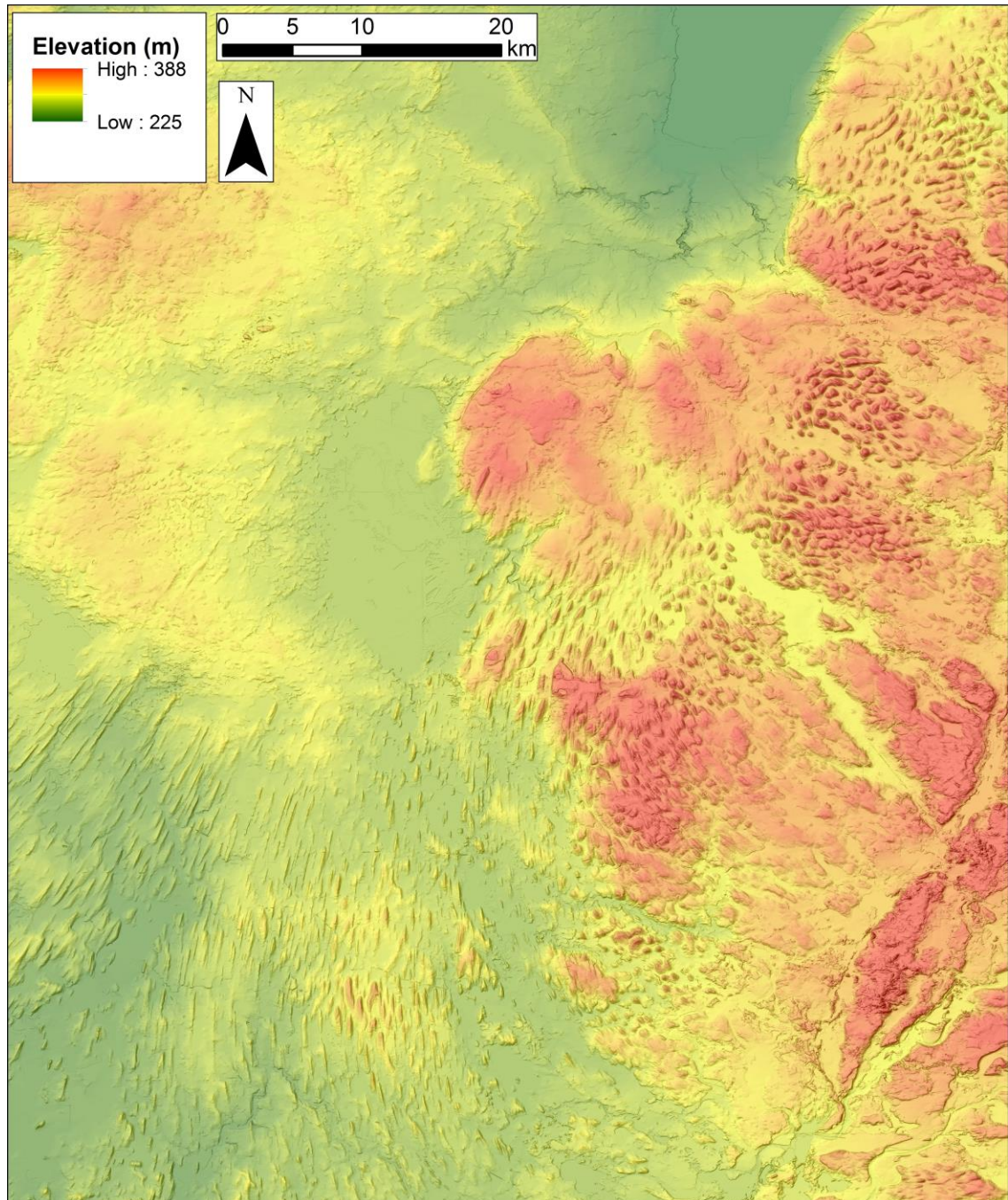
Ely, J.C. and Clark, C.D., 2016. Flow-stripes and foliations of the Antarctic ice sheet. *Journal of Maps*, 12(2) pp.249-259.

This paper presents the maps presented on Plate 1 and how these maps were created (Section 4.3). No analysis of the mapping (other sections in Chapter 4) is included in this paper.

Ely, J.C., Clark, C.D., Spagnolo, M., Stokes, C.R., Greenwood, S.L., Hughes, A.L., Dunlop, P. and Hess, D., 2016. Do subglacial bedforms comprise a size and shape continuum?. *Geomorphology*, 257, pp.108-119.

Chapter 3 was shortened and adapted to create this paper.

## Section A: Insights into the Characteristics and Formation of Subglacial Bedforms



Section A: Hill-shaded digital elevation model of Dodge County, Wisconsin, USA. Note the numerous subglacial bedforms imprinted onto the landscape. Source: [ned.usgs.gov/](http://ned.usgs.gov/)

# Chapter 2 Patterning and Growth of Subglacial Bedforms

## 2.1 Introduction

A pattern is a discernible regularity of form, composed of a number of elements which have been organised by a process (Ball, 1999). Some of the most striking natural patterns are geomorphological (Werner, 1999); exemplars include dunes (Kocurek and Ewing, 2005), freeze-thaw patterned ground (Kessler and Werner, 2003) and river meander networks (Hallet, 1990). The regularity of a pattern gives the impression of simplicity; however, pattern forming processes are often non-linear, involving complex interactions between elements of the pattern (Cross and Hohenberg, 1993; Phillips, 2003; Kocurek et al., 2010; Murray et al., 2014). Patterns often emerge through self-organisation due to local interactions between pattern elements, rather than a collection of discrete events (Werner, 1999; Baas, 2007). For example, rather than simply being a collection of individuals, a field of dunes can be considered to be a phenomenon in itself (e.g. Ewing et al., 2006; Eastwood et al., 2011).

When observed from the ‘bird’s-eye’ view provided by remote sensing and subsequent application of GIS techniques, subglacial bedforms often appear to belong to a pattern (e.g. Aylsworth and Shilts, 1989; Clark, 1994, 1999; Dunlop et al., 2008; Stokes et al., 2013a; Figure 2.1). Yet, ideas developed within the field of pattern formation are rarely considered within the context of subglacial bedforms. This is perhaps due to a lack of observations of subglacial bedforms as they are formed (c.f. King et al., 2009), leaving the static view provided by the exposed subglacial bedforms of palaeo-ice sheets. If fields of subglacial bedforms display patterning behaviour, this suggests that they co-evolve as a phenomenon. Such a monogenetic interpretation would conflict with the polygenetic view often derived from the diverse internal structures of subglacial bedforms (Lundqvist, 1997; Möller, 2006; Sutinen et al., 2009; c.f. Section 1.2.1; Figure 1.4), yet it is consistent with the commonality found in bedform morphology and spatial distribution (Dunlop et al., 2006; Clark et al., 2009; Spagnolo et al., 2014a). Thus, the consideration of subglacial bedforms within a patterning context may provide useful insight into their formation. Here, I address the above deficiencies by asking whether subglacial bedforms from palaeo-ice sheet beds display characteristics similar to that of other phenomena formed by processes that tend to spatially organise landforms into patterns.

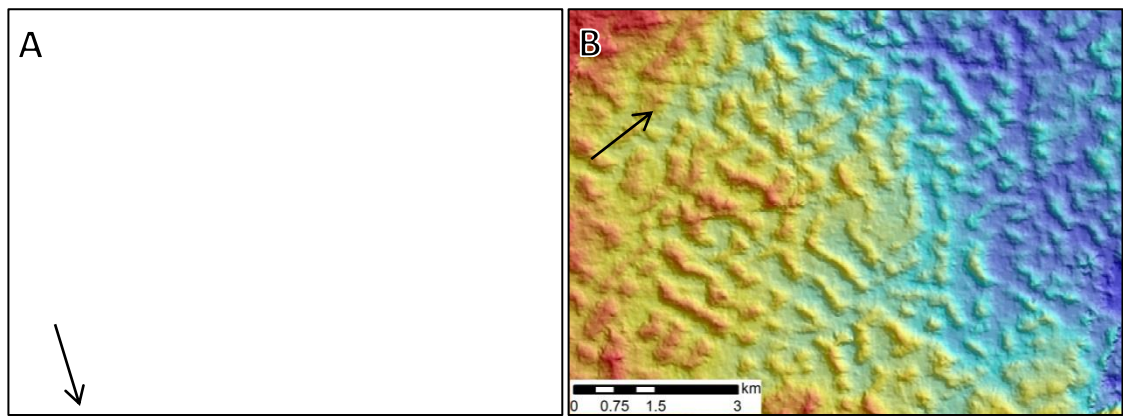


Figure 2.1. Subglacial bedform patterns. Arrows denote palaeo-ice flow direction. All images are hill-shaded digital elevation models. A) The Leitrim drumlin field, Ireland. Note the consistency of form and ordered spacing of the drumlins. B) Subglacial Ribs, Northern Ireland, east of Dromore. Note the almost wave-like morphology and consistent down-flow spacing. C) MSGL of the Getz Shelf, offshore Amundsen Sea, Antarctica. Note the apparent regular across flow arrangement. Figure from Spagnolo et al. (2014).

## 2.2 Previous Work

### 2.2.1 Pattern Formation and Interactions within Bedform Fields

Patterns result from numerous natural and anthropogenic systems (Ball, 1999). They are often thought to be self-organising, emergent phenomena resulting from complex systems (e.g. Werner, 1999; Kocurek and Ewing, 2005; Baas, 2007). Much work has been done upon the formation of patterns within aeolian dune fields (Wasson et al., 1988; Werner, 1995; Kocurek and Ewing, 2005; Ewing and Kocurek, 2010; Fourriere et al., 2010). Therefore, it is useful to review this work, in order to provide a background for considering whether subglacial bedforms display similar patterning behaviour.

A key component of a pattern is the spatial regularity of its components. Often patterns are initiated by an instability, whereby disturbances or random forcing fluctuations are amplified in an otherwise uniform field (Kennedy, 1969; Sivashinsky et al., 1983; Hansen et al., 2001). This amplification triggers feedbacks within the system, causing the further growth of the perturbations. Although growth occurs at multiple wavelengths (or spacings), typically a single wavelength dominates at which perturbations preferentially grow (Dunlop et al., 2008). Hence, the regularity of a pattern is often a consequence of the instability from which it develops (Murray et al., 2014; c.f. Figure 2.2A). This preferred wavelength can often be controlled by the boundary conditions of the system. Hence, the wavelength, or spacing of the components within the pattern, that initially develops may change spatially and temporally in accordance with fluctuations in boundary conditions.

After a pattern has developed, interaction between elements within that pattern may lead to numerous pattern altering behaviours. Murray et al. (2014) review common behaviours of patterning in aeolian, fluvial and marine bedforms that occur after pattern initiation. Firstly, patterns can stabilize as the forms of the elements within the pattern adapt to flow conditions (Figure 2.2B). For example, the development of slip planes in the lee of barchans dunes limits their growth, causing stabilization (Evans, 2003). In other cases, the elements of a pattern can interact. Growth, migration and collision of pattern elements can lead to coarsening of a pattern, whereby a pattern becomes composed of fewer elements which are spaced further apart (e.g. Werner, 1995). This either happens until a new stable state is reached and coarsening stops, or until the whole spatial domain is composed of a singular pattern element (Murray et al. 2014;

Figures 2.2C and D). Additionally, patterns can also return toward their initial state, via a number of regenerative processes whereby pattern elements, in this case bedforms, split to create new bedforms (Kocurek et al., 2010; Figures 2.2E and F). These patterning behaviours are summarised in Figure 2.2.

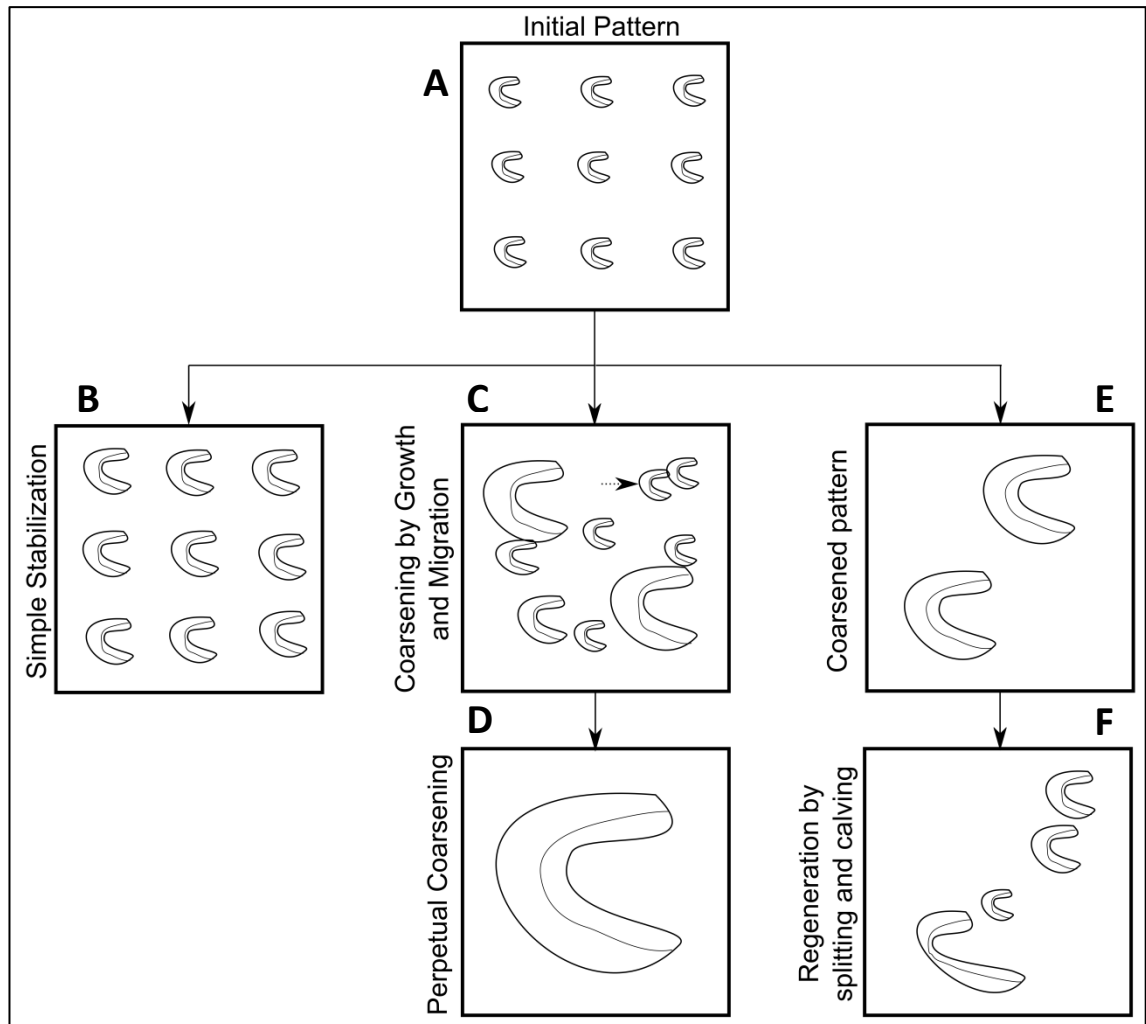


Figure 2.2. Summary of patterning behaviour for dunes. Wind-flow from the left. Note, in reality the morphology of dunes is likely change as pattern interactions occur, but for simplicity the same representation of a barchans is used here. See text and Kocurek et al. (2010) and Murray et al. (2014) for more details.

### 2.2.2 Patterning and Subglacial Bedforms

Although the concept of patterning has been adopted frequently in the study of bedforms in other disciplines (e.g. Kocurek et al., 2010), patterning, and pattern forming processes, have been rarely addressed for subglacial bedforms. This is likely influenced by a lack of *in situ* observations, hindering our ability to observe any possible stages of



pattern development. However, the static snapshot provided by the exposed subglacial bedforms of palaeo-ice sheets may provide us with insight into whether they display patterning behaviour.

As noted above (Section 2.2.1), a key aspect of any pattern is its regularity. Many have remarked upon the apparent regularity of subglacial bedforms (e.g. Werth, 1909 cited in Baranowski, 1969; Baranowski, 1977; Carl, 1978; Fowler, 2000; Clark, 2010). As Figure 2.1 demonstrates, when viewed from above subglacial bedforms often form a repetitive, systematic arrangement within the landscape. Statistical work attempting to describe this regularity has focused upon drumlins (Table 2). The simplest technique for assessing the regularity is to measure bedform spacing. This approach has been employed for subglacial ribs (Dunlop and Clark, 2006b) and MSGL (Spagnolo et al., 2014a), utilising large datasets of mapped bedforms. Dunlop and Clark (2006) measured the wavelength of subglacial ribs through spectral analysis, across transects totalling 12,000 km in length. They found a strong preferred spacing for subglacial ribs in the down-stream direction, varying between locations, but typically between 300-1200 m (Figure 2.3A). Similarly, Spagnolo et al. (2014a) measured the across flow spacing of 8 fields of MSGLs, finding a consistent modal spacing of 200-300 m (Figure 2.3B).

Subglacial ribs and MSGLs can be considered as wave-type phenomena (Schoof, 2007; Fowler 2010b), hence measuring only their spacing either down flow or across flow respectively is appropriate. When considered this way, they are essentially only two dimensional, these dimensions being spacing and amplitude. However, drumlins are often considered to be three-dimensional (e.g. Chapwanya et al., 2011), making both across and down-flow spacing relevant. Subglacial bedform spacing frequency histograms have a strong peak, interpreted as showing that drumlins have a preferred spacing (Table 2; Reed et al., 1962; Baranowski, 1969; Hill, 1973). For drumlins specifically, Spagnolo et al. (in prep.) have demonstrated that a peak is present both in the down-flow and across-flow spacing frequency distribution, and verified this across different flowsets (Figures 2.3C-D).

<b>Reference</b>	<b>N of drumlins</b>	<b>Statistical Methods</b>	<b>Concluded Distribution of drumlins</b>
Reed et al., 1962	204, across 2 fields	Spacing measurements	Preferred spacing.
Smalley and Unwin, 1968	203, across 4 fields.	Comparison to random placement model and Clark and Evans (1954) statistic	Random
Vernon, 1966	733	Density estimates and nearest neighbour distance	Variable spacing, throughout sections of drumlin field
Baranowski, 1969	1054 spacing measurements, 2 fields	Nearest neighbour, across profile measurements	Regularly spaced
Trenhaile, 1971	Between 6000-7000, across several fields	Comparison to two random distribution models, and order-rank nearest-neighbour analysis	Between random and uniformly spaced
Hill, 1973	≈3900	Nearest neighbour distance measurements, trend surface analysis and cumulative frequency distribution of nearest neighbour distances	Non-randomly distributed, mostly clustered, peaked histogram of nearest-neighbour distances
Jauhiainen, 1975	1137 across 12 fields	Clark and Evans (1954) statistic	Clustered to random
Boots and Burns, 1984	102, across 2 fields	Two phase mosaic	Random
MacLachlan and Eyles, 2013	≈3000	Ripley' s K-function	Clustered

Table 2 – Compilation of previous studies on the regularity of drumlin spatial distribution.

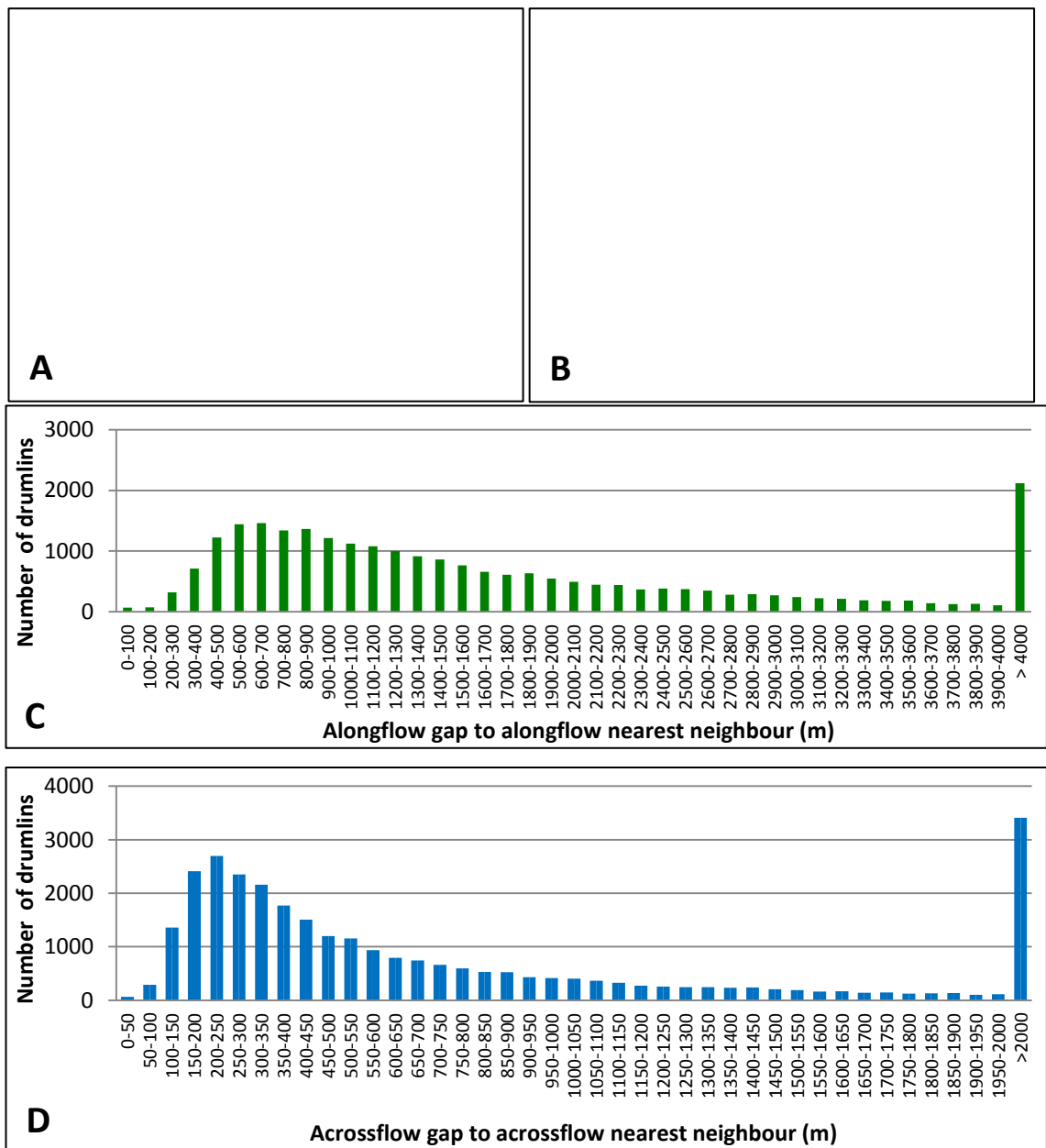


Figure 2.3. Histograms of spacing measurements of subglacial bedforms. A) Downstream spacing of subglacial ribs. From Dunlop and Clark (2006), who report a mean wavelength of 505 m. B) Across flow spacing of MSGL. From Spagnolo et al. (2014), who report a mean spacing of 458 m. Modal spacing is between 200 and 300 m. C) Downstream spacing of drumlins. Modal spacing is between 600 and 700 m. D) Across flow spacing of drumlins. Modal spacing is between 200 and 250 m. C and D from Spagnolo et al. (in prep), and is amalgamated from mapping of 43,432 drumlins from Britain, Ireland, Canada and the USA.

Whilst the preferential spacing of subglacial bedforms hints at regularity within drumlin fields, better spatial statistical tools may be needed to test this hypothesis. Currently, there is no consensus regarding whether drumlins are placed regularly, randomly, or within clusters in a drumlin field (Table 2, c.f. Unwin, 1996, p.545).

Additionally, many of the studies in Table 1 have relatively small sample sizes (<1000). Drumlin identification is also an issue, a problem most pertinent to the latest study in Table 1 (MacLachlan and Eyles, 2013); during the mapping procedure a minimum threshold of 10 m of relief was employed in drumlin identification, yet a large sample of drumlin relief reveals the majority of drumlins to possess a relief below this threshold (Spagnolo et al., 2012). This further problem of drumlin identification and representation can lead to systematic errors when testing for spatial regularity. Hence, debate about appropriate statistics and a lack of detailed analysis leaves the question of whether drumlins are randomly positioned within a flowset unsolved.

Beyond regularity, the characteristics of exposed drumlins can provide us with hints that other patterning interactions have occurred. As outlined in Section 2.2.1, elements within a pattern may interact once they have developed. One way in which this occurs is through the growth of elements within the pattern. Many have argued that, all other things being equal, the length of drumlins can be considered as a function of ice-velocity and time (e.g. Clark, 1993; Hart, 1999). This is based upon the identification of palaeo-ice stream signatures, within which the longest drumlins are found where the highest ice velocities might be expected (e.g. Stokes and Clark, 2002). Additionally, observations of progressive downstream increases in drumlin length corresponding to expected increases in palaeo-ice flow velocity (e.g. Briner, 2007). However, it is difficult to distinguish whether this shows a progressive growth of drumlin length, or a near instantaneous ‘printing’ of drumlins at these various lengths in correspondence with subglacial boundary conditions. Stokes et al. (2013b) concluded that the former is more likely, at least for the bedforms of the Dubawnt Lake palaeo-ice stream, Canada. They found that shorter bedforms can be found neighbouring much longer bedforms. Rather than representing abrupt jumps in subglacial conditions, Stokes et al. (2013b) argue that a more likely explanation for this juxtaposition is a mixed age population of bedforms, whereby longer subglacial bedforms have had more time to grow. This supports the idea of a rapidly evolving subglacial environment, where bedforms can initiate, grow, shrink or be erased over time. Such an environment would provide ideal ground for subglacial bedform patterning interactions to occur (e.g. Figure 2.2).

Supporting evidence that drumlins grow over time has recently been inferred from the frequency distribution of their morphological properties. Commonly, these conform to a log-normal distribution (e.g. length and width in Clark et al., 2009 and relief in Spagnolo et al., 2012), as demonstrated in Figure 2.4. As argued by both Hillier et al.

(2013) and Fowler et al. (2013), such log-normal distributions are common for many phenomena which stochastically grow and shrink in multiple random events. Fowler et al. (2013) expanded upon this, arguing that drumlins form from an incremental growth process; growing during transient events such as high subglacial discharge periods and ice spurts. Indeed, drumlin growth phases may occur over multiple glaciations (e.g. Hättestrand et al., 2004). An alternative explanation is that drumlin size mirrors stochastically distributed subglacial parameters pertinent to drumlin formation (e.g. ice velocity, effective pressure, sediment supply). Analysis of size metric distributions has thus far focused upon morphological metrics of drumlins collated from multiple flow events, at the ice sheet scale. A comparison of size distributions of drumlins between different flow-sets, where one might infer that similar subglacial conditions have occurred within the flow-set, may provide further insight into the nature of how such log-normal distributions occur.

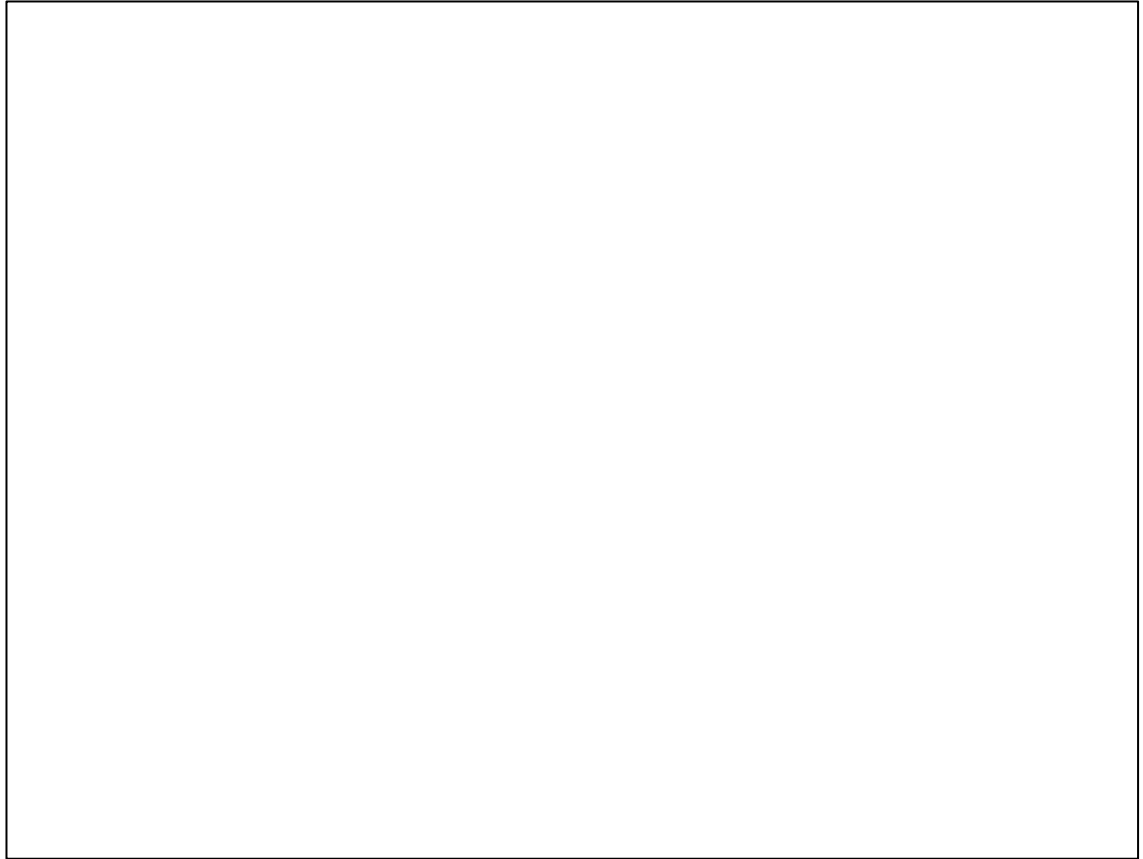


Figure 2.4. Frequency ( $f_i$ ) histogram of drumlin width, plotted with a logarithmic scale. Blue line indicates a theoretical Gaussian probability function, which approximates the shape of the histogram. Hence, Fowler et al. (2013) interpret drumlin width to be approximately log-normal. Figure from Fowler et al. (2013).

As discussed in Section 2.2.1, a consequence of elements within a pattern growing, is that secondary pattern interactions occur. Thus, the same may be the case for drumlins. This may take the form of coarsening, either by selective preferential growth of some drumlins leading to sediment starvation for other drumlins, or via collisions which occur by growth or migration. If subglacial bedforms coarsen over time, then an expectation would be that flow-sets where bedforming occurred for a long duration would be comprised of fewer elements, spaced further apart. If drumlins grow, stabilisation may also occur. Here, the expectation would be that drumlin size reaches a certain threshold beyond which it becomes more difficult for the drumlins to grow. However, such a limit on length, width and relief has not been found (Clark et al., 2009; Spagnolo et al., 2012).

Interactions within a pattern can also occur through migration of pattern elements. Migration of subglacial bedforms has been inferred from geophysical studies (e.g. Smith et al., 2007; King et al., 2009) and theoretical studies (Hindmarsh, 1996). Hence, a second mechanism controlling the distribution and size of drumlins may be their migration along an ice sheet bed.

In summary, subglacial bedforms often display a preferential spacing, either in an across or down-flow direction (Dunlop and Clark, 2006b; Spagnolo et al., 2014a; in prep.). However, it is unclear whether bedform spacing is the best way to describe and test patterning and other, more or less sophisticated statistical techniques applied in the literature have shown opposing results, sometimes stating that drumlins are spatially regular, random or clustered within a drumlin field (Table 2). Both the distribution of drumlin sizes within a field, and the log-normal distribution of drumlin size metrics have been used to argue that drumlins grow over time. If growth of drumlins occurs, other patterning interactions such as coarsening and stabilization may occur. Subglacial bedforms have rarely been thought about in this context. In line with most of the previous literature, the remainder of this chapter will focus specifically on drumlins. Additionally, the consequences for our interpretation of other subglacial bedforms will be discussed.

## **2.3 Dataset**

A GIS database comprising of 36,222 drumlins mapped by Hughes et al. (2010) across Britain from a high resolution (5 m) digital elevation model (DEM), with multiple illumination angles was analysed here. A high identification level is reflected in that extremely low relief ( $\approx 0.5$  m) drumlins are identified within the dataset (Spagnolo et al., 2012). Each drumlin is represented within the dataset by a smooth polygon manually digitised around its break of slope (Figure 2.5).

Figure 2.5. Representation of drumlins within the dataset. A) Relief-shaded digital elevation model of drumlins in the Yorkshire Dales, England. B) Representation of drumlins within studied dataset. Smooth polygons drawn around the break of slope of each drumlin. From Hughes et al. (2010).

The dataset was divided into 100 flowsets, which were previously identified for the purpose of palaeo-ice sheet reconstruction (Hughes et al., 2014; Figure 2.6). The delineation of these flowsets was based upon drumlin spatial arrangement, with consideration of their morphology, parallel conformity, spacing and orientation (Clark, 1997; Greenwood and Clark, 2009a). Here, these flow-sets were used as a first approximation of the study area (see Section 2.4.1), an essential ingredient in many spatial statistical tools. However, some flow-sets contained small numbers of drumlins, therefore a threshold of minimum 30 drumlins was applied, leaving 72 flow-sets which were used in this study. All following analyses were done on a per-flowset basis. This was done based on the assumption that each flowset represents a field of drumlins at a different stage of development (see Section 3.5 for discussion). Although across a flowset geological and glaciological conditions are likely to change, producing differences in drumlin morphology (e.g. Rattas and Piotrowski, 2003; Stokes and Clark, 2003), analysing the drumlins observed by flowset enables the constraint that the area being studied was subjected to a similar time for drumlin development to occur. However, if drumlins erode, migrate and spawn during drumlinisation (Section 2.2.2), this may mean that the drumlins within the flowset are of mixed ages.



Figure 2.6. Flowsets of the last British-Irish Ice Sheet. From Hughes et al. (2014).

## **2.4 Are Drumlins Regularly Positioned?**

### **2.4.1 Methods: Spatial Statistics**

If drumlins are patterned, then they should be regularly positioned. Multiple statistical tools exist for assessing whether spatial phenomena positioned randomly, regularly or within clusters. Previous statistical studies examining the positioning of drumlins have typically relied upon spatial descriptive statistics (Table 2), such as the

Clark and Evans (1954) statistic. The Clark and Evans (1954) statistic ( $R$ ) is a comparison between the mean observed nearest neighbour distance of points ( $\bar{r}_A$ ) and the random expectation ( $\bar{r}_E$ ) using the equation:

$$R = \frac{\bar{r}_A}{\bar{r}_E} \quad \text{Eq.1}$$

Whereby:

$$\bar{r}_A = \frac{\sum r}{N} \quad \text{Eq.2}$$

And:

$$\bar{r}_E = \frac{1}{2\sqrt{\rho}} \quad \text{Eq.3}$$

Where  $\sum r$  is the sum of measurements between points and their nearest neighbour,  $N$  is the number of observed measurements and  $\rho$  is the number of points per unit area in the observed distribution. A value of 0 indicates maximum clustering of points, whilst a value of 2.1491 indicates that points are as regularly and widely spaced as possible. Whilst providing a useful summary of a study area, this technique provides no information pertaining to the scale at which clustering or regularity occurs. Furthermore, the Clark and Evans statistic does not account for mutual nearest neighbours, essentially double counting of the same nearest neighbour distance from each point (Dixon, 2006). Neither does it take account of edge effects, which can lead to a bias when calculating  $\bar{r}_A$ . Such effects can be minimised through the use of an edge buffer area, inside which the nearest neighbour of a point is not included in the calculation, but points inside the buffer area can be used to calculate the nearest neighbour distance for other points. Previous studies using the Clark and Evans statistic did not use edge corrections, and used rectangular bounding boxes (Jauhiainen, 1975; Smalley and Unwin, 1968). Here, I will use the Clark and Evans statistic with more advanced bounding boxes and utilise edge corrections.

Instead of spatial descriptive statistics, a second approach to describing the regularity, or otherwise, of events within a study area is to compare a function of the distance between points to expectations of complete spatial randomness (CSR). The only study known to the author to adopt this approach for drumlins was conducted by MacLachlan and Eyles (2013). Using the Ripley K function ( $K(r)$ ), they concluded that drumlins in the Peterborough Drumlin Field, Ontario, Canada were significantly clustered within the field. However, MacLachlan and Eyles (2013) do not explicitly

refer to bounding box issues or edge corrections, and, as previously mentioned, numerous drumlins may have been missing from their dataset due to a minimum relief threshold adopted during mapping. Numerous adaptations of Ripley's K function exist (Ripley, 1988; Dixon, 2012) but a commonly used function is defined as:

$$K(r) = \frac{\lambda^{-1} \sum_{i \neq j} (e_{ij} < \pi r^2)}{n} \quad \text{Eq.4}$$

where  $\lambda$  is the mean density of points,  $e_{ij}$  is the Euclidean distance between the  $i^{\text{th}}$  and  $j^{\text{th}}$  points in the dataset,  $r$  is the radius of the search area and  $n$  is the number of points within the dataset. Under CSR, the expected value of  $K(d)$  is:

$$E(K(d)) = \frac{\lambda \pi r^2}{\lambda} \quad \text{Eq.5}$$

Since for a CSR pattern, we would expect the average number of points within the searched circle to be dependent upon  $r$  (O'Sullivan and Unwin, 2010, p. 146). To emphasize the difference between expected and observed results,  $K(d)$  is commonly converted into Ripley's L function ( $L(r)$ ):

$$L(r) = \sqrt{\frac{K(r)}{\pi}} \quad \text{Eq.6}$$

Making the expectation of CSR directly proportional to  $r$  for  $L(r)$ . Here, values lower than the expected value of CSR are referred to a dispersed pattern. Those above the expectation, that possess more points than under CSR, indicate clustering. A perfectly regular pattern (e.g. a grid of points evenly spaced) would only have values on the dispersed side of the expected CSR function.

$K(r)$  and  $L(r)$  are both cumulative functions. This means that each value considers the previous measurements. This means that  $K(r)$  and  $L(r)$  can only be used to infer clustering or dispersion up to a certain distance (Wiegand and Moloney, 2004). The pair correlation function (PCF;  $g(r)$ ) is non-cumulative, and therefore allows for inferences at specific distances (Perry et al., 2006; see Figure 2.9).  $g(r)$  is defined as:

$$g(r) = \frac{1}{2\pi r} \frac{\delta K(r)}{\delta r} \quad \text{Eq.7}$$

Under CSR,  $g(r)$  is equal to 1. Homogeneous Poisson processes display a value of  $g(r) = 1$  for all values of  $r$ , thus under CSR  $g(r) = 1$ . If  $g(r) < 1$ , then this means that fewer points are measured within the point array than under CSR.  $g(r) < 1$  therefore indicates that "repulsion" between points at the measured value of  $r$  has occurred, or that points have been inhibited from occurring at this scale. When  $g(r) > 1$ , "attraction"

of points to this distance as occurred, i.e. there are more points at this  $r$  for this specific distance. A truly regular pattern would display repulsion at most values of  $r$ , but a high value of  $g(r)$  at the scale of the regularity.

The analyses described so far are applicable to stationary, or homogeneous, sets of data. This means that they assume the intensity (density of points) of a process is the same across the entire study area. Often this is not the case. For example, in ecological studies the position of trees may be influenced by variables such as soil availability and nutrition, which introduces inherent clustering (Perry et al., 2006). One might expect similar second-order effects to occur in the formation of drumlins. Initially, the domain over which drumlin formation occurs is inhomogeneous in nature due to variations in topography, sediment supply and sediment nature. Indeed, such variables can have a local effect upon drumlin morphology (e.g. Rattas and Piotrowski, 2003). Furthermore, as the drumlins I am studying are not observed *in situ*, post formational erosion, or masking by human activity may remove some of the drumlins from the study area (Figure 2.7). One approach to address this problem is to individually study carefully delineated homogeneous areas or clusters (e.g. Couteron et al., 2003). However, the variables influencing drumlin formation and preservation may be unknown and vary between each flowset, meaning delineation of such smaller areas may be arbitrary (see Figure 2.8). A second approach for inhomogeneous study areas was proposed by Baddeley and Turner (2000), whereby the chosen function is varied in correspondence to the local density of points at each given point. When this adaptation is applied, the functions  $K(r)$ ,  $L(r)$  and  $g(r)$  are referred to as  $K_{inhom}(r)$ ,  $L_{inhom}(r)$  and  $g_{inhom}(r)$  respectively. This approach enables the entire flowset to be examined, without arbitrarily defining ill-justified sub divisions of data.

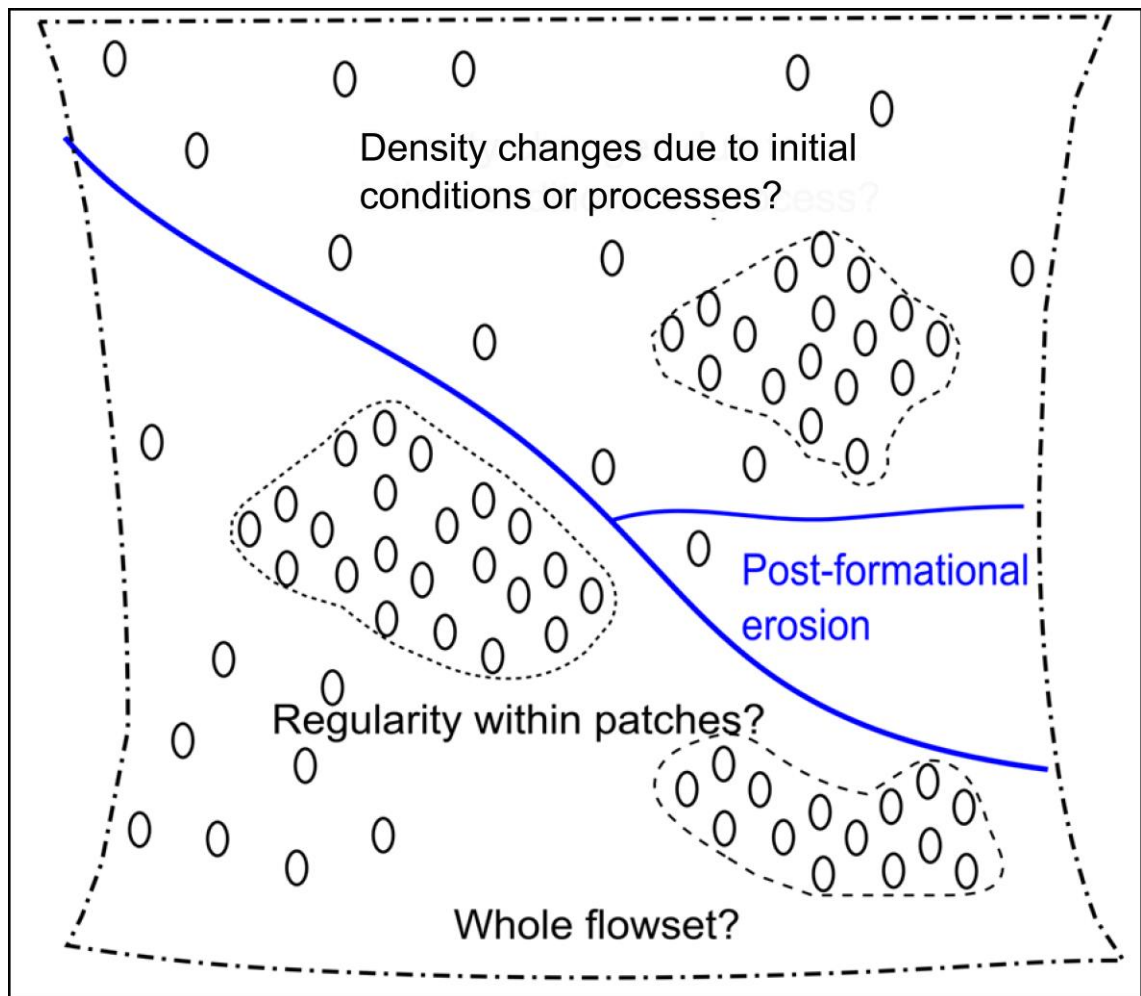


Figure 2.7. The problem of defining a study area or bounding box. The drumlin patterns we observe may have been influenced by post formational erosion. Additionally, the density of drumlins may be affected by initial conditions such as the availability of sediment. Delineating well preserved patches may be arbitrary, as may the definition of the whole flow-set bounding box. For either option, edge corrections are critical.

For inhomogeneous spatial statistics, the intensity of the point pattern must be calculated. The default intensity is calculated by the procedure outlined by Baddeley et al. (2000). Here, each point is iteratively removed from the pattern and its smoothed intensity is calculated through a density kernel estimator operation with an edge correction applied. The result of this ‘leave-one-out’ function is then gridded to provide a spatially variable intensity function. However, all such kernel based approaches to estimating density are sensitive to the selected kernel bandwidth (O’Sullivan and Unwin, 2010, p. 70). Sensitivity analysis of the inhomogeneous point pattern procedure to the intensity function was conducted upon flowset 29 (1,473 drumlins) by altering the default bandwidth by a fixed percentage per iteration. This flowset, located to the west

of Dumfries, Scotland, is likely deglacial in origin (Hughes et al., 2014) and was chosen due to the relatively high number of well-preserved drumlins.

Although each function has its own expectation under CSR, to determine if the magnitude of any departure from CSR is abnormally high or low, Monte Carlo simulations of CSR are often used to generate an envelope of CSR to compare to the observed function (O’Sullivan and Unwin, 2010, p. 148). Usually, such deviation is assessed visually. However, Myllymäki et al. (2013) proposed a method for assigning statistical significance to the confidence envelope. Their technique produces conservative and optimistic  $p$ -values for rejecting the null-hypothesis of randomness (CSR).

In the absence of a single clear test for spatial regularity, many have advocated the approach of comparing the output for multiple tests (e.g. Ripley, 1981; Diggle, 2003; Perry et al., 2006). Here, each flowset was bounded by a Ripley-Rasson estimator of the bounding box. This is a convex hull (the smallest convex set that contains the points) enlarged by a factor dependent upon the number of points within the study area designed to minimise edge-effects (Ripley and Rasson, 1977). The Clark and Evans (1954) statistic for each flowset was calculated with edge corrections implemented through the use of a buffer region. The functions  $L(r)$ ,  $g(r)$ ,  $L_{inhom}(r)$  and  $g_{inhom}(r)$  were also performed on each flowset. For the inhomogeneous functions ( $L_{inhom}(r)$  and  $g_{inhom}(r)$ ) sensitivity analysis of the density estimation was also conducted upon flowset 29, chosen due to its high level of preservation, and numerous drumlins. Each function was compared to 499 simulations of CSR, yielding  $p$ -values when using the technique of Myllymäki et al. (2013). Deviations from CSR, the scale at which this occurred, and the  $p$ -values obtained were recorded. The statistical software ‘R’ was used in data preparation and to perform these analyses, using functions available in the libraries ‘spatstat’ (Baddeley et al., 2005) and ‘spptest’ (Myllymäki et al., 2013). Figure 2.8 highlights how the functions differ and provides a framework for interpreting the output.

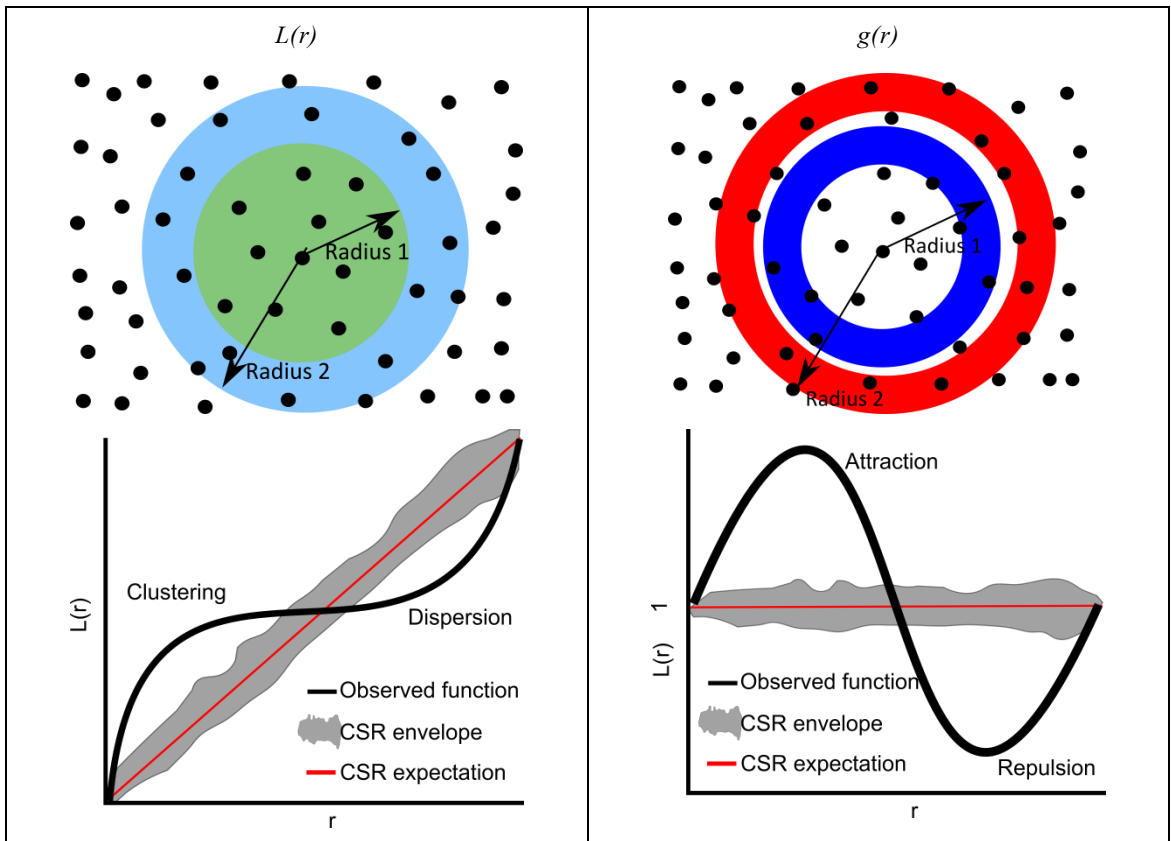


Figure 2.8. Summary of the Ripley K function and pair correlation function procedures. Top image shows the difference between the search regions. All points within a colour are measured per test. Upper left: For  $L(r)$ , as the search radius increases, so does the number of points measured. Upper right: For  $g(r)$ , the search radius forms a ring or doughnut shape. Bottom images show interpretation of theoretical outputs from spatstat tests. Lower left: Output from  $L(r)$  procedure. CSR envelope is derived from Monte Carlo simulations of CSR. When the observed line is within this envelope the point pattern is under CSR. Below this envelope there is dispersion of points, and above points are clustered for the value of  $r$ . Lower right: Output from the  $g(r)$  procedure. Envelope of CSR again derived from Monte Carlo simulations of CSR. Below the envelope there are fewer points than expected by CSR, hence point repulsion has occurred. Above the envelope there is an attraction of points to this scale, i.e. there are more points than expected under CSR. In this example there is a strong preference for regularity at the smaller scale, with few points occurring larger distances apart.

In summary, unlike previous analyses of the spatial positioning of drumlins within a flowset, I deploy a robust portfolio of techniques, accounting for issues such as edge corrections and bounding box estimates, without reliance upon a single technique. Furthermore, the analyses are performed on a large sample of drumlins, with a high level of mapping identification. These should illuminate the presence or absence of spatial regularity of drumlins, a key component in identifying patterning.

## 2.4.2 Results: Spatial statistics

Figure 2.9 shows the frequency of Clark and Evans ( $R$ ) values for all tested drumlin flowsets. The  $R$  values for all but one flowset are less than  $R = 1$ , which indicates a clustered pattern. The lowest  $R$  value is 0.15 (3 s.f.), and the mean  $R$  value for all flowsets is 0.65. The maximum  $R$  value is only just over the threshold value of 1 ( $R = 1.01$ ). Thus, the  $R$  values indicate clustering of drumlins for all tested flowsets.

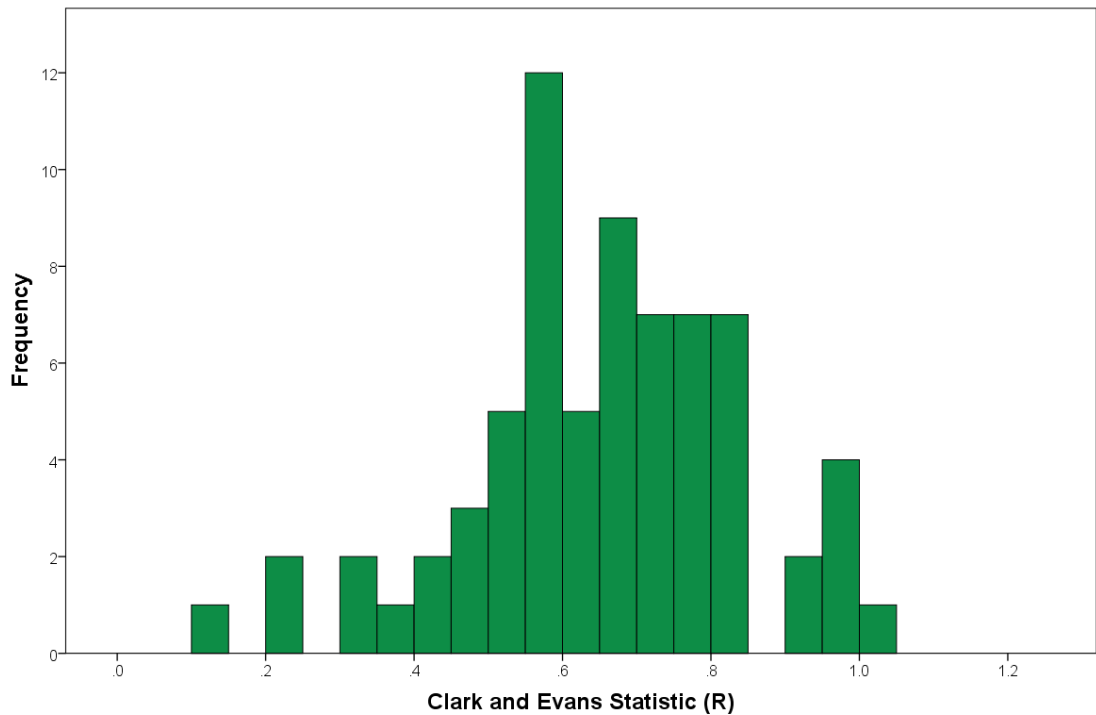


Figure 2.9. Histogram of Clark and Evans statistic value for British drumlin flowsets. A value of 0 would equal perfect clustering, 1 equals randomly placed and a value of 2.1491 would indicate regular.

Figure 2.10B shows typical output of the Ripley L homogeneous test ( $L(r)$ ). Here, the observed function deviates from CSR toward dispersion of points at small values of  $r$ . Figure 2.10C further highlights this initial dispersion (regularity) of points. However, after  $r \approx 200$  m, the observed  $L(r)$  crosses into the CSR envelope, and thereafter the observed  $L(r)$  plots to indicate a clustered pattern. Of the 72 flowsets studied, 38 showed qualitatively similar results (53%), whereby the observed  $L(r)$  initially displays dispersion of points, but then a clustering signal predominates. Also observed were flowsets where only clustering was initially indicated ( $n = 16$ ). However, by altering the smoothing kernel estimation of the function, initial dispersion of points was found for all of these additional flowsets. Rarely ( $n = 8$ ), the observed function plotted within the CSR envelope at all values of  $r$ , indicating a randomly placed pattern.



Figure 2.11B shows a typical output of the pair correlation function ( $g(r)$ ) test. Initially, the observed function plots below CSR envelope, indicating repulsion (less points at this distance) of points until  $r \approx 300$  m. The observed  $g(r)$  then passes through the CSR envelope, peaking at  $r \approx 900$  m in the ‘attraction’ section of the graph. The observed  $g(r)$  then decays into the CSR envelope, indicating attraction of points up to  $r \approx 4000$  m, beyond which it is contained within the CSR envelope. 57 flowsets (79%) showed qualitatively similar results to this (e.g. Figure 2.11B). However, the scale at which the observed function passes the envelope differed between flowsets. Only 9 flowsets, remained within the CSR envelope after initial point dispersion. Others display an initial attraction peak, found later to be a function of the smoothing operations in R. This is similar to the initial dispersion which was initially not revealed for  $L(r)$  (e.g. Figure 2.10C).

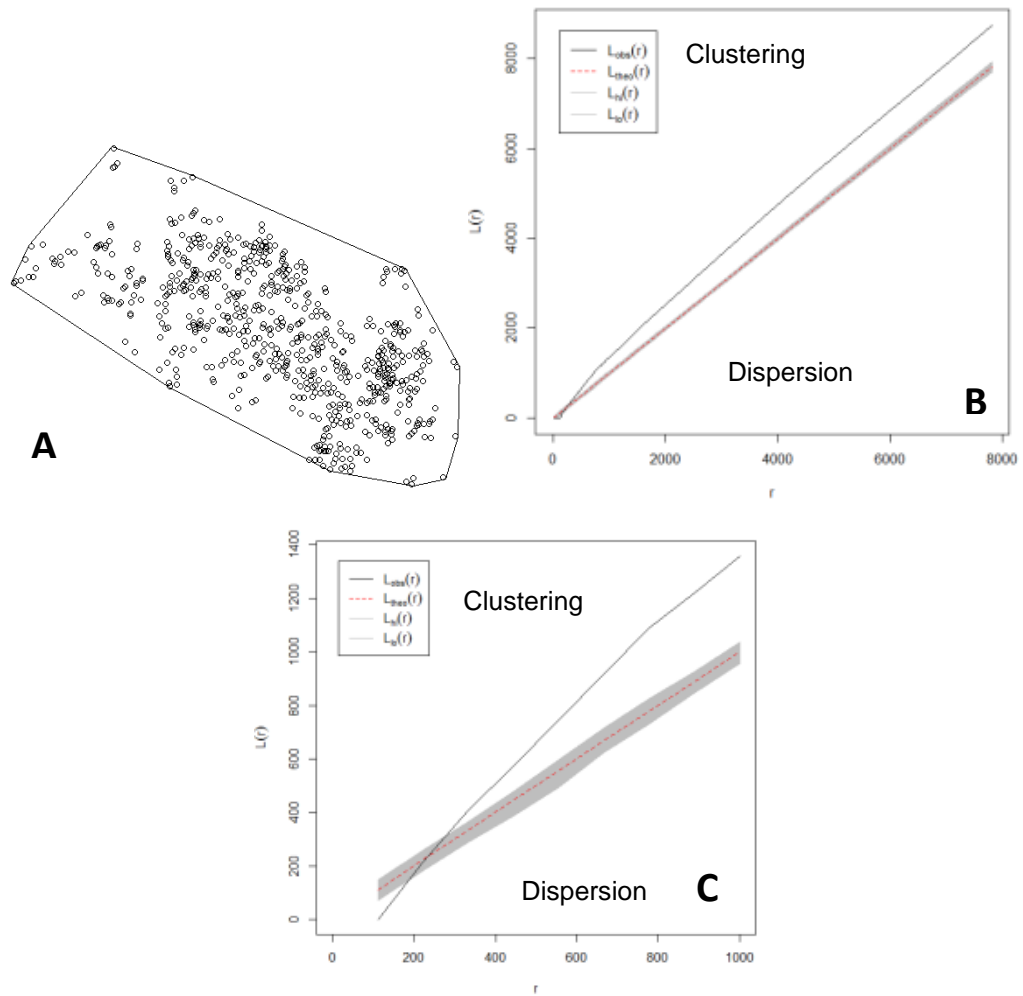


Figure 2.10. Typical output from the  $L(r)$  test. A) Point pattern of flowset 14, approximately 44 km across by 17 km wide. B) Output of the  $L(r)$  function. Deviation from the envelope is at least significant at  $p = 0.05$ , and at most  $p = 0.002$ . C) Output limited to the first 1000 m. Where the observed black line lies above the envelope, this indicates clustering of points. Where the observed black line lies below the envelope this indicated dispersion (regularity) of points.

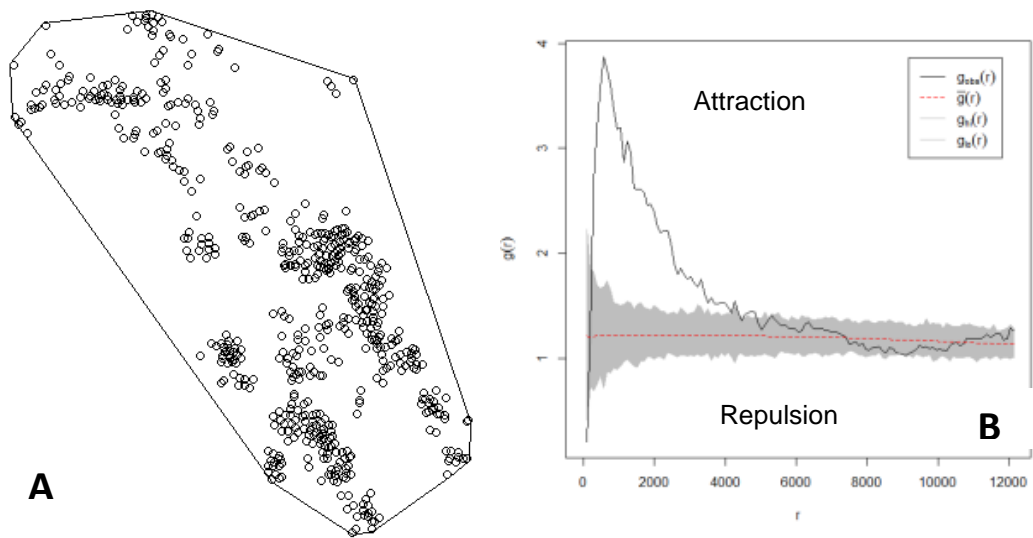
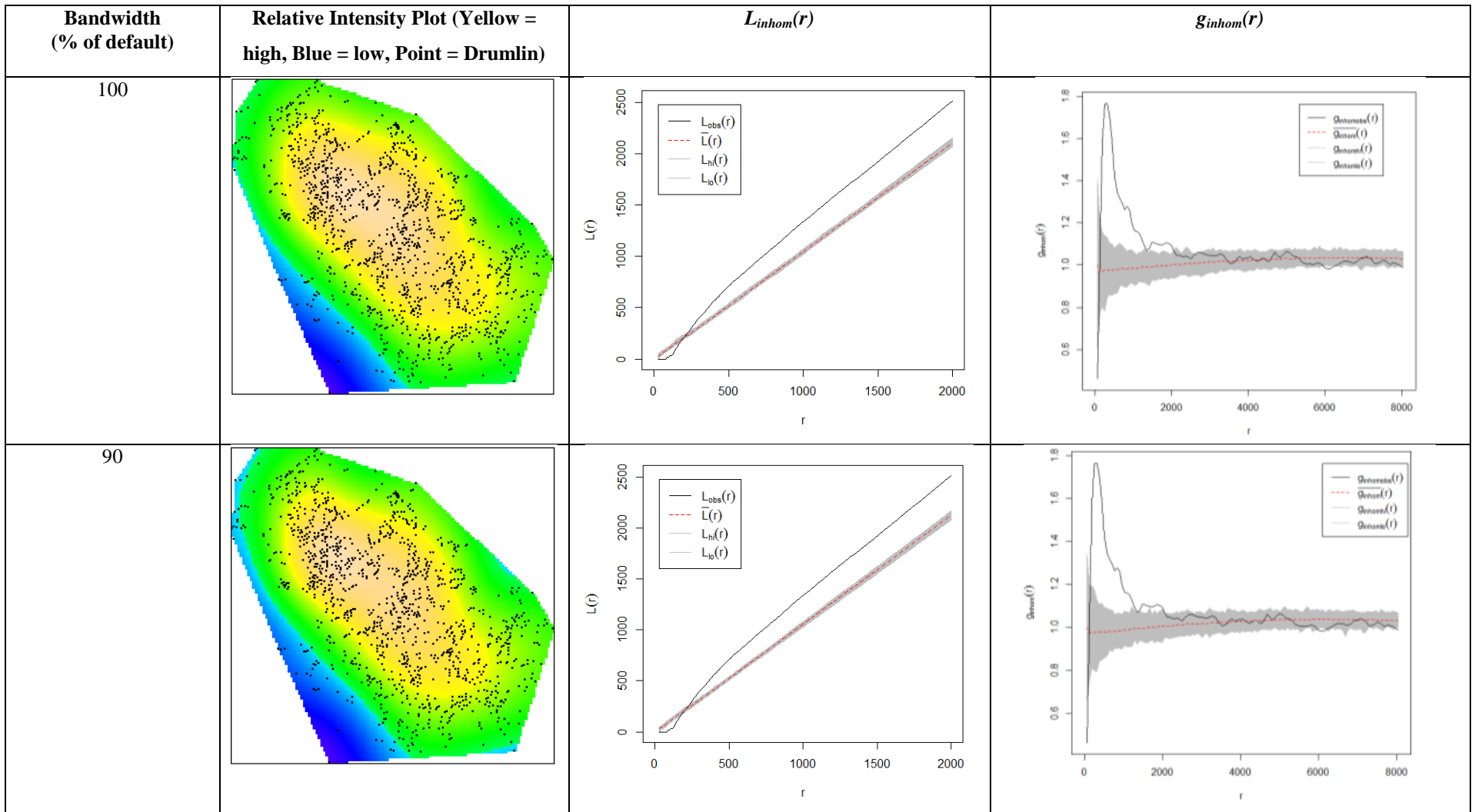
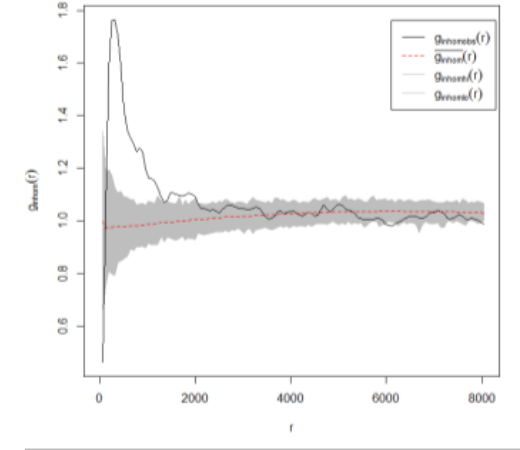
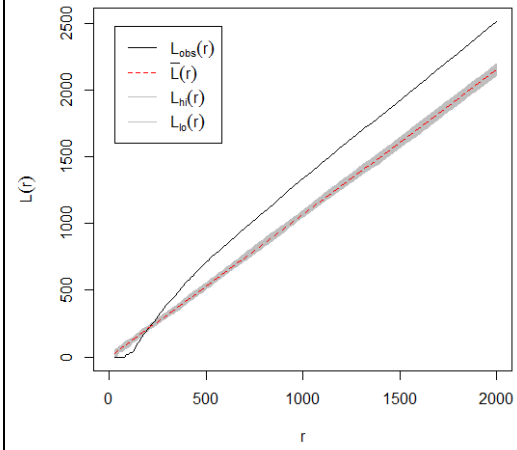
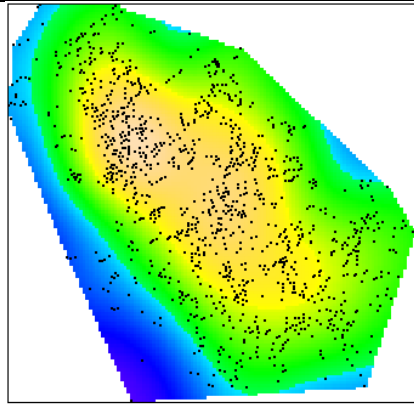


Figure 2.11. Typical output of the  $g(r)$  test. A) Point pattern of flowset 20, approximately 63 km long by 21 km wide. B) The function  $g(r)$  plotted against 499 simulations of CSR. Deviation from the envelope is at least significant at  $p = 0.116$ , and at most  $p = 0.001$ .

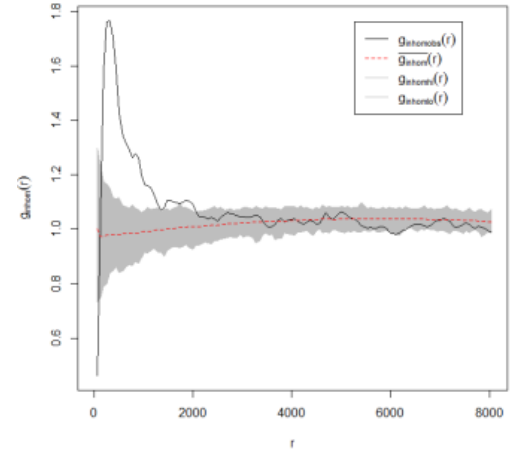
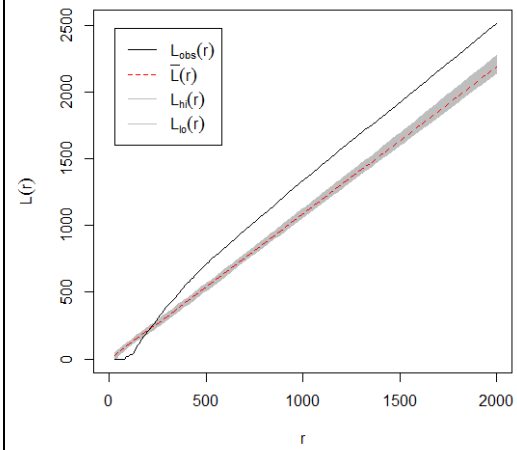
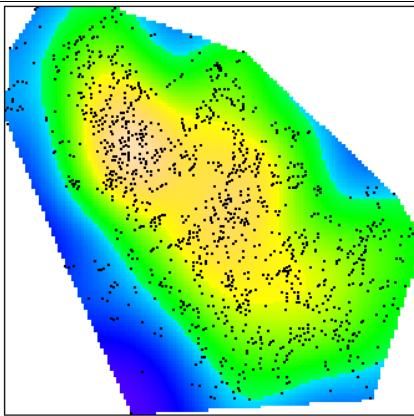
Table 3 plots the results of sensitivity analysis of the bandwidth of the intensity (density) estimator for the inhomogeneous versions of the Ripley L function ( $L_{inhom}(r)$ ) and the pair correlation function ( $g_{inhom}(r)$ ). For the default value, the intensity of points across the flowset is smooth, increasing away from the edges of the flowset due to edge corrections. Therefore, this estimates the point pattern intensity to be near homogenous across the flowset, producing results similar to Figures 2.10 and 2.11. Smaller scale repulsion of points and then a more predominant clustering signal occurs for  $L_{inhom}(r)$  (Table 3, column 3), and small scale dispersion, a peak in attraction (regularity) at  $r \approx 400$  m, and a decay to CSR occurs for  $g_{inhom}(r)$  (Table 3, column 4). As the magnitude of intensity function decreases, clusters within the data become apparent (Table 3, column 2). The results for both functions remain similar, between 20% and 100% of the default value. However, further reduction to 10% shows that drumlins are CSR after initial dispersion for  $L_{inhom}(r)$ , and the peak in attraction values for  $g_{inhom}(r)$  does not escape the CSR envelope. At 5% of the default value, clustering is not detected by  $L_{inhom}(r)$ , and the peak in attraction does not occur above CSR for  $g_{inhom}(r)$ . However, at 5% of the default bandwidth intensity, the intensity map is such that often only a single drumlin or pair of drumlins is within a single intensity cluster. For all other flowsets, a similar pattern of an initial smoothing across the flowset with an increasing clustering at 10% is apparent. Thus, all flowsets were tested at 20% of the default intensity estimate.



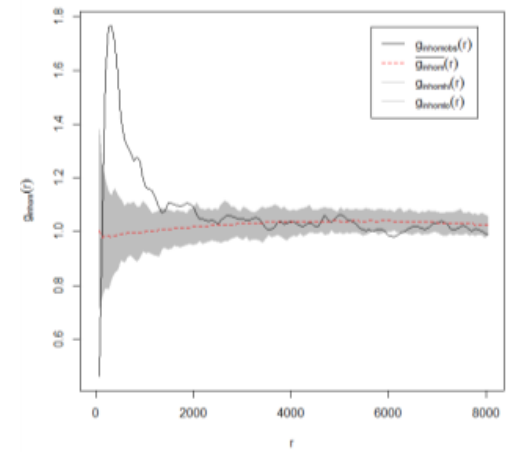
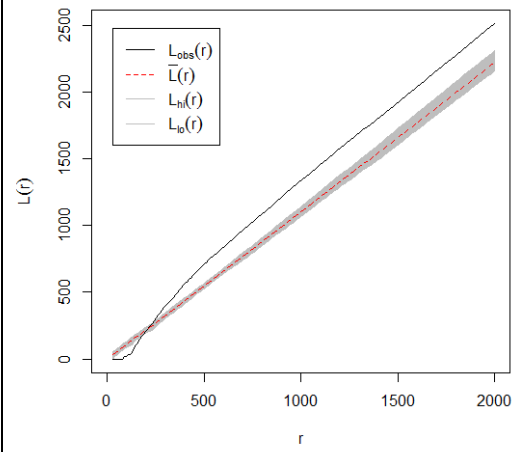
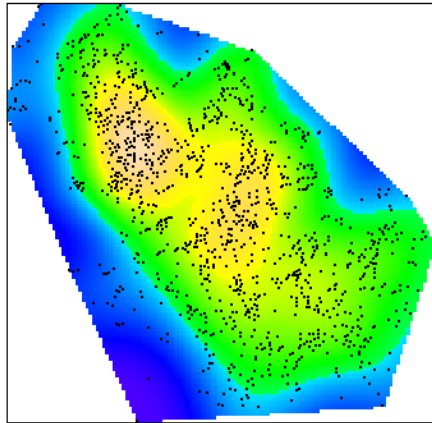
80



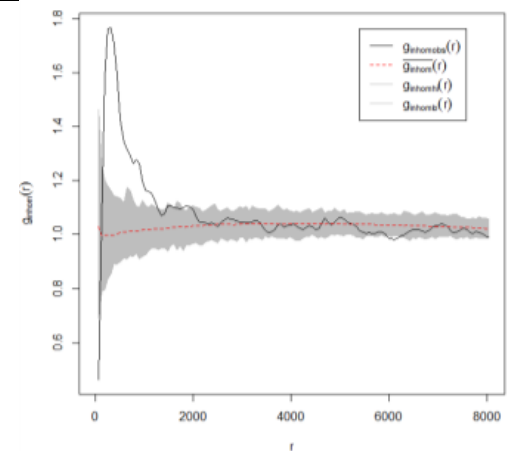
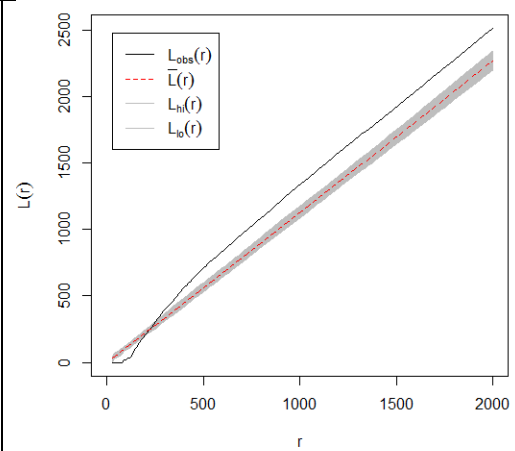
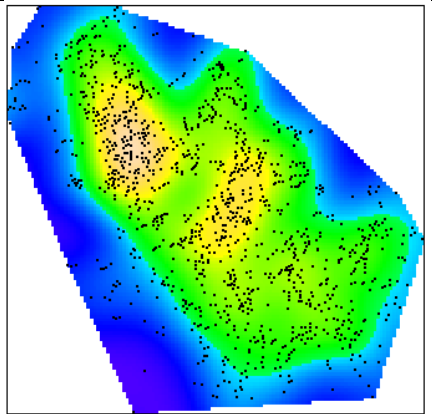
70



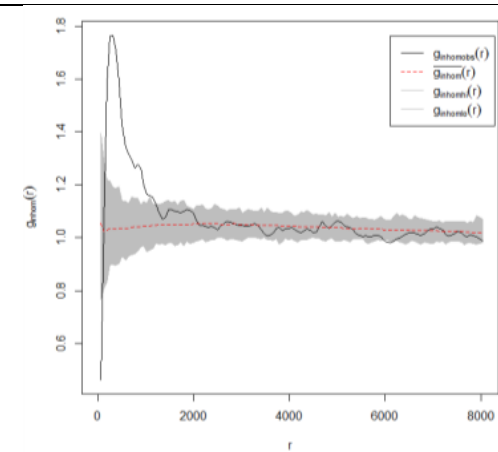
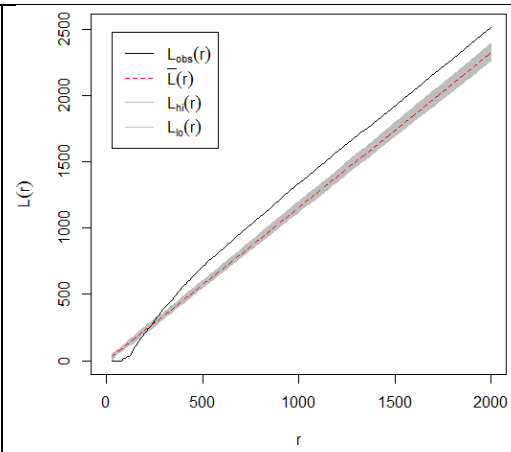
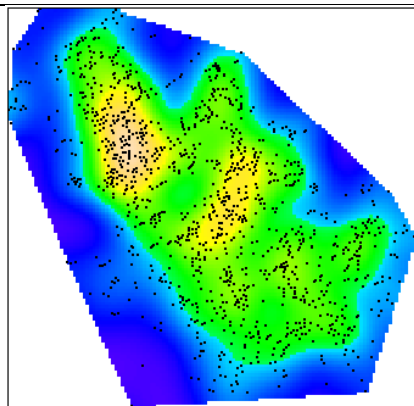
60



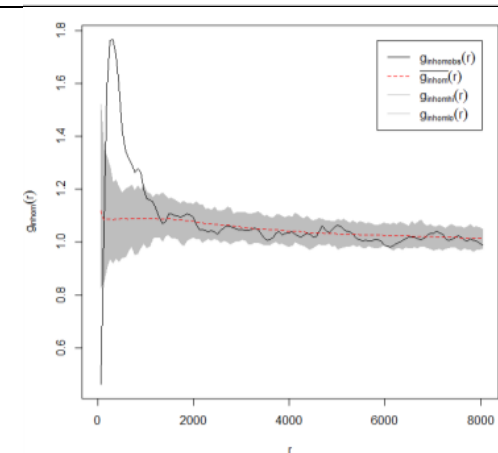
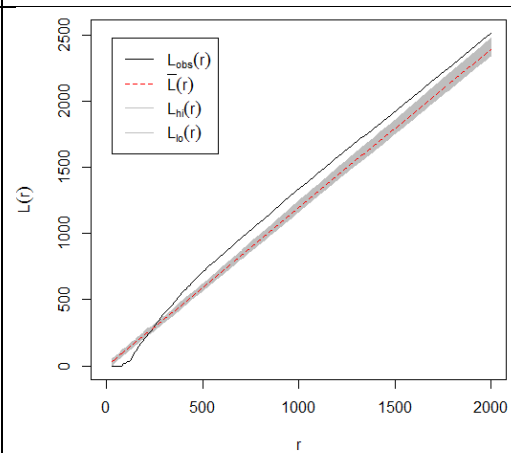
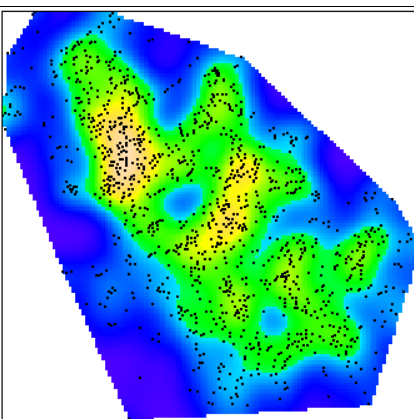
50



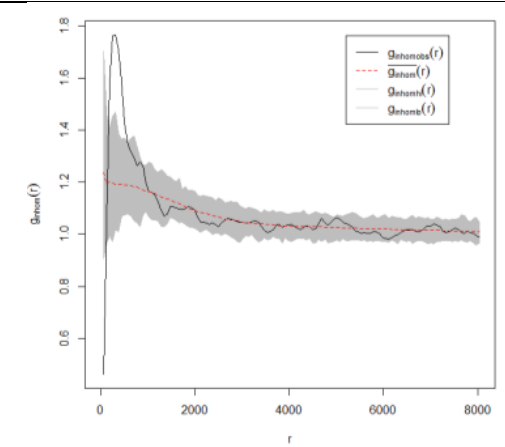
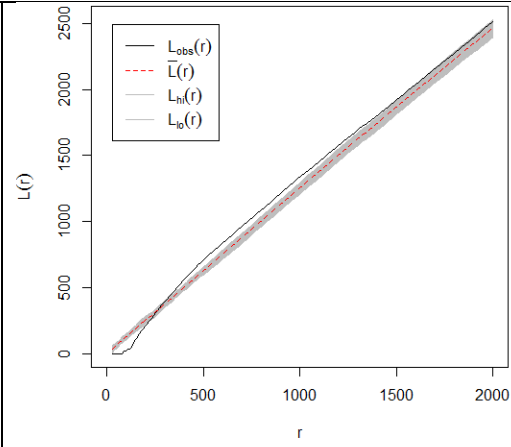
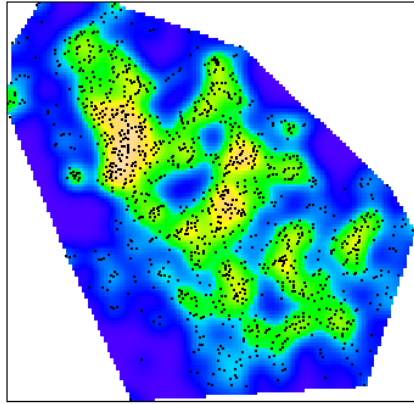
40



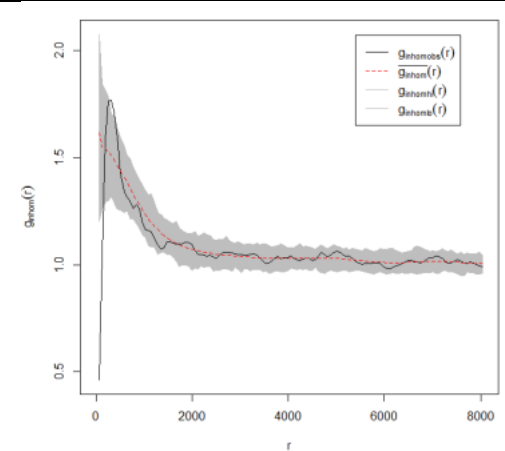
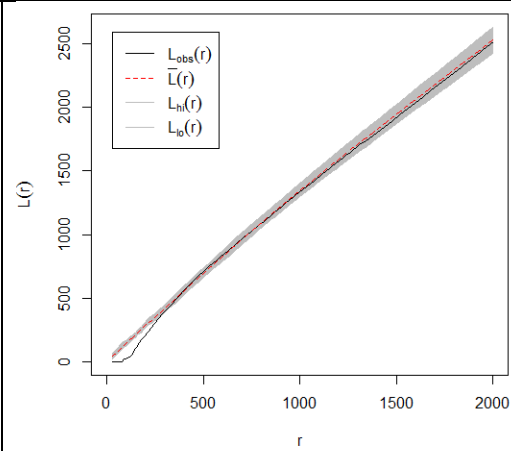
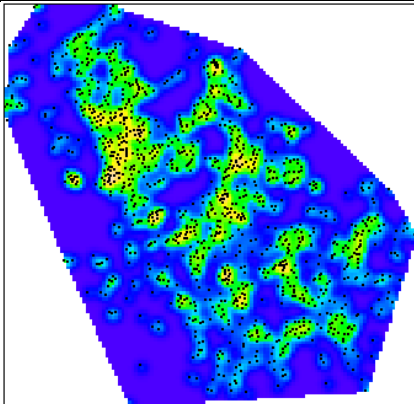
30



20



10





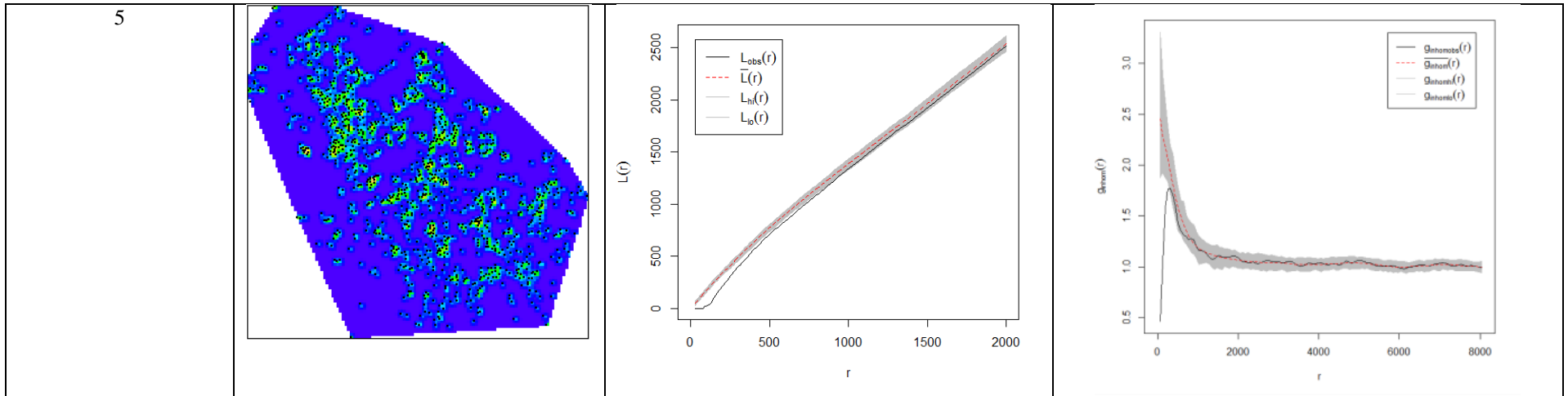


Table 3. Sensitivity analysis results of the functions  $L_{inhom}(r)$  and  $g_{inhom}(r)$  to different intensity search radii. Envelopes are significant to at least  $p = 0.044$ , and at most  $p = 0.002$ .

The flowset shown is flowset 29, which is approximately 42 km long by 23 km wide.

For the inhomogeneous Ripley K function test ( $L_{inhom}(r)$ ), 35 of the 72 flowsets studied displayed similar results to Table 3, column 3 whereby there was initial dispersion of points, indicating regularity up to this scale (typically 300-500 m), and then a signal of clustering. However, for many flowsets (32), only a signal of clustering was detected. By altering the smoothing estimator of the function, these all detected a small deviation from CSR into repulsion at small values of  $R$  ( $\approx 50$ -100m). The remaining 5 flowsets did not deviate from CSR, but tended to contain small numbers of drumlins.

The majority of flowsets studied (74%) displayed a  $g_{inhom}(r)$  function similar to that in Table 3, column 4. These are graphically plotted on Figure 2.12. The shape of this function is indicative of regularity, as it shows inhibition of points at small scales (i.e. points do not occur in close proximity), and then the attraction peak demonstrates that more points than would occur under CSR occur at a specific distance. For each flowset, the occurrence or absence of an attraction peak, and its location with respect to  $r$ , was recorded. As was the location where this peak decayed to randomness and the occurrence of any initial inhibition of points. Many flowsets (26) did not exhibit regularity, instead displaying CSR at most scales. However, these tend to be flowsets which contain fewer drumlins (Figure 2.13), meaning that any signal of regularity is harder to detect. This is especially true for inhomogeneous tests, where the sample is effectively subdivided by the observed density function. Drumlin flowsets which display regularity have a mean number of drumlins of 990, whilst the random flowsets have a mean number of drumlins of 225.

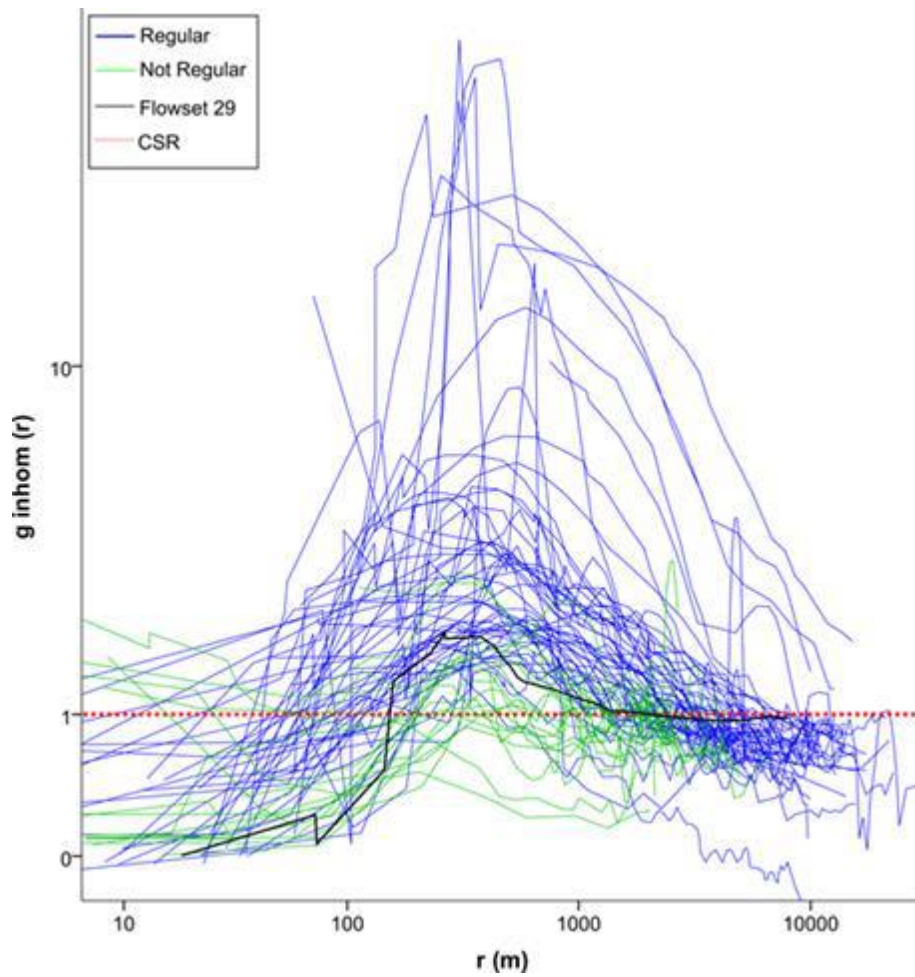


Figure 2.12. The inhomogeneous pair correlation function for all studied flowsets. This shows that the main signal is of regular positioning. The majority of flow sets (blue lines – 74%) are found to have a statistically significant demonstration of regularity, and represent 93% of the total drumlin sample. The green lines are for those flowsets that did not exhibit regularity (26% of the sample) approximating complete spatial randomness or clustering. The black line is for flow-set 29, where sensitivity analysis has been conducted, above.

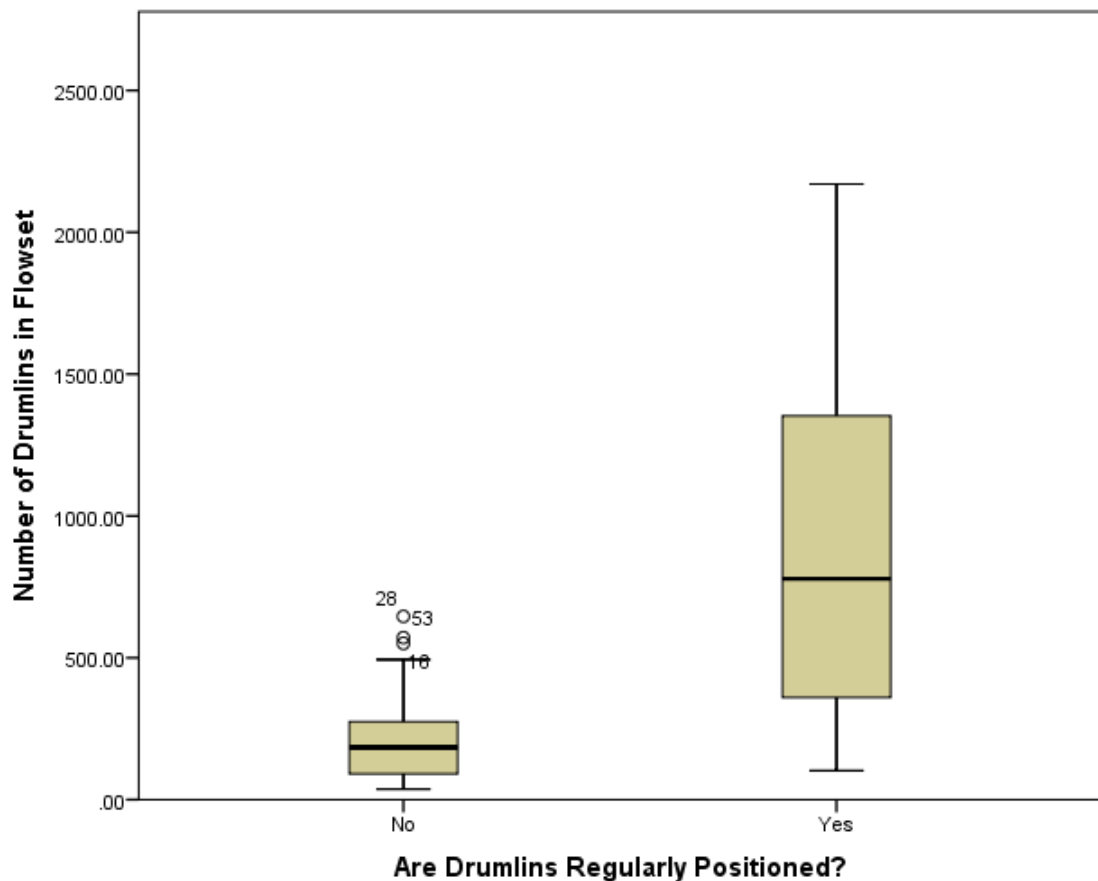


Figure 2.13. Comparative box plot of the number of drumlins within a flowset and whether the drumlins are regularly positioned or not. Note that those that are not regularly positioned tend to have a smaller number of drumlins.

### 2.4.3 Interpretation: Regular, Random or Clustered?

Depending on the test applied and whether the focus is on the number of drumlins or the number of flowsets, the outcome of the spatial statistics give conflicting results as to whether drumlins are positioned randomly, regularly or within clusters (Section 2.4.2). Hence, it is appropriate to distinguish between tests by asking which is most applicable for drumlins, providing the most information for how they form. If only the Clark and Evans (1954) statistic ( $R$ ) is considered, then the conclusion would be that drumlins are clustered within a field. However, as outlined in Figure 2.7, such clustering may be the consequence of pre-existing conditions or post formational modification. For palaeo-ice sheet beds the two are difficult to distinguish. For instance, a flowset may have originally been comprised of a regular and uniform drumlin field but later fluvial incision caused apparent clustering to occur. Conversely, these rivers may exploit topographic lows which are a consequence of drumlinisation, and thus the drumlin flowset we observe now was preconditioned to form clusters through the

drumlin forming process. Furthermore,  $R$  only considers the drumlin flowset as a whole, and not the scale at which this clustering occurs. It is therefore difficult to isolate relevant scales to other landscape features which might precondition clustering. Therefore, whilst  $R$  provides a useful first approximation of the flowset in general, and indeed as a first order observation drumlin flowsets are clustered, it contains little information for studying drumlin forming processes.

If we consider the likelihood of drumlin formation to be equal across a flowset, then results from the homogenous spatial statistical tests are applicable (Figures 2.10 and 2.11).  $L(r)$  generally shows small scale repulsion of points, but a predominately clustered signal, in agreement with the  $R$  statistic. This small scale repulsion may represent inevitable spatial inhibition (i.e. that drumlins possess an area and do not overlap). However,  $g(r)$  provides a different insight, showing that most drumlin flowsets actually have a preferred spacing (attraction), with small scale dispersion of points. This attraction peak has a mean value of 612 m, and this peak decays into the CSR envelop at a mean value of 2675 m. This shows that such an attraction peak exists beyond the mean size and spacing of drumlins (length = 629 m; width = 209 m; across flow spacing = 250 m; Clark et al., 2009; Spagnolo et al., in prep). For most localities, one would assume that drumlin formation and preservation is unlikely to be equal across a flowset. Therefore, the results from a homogenous statistical test are likely to be biased toward clustering. However, in well-preserved and flat areas, comparatively homogenous spatial statistical tests may be applicable. Additional analysis of a well preserved portion of the Leitrim drumlin field, Ireland, confirms this. As Figure 2.14 shows, both  $L(r)$  and  $g(r)$  have even greater typical deviations from CSR at this locality, and importantly the dispersion signal from  $L(r)$ , is much larger than the spacing of drumlins. Therefore, I interpret that this is not a product of just spatial inhibition, but a regularity of drumlin positioning. However, regions similar to Leitrim, which display homogeneous regularity, may either form or be preserved rarely. Research on pristine drumlin fields, perhaps imaged under contemporary ice sheets, is required to further elucidate the utility of homogenous spatial statistics on drumlins.

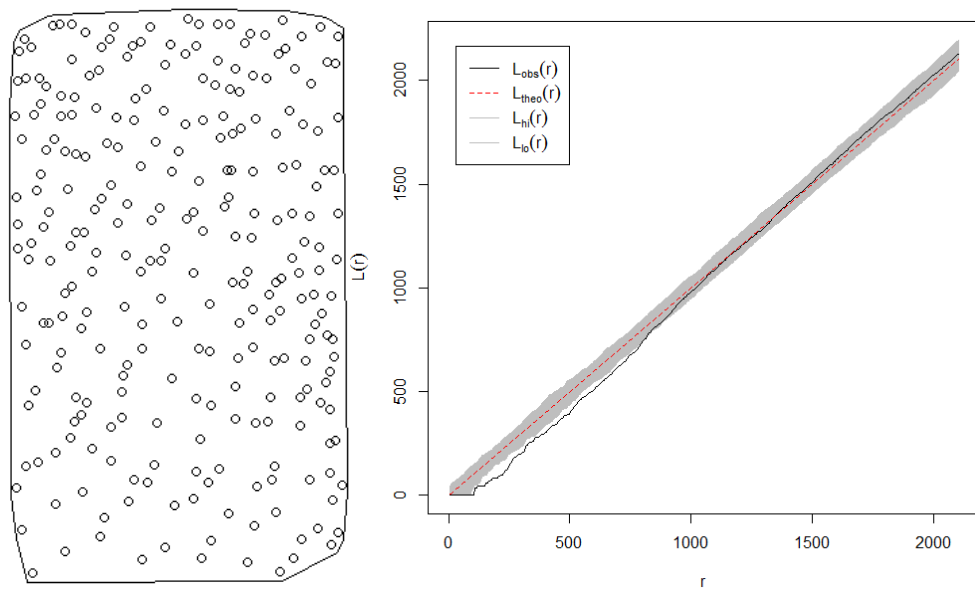


Figure 2.14. Left – Point pattern of the Leitrim drumlin field. Right – Results from the  $L(r)$  test, showing repulsion of points up to nearly 1000 m. Result is significant to at least  $p = 0.008$ , and at most  $p = 0.002$ .

When the inhomogeneous statistical tests,  $L(r)_{inhom}$  and  $g(r)_{inhom}$ , are conducted, there is little change in comparison to the homogenous counterparts. For the majority of drumlins there is small scale dispersion and larger scale clustering for  $L(r)_{inhom}$ , and small scale inhibition with a peak in attraction which decays to CSR for  $g(r)_{inhom}$ . Unless the bandwidth is so small that only the local area is considered (Table 6), or there are insufficient drumlins within a flowset (Figure 2.13). The small-scale dispersion of points detected by  $L(r)_{inhom}$  and the small-scale repulsion of points detected by  $g(r)_{inhom}$  could again be attributed to spatial inhibition. However, drumlins are rarely found touching each other within a flowset; the boundaries between drumlins outlines are typically 25 to 400 m apart (Spagnolo et al., in prep.). Drumlins can be thought of as either discrete “bumps” (blisters) or as continuous waveforms, whereby the edges of the drumlin represent post-glacial infill (Spagnolo et al., 2012; Figure 2.15). If drumlins are bumps, this indicates that not only do drumlins have a specific size at which they form, but they also prefer to be a set distance apart. Under the waveform interpretation, the non-random repulsion of points indicates that drumlins prefer to be a set-wavelength apart.

Figure 2.15. Drumlins as either discrete bumps (“blisters”) or as continuous waveforms. From Spagnolo et al. (2012). Drumlins can either be thought of as individual bumps on the landscape (A), or as continuous waveforms with sediment masking the flanks to give the appearance of individuals (B).

The attraction peak commonly found for the  $g(r)_{inhom}$  function, provides the strongest case for drumlins being regularly placed within a flowset. This shows that there are more drumlins at this peak distance than would be expected under CSR. For flowsets with less drumlins, this attraction peak is not apparent, this is likely the result of a sample size issue, as not enough drumlins are present compared to the number of simulations of CSR, and drumlins are further subdivided within a flowset according to clustering. Consequently, I recommend a minimum sample of at least approximately 300 drumlins for future work. The mean value of  $r$  that this peak occurs at is  $\approx 600$  m, and the attraction signal continues to an average value of  $\approx 1750$  m, indicating a regularity of points greater than the scale of drumlin size. The results are similar to that found for a Matérn hard-core point process, whereby a point pattern is “thinned” so that points must be a minimum distance apart (Stoyan and Stoyan, 1985; Hahn, pers. comm. 2013; Figure 2.16). Furthermore, Figure 2.17 demonstrates the results of applying  $g(r)_{inhom}$  to a regular grid of points with clusters artificially created. The results (Figure 2.17C) are similar to that found for most drumlins (Section 2.4.2; Table 3; Figure 2.12). Therefore, I can interpret the results of  $g(r)_{inhom}$  as indicating that drumlins prefer to be a non-random distance apart, which is independent of drumlin size. The clustering signal detected by  $L(r)_{inhom}$  is likely a function of its cumulative nature, meaning it cannot determine the scale at which dispersion of points continues to (Condit et al., 2000;

Wiegand and Moloney, 2004), and therefore provides us with less information about drumlin formation.

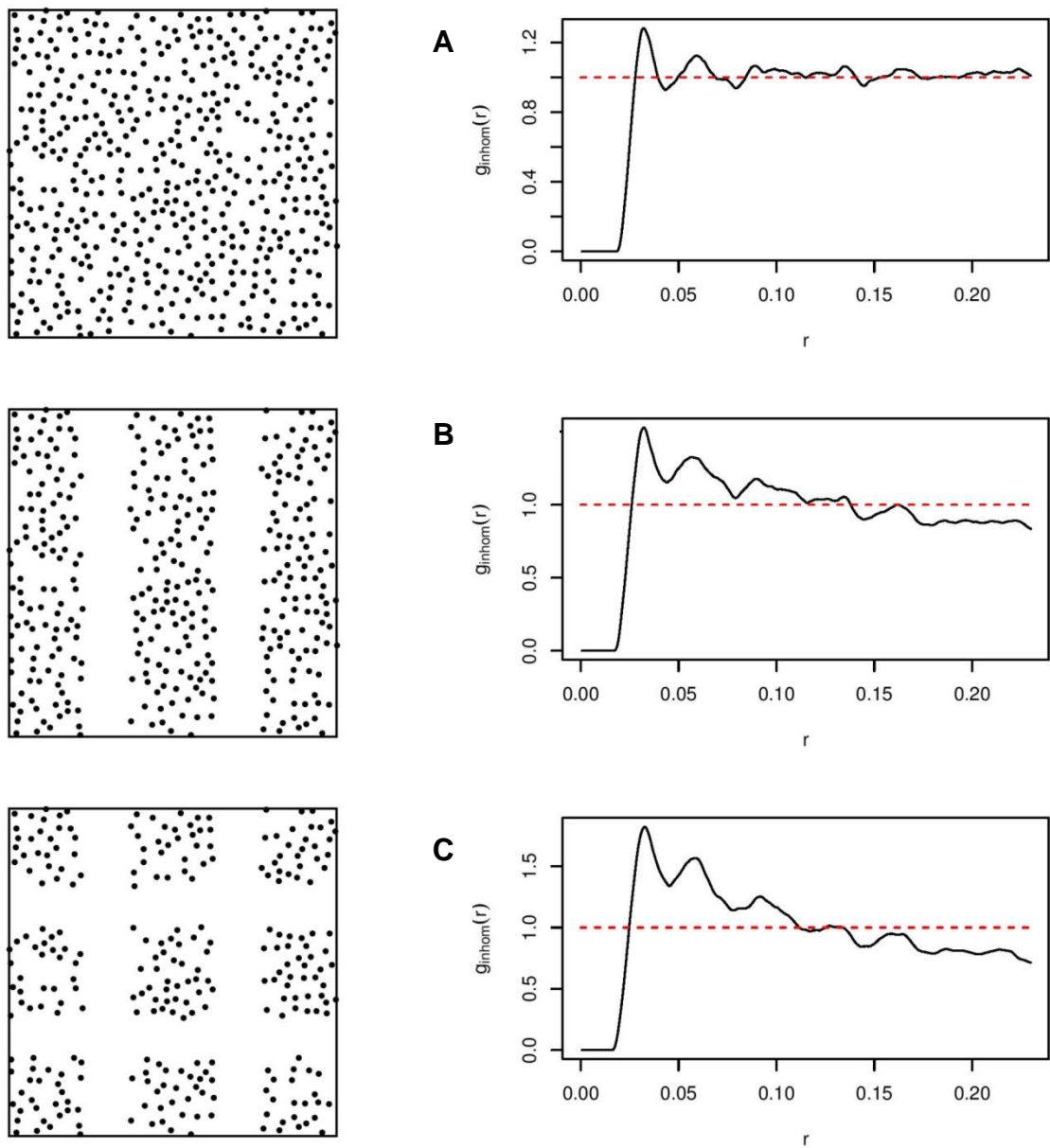


Figure 2.16. Results of  $L(r)_{inhom}$  compared to a Matérn hard-core point process. A) Original point pattern. B) and C) artificially induced clustering. Note the peak in attraction and similarity to results in Table 6. Figure from Hahn (pers. comm.). This denotes that points both here and in my drumlin tests are regularly positioned.



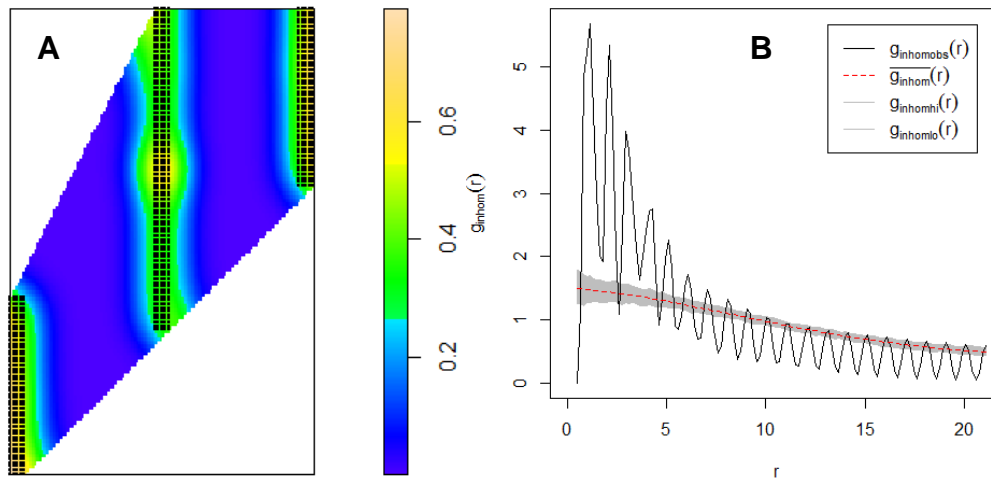


Figure 2.17. Results of the inhomogeneous pair correlation function applied to a regular grid of points which has been artificially clustered. A) Artificially clustered points (black dots) and the intensity function of these points (colour scale). B) Results of  $g_{\text{inhom}}$  test. Note the small scale inhibition and then attraction peak. Harmonics of this peak are then repeated throughout the graph. This is significant to at most  $p = 0.002$  and at least  $p = 0.144$ . The result is similar to that found for most drumlins.

Overall, as a first order observation is clear that drumlins are clustered within a flowset. However, it is difficult to distinguish whether this clustering is a consequence of drumlin forming processes, pre-formational conditions or post-formational modification. This clustering means that inhomogeneous spatial statistics are required for the study of drumlins. Previous studies on drumlins did not consider this, and wrongly concluded that drumlins were either clustered or random within a flowset. Therefore, the results from the  $g_{\text{inhom}}$  are the most applicable to our problem, and suggest that most drumlins are placed a non-random distance apart within a flowset.

As a key component of a pattern is the regularity of its components, the regular positioning of drumlins found here could be considered to be a consequence of a pattern forming process. Alternatively, the spatial regularity of drumlins could be a consequence of preconditioning, perhaps by a regular array of initiating bedrock protuberances (e.g. Raukas and Tavast, 1994) or by regular differential shear properties of drumlinised sediment (e.g. Smalley and Piotrowski, 1987). Whilst such variations may account for individual drumlins (e.g. the drumlin clones of Clark, 2010), there is no evidence for the regularity of such underlying triggers within a flowset and across multiple flowsets. Hence, this specific drumlin view is rejected. Therefore, I interpret this regular positioning of drumlins within clusters as indicating that they can constitute a patterned phenomenon.

A caveat of the above approach and interpretation is that drumlins that lie outside clusters also require explanation. A possible interpretation is that the distribution of clustered and non-clustered drumlins is a product of the drumlinisation process itself. Perhaps drumlinisation partitions the ice-bed interface into regions of clustered and non-clustered bedforms. Although this cannot be ruled out, I find it unlikely that drumlinisation would act unequally (causing clusters) where there was a homogenous sediment supply, sediment properties and conditions at the ice-bed interface. If this was the case, no sedimentologically significant differences between clustered drumlins, isolated drumlins and intercluster regions would be expected. This interpretation also neglects any deglacial or post glacial erosion which may have formed clusters. Given that sediment availability is likely to be spatially concentrated prior to drumlin formation, and that drumlin preservation may erode an otherwise homogenous drumlin field into clusters, I favour the interpretation that these factors are the primary cause of the drumlin clustering (e.g. Figure 2.7). Given the regularity of drumlins within these clusters, I therefore retain the interpretation that drumlinisation is a pattern forming process. Some aspects of the above could be tested in future work by investigating whether isolated drumlins are anchored on bedrock forming clones (Clark, 2010), or occur on isolated patches of till. Alternatively, it may be the case that drumlins are initially regularly distributed, but secondary pattern interactions (e.g., migration, coarsening) may cause clustering (Section 2.5).

## **2.5 Secondary Patterning Interactions**

In the previous section (2.4), we saw that drumlins are regularly positioned within clusters across a flow set. This is taken to be an indication that a patterning process could have caused their formation, producing drumlins at a set distance apart. Therefore, it is apt to consider whether secondary patterning interactions have occurred during drumlin formation (i.e. coarsening, migration). We are yet to observe the formation and evolution of drumlins evolving *in situ* in enough detail to determine whether such interactions occur. However, the size and shape metrics of drumlins from palaeo-ice sheets, which represent the end-product of any such interactions, may be able to provide us with insight into whether patterning interactions have occurred.

### **2.5.1 Methods: Drumlin Size and Spacing Metrics**

Within each flow-set, the across and along flow spacing between each drumlin and its nearest neighbour was calculated using the technique of Stokes et al. (2013b)

developed by Spagnolo et al. (in prep). To calculate lateral spacing, the longest line within each drumlin polygon was created using the Geospatial Modelling Environment (GME; [www.spatialecology.com](http://www.spatialecology.com)) plugin ‘geom.polygonfetch’, and its azimuth was calculated. The azimuth of the 10 nearest drumlins, identified using the GME plugin ‘pointdistances’, was then used to calculate the local mean ice flow direction for each drumlin. Using the mean azimuth, Pythagorean Theorem was used to calculate the across-flow distance between each drumlin polygon centroid and its 10 nearest neighbours. The shortest distance between each pair of drumlins, that is not smaller than the sum of the two drumlins’ half widths, was used to identify the nearest drumlin centroid in an across flow direction. For the along-flow spacing of drumlins, the same approach is adopted, except the azimuth is rotated by 90 degrees, and the nearest neighbour cannot be at a distance lower than the sum of the two drumlins’ half lengths.

The length (L) and width (W) of each drumlin was estimated via Euler’s approximation for an ellipse (Clark et al., 2009), whereby:

$$L = \frac{1}{\pi} \sqrt{P^2 + \sqrt{P^4 - 16 \pi^2 A^2}} \quad \text{Eq.8}$$

$$W = \frac{1}{\pi} \sqrt{P^2 + \sqrt{P^4 - 16 \pi^2 A^2}} \quad \text{Eq.9}$$

where A is the area of a polygon, and P is its perimeter. Both A and P were calculated within ArcGIS. A limitation of this approximation is that it underestimates the length (and overestimates the width) of elongate or irregular polygons (Clark et al., 2009). The relief of each drumlin was calculated by Spagnolo et al. (2012).

Hillier et al. (2013) proposed that, as most distributions of metrics relating to subglacial bedforms conform to an exponential or log-normal distribution, the mode ( $\phi$ ) and the gradient of the distribution after the mode ( $\lambda$ ; Figure 2.18) are best suited to characterise the distributions of drumlin metrics. After Hillier et al. (2013), the mode ( $\phi$ ) was calculated using the method of moments, via the equation:

$$\phi = \frac{\left(\frac{\bar{x}}{s_x}\right)^2 - 1}{\left(\frac{\bar{x}}{(s_x)^2}\right)} \quad \text{Eq.10}$$

where  $\bar{x}$  is the mean of the distribution and  $s_x$  is the standard deviation of the data.  $\phi$  was then subtracted from each data value, and values below the modal value were then removed from the data, and the gradient ( $\lambda$ ) of the remaining data calculated using the equation:

$$\lambda = \frac{1}{\bar{k}} \quad \text{Eq.11}$$

where  $\bar{k}$  is the mean value of the remaining dataset (above the mode). A disadvantage of the  $\lambda$  metric is that it ignores all values below the mode (Fowler et al., 2013). Hence, here I also calculate  $\Lambda$ , the slope of the distribution before the mode, through the equation:

$$\Lambda = \frac{1}{\bar{K}} \quad \text{Eq.12}$$

where  $\bar{K}$  is the mean of the data less than  $\phi$  where each value has been subtracted by  $\phi$ . Thus,  $\phi$  describes an average value per flowset, and the parameters  $\lambda$  and  $\Lambda$  describe the shape of the probability distribution function of the flowset. These two metrics are illustrated in Figure 2.18. The  $\phi$  and  $\lambda$  of the across flow spacing, down flow spacing, length, width and relief of each were calculated for each flowset. Importantly,  $\lambda$  and  $\Lambda$  are independent of each other. However,  $\Lambda$  may be influenced by  $\phi$  as I am dealing with scalar variables.

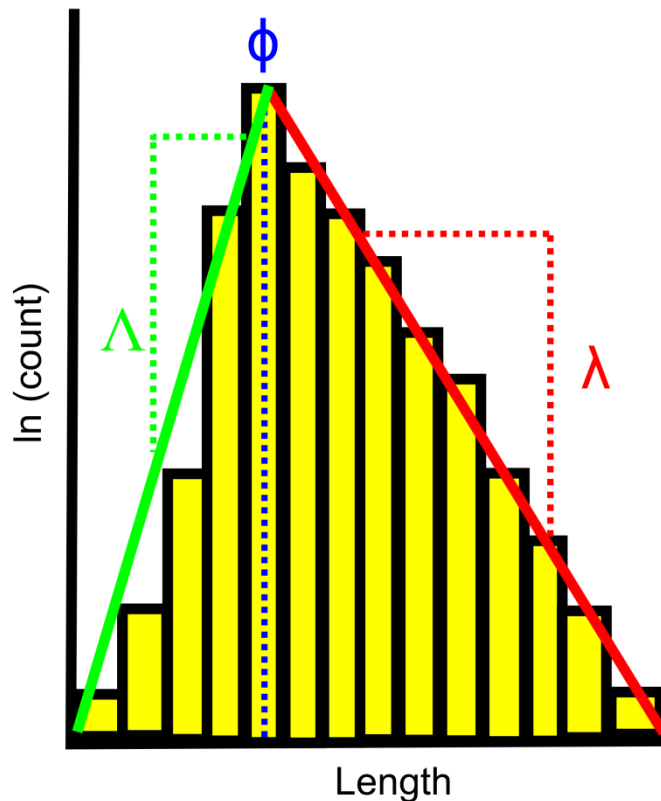


Figure 2.18. Illustration of  $\phi$ , the modal value of the distribution, and  $\lambda$ , the gradient of the tail of the distribution and  $\Lambda$ , the gradient of the distribution before the mode.

If the different patterning processes occur during drumlin flowset development, as outlined in Figure 2.2 and Section 2.2.1, one might expect the size and shape parameters to behave in the following ways:

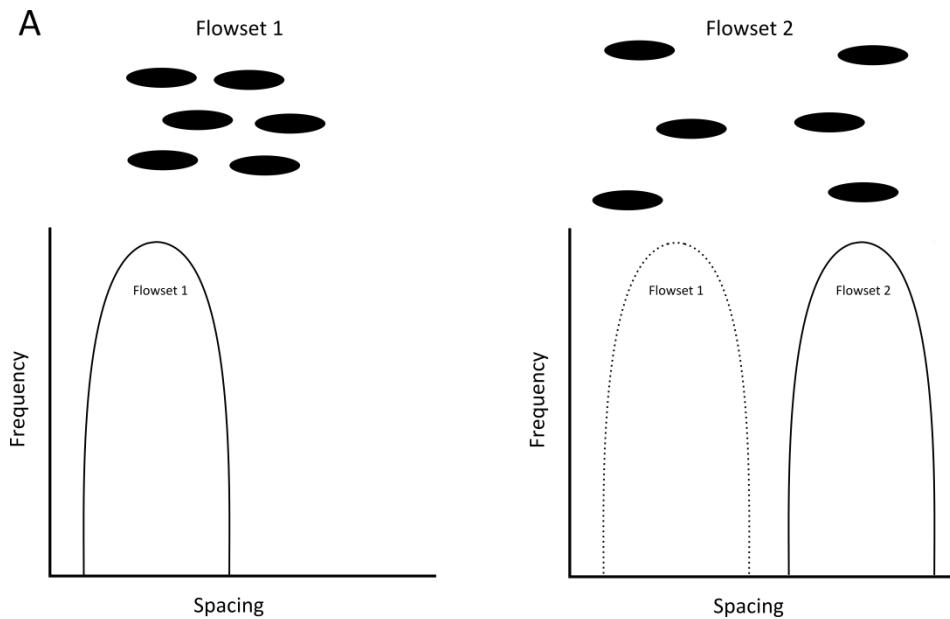


Figure 2.19A. Drumlins are printed at a different spacing in different localities due to local conditions at the ice bed interface. This would produce two different spacing populations.

- Drumlins are ‘printed’ at a certain size and distance apart, which changes according to glaciological and sedimentological conditions (e.g. variations of Figure 2.2A). Under this scenario, and assuming conditions across a flowset are sufficiently similar,  $\lambda$  and  $A$  would show little variability between flowsets but the  $\phi$  of spacing metrics would change across flowsets (Figure 2.19A).

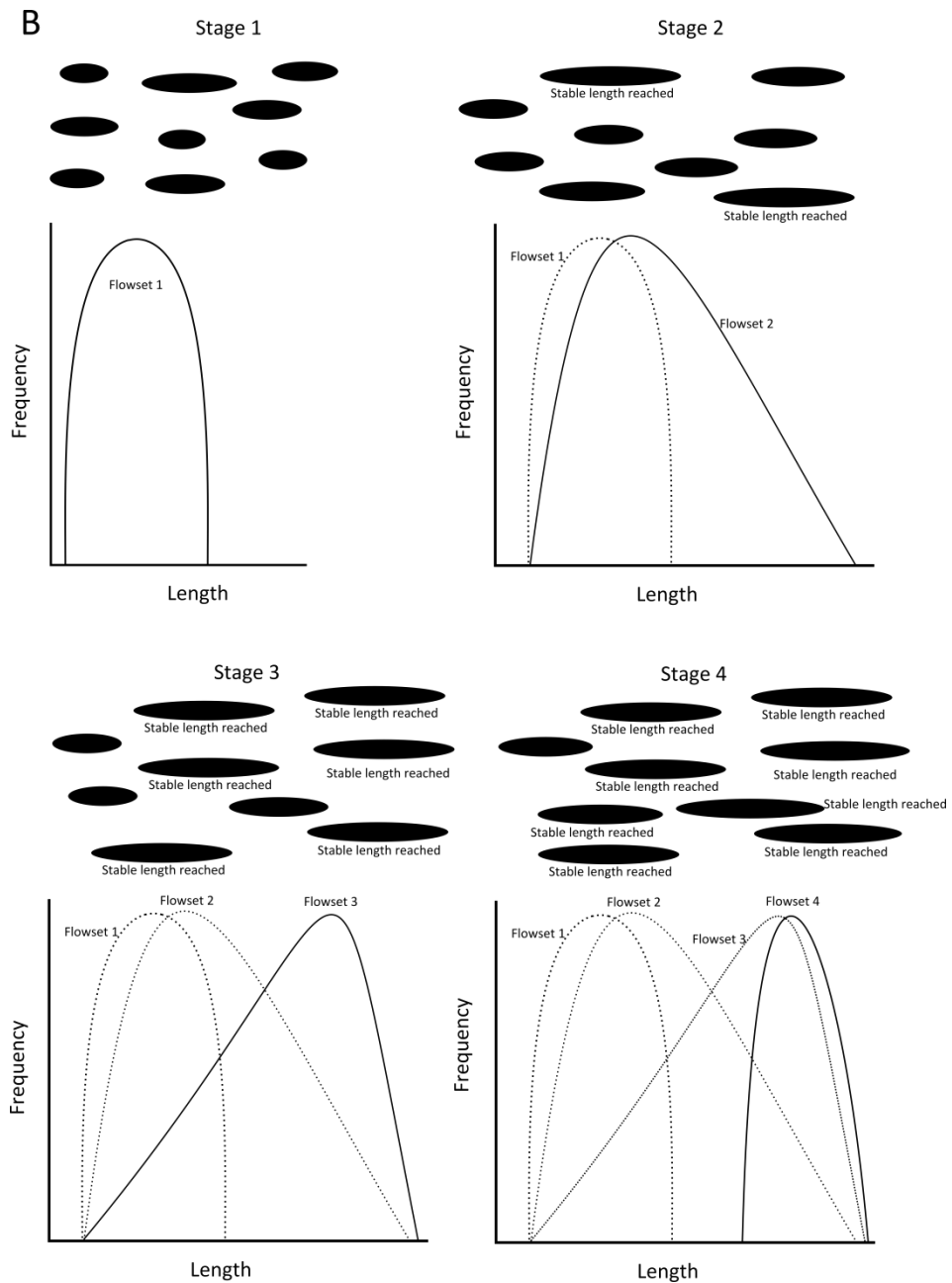


Figure 2.19B. Stabilisation of drumlin length. 1) Drumlins initiate at certain lengths. 2) Lengthwise growth of some individuals leads to an increase in the tail of the histogram. 3) Once a threshold is reached, drumlin growth stops, and the histogram tail steepens. 4) Eventually no drumlins can grow any longer.

- Drumlins are all formed at once, but grow in size through time. If simple stabilisation occurs (e.g. Figure 2.2B), then I may expect  $\lambda$  to rapidly increase beyond a threshold of that parameter, and  $\lambda$  to increase as more of the flowset reaches this threshold. For example, if drumlins grow longer over time, once a threshold of length is reached it may become harder for a drumlin to grow longer. Shorter forms would continue to grow, but growth rate of longer forms would decrease, increasing the value of  $\lambda$  for length, whilst  $\lambda$  remains comparatively small.  $\lambda$  will then increase as more short forms approach the stabilisation threshold, as the shorter forms will find it easier to grow (Figure 2.19B).

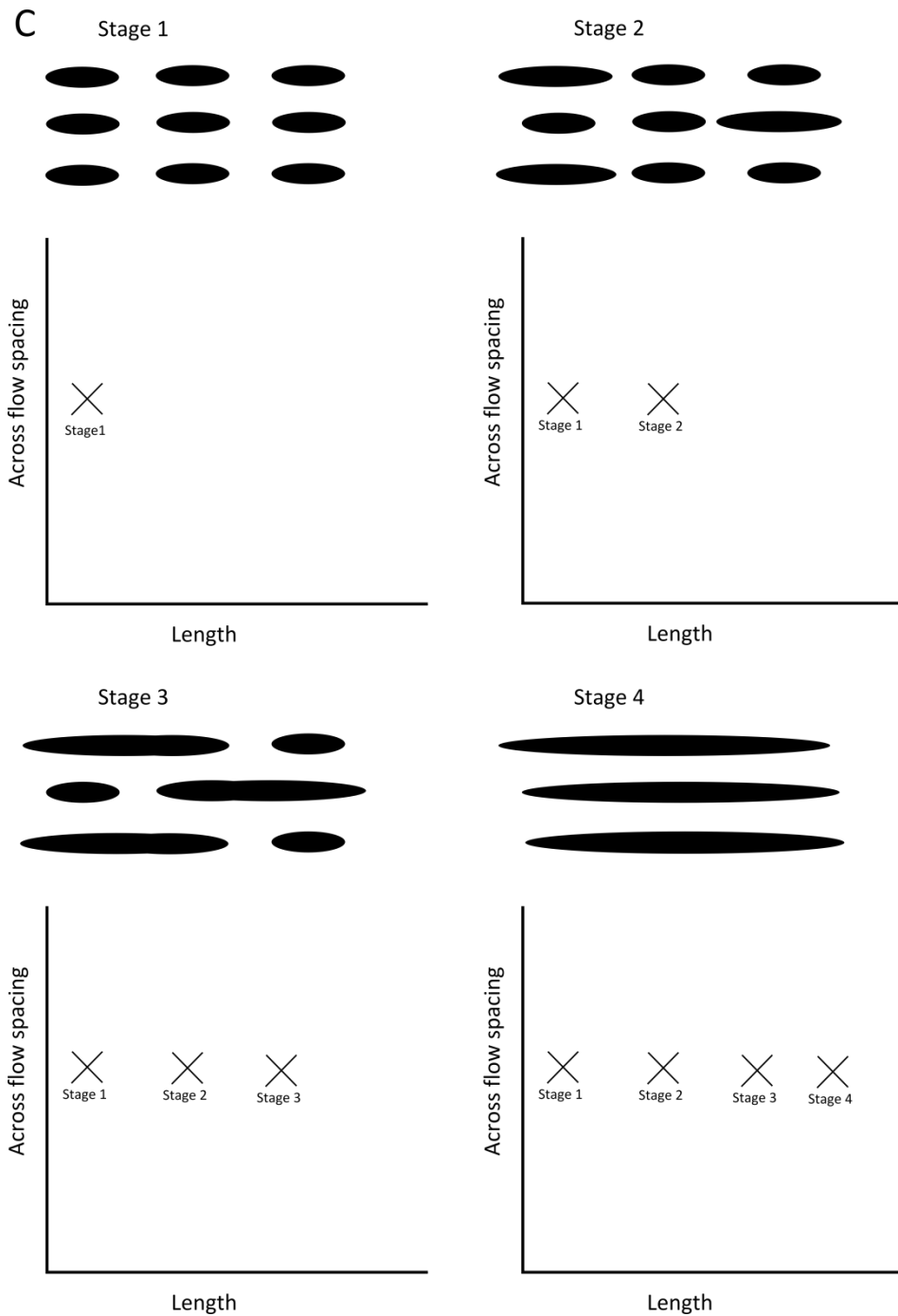


Figure 2.19C. Growth and coarsening without migration. 1) Drumlins printed at a set distance apart. 2) Drumlins begin to grow. 3) Collisions between drumlins as length increases leads to coarsening. 4) Drumlins eventually merge.

- If drumlins grow longer, but remain static (i.e. no migration occurs) then eventually collisions between drumlins would lead to coarsening. Assuming across flow spacing does not systematically change between flowsets, inter-flowset across flow spacing of drumlins would remain constant as the  $\phi$  value of length changes (Figure 2.19C).

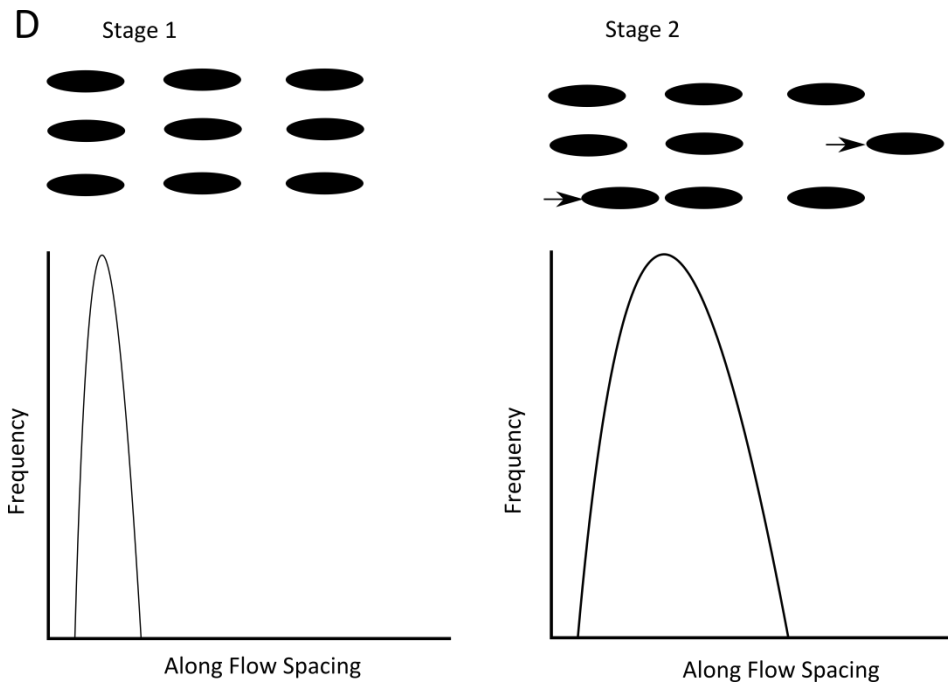


Figure 2.19D. Migration of drumlins leads to more variability in the spacing values.

- Migration of drumlins down-flow. The movement of drumlins would vary the spacing values of  $\lambda$  and  $\lambda$ . This is because a larger spread of distances between drumlins would occur as drumlins move further apart and closer together (Figure 2.19D). This would be the case unless drumlins migrate uniformly, which given a spread of sizes within a drumlin field may be unlikely.

### 2.5.2 Results: Drumlin Spacing and Size Metrics

The across-flow spacing of 30,641 drumlins and the along flow spacing of 19,210 drumlins across the 72 chosen flowsets of Britain were calculated. Figure 2.20 plots the across flow spacing of all measured drumlins per flowset. Overlap occurs between all flowset spacing measurements. However, an ANOVA test shows that there are significant differences between the means of many flowsets. The most extreme example is flowset 8, where the mean is significantly different to the mean of 69 other flowsets. Conversely, the mean flowset 38 is significantly different to only 25 flowsets. Figure 2.21 shows the down flow spacing of all measured drumlins per flowset. Again, overlap occurs between all flowset populations. ANOVA tests again reveal significant differences between the means of populations. Flowset 11 is the most distinguishable, as its mean is significantly different to the means of 69 other flowsets. The least distinguishable is flowset 40, with a mean significantly different to the mean of 28 other flowsets.



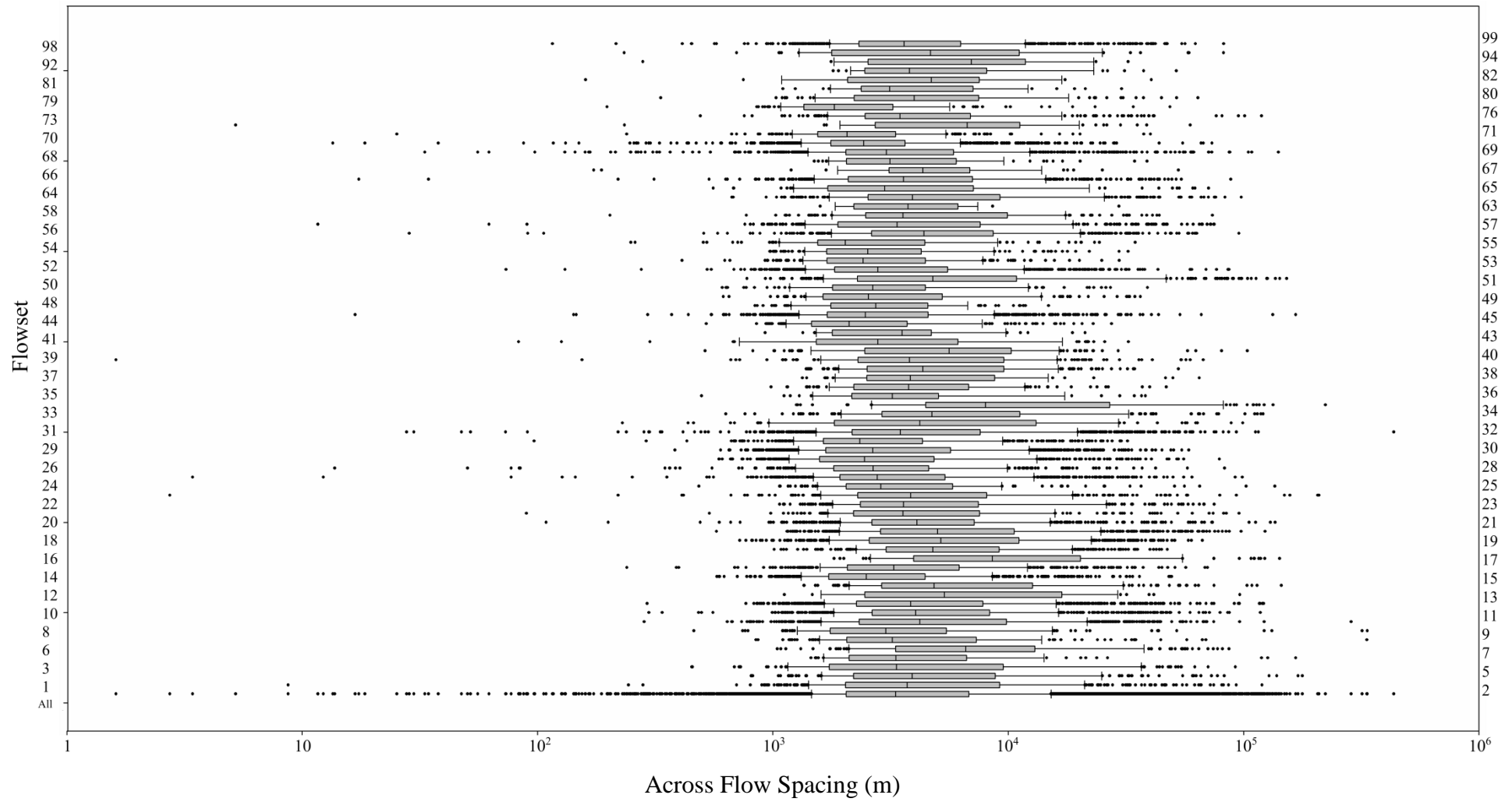


Figure 2.20. Comparative boxplots of drumlin across-flow spacing measurements grouped by flowset.

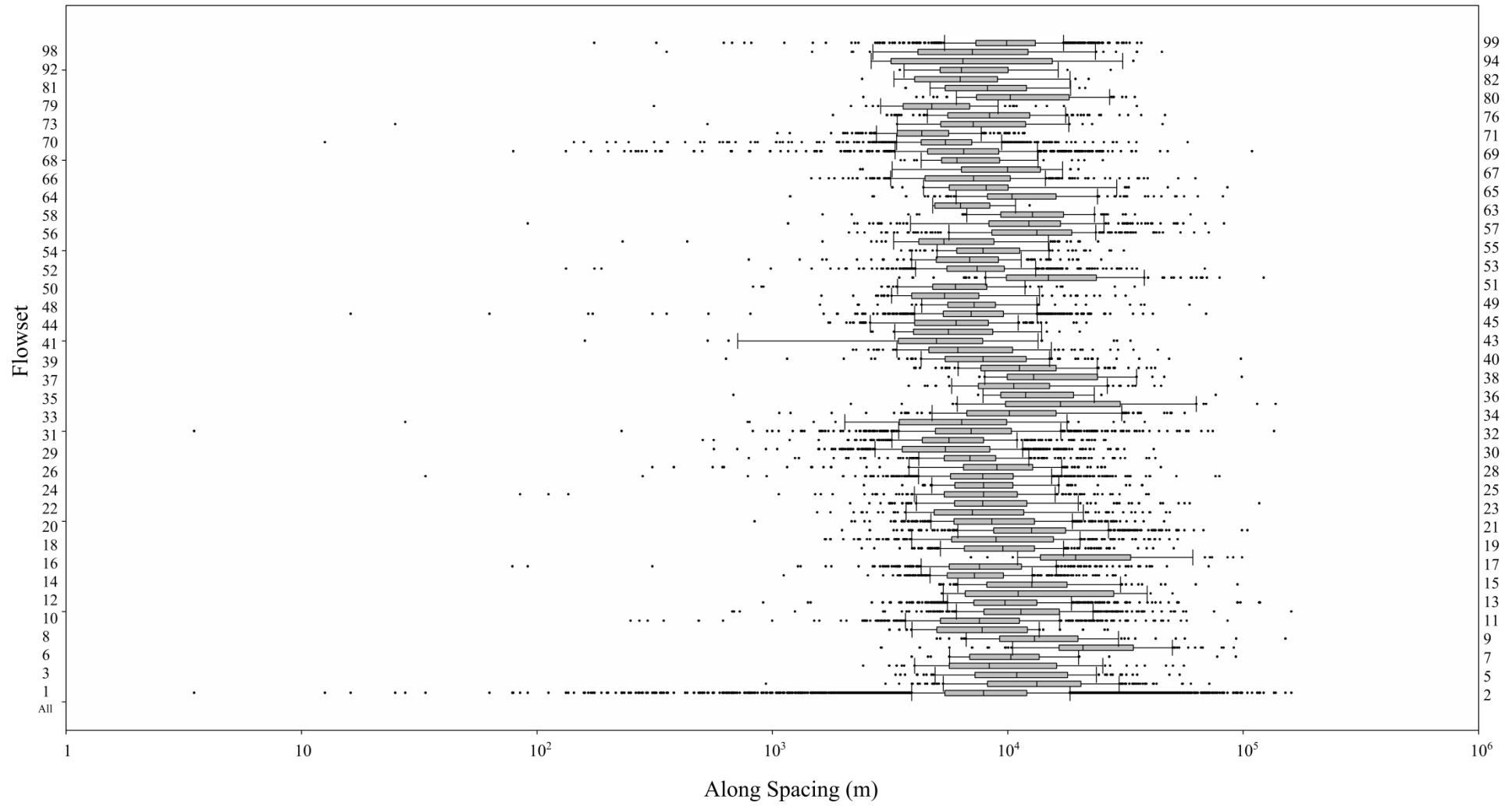


Figure 2.21. Comparative boxplots of drumlin along flow spacing measurements, grouped per flowset.

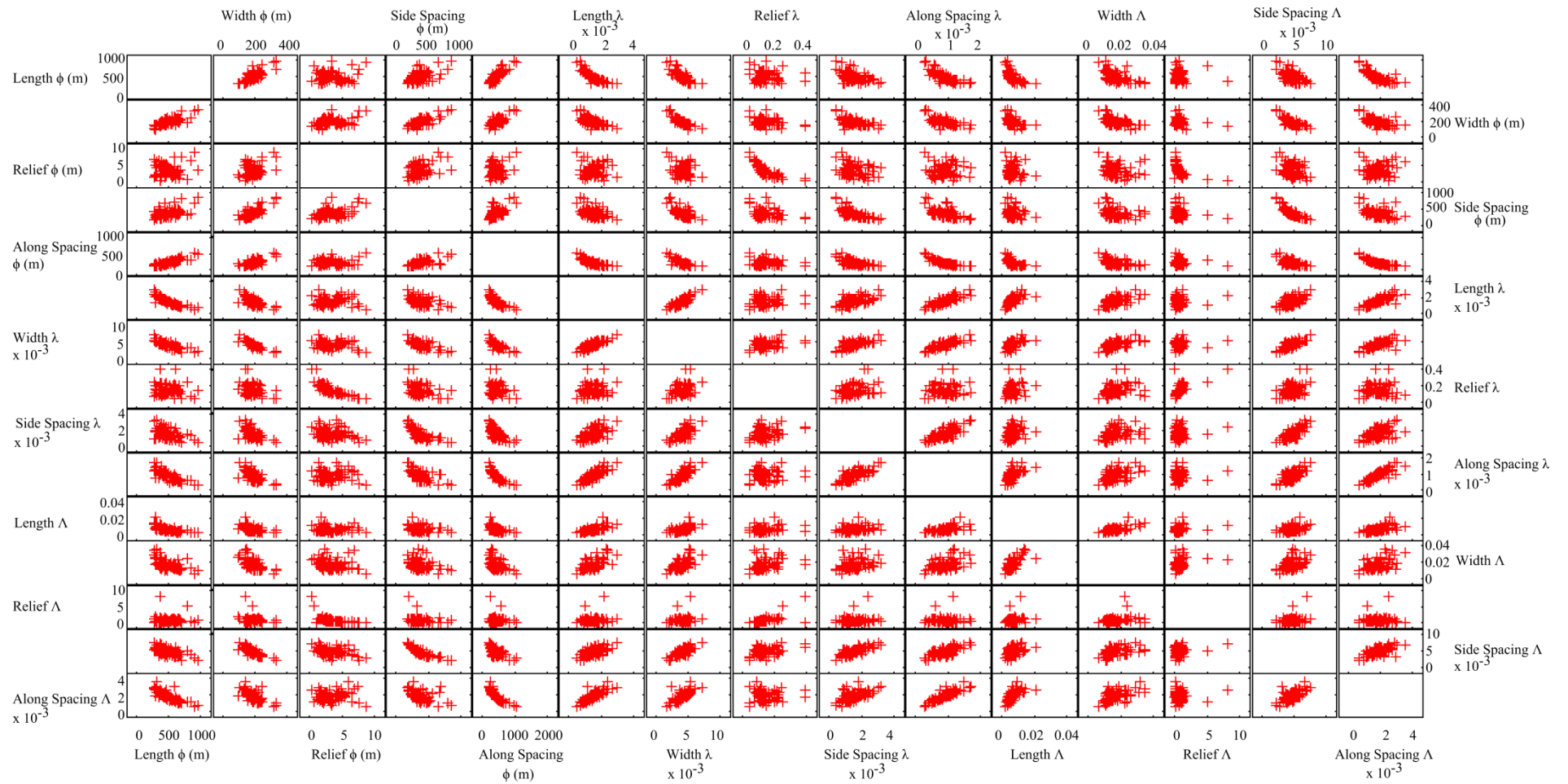


Figure 2.22. Scatter plot matrix of the shape of the distribution ( $\phi$ ,  $\lambda$  and  $\Lambda$ ) for all variables studied.

	Length $\phi$	Width $\phi$	Relief $\phi$	Side Spacing $\phi$	Along Spacing $\phi$	Length $\lambda$	Width $\lambda$	Relief $\lambda$	Side Spacing $\lambda$	Along Spacing $\lambda$	Length $\Lambda$	Width $\Lambda$	Relief $\Lambda$	Side Spacing $\Lambda$
Width $\phi$	<b>0.64</b> , $y = 3.6739x^{0.6346}$													
Relief $\phi$	0.0018, $y = 5.3309x^{-0.086}$	0.08, $y = 0.0742x^{0.7188}$												
Side Spacing $\phi$	0.29, $y = 0.0008x^2 - 0.4553x + 386.85$	<b>0.6</b> , $y = 2.3287x - 62.059$	0.13, $y = 27.452x + 277.23$											
Along Spacing $\phi$	<b>0.77</b> , $y = 2.006x - 103.36$	<b>0.62</b> , $y = 0.0173x^2 - 1.5668x + 537.45$	0.006, $y = 15.29x + 832.01$	0.39, $y = 1.5559x + 302.21$										
Length $\lambda$	<b>0.87</b> , $y = 1.4763x^{-1.125}$	0.5, $y = 0.3849x^{1.072}$	0.001, $y = 9E-06x + 0.0015$	0.24, $y = 17.767x^{-0.459}$	<b>0.82</b> , $y = 2.3505x^{-0.898}$									
Width $\lambda$	<b>0.71</b> , $y = 0.435x^{0.761}$	<b>0.85</b> , $y = 0.9429x^{-1.048}$	0.05, $y = 0.0045x^{-0.096}$	0.57, $y = 1.9182x^{-0.946}$	<b>0.7</b> , $y = 1.7835x^{-1.114}$	<b>0.72</b> , $y = 1.6834x^{0.0016}$								
Relief $\lambda$	0.008, $y = 0.2958x^{-0.131}$	0.13, $y = 3.9852x^{-0.653}$	<b>0.8</b> , $y = 0.2797x^{-0.653}$	0.01, $y = 687.45x^{0.097}$	0.01, $y = 687.45x^{-0.097}$	0.02, $y = 0.4145x^{0.1745}$	0.14, $y = 3.5596x^{-0.5962}$							
Side Spacing $\lambda$	0.22, $y = 0.0969x^{-0.688}$	0.37, $y = 0.4913x^{1.124}$	0.06, $y = 0.0017x^{-0.176}$	<b>0.69</b> , $y = 0.7915x^{-1.078}$	0.48, $y = 0.4149x^{-0.846}$	0.28, $y = 0.0931x^{0.6416}$	0.51, $y = 0.8354x^{-1.1575}$	0.11, $y = 0.0027x^{-0.3265}$						
Along Spacing $\lambda$	<b>0.62</b> , $y = 0.6205x^{-1.071}$	0.52, $y = 0.3999x^{-1.183}$	N/A	0.46, $y = 0.0787x^{0.772}$	<b>0.93</b> , $y = 0.9135x^{-1.039}$	<b>0.73</b> , $y = 0.3442x^{0.9192}$	<b>0.72</b> , $y = 0.699x^{1.2173}$	0.01, $y = 0.001x^{0.0898}$	0.46, $y = 0.0787x^{-0.772}$					
Length $\Lambda$	<b>0.62</b> , $y = 5.3476x^{-1.097}$	0.3, $y = 0.9607x^{0.968}$	0.003, $y = 0.0065x^{-0.038}$	0.05, $y = 0.0304x^{-0.27}$	0.49, $y = 1.4925x^{0.815}$	<b>0.63</b> , $y = 2.5043x^{0.9175}$	0.37, $y = 1.0725x^{0.9333}$	0.04, $y = 0.009x + 0.0054$	0.05, $y = 0.0304x^{0.27}$	0.39, $y = 0.723x^{0.6722}$				
Width $\Lambda$	0.37, $y = 1.2853x^{-0.712}$	0.43, $y = 2.4231x^{-0.964}$	0.07, $y = 0.0191x^{0.155}$	0.13, $y = 0.1359x^{-0.364}$	0.32, $y = 0.656x^{-0.552}$	0.42, $y = 2218.1x^2 + 0.5456x + 0.0104$	0.43, $y = 1.7157x^{0.8471}$	0.13, $y = 0.0288x^{0.2911}$	0.13, $y = 0.1359x^{-0.364}$	0.24, $y = 0.3651x^{0.4421}$	0.52, $y = 0.3463x^{0.6053}$			
Relief $\Lambda$	N/A	0.03, $y = 12.541x^{-0.578}$	<b>0.65</b> , $y = 2.0112x^{1.03}$	0.03, $y = 0.0015x + 1.4177$	N/A	0.004, $y = 153.1x + 0.6201$	0.01, $y = 3.3971x^{0.3086}$	0.45, $y = 6.6008x^{1.171}$	0.03, $y = 0.0015x + 1.4177$	0.002, $y = 0.318x^{0.094}$	0.02, $y = 2.492x^{1.2743}$	0.12, $y = 13.55x^{0.7462}$		
Side Spacing $\Lambda$	0.34, $y = 0.1074x^{-0.512}$	<b>0.69</b> , $y = 0.5454x^{-0.918}$	0.13, $y = 0.0055x^{-0.155}$	<b>0.89</b> , $y = 0.3333x^{-0.73}$	0.49, $y = 0.1457x^{-0.514}$	0.32, $y = 0.0678x^{0.4123}$	<b>0.68</b> , $y = 0.3766x^{0.799}$	0.14, $y = 0.0072x^{0.2221}$	<b>0.89</b> , $y = 0.3333x^{-0.73}$	0.54, $y = 2.7194x + 0.0023$	0.13, $y = 0.0142x^{0.223}$	0.23, $y = 0.0203x^{0.3609}$	0.04, $y = 0.0047x^{0.0674}$	
Along Spacing $\Lambda$	<b>0.74</b> , $y = 0.9457x^{-1.023}$	0.48, $y = 0.3957x^{-1.042}$	N/A	0.28, $y = 0.045x^{0.554}$	<b>0.94</b> , $y = 1.1x^{-0.959}$	<b>0.76</b> , $y = 0.4863x^{0.862}$	<b>0.6</b> , $y = 0.4903x^{-1.0226}$	0.002, $y = 0.0019x^{0.0346}$	0.28, $y = 0.045x^{0.554}$	<b>0.86</b> , $y = 0.7281x^{0.8535}$	0.52, $y = 0.0402x^{0.6189}$	0.31, $y = 0.0178x^{0.5635}$	N/A	0.43, $y = 0.2114x^{0.8918}$

Table 4 – Pearson product-moment correlation coefficients ( $R^2$ ) and best-fit line equation for all studied bivariate relationships. N/A indicates an  $R^2$  value of less than 0.001. Bold values indicate  $R^2$  larger than 0.6.

Figure 2.22 shows scatterplots of all studied variables and Table 4 shows the Pearson product-moment correlation coefficient ( $R^2$ ) and the best-fit equation between all bivariate pairs. These were used to identify significant relationships between variables. The weakest relationships relate to relief measurements. This is especially so for the  $\Lambda$  parameter for relief due to a low number of observations below the mode, relating to a filter applied during measurements (Spagnolo et al., 2012). The strongest relationships exist between a measured parameters'  $\phi$  value and its corresponding  $\lambda$  value. The relationship between which takes the form of a negatively correlated power law, indicating that as the size or spacing of drumlins increases, the gradient of the tail of the distribution decreases (Figure 2.23). Similarly,  $\phi$  and  $\Lambda$  also have high correlations for the same variable, again generally taking the form of a negative power-law relationship (Figure 2.24). This indicates that as drumlins get larger, or further apart, the gradient before the mode increases. Note that the relationship is weaker between  $\phi$  and  $\Lambda$  for the variable width. There are also strong  $R^2$  values between  $\lambda$  and  $\Lambda$ , taking the form of positive power laws (Figure 2.25). For each flowset and variable,  $\lambda$  is always greater than  $\Lambda$ , meaning that the distribution of each variable always conforms to an approximately log-normal shape. Furthermore, as shown in Figure 2.20 and Table 4, the form of the power law relationships means that for an increase in  $\lambda$  there is a corresponding larger increase in  $\Lambda$ . This means that as the tail of the distribution becomes shallower, so does the slope of the distribution before the mode. The general form of drumlin flowset metric distributions is schematically shown in Figure 2.26.

The  $R^2$  value between  $\phi$  length and  $\phi$  width is higher than that between per drumlin length and width measurements (Table 4; 0.45 in Clark et al., 2009), this may be due to less consideration for extreme outlier values. This relationship between length and width may explain the high  $R^2$  value between  $\phi$  width and  $\phi$  along-flow spacing. However, a similarly strong  $R^2$  does not occur between  $\phi$  length and  $\phi$  across-flow spacing (Table 4). Interestingly,  $\lambda$  length and  $\lambda$  width display a high positive correlation, such that as the tail of the distribution of length increases, so does the tail of the distribution for width. Further high  $R^2$  values in Table 4 may be the consequence of the variables not being dependent (i.e.  $\phi$  length and  $\phi$  along-flow spacing).

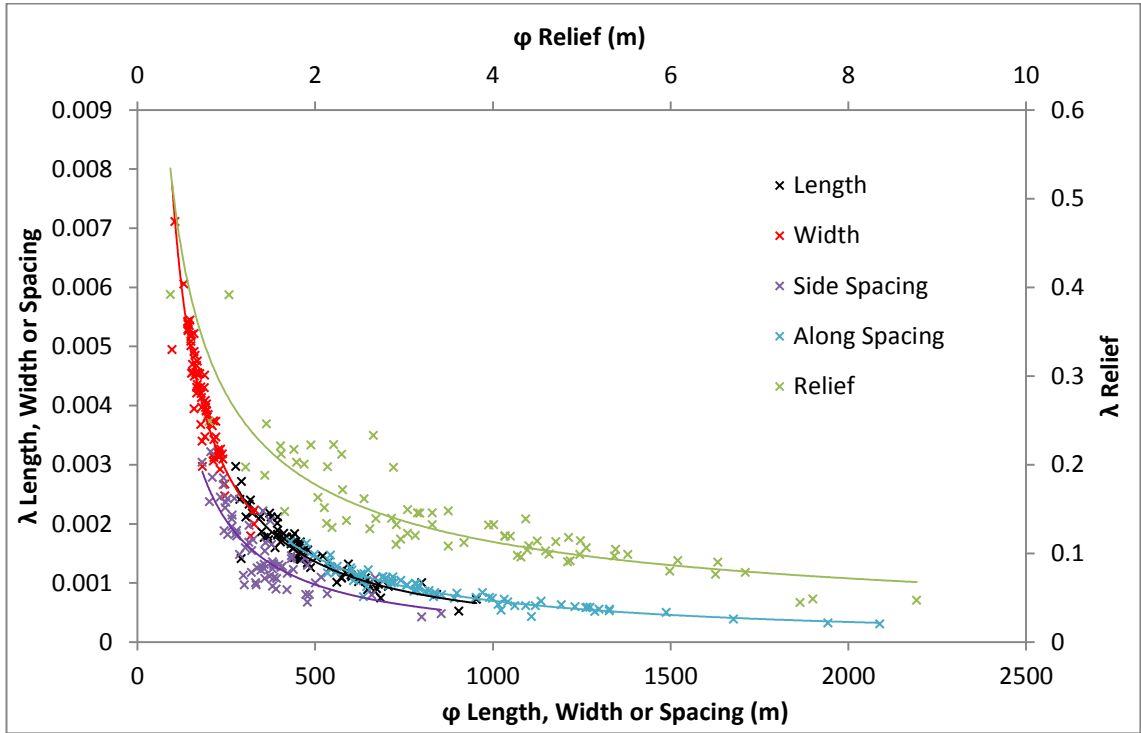


Figure 2.23. The relationships between  $\phi$  and  $\lambda$ . For  $R^2$  values see Table 6.

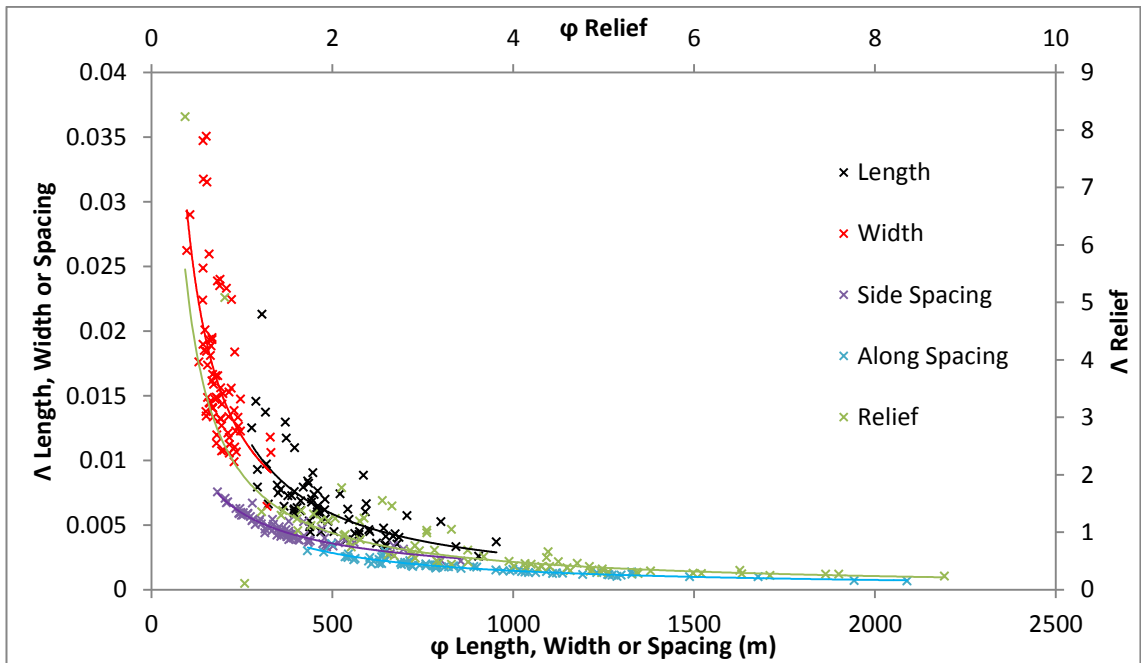


Figure 2.24. The relationships between  $\phi$  and  $\Lambda$ . For  $R^2$  values see Table 6.

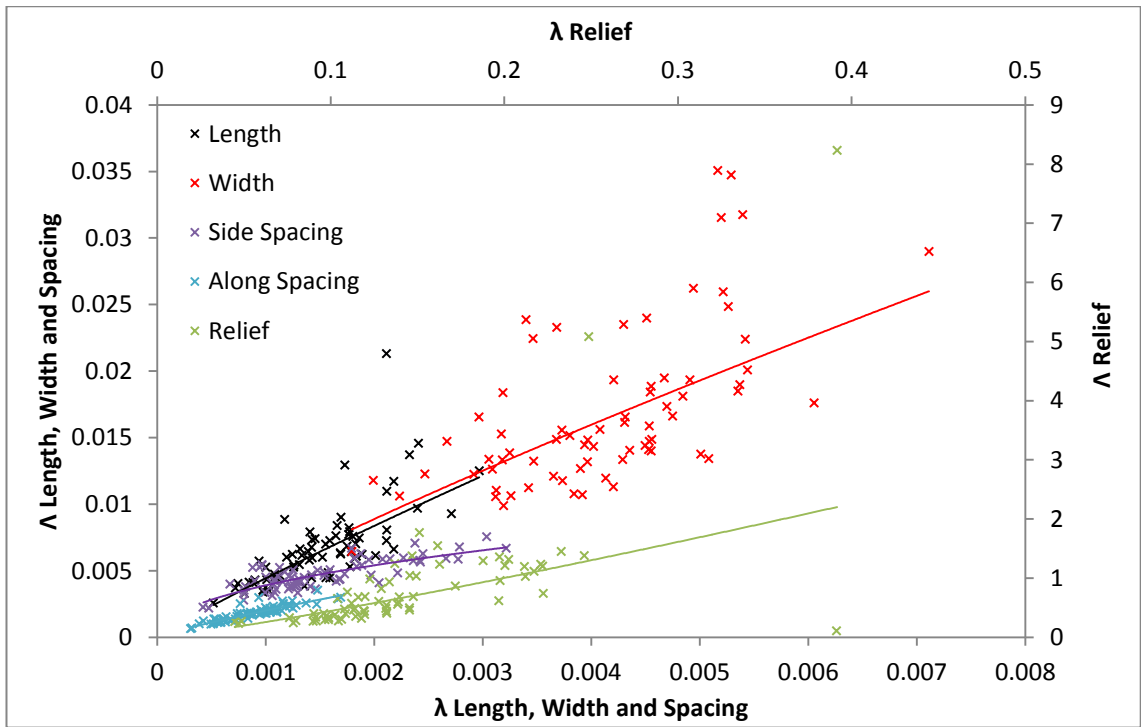


Figure 2.25. The relationship between  $\lambda$  and  $\Lambda$ . For  $R^2$  values see Table 6.

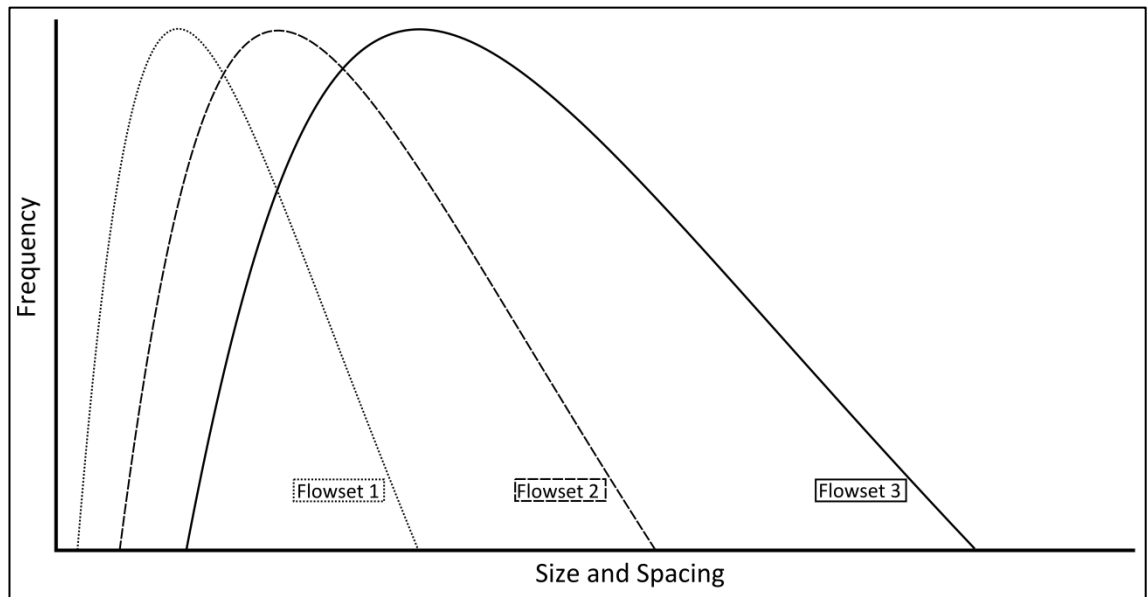


Figure 2.26. Schematic summary of the shape of probability distribution functions for different flowsets.

### 2.5.3 Interpretation: Are Drumlins “Printed”?

As shown in Section 2.4, spatial statistical analysis shows that drumlins within a cluster are regularly spaced, explaining the peaked histograms of their spacing metrics. Size metrics of drumlin dimensions also display a preferred modal class (e.g. Clark et al., 2009; Spagnolo et al., 2012). However, as shown in Section 2.5.2, the modal spacing and size of drumlins differs between flowsets. One possible explanation for this

inter-flowset variability is that drumlins are near-instantaneously “printed” at different sizes and spacing’s in accordance with local conditions at the ice-bed interface. Such a hypothesis would account for the log-normal distribution of drumlins by invoking a similar distribution of variables influencing the size and spacing of drumlins at the ice-bed interface (Fowler et al., 2013).

One line of evidence that drumlins are not printed in the above manner is found where drumlins cross cut (e.g. Clark, 1993; Mitchel, 1994; Hättestrand et al., 1999). Such drumlins are made of the same sediment, yet often have separate size and spacings. A clear example of this in Britain is shown in Figure 2.27. Indeed, Greenwood and Clark (2010) showed that differences in substrate lithology do not account for variations in drumlin spatial density or length. A shift in ice dynamics between cross cutting events could produce a different set of drumlin forming/influencing glaciological variables. However, drumlins of different sizes thought to have formed within the same ice flow configuration can be found next to each other. This juxtaposition is most apparent at the Dubawnt lake ice stream, where neighbouring drumlins can vary by an order of magnitude in length (Stokes et al., 2013b). Instead, Stokes et al. (2013b) argue that this juxtaposition requires drumlins to be of different ages, supporting the idea that the subglacial environment under which drumlins form is rapidly changing (e.g. Smith et al., 2007). Thus, drumlins formed under near identical glaciological conditions and from similar sediment can be of vastly different lengths, at odds with the printing hypothesis.



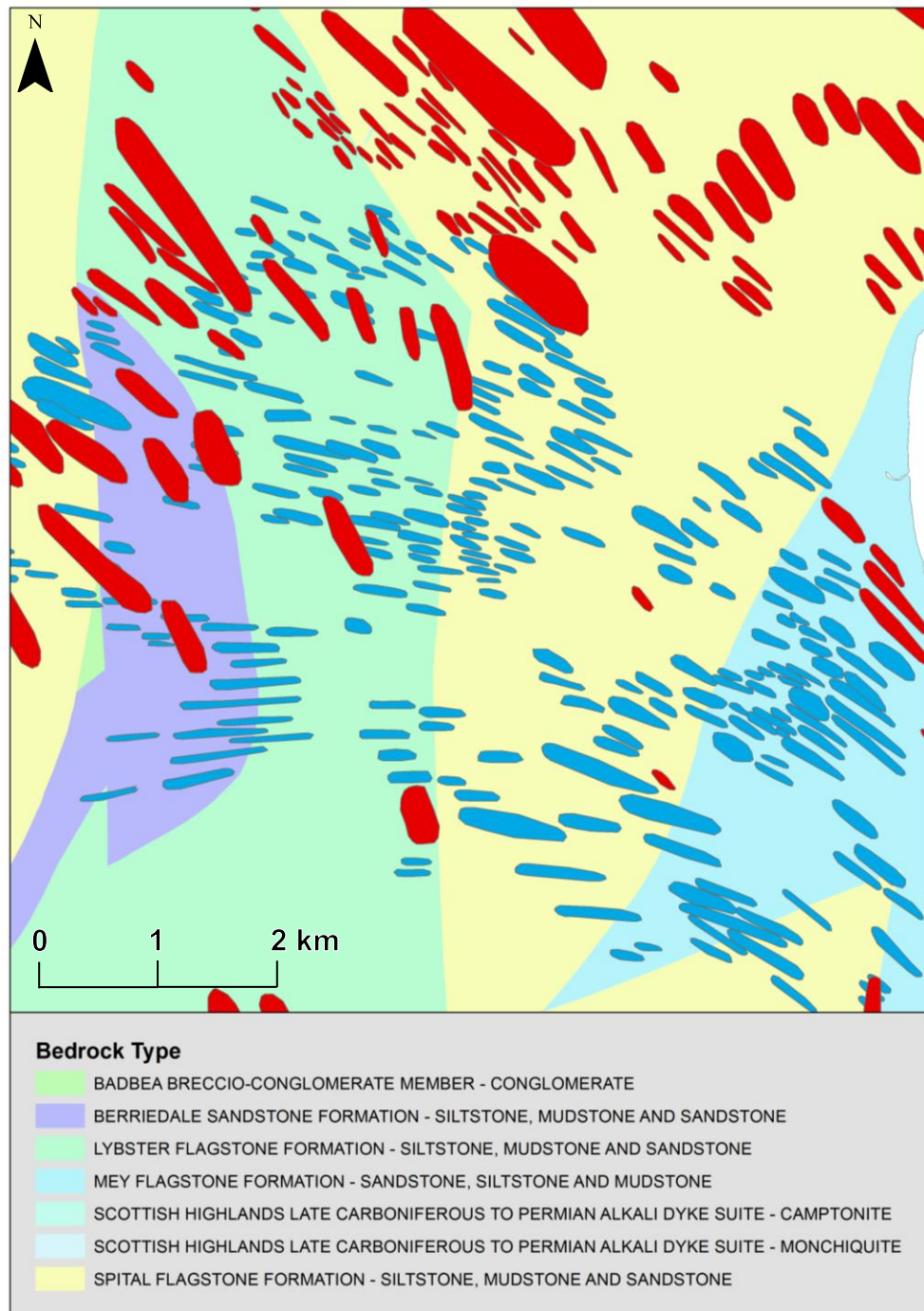


Figure 2.27. Cross cutting drumlins in NE Scotland, near Thurso. Background is a geology map supplied by EDINA Digimap service and the BGS. Note the difference in scale between drumlins from flowset 1 (red) and 26 (blue), yet they occur on the same geology. Mapping from Hughes et al. (2010).

An adaptation of the printing interpretation was presented by Clark et al. (2009). They pointed to the cone-shaped scatter of drumlin length and width, with abrupt boundaries as evidence that drumlins initiate at the order of 100 m before other interactions cause these metrics to evolve (Figure 2.28A). A similar shaped scatter is

found for the spacing of drumlins per flowset (Figure 20.28B), invoking a similar interpretation, that drumlins are initially printed at a minimum spacing. Indeed, if one considers drumlins to be waveforms, rather than “blisters” (Spagnolo et al., 2012; Figure 2.15), then perhaps the spacing of drumlins is a more fundamental measure than their size. Overall, the “printing” interpretation does not seem compatible with the observations of drumlins presented here and elsewhere. A more feasible explanation is that drumlins initiate at a minimum size and spacing, before other pattern forming interactions alter this. This interpretation supports the previous assumption that each flowset represents a different snapshot in time of the evolution of a drumlin pattern.

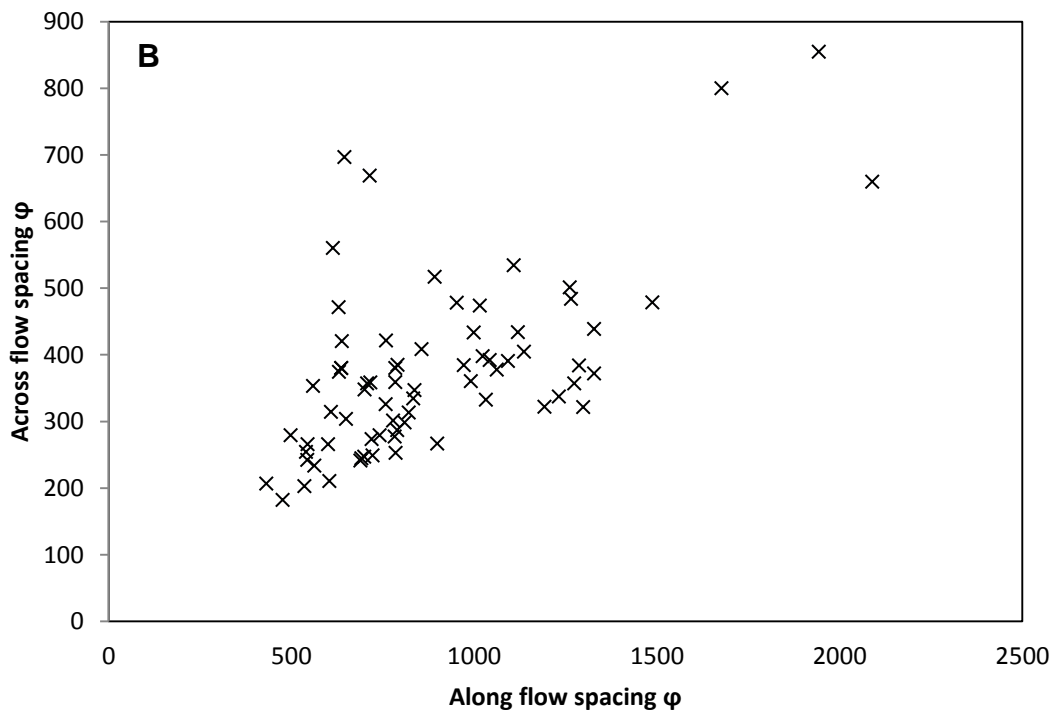
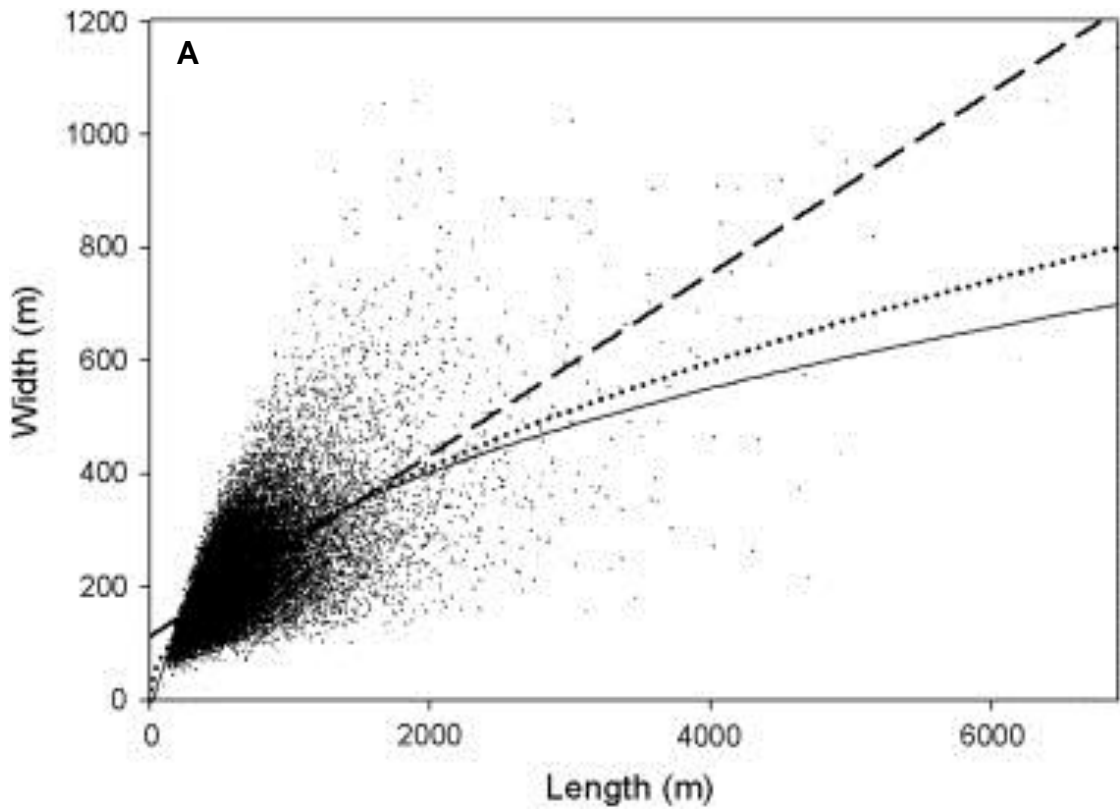


Figure 2.28. A) The length and width of drumlins from Clark et al. (2009). Note the cone shape of the distribution. B) Modal across and along flow spacing per flowset from authors own dataset.

#### 2.5.4 Interpretation: Simple Stabilisation

None of the probability distributions of the metrics conform to the expectation of simple stabilisation outlined in Figure 2.19B. Indeed, all probability distributions are broadly log-normal, suggesting that the size and shape continues to change, either growing or shrinking. The lack of an upper limit on length leaves open the question of a subglacial bedform continuum (Aario, 1977; Rose, 1987), whereby drumlins continue to get longer and possibly merge into MSGL (Chapter 3).

#### 2.5.5 Interpretation: Drumlin Growth

Based upon analogy to other disciplines (e.g. Limpert et al., 2001), and a statistical model, the log-normal distributions of drumlin size metrics have been interpreted elsewhere as an indication that drumlins grow in a number of stochastically distributed events (Fowler et al., 2013; Hillier et al., 2013). An alternative mechanism as to how such distributions can occur is through a random spread of flow conditions (e.g. Dunlop et al. 2008). Such a random spread may apply when explaining the log-normal distributions of subglacial bedforms at the ice-sheet scale (e.g. Clark et al., 2009; Dunlop and Clark, 2006b; Spagnolo et al., 2012). However, the log-normal distributions of drumlin metrics also occur at the individual flowset level, where one would expect gradually rather than stochastically varying flow conditions (Section 2.4.2). Furthermore, if drumlin size and shape metrics correspond to flow conditions at the ice sheet scale, this would require simple stabilisation of the drumlins in accordance with such conditions, which is not apparent from their probability distribution functions (Section 2.5.3). Therefore, my results favour the interpretation that the log-normal distribution of drumlins can be attributed to growth in stochastic phases. Alternatively, drumlins could shrink over time, due to erosional processes. Thus far, the possibility that drumlins shrink has been largely overlooked. Instead, links between ice velocity and drumlin length, which infer that longer drumlins have grown more than shorter ones (e.g. Hart, 1999; Stokes and Clark, 2002; Briner, 2007; Stokes et al., 2013b), have been favoured. Future work should also consider whether drumlins can shorten during the course of their development.

For width and relief, the general direction of growth is less clear. Stokes et al. (2013b), interpreted the size and shape metrics of the long drumlins on the Dubawnt Lake ice stream bed to have grown longer at the expense of their width, suggesting that the growth rate of width is less than that for length. Both the  $\lambda$  and  $\Lambda$  values for width

are much higher than for other size metrics (Figures 2.23 and 2.24), meaning the probability distribution functions of width are constrained. Building on the balance of growth and shrinking interpretation of log-normal distributions, either drumlin width increases at a slower growth rate than for other metrics, or the width of drumlins is regulated by erosional processes acting between them (e.g. Boyce and Eyles, 1991; Fowler, 2010a; Stokes et al., 2013b). Relief shows a larger spread of  $\lambda$  and  $\Lambda$  values, however an intuitive direction of growth or shrinkage is not apparent. Drumlin relief has little correlation with length, but never exceeds 7% of the width (Spagnolo et al., 2012), implying that a wide enough base of the drumlin is required to stand against ice flow and accumulate sediment. However, MSGL, which may form a continuum of morphology with drumlins (Chapter 3), are generally much lower in relief (Spagnolo et al., 2014a). Perhaps as drumlins get longer, erosional processes redistribute material from the relief of a drumlin enabling it to get longer, fitting with the interpretation of drumlin length being related to ice velocity, as higher velocities would create a higher erosion rate underneath the ice. Further work is required to establish such a link.

The negative correlation found between  $\phi$  and  $\lambda$  for length, width and relief (Figure 2.23) can be interpreted under the paradigm of drumlin growth. One possible interpretation of an increasing mode, but decreasing slope of the tail of the distribution, is that some drumlins preferentially grow more than others. This either indicates that growth is not evenly distributed amongst all the drumlins, with some preferentially growing more than others, or that drumlins within a flowset were created at different times, making the longest drumlins are older. The relationship between  $\phi$  and  $\Lambda$  for drumlin size metrics also gives insight into the nature of drumlin growth. If  $\Lambda$  had remained constant as  $\phi$  changed, this would be an indication that drumlins initiate at different sizes before growing to the mode (c.f. Section 2.5.2). However, the negative correlation between  $\phi$  and  $\Lambda$ , shown in Figure 2.24, may be a further indication that drumlins initiate at a single size in a flowset, before growing or shrinking occurs. Again, this either indicates a mixed age population, where the smallest drumlins are the youngest, or that drumlin growth is unevenly distributed across a drumlin field.

### 2.5.6 Interpretation: Static or Migratory?

As discussed in Section 2.5.5, a likely explanation for the nature of the probability distribution functions of the size metrics of drumlins is that drumlins grow. Whilst they grow, drumlins either remain static and accrete material, or they become mobile and

collisions between drumlins become an important mechanism by which drumlin size changes. Distinguishing between these from the snapshot provided by palaeo-ice sheet beds is difficult, but nevertheless important to consider as both are plausible mechanisms by which other interactions such as coarsening could occur.

Considering only growth in length, if drumlins grow without migrating, then I would expect one of three things in the metrics plotted in Figure 2.22 and Table 4. Firstly, if drumlins were to collide with each other in the manner shown in Figure 2.19C, then I would expect no correlation between length and across flow spacing. This is indeed the case, as shown in Figure 2.22 and Table 4. Secondly, a negative trend would imply that as drumlins grew longer, the tail of the growing drumlin was filling the space between downstream intervening drumlins. This was not found in the analysis of spacing. Thirdly, both along and across flow spacing metrics  $\lambda$  and  $\Lambda$  behave in the manner expected for migration (Figure 2.19D), whereby the probability distribution functions of spacing become less constrained (i.e. Figure 2.25). Therefore, it is difficult to distinguish between static growth and migration from the palaeo-record. One possibility is that some drumlins remain static once a critical size is reached, whilst smaller, more readily moveable drumlins migrate. Indeed, some drumlins are composed of bedrock or gravel cores, which are unlikely to have migrated (Schoof, 2007). However, this is not true for all drumlins, as others are composed purely of glacial diamict, and some show signs of a carapace which has eroded underlying sediment and could thus migrate as the surface is lowered (Hart, 1997; Stokes et al., 2013a). Whilst there is no obvious morphological evidence within drumlin fields of collision and cannibalisation occurring, further imaging of drumlins evolving in situ is required to solve this debate (e.g. King et al., 2007; 2009; Smith et al., 2007).

## 2.6 Discussion and Implications

### 2.6.1 Subglacial Bedforms as Patterns

As stated above, a key component of a pattern is its regularity (Section 2.2.1). Drumlins, MSGL and subglacial ribs all display preferred measured spacings (Dunlop and Clark, 2006b; Spagnolo et al., 2014a; Spagnolo et al. in prep), indicating that regularity might exist. For drumlins, results from the inhomogeneous pair-correlation function mostly showed this preferred spacing to be distinct from CSR (Section 2.4.1). Although the results of the  $g(r)_{inhom}$  tests provide evidence that drumlins are regularly placed within a drumlin field, variability is still found between flowsets and drumlins

(i.e. they are not placed in a perfect grid). Drumlins are likely to grow and shrink over time, and possibly migrate and coarsen (Section 2.5), providing mechanisms by which patterning interactions can occur. Therefore, one possible explanation for the deviation of drumlins from a regular grid is that other patterning interactions act to cause changes to the initial spacing of drumlins. This fits with the interpretation of Clark et al. (2009), that drumlins initiate at a minimum size and shape from which they grow (c.f. Evans, 2003). Perhaps, drumlins initiate at a minimum spacing which is regular (e.g. Figure 2.28), and then interactions such as growth, migration and coarsening occur which cause deviation from this pattern. Sediment supply may also be an important control upon drumlin patterning. In a sediment starved system, available sediment may be more spatially limited, leading to a clustered drumlin landscape. Additionally, drumlin growth may be more limited due to less sediment being available. Conversely, drumlins may form and grow more readily where there is a net sediment production underneath the ice sheet. To some extent, this is supported by observations offshore Antarctica, where drumlins form on thin sediment areas and much longer MSGL form where sediment is more readily available (Ó Cofaigh et al., 2002; See Chapter 3). Another possibility is that drumlin regularity is often destroyed by post-formational modification of the drumlin field removing many of its elements. Furthermore, drumlins with a resistant core (i.e. the obstacle drumlins of Clark (2010)), may induce predetermined defects into the pattern. Further work is required to determine the role of sedimentology, sediment supply and drumlin structure upon regularity within drumlin fields.

My above conclusion, that drumlins are mostly found to be regularly spaced within clusters in a field, and that drumlins can grow over time, indicates that many of the considerations of pattern forming processes may be applicable to drumlins (Section 2.2.1). Such a framework may be applicable to other subglacial bedforms which also display regularity and log-normal metric distributions (Section 2.2.2). Further geophysical work (e.g. King et al., 2009), observing drumlins evolving *in situ* may provide a clearer picture of how drumlin patterns evolve over time. As subglacial bedforms are here concluded to be patterned phenomena, future work should consider subglacial bedforms as a field phenomena, considering the co-evolution of bedforms within a flow-event or flowset, rather than as individual landforms. Such an interpretation has much in common with bedforms from other disciplines (e.g. Rose and Menzies, 1987; Werner and Kocuerk, 1999; Bartholdy et al., 2002; Kocurek et al., 2010). Isolated drumlins, which do not belong to regularly spaced drumlin clusters, also

require further investigation. Perhaps they are drumlin ‘clones’ (Clark et al., 2010), or the clustering/isolated partitioning of drumlins is a true result of the drumlinisation process (Section 2.4.3).

## 2.6.2 Implications for Drumlin Formation Theories

The regularity displayed by drumlin fields is strong evidence against formation theories, which view drumlins as individual entities (e.g. Möller, 1987). Instead, it appears that the initiation and growth of drumlins occurs at a field-wide scale, explaining both the regularity in distribution and spacing, and their size and shape metrics and probability distribution functions. This does not mean that the formation of drumlins can be elucidated from morphological properties alone. Indeed, many common sedimentological features such as lee-side cavities (e.g. Dardis et al., 1984; McCabe and Dardis, 1989) and rock cores (Clark, 2010) may provide further insight into the mechanisms of drumlin generation. Furthermore, remote sensing and GIS techniques cannot elucidate previous phases of drumlin building (e.g. Hart, 1995). However, the evidence shown here for field scale interactions does imply that sedimentological studies need to expand the area studied in order to account for the variation in the internal architecture of drumlins across a whole field and the implications this has for drumlin initiation, growth and interaction, rather than focussing on individual drumlins. Tools such as ground penetrating radar may be able to provide such information at this scale (e.g. Spagnolo et al., 2014b; see Section 3.6.1 for more on sedimentology and morphology).

Instabilities usually create regular patterns (Ball, 1999). Hence, the regularity of drumlins within a field found here could be interpreted as supportive of theories which involve an instability. Furthermore, any drumlin formation theory must also explain how drumlins grow or shrink over time. Three main instability based theories currently exist. The Shaw (2010) mega-flood hypothesis involves an instability in the flow of flood water as it erodes the substrate and overlying ice (see Figure 1.5; Shaw, 2002). This process could account for the regular distribution of drumlins within a field, through the creation of regular vortices during the turbulent flow of flood water. In order to account for my inference of drumlin growth (Section 2.5.4), drumlins would either have to grow within a single flood event, or floodwater erosion capacity would have to conform to a log-normal distribution across a flowset. Both of these seem unlikely. The former would either require multiple flood events to generate stochastic



growth events, which at the current magnitude proposed by the hypothesis, are likely to destroy previous drumlins. The latter would need the flood event to last long enough for drumlin forming erosional marks to grow and adapt, which would require additional water on top of an already unfeasibly large amount (Clarke et al., 2005; Livingstone et al., 2013).

Hooke and Medford (2013) propose that a drumlin forming instability originates from the unequal freezing and thawing of sediment at the bed creating obstacles for mobile sediment to accumulate around. This model therefore proposes a mechanism whereby drumlins can grow, similar to that originally described by Smalley and Unwin (1968) and later Boulton (1987), and accurately recreates drumlin relief. However, the model does not provide any quantitative estimates of spacing, and so in order to account for drumlin regularity the initial freeze-thaw instability must produce regular frozen patches. Such regular patches in subglacial sediment were proposed by Baranowski (1969) for the formation of flutes, but at a smaller scale than the drumlins studied here (the relationship between flutes and other subglacial bedforms will be discussed further in Chapter 3). Hooke and Medford (2013) concede that their formation mechanism may not be able to account for drumlins which form in regions away from the frozen bed zone (e.g. under an ice stream). Therefore, further adaptations are required in order for this model to account for all drumlin formation.

If drumlins are triggered by stiff patches of sediment, or another preconditioning of the bed, then we must seek an explanation for why these irregular patches are converted into a field of regularly positioned drumlins. Potentially, triggering of drumlins by such preconditioning would then cause drumlins to grow, such that they meet and interact with their neighbours. Regularity would then emerge from these interactions, causing self-organisation of the bed to occur. Hence, future drumlin formation theories should attempt to address this interaction.

The Hindmarsh-Fowler instability theory also builds drumlins from a mobile layer of deforming sediment (Hindmarsh, 1996; 1998a, b; Fowler 2000; Fowler 2010a). However, rather than requiring pre-existing resistant cores of sediment, like in the Hooke and Medford (2013) model, they propose that the coupled flow of ice, water and sediment at the base of an ice stream is inherently unstable, amplifying infinitesimally small perturbations which do not need to be already regularly placed. This theory accounts for the regularity of drumlins as it predicts the maximum growth rate of

instabilities (Fowler and Chapwanya, 2014). Once the drumlin forming perturbation is initiated, the theory also provides mechanisms via which the drumlins will grow. Sediment will either squeeze into the bump due to differential compressive stresses (Schoof, 2007), or once the drumlin is high enough a cavity will form behind it, which fills with water and sediment (Fowler, 2009). Therefore, the initial wavelength of regularity that the theory predicts may change as the bedform field produced grows and changes over time. Interestingly, the theory also predicts that some drumlins, below a threshold height, are able to migrate (Hindmarsh, 1998b). Therefore, the Hindmarsh-Fowler instability theory already accounts for both the regularity and growth of drumlins. Numerical models so far have only been able to reproduce subglacial ribs (Chapwanya et al., 2011), with further developments required to produce three-dimensional models of drumlins which initiate and evolve (c.f. Fowler and Chapwanya, 2014). Future models should also include stationary patches of sediment or bedrock, as well as including outputs that show the evolution of the ice-bed interface as the pattern of bedforms develops.

### 2.6.3 Implications for the subglacial environment

The above findings have implications for our understanding of the subglacial environment. Drumlins can act as a source of drag, limiting the sliding speed of an ice body (Schoof, 2002; 2004). As they are regularly distributed throughout a flowset, this implies that the drag imparted by drumlins is distributed evenly at the flowset scale. However, since drumlins grow over time, the drag imparted by drumlins across a flowset also increases as the drumlins grow. In this manner, the balance of forces at the ice-bed interface must evolve through time as drumlins develop. Theoretically, drumlins can also develop cavities in their lee, which are likely filled with water or saturated sediment (Fowler, 2009). Such water fluctuations are likely to cause changes in effective pressure at the ice-bed interface, increasing sliding across the cavity. As cavity size increases with the size of a drumlin (Fowler, 2009), this effect may counteract out the drag imparted by the drumlin itself (Figure 20.29).

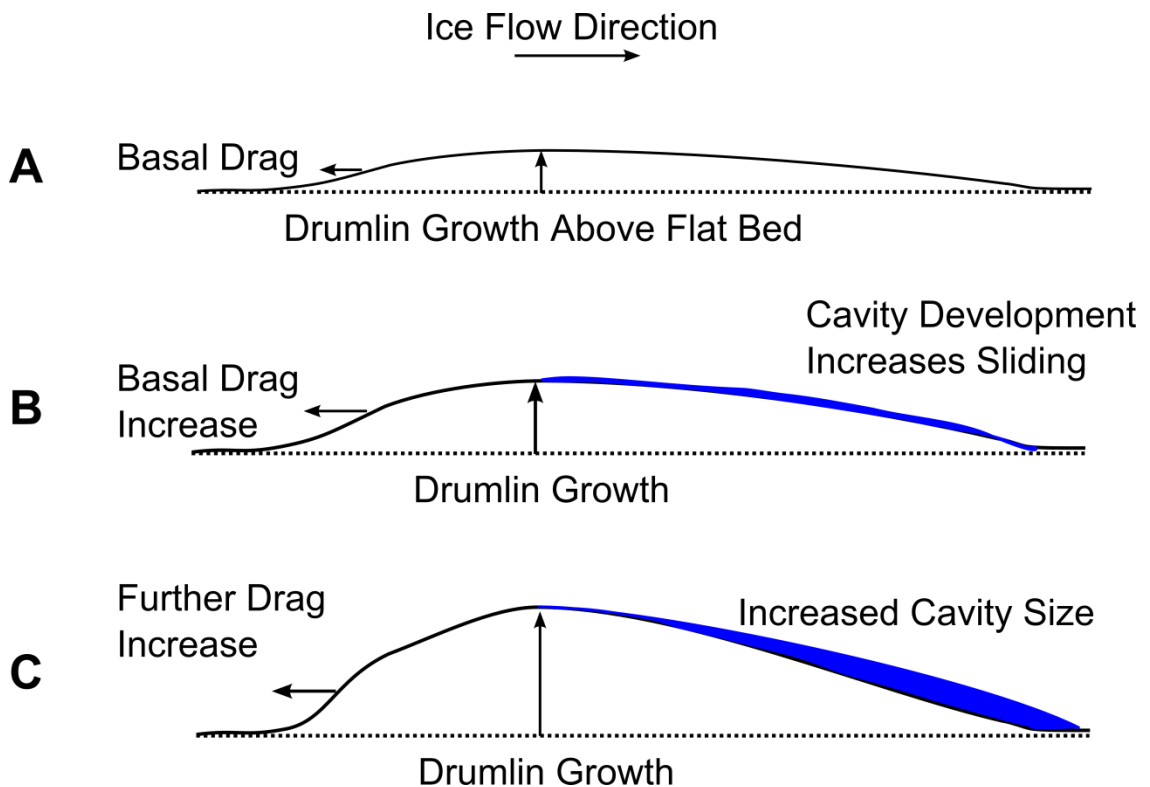


Figure 20.29. Hypothetical interplay between drumlin growth and drag. A) Initial development of a drumlin increases drag. B) Continued drumlin growth leads to cavitation. This creates a contrast between the high drag region at the stoss of the drumlin, and low effective pressure and high sliding region in the lee. C) Continued drumlin growth increases this contrast.

Deforming subglacial sediment underneath modern day ice masses has been observed (e.g. Boulton and Jones, 1979; Alley et al., 1986; Tulaczyk et al., 2000), and inferred (Engelhardt and Kamb, 1998), and in many cases may regulate ice flow (Boulton and Hindmarsh, 1987). If drumlins form through the deformation of subglacial sediment (e.g. Smalley and Unwin, 1969; Boulton, 1987), the abundance of drumlins and other subglacial bedforms on the beds of palaeo-ice sheets where deformation has occurred suggests that drumlins may be an indicator of subglacial deformation, as well as altering its characteristics. Indeed, if subglacial bedforms arise from an instability in the flow of subglacial sediment (Section 2.6.2), they are a spontaneous result of subglacial sediment deformation (Hindmarsh, 1996; 1998a, b). Bumps in the deforming layer may increase deformation in regions surrounding the bumps due to higher overburden pressures. Such streams of sediment have been invoked for the drumlins of the Peterborough drumlin field (e.g. Boyce and Eyles, 1991). This suggests a mosaic of subglacial deformation, rather than a continuous sheet, whereby sediment at the flanks of a subglacial bedform deforms at a higher rate than the

crests (e.g. Piotrowski et al., 2004). As drumlins grow in stochastic events, deformation may not only be spatially concentrated, but also temporarily, with growth and enhanced deformation occurring during events such as seasonal meltwater pulses or even from subglacial lake floods (Wingham et al., 2006; Fowler et al., 2013).

## **2.7 Summary and Conclusions**

Drawing from other disciplines of geomorphology, here I consider whether drumlins are a patterning phenomenon. The positioning of drumlins within a flowset is at first order clustered, but it is unclear whether this clustering is a true consequence of drumlin forming processes, inheritance from a pre-glacial phase or post formational modification. Within these clusters, spatial statistical techniques indicate that drumlins are regularly placed, demonstrating that they have a preferred wavelength in common with other patterned phenomena. The inhomogeneous pair correlation function was found to be the most useful statistic used for the study of drumlins. Furthermore, the spacing metrics of drumlins suggest that they initiate at a specific distance apart, in common with previous interpretations of their size. The probability distribution functions of drumlins per flowset are interpreted here to show that drumlins grow over time. Growth is either unevenly distributed across drumlins within a flowset, or drumlins of mixed ages are evident within the flowset. However, it is unresolved whether drumlins remain stationary during growth or migrate. Drumlins, and in turn other subglacial bedforms, are likely formed by a patterning process, and therefore interactions at the scale of a cluster are important for consideration in their formation. These findings are most compatible with the instability theory of drumlin formation, which both explains the regularity of drumlins and incorporates mechanisms by which they grow. The initiation and development of drumlins also has implications for mechanisms of ice flow interacting with the subglacial environment.

# Chapter 3 **A Size and Shape Continuum of Subglacial Bedforms? Implications for their Genesis**

## **3.1 Introduction**

The interface between water, air or ice and unconsolidated sediment is often populated by undulating landforms, collectively referred to as bedforms (Allen, 1968; Wilson, 1972; Aario, 1977; Rose and Letzer, 1977). Rather than being individuals, bedforms commonly occur in swathes or fields; configurations which cover large portions of Earth's deserts, river beds and sea floors (e.g. Costello and Southard 1981; Amos and King, 1984; Carling, 1999), as well as the surfaces of extra-terrestrial bodies (Cutts and Smith, 1973; Kargel and Strom, 1992; Radebaugh et al., 2008). The morphological properties of bedforms provide constraints for hypotheses and models of their formation (e.g. Jackson, 1975; Clark et al., 2009; Worman et al., 2013). Fluvial, aeolian and marine bedforms can form distinct, often hierarchical, size and shape populations (Allen, 1968). For example, in deserts discrete populations of bedforms are found, increasing in size from ripples to dunes then draas (Wilson, 1972; Lancaster, 1988). Conversely, bedforms can belong to populations within which there are no clear size distinctions, forming size and shape continua (e.g. aeolian ripples (Ellwood et al., 1975), aeolian dunes (Lancaster, 2013, p. 159) and subaqueous dunes (Ashley, 1990)). For subglacial bedforms, it is unclear whether they form separate distinct morphological populations, or form a single continuous morphological population with no natural breaks (i.e. a size and shape continuum).

Subglacial bedforms are often subdivided and named on the basis of perceived distinctions in scale and morphology. Commonly, subglacial bedforms that form aligned with ice-flow direction are divided into drumlins, mega-scale glacial lineations (MSGs) and flutes (Figure 3.1). Ribbed moraine form transverse to flow direction (Figure 3.1), with a potentially separate "mega-scale" variant having recently been discovered (Greenwood and Kleman, 2010; Klages et al., 2013). Quasi-circular bedforms, which have no clear orientation to ice flow direction, are less frequently studied, but have been previously noted (Hill, 1973; Markgren and Lassila, 1980; Bouchard, 1989; Greenwood and Kleman, 2010). Beyond this, a wealth of further nomenclature exists (e.g. mega-flutes, fluting, mega-drumlins, and minor ribbed,

Blatnick, Rogen and Niemsel moraines). The plethora of terms suggests that multiple, potentially hierarchical, populations of subglacial bedforms exist.

Figure 3.1. Different types of subglacial bedform and their orientation to ice flow direction (denoted by black arrow). Scales are approximate. A) A drumlin in N.E. England. These streamlined hills, typically 250-1000 m along-flow and 120-300 m across-flow (Clark et al., 2009). B) Transverse ridges, termed ribbed moraine, in Nunavut, Canada, typically 300-1200 m across-flow, and 150-300 m along-flow (Hättestrand and Kleman, 1999). C) A flute formed parallel to ice flow direction, Svalbard. Note the accumulation of sediment in the lee of a boulder. D) A MSGL in Nunavut, Canada. MSGLs are typically 100-200 m across-flow and 1-9 km along-flow (Spagnolo et al., 2014a), but have been reported to be much longer (e.g. 180 km, Andreassen et al., 2008). All photographs from [www.shef.ac.uk/drumlins](http://www.shef.ac.uk/drumlins).

Despite the array of terms applied to subglacial bedforms, a long-standing hypothesis within the literature is that they actually belong to a continuum of size and shape (Aario, 1977; Rose, 1987). This ‘continuum hypothesis’ was originally based upon observations of downstream spatial transitions between subglacial bedform types and orientations, suggesting a single continuum of form stretching from ribbed moraine, through quasi-circular forms to drumlins (Aario, 1977; Markgren and Lassila, 1980; Punkari, 1984; Lundqvist, 1989). However, subsequent work on the continuum hypothesis has focussed solely upon flow-aligned subglacial bedforms (e.g. Rose, 1987;

Stokes et al., 2013b). Furthermore, morphological studies often focus upon previously labelled categories of subglacial bedforms (e.g. drumlins in Clark et al. (2009) and Maclachlan and Eyles, (2013); ribbed moraines in Hättestrand (1997) and Dunlop and Clark (2006b); MSGL in Spagnolo et al. (2014a)), leaving the continuum hypothesis unresolved.

Here, I address the question of whether subglacial bedforms comprise of a continuum of size and shape by assembling and analysing the largest ever database of subglacial bedform size and shape measurements ( $\approx 100,000$ ). Thus, I provide the first rigorous test of the continuum hypothesis, and discuss its implications for subglacial bedform formation.

### **3.2 Previous Work**

The word continuum is defined as “a continuous sequence in which adjacent elements are not perceptibly different from each other, but the extremes are quite distinct” (Concise Oxford English Dictionary, Luxury Edition, 2011, P.309). The clearest example of a natural continuum is the electromagnetic spectrum. Within the visible wavelengths of light, the extremes of violet and red are distinct, but adjacent wavelengths vary continuously (Newton, 1730). Whilst the continuous nature of light can be demonstrated by refracting light through a prism, such an elegant experiment for subglacial bedforms does not exist. Instead, observations of subglacial bedforms have been piecemeal. Thus, whilst a morphological continuum of subglacial bedforms has been hypothesised (Aario, 1977; Rose, 1987), it is unclear whether a single continuum, several continua, or multiple unrelated populations of bedforms exist.

The idea that subglacial bedforms belong to a morphological continuum began with observations of gradual spatial transitions of bedform morphology (e.g. Aario, 1977; Markgren and Lassila, 1980; Punkari, 1984; Lundqvist, 1989). Figure 3.2 conceptualises such a landscape, and provides further examples of such transition zones (Figure 3.2D and 3.2E). These transition zones often include a switch from flow-transverse ribbed moraine, through quasi-circular forms, to flow parallel drumlinoid bedforms, which progressively elongate downstream. Bedform transition zones cast doubt upon morphological distinctions between bedforms, and also lead to the supposition that ribbed moraines and drumlins are not mechanistically exclusive (e.g. Aario, 1977; Aario, 1987). Subsequently, examples of circular subglacial bedforms have been noted (Hill, 1973; Markgren and Lassila, 1980; Bouchard, 1989; Greenwood

and Clark, 2008), and other transitions have been documented (e.g. Carl, 1978; Aylsworth and Shilts, 1989; Dyke et al., 1992; Knight et al., 1999; McCabe et al., 1999; Clark and Meehan, 2001; Dunlop and Clark, 2006b; Clark, 2010).

The first quantitative test of the continuum hypothesis was conducted by Rose (1987), who measured the length, width and elongation ratio (length divided by width) of flow-aligned subglacial bedforms. His dataset revealed a size distinction between drumlinoid and flute forms (Figure 3A), whereby flutes were much smaller than drumlins, but a continuum between other streamlined landforms. Subsequently, Clark (1993) recognised MSGLs as a new category of subglacial bedforms and distinguished them from drumlins on the basis of their great length. Thus, three continua of flow aligned subglacial bedforms had emerged by the 1990s (Figure 3.4A). The distinction between drumlins and MSGL (Figure 3.4A) has since been questioned, because downstream increases in drumlin elongation have often been observed (e.g. Hart, 1999; Stokes and Clark, 2002; Briner, 2007; Hess and Briner, 2009), including transitions from drumlins to MSGL (e.g. Ó Cofaigh et al., 2002; Heroy and Anderson, 2005; Graham et al., 2009; Stokes et al., 2013b; Figure 3.4B). However, a thorough quantitative analysis of MSGLs and drumlins that looks at a variety of settings is still missing: and no recent studies have tried to re-address the possible link with these and flutes.



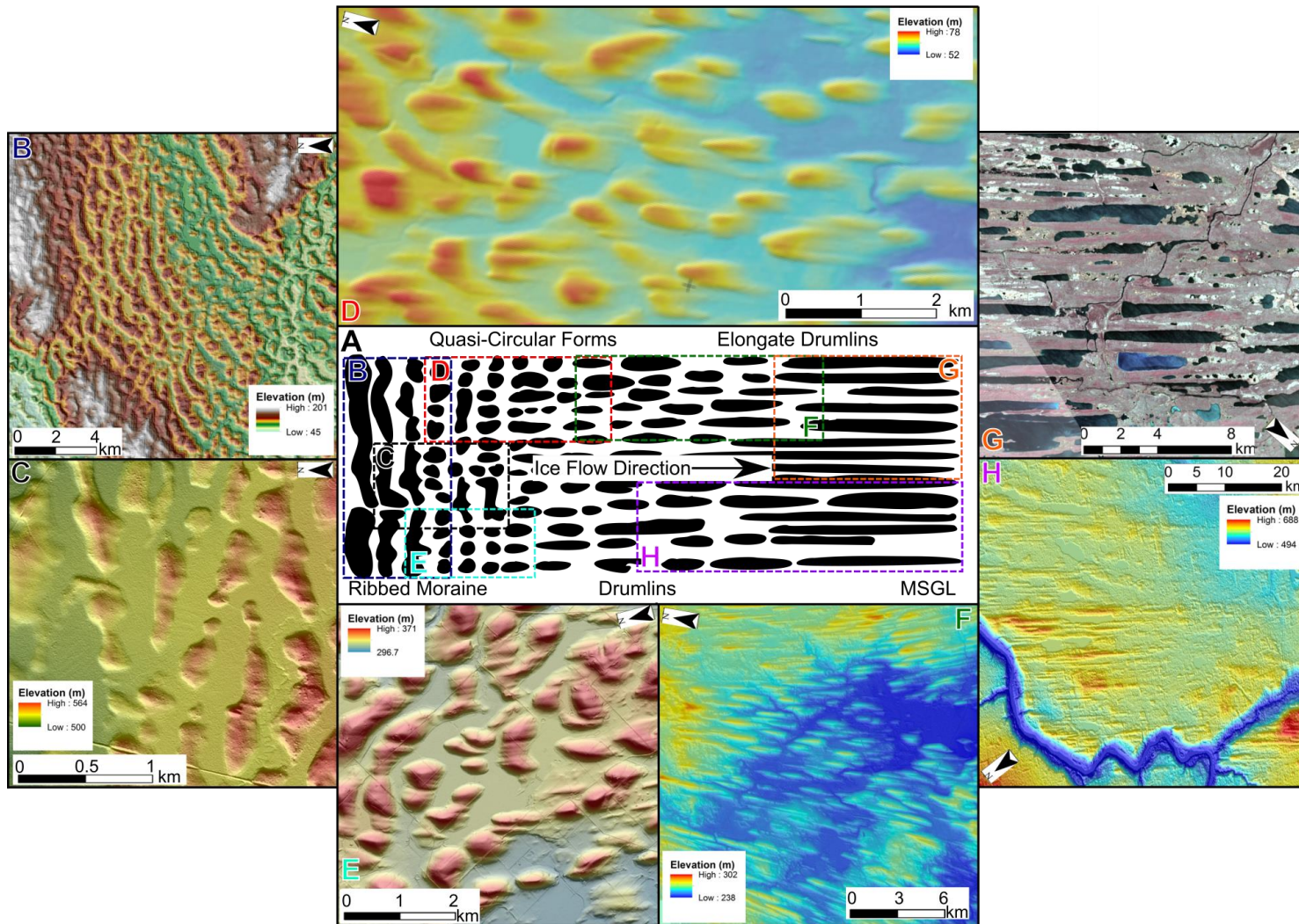


Figure. 3.2. A schematic representation of bedform transitions (A), after Aario (1977) and Stokes (2013b), with hill-shaded digital elevation models showing examples of subglacial bedforms. In all cases ice flow is broadly from left to right. Coordinates for the centre of the image provided. (B) a field of ribbed moraine near Monaghan, Ireland (54°13'51.69"N, 7° 3'5.47"W); (C) slightly drumlinised ribbed moraines in Lake county, Michigan, USA (47°42'9.38"N, 91°14'53.98"W); (D) a transition between ribs and drumlins near Leitrim, Ireland (53°52'19.68"N, 7°54'48.10"W); (E) a transition between ribs and drumlins in Fon du Lac county, Wisconsin, USA (43°35'19.65"N, 88°21'2.59"W); (F) elongated drumlins and drumlins in Dodge county, Wisconsin, USA (43°21'16.23"N, 88°45'58.80"W); (G) Landsat ETM+ false colour composite of MSGL of the Great Bear Lake ice stream, NWT, Canada (64° 6'2.95"N, 120°23'8.19"W) and (H), 'flutings' or MSGL of the Athabasca fluting field, Alberta, Canada (54°46'24.30"N; 113° 4'51.57"W). Why do the gradual transitions seen in (D) and (E) occur if formed by separate processes?

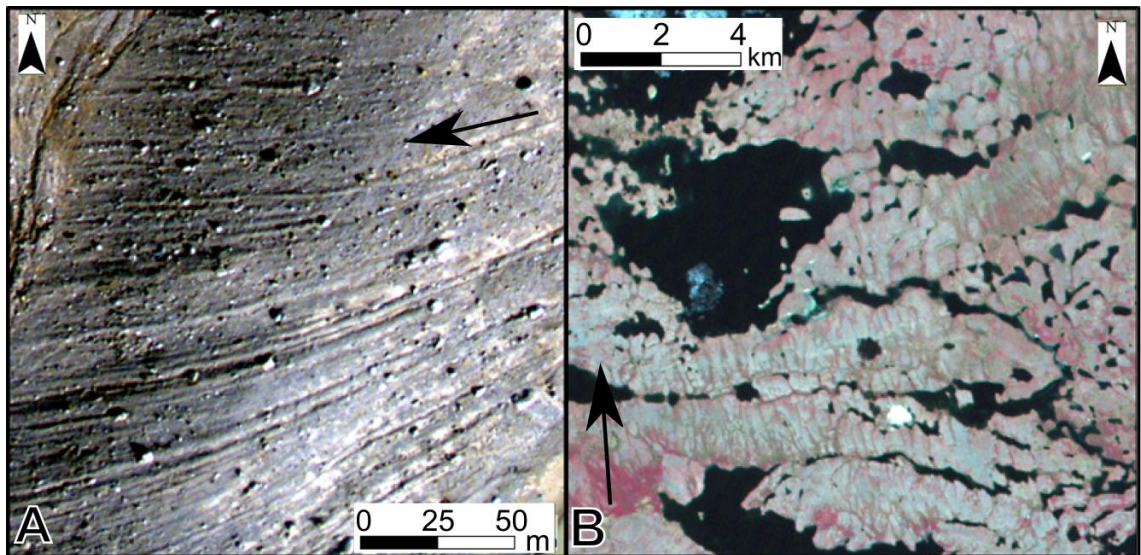


Figure. 3.3. Subglacial bedforms not considered within the transition-based continuum hypothesis (e.g. Aario, 1977), and thus not shown in Figure 3.2. (A) Aerial photography of a field of flutes in front of Conwaybreen, Svalbard. (B) mega-scale ribbed moraine in Nunavut, Canada (see Greenwood and Kleman, 2010).

The original idea of a subglacial bedform continuum included ribbed moraines (e.g. Figure 2A; Aario, 1987), but there are few recent reports of them in relation to a bedform continuum, including those thought to be of a larger, potentially separate, scale (Greenwood and Kleman, 2010; Klages et al., 2013; Fig 3B). Furthermore, quasi-circular bedforms (e.g. Markgren and Lassila, 1980) have not been morphologically defined and considered within a continuum context, which could potentially bridge the gap between the alignments of subglacial bedforms. Thus, whether subglacial ribs, mega-ribs and circular features are morphologically separate (Figure 3.4C), or form a much larger continuum of bedforms (Figure 3.4D), is yet to be resolved.

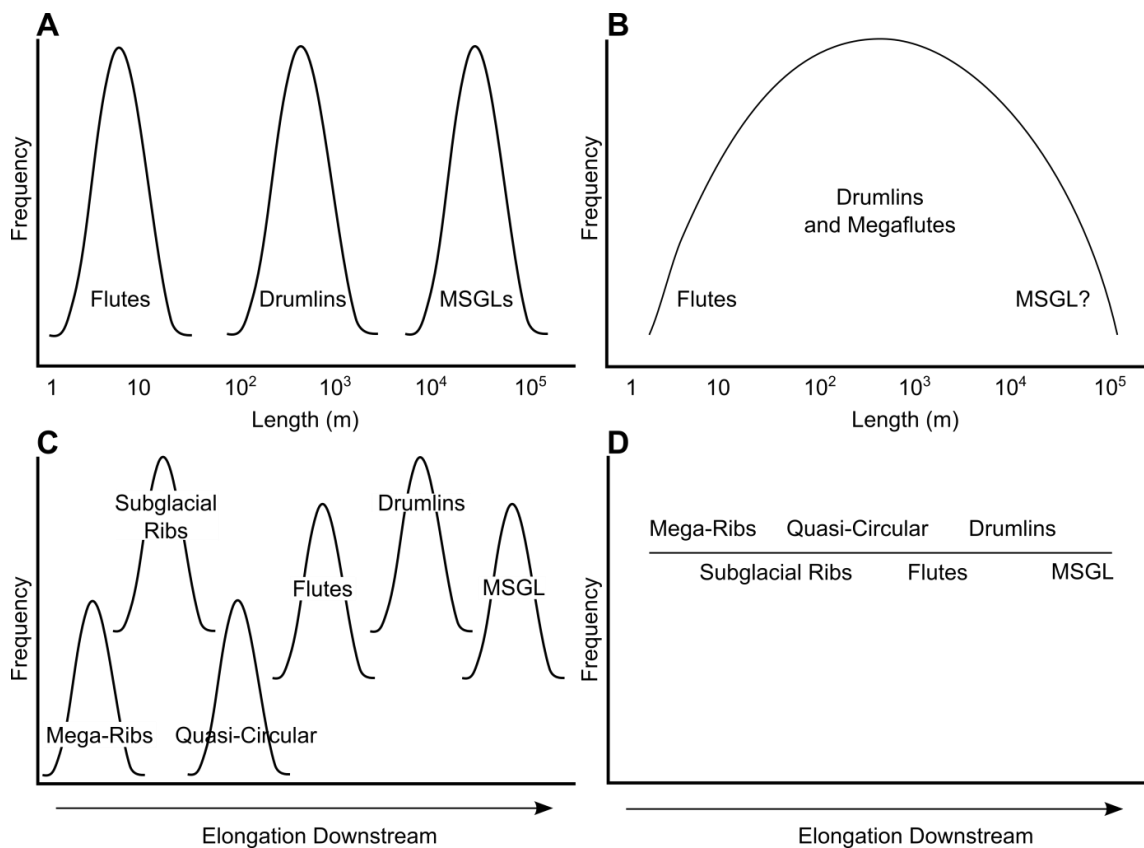


Figure 3.4. Schematic representations of different continuum hypotheses. Scales are approximate and relative. Clark (1993) suggested three continua of subglacial bedforms (A). Stokes et al. (2013b) proposed a continuum of flow aligned subglacial bedforms (B). However, flow transverse and quasi-circular bedforms should also be considered, and could form separate continua (C), or a morphological continuum between all different reported types (D).

The existence or absence of a morphological continuum has important implications for deciphering subglacial bedform origin. One possibility is that they have multiple, ‘equifinite’ origins. Thus, multiple hypotheses may be valid and, as such, the term ‘subglacial bedform’ may accidentally group together phenomena which are not genetically related (c.f. Clark, 2010). If true, the term should not be used to imply a common origin, but should be used merely as a convenient label for referring to subglacial landforms. Based upon the internal composition of subglacial bedforms, others have argued that multiple phases of bedform development are required in order to adequately account for their formation (e.g. Kurimo, 1980; Möller, 2006; Johnson et al., 2010). Such ‘polygenetic’ hypotheses highlight the differences within and between different fields (e.g. Lindén et al., 2008; Möller, 2010; Sutinen et al., 2010), rather than the commonality that a morphological continuum would imply. Conversely, a number of ‘bedform specific’ formation hypotheses have also been proposed, whereby named

bedform categories (e.g. drumlin, ribbed moraine) are formed by separate processes (e.g. Bouchard, 1989; Gordon et al., 1992; Hättestrand and Kleman, 1999; Clark et al., 2003; Hooke and Medford, 2013). This view may be more compatible with subglacial bedforms conforming to discrete continua (e.g. Figure 3.4A and C). Perhaps prematurely, the continuum hypothesis has been used to argue for a process continuum between subglacial bedform types (e.g. Aario, 1977; Stokes et al., 2013a). Indeed there are a number of ‘unifying’ hypotheses for subglacial bedform formation (e.g. Hindmarsh, 1998b; Shaw, 2010; Fowler and Chapwanya, 2014), which seek to account for all subglacial bedforms through the same process acting under different conditions (Clark, 2010).

### **3.3 Methods**

When testing for the presence of a continuum it is important to minimise the effect of potentially arbitrary labels contaminating the findings. In the absence of an experiment as elegant as Newton’s prism (see Section 2), I must rely instead upon measurements. If one were to adopt a similar approach for light, if only the regions of the spectrum with distinctive names were measured (e.g. red and yellow) then others (e.g. orange) would be overlooked, and the conclusion that red and yellow are separate entities may be reached (Figure 3.5A). With the addition of a multitude of terms, a sufficiently high number of named colours could be included and a continuum of light would be recorded (Figure 3.5B). However, oversampling toward the predefined nomenclature may still occur (Figure 3.5B). Furthermore, if the study area contained no surfaces which reflect light at a specific wavelength then one may conclude that such a wavelength of light does not exist. Thus, my experimental design must: (i) minimise the effects of nomenclature bias and (ii) include sufficient localities to account for the true population of subglacial bedforms.



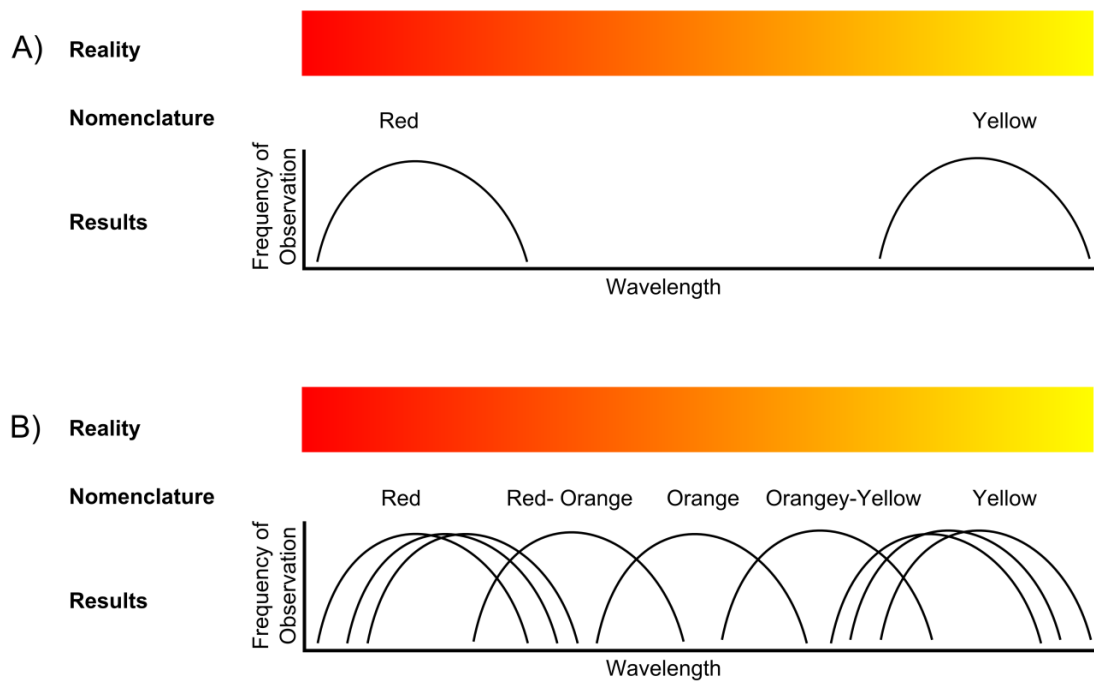


Figure 3.5. Thought experiment for testing light as a continuum, illustrating the sampling bias introduced by nomenclature. Each plot displays the reality that light forms a continuous spectrum between red and yellow (top), the known nomenclature for the experiment (middle) and the distribution of measurements in the results (bottom). In (A) minimal nomenclature leads to the conclusion that red and yellow are separate phenomena. The addition of further nomenclature in (B) leads to more overlap between populations. However, the initial bias introduced from (A) leads to a higher sampling density for red and yellow.

In order to test whether a morphometric continuum of subglacial bedforms exists, a large database of 96,900 mapped subglacial bedforms was compiled from previous studies, and additional mapping conducted using standardised techniques (Table 5). When mapping from digital elevation models, a break of slope was identified around each bedform on hill-shaded images (e.g. Hughes et al., 2010). Azimuth biasing was minimised through the use of multiple hill-shade directions (Smith and Clark, 2005). On satellite images and aerial photography, boundaries around each bedform often correspond to a change in vegetation and soil moisture, taken to correspond to a break in slope (Spagnolo et al., 2014a). Additionally, the angle of the sun can naturally highlight topography (Clark, 1997; Jansson and Glasser, 2005). A number of automated mapping methods exist (e.g. Saha et al., 2011; Machlachlan and Eyles, 2013), but require predefinition of parameters such as shape and scale of expected bedforms, and

hence contain biases toward a certain size or shape of bedform. Thus, a smooth polygon was manually digitised around the perimeter of each bedform.

A wide range of sites were chosen from the literature, in order to include a variety of typically reported bedform morphologies (i.e. to address issue (ii), above). These sites cover a large area of the Northern Hemisphere (Figure 3.6). At each site, the highest resolution data available were used (Table 6). Importantly, this was always higher than 30 m, as coarser resolutions hinder bedform identification and derived morphometric variables (Napieralski and Nalepa, 2010).

Figure 3.6. Location of mapped subglacial bedforms. Numbers refer to Table 5.

Bedform Category	Location	Central Coordinates (Decimal Degrees)	Number of Bedforms	Dataset	Previous Study (* denotes mapping is original to this study)	Location Number
Drumlins	Britain	54.069, 2.258	30,304	NEXMap DEM	Hughes et al., 2010.	1
	New York State, USA	44.830, -75.268	5,650	USGS NED	Hess and Briner, 2009.	2
	Alta, Norway	69.476, 23.139	1,638	Landsat ETM+	Spagnolo et al., 2010.	3
	Ungava Bay, Quebec, Canada	57.176, -67.299	5,903	Landsat ETM+	Spagnolo et al., 2010.	4
MSGL	Cameron Hills, Alberta, Canada	59.950, -117.826	581	SPOT	Brown et al., 2011. *	5
	Dubawnt Lake, Nunavut, Canada	64.171, -100.415	17,038	Landsat ETM+	Stokes et al., (2013b)	6
	Eskimo Bay, Nunavut, Canada	61.387, -94.829	4,499	SPOT	Clark, 1993. *	7
	Great Bear Lake, NWT, Canada	64.454, -122.069	1,260	SPOT	Winsborrow et al., 2004. *	8
	Haldane Ice Stream, NWT, Canada	67.008, -121.299	489	SPOT	Winsborrow et al., 2004. *	9
	Liard Ice Stream, NWT, Canada	61.217, -121.701	340	SPOT	Brown et al., 2011. *	10
	Great Slave Lake, NWT, Canada	61.703, -116.576	784	SPOT	Brown et al., 2011. *	11
	Payne Bay, Quebec, Canada	59.618, -70.430	531	SPOT	This study. *	12
	M'Clintock Channel Ice Stream, Canada	72.743, -105.753	2,796	Landsat ETM+	Storrar and Stokes, 2007. *	13
	West James Bay Ice Stream	54.478, -87.280	3,350	SPOT	Clark, 1993. *	14
Quasi-Circular Bedforms	Ireland	53.723, -7.803	1955	Landmap DEM, SRTM, Landsat ETM+	Greenwood and Clark, 2008.	15
Flutes	Skeiðarajökull, Iceland	63.977, -17.219	101	NERC ARSF Aerial Photography	Waller et al., 2008. *	16
	Breiðamerkurjökull, Iceland	64.071, -16.3275	131	NERC ARSF Aerial Photography	Evans and Twigg, 2002. *	17
	Conwaybreen, Svalbard	78.994, 12.486	432	NERC ARSF Aerial Photography	This study. *	18
Ribbed Moraine	Ireland	53.723, -7.803	5464	Landmap Dem, SRTM, Landsat ETM+	Greenwood and Clark, 2008.	19
	Lac Naococane, Quebec, Canada	52.972, -70.921	501	Landsat	Dunlop and Clark, 2006a.*	20
	St. Lawrence Valley, New York	44.831, -75.268	921	USGS NED	Carl, 1978. *	21
	Lake Rogen, Sweden	62.328, 12.394	3,357	Landsat ETM+	Dunlop and Clark, 2006b. *	22
	Ungava Bay, Quebec,	59.618, -70.430	7582	Landsat ETM +	Dunlop and Clark, 2006b. *	23



Mega Subglacial Ribs	Canada Great Slave Lake, NWT, Canada	61.703, -116.576	559	SPOT	Brown et al., 2011. *	24
	Keewatin, Canada	64.171, -100.415	733	Landsat ETM+ and SPOT	Greenwood and Kleman, 2010.	25

Table 5. Location and reference of collated mapping of subglacial bedforms.

Dataset	Type of Data	Horizontal Resolution	Source
NEXTMap Great Britain™	DEM	5m	<a href="http://arsf.nerc.ac.uk/">http://arsf.nerc.ac.uk/</a>
USGS NED	DEM	1/3 arc second (≈10m)	<a href="http://ned.usgs.gov/">http://ned.usgs.gov/</a>
Landsat ETM+	Imagery	15m Pan-chromatic, 30m Colour.	<a href="http://earthexplorer.usgs.gov/">http://earthexplorer.usgs.gov/</a>
SPOT	Imagery	10m Pan-chromatic, 20m colour	<a href="http://geobase.ca/">http://geobase.ca/</a>
Landmap DEM	DEM	25m	<a href="http://landmap.ac.uk/">http://landmap.ac.uk/</a>
NERC ARSF Aerial Photography	Imagery	≈15cm	<a href="http://arsf.nerc.ac.uk/">http://arsf.nerc.ac.uk/</a>
SRTM	DEM	3 arc seconds	<a href="http://earthexplorer.usgs.gov/">http://earthexplorer.usgs.gov/</a>

Table 6. Data type and source for the mapping described in Table 5.

The length ( $L$ ) and width ( $W$ ) of each mapped bedform polygon was estimated via Euler's approximation for an ellipse (Equations 8 and 9 in Chapter 2, Section 2.3.3; Clark et al., 2009). A limitation of this approximation is that it underestimates the length (and overestimates the width) of elongate or irregular polygons, but this error is insignificant compared to the size of the bedforms (Clark et al., 2009). Rather than change measurement technique for different categories, the same technique was used for the whole dataset in order that systematic changes or classifications were not introduced. These polygon measurements were then converged into  $a$ -axis (distance down-ice flow) and  $b$ -axis (distance across-ice flow) measurements according to bedform orientation to ice flow (Figure 3.7). For near-circular bedforms, no clear long axis is apparent. Thus, bedform  $a$ -axis and  $b$ -axis were manually measured within a GIS using regional ice flow patterns as an indicator of flow alignment. Elongation ratio, often used as a proxy for shape (e.g. Clark et al., 2009; Rose, 1987; Stokes and Clark, 2002; Dowling et al., 2015), was simply measured as  $a$ -axis divided by  $b$ -axis.. Unfortunately, due to the lack of high-resolution digital elevation models for each study site, relief could not be calculated here (e.g. Smith et al., 2009; Spagnolo et al., 2012). The compiled dataset contains 96,900 mapped subglacial bedforms, the largest data set on subglacial bedforms ever collated.

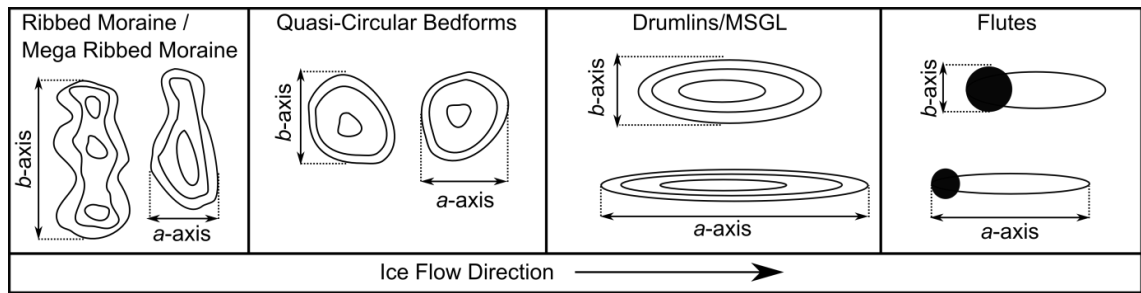


Figure 3.7. Schematic of derived bedform axes. *a*-axis and *b*-axis are normalised in correspondence to palaeo-ice flow direction.

Testing the subglacial bedform continuum hypothesis requires the detection and definition of populations within my dataset. If the variously-named types of bedforms are found to vary continuously in size and shape such that, for example, a large drumlin is the same as a small MSGL, then a size and shape continuum between these exists (Figure 3.8A and B). When plotted on a scatter graph, this would show a single continuous data cloud, or cluster (Figure 3.8B). On the contrary, if the derived metrics reveal gaps or jumps in scale or shape then they are better interpreted as discrete phenomena (Figure 3.8C and D), leading to the rejection of the continuum hypothesis. Here, a scatter graph of bedform metrics would show several distinct clusters (Figure 3.8D). Whilst all attempts were made to be objective when mapping the outlines of each bedform, the existing nomenclature introduces preconceived notions into the mapping of any landscape. Such bias might push mappers toward defining shapes that conform to previously established labels (i.e. issue (i), above). Therefore, my dataset was analysed both with and without reference to previously established nomenclature.

Figure 3.8. Schematic of how a continuum (A and B) or different populations (C and D) may be detected in my dataset. If a continuous sequence in the size and shape of bedforms exists, e.g. between drumlins and MSGs (A), then a scatter plot of their metrics would show a single cluster. If separate size and shape populations occur (C), then separate clusters would be shown on a scatter plot (D).

The human eye is an excellent tool for detecting clusters (Jain, 2010). As such, my first attempt at detecting clusters in my dataset was to plot the data and visually assess clustering qualitatively. That said, different interpreters may see different clusters. Thus, in an effort to make my analysis more objective and quantitative I employed the density-based clustering algorithm DBSCAN (Ester et al., 1996) using the package ‘fpc’ in R statistical software. This method requires no predefinition of the number of expected clusters within a dataset; hence it requires no *a priori* categorisation of bedforms into separate populations. In order to define dense regions (clusters) within a point cloud, DBSCAN creates a window at each point and determines which points are sufficiently reachable from each other in order to warrant definition as a cluster (Ester et al., 1996). The algorithm requires two input parameters; the window size ( $\epsilon$ ) and the minimum number of points within a cluster (MinPts). Sensitivity analysis of cluster-definition to window size ( $\epsilon$ ) was run from  $\epsilon = 1.0$  to  $\epsilon = 0.01$  with steps of  $\epsilon = 0.01$ . The sensitivity of minimum points per cluster (MinPts) was also tested at values of 10, 50 and 100. DBSCAN was only conducted on the independent variables of length and width; elongation being derived from the two. DBSCAN was run on all mapped

landforms, without any separation across the various types of landforms. Identified clusters were only discussed in light of the conventional nomenclature of subglacial bedforms after this cluster analysis was conducted.

Significance testing of cluster cohesion and separation was conducted in order to test the validity and quality the clusters produced by DBSCAN. The silhouette measure of cohesion and separation, as proposed by Rousseeuw (1987), was conducted using the software IBM SPSS Statistic v.10. A value close to 1 indicates the data is “well clustered”, where as a value of -1 indicates misclassification (Jain and Koronios, 2008; Kaufmann and Rousseeuw, 1990).

A second approach, based on a direct, visual assessment of the degree of overlap between assigned bedform categories’ metrics was also applied (Table 1). In binary plots of the morphological variables (e.g. length vs. width) the density of observations per category were calculated and contoured, whereby the highest density contour contained 75% of the observations, the middle 95% and the lowest 99%. The degree of overlap between adjacent categories were then evaluated in order to test the validity of frequently used bedform nomenclature. A similar approach was also taken in order to analyse bedforms by location.

## 3.4 Results

### 3.4.1 Cluster Analysis

The size and shape of all 96,900 subglacial bedforms in my dataset is displayed in Figure 3.9. Arguably, the most striking aspect is that data are concentrated into a narrow range of values, leaving a large proportion of the available space blank. When plotted on linear axes (Figure 3.9A), there appears to be two clouds of data which merge toward the origin of the plot. Larger bedforms (>10,000 m) are less frequent in my dataset, but importantly plot as extensions of the same data clouds, rather than forming separate clusters. Due the skew imposed by these large values, data was also plotted on a logarithmic scale (Figures 3.9B-D). At first order, two clusters of data are visually discernible: a small cloud of narrow and elongate bedforms aligned with flow direction, and a much larger cloud comprising the remaining bedforms (Figure 3.9D). Within this larger cloud, density variations occur, perhaps delimiting three further populations which overlap, or sampling irregularities. Furthermore, separate trends of data can also be discerned within the larger cloud, with bedforms with a larger *a*-axis than *b*-axis following a separate trajectory to transverse bedforms (Figure 3.9B). Interestingly, there

are bedforms with no clear orientation (i.e. circular) which fall between these two groups.

The results of DBSCAN are dependent upon the combination of parameters chosen (Figure 3.10). At the extremes of the window size parameter ( $\epsilon$ ), the algorithm groups the data into inappropriately sized clusters. When  $\epsilon$  is large, the window size is such that the whole dataset is seen as a single cluster (Figure 3.10 A). When  $\epsilon$  is small, numerous small clusters are detected due to an insufficient search radius (Figure 3.10O). The most common result is that two clusters are detected (Figure 3.10 B-F). These two clusters occur in the same positions as the first order visual clustering (Figure 3.9D). Figure 3.11 plots this typical result. When the data are separated in such a way, the silhouette measure of cohesion and separation yields a value of 0.821, indicating that the dataset is significantly well clustered when considered as two separate clusters. The larger cluster is not separated when the search window size parameter is adjusted from 0.5 to 0.06 (Figure 3.10 H-J). Beyond this, the larger cloud is separated into two clusters, one with bedforms aligned with flow direction and another with bedforms transverse to flow (Figure 3.10 K-N). For only a very small parameter space, DBSCAN distinguishes subglacial bedforms with no clear orientation to flow direction from flow-aligned and flow-transverse bedforms (Figure 3.10 M).

Figure 3.9. The size and shape of all 96,900 subglacial bedforms, paying no regard to their nomenclature. (A) Plot of  $a$ -axis (down-flow) and  $b$ -axis (across flow) dimensions. (B) The same dimensions, plotted on logarithmic axes. (C) Combined plot of  $a$ -axis,  $b$ -axis and elongation ratio ( $a/b$ ). Although elongation ratio is dependent upon  $a$  and  $b$  axis, it is plotted for visualisation purposes. (D) Two possible qualitative (visual) interpretations of clusters. See text for further details.

$\epsilon = 1$	MinPts = 100	$\epsilon = 0.5$	MinPts = 100	$\epsilon = 0.25$	MinPts = 100
$\epsilon = 0.25$	MinPts = 10	$\epsilon = 0.15$	MinPts = 100	$\epsilon = 0.1$	MinPts = 100
$\epsilon = 0.09$	MinPts = 100	$\epsilon = 0.08$	MinPts = 100	$\epsilon = 0.07$	MinPts = 100
$\epsilon = 0.06$	MinPts = 100	$\epsilon = 0.05$	MinPts = 100	$\epsilon = 0.045$	MinPts = 100

$\mathcal{E} = 0.04$	MinPts = 100	$\mathcal{E} = 0.04$	MinPts = 50	$\mathcal{E} = 0.01$	MinPts = 100

Figure 3.10. DBSCAN sensitivity analysis to assess how many clusters exist. Red, green and blue indicate different clusters. Black points are disregarded by the clustering algorithm as being outside of any cluster, due to a lack of density and cohesiveness with other points. The most common result is that two clusters are detected (B, C, D, E and F): narrow elongate bedforms and a larger cluster comprising of the remaining data. This occurs when  $\mathcal{E} = 0.5 - 0.1$ , and MinPts = 10-100 (B-F). For  $\mathcal{E} = 0.09 - 0.06$  (G-J), the smaller cluster is not detected, but the large cluster remains. When  $\mathcal{E} = 0.05-0.045$ , clusters distinguish between flow alignment (K). At  $\mathcal{E} = 0.04$  and MinPts = 100, a further small cluster between flow alignments is detected (blue in 'M'). Yet, a slight change in parameter values alters this result (N). When  $\mathcal{E}$  is too large, the whole dataset is considered a cluster (A), or when  $\mathcal{E}$  is too small, clusters of an inappropriate size are detected (O).



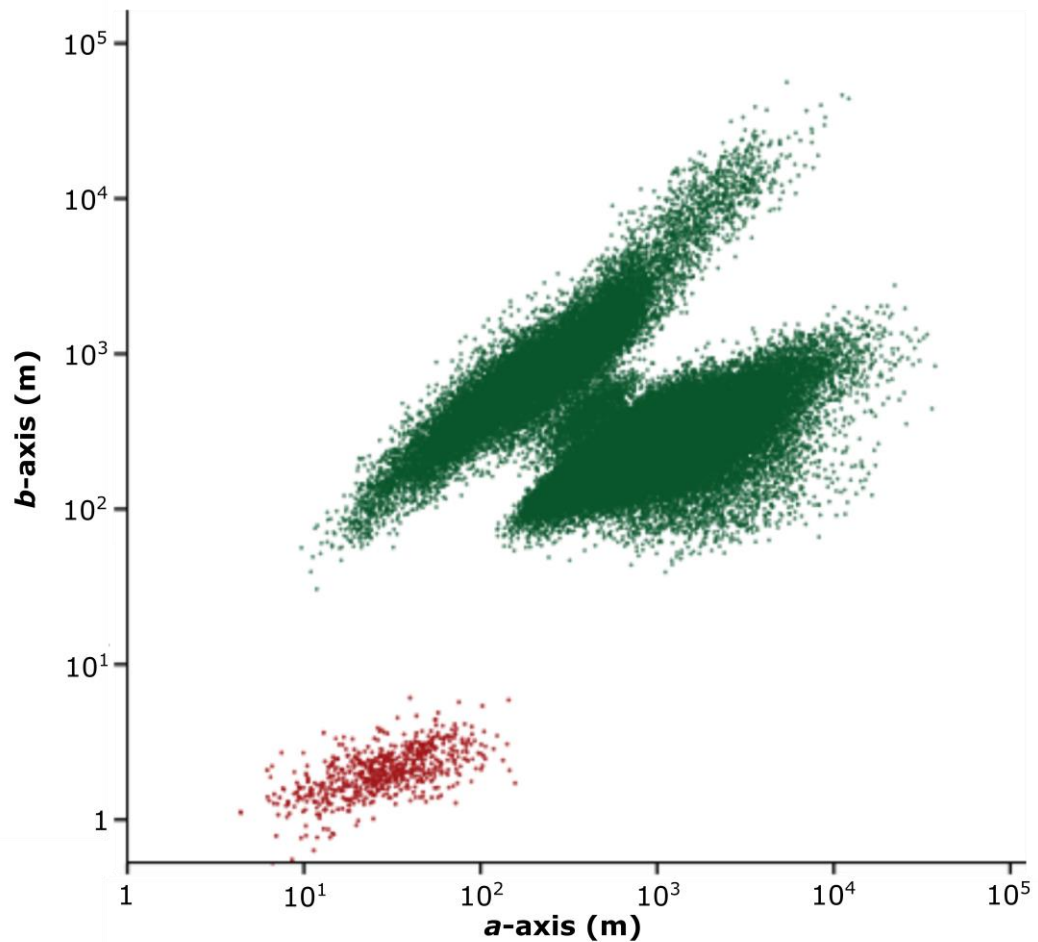


Figure 3.11. DBScan results. DBScan algorithm detects two clusters when the parameters  $\mathcal{E} = 0.25$  and  $\text{MinPts} = 100$  are used. Separate colours denote detected clusters. These results are typical for a wide range of input parameters (Figure 3.10).

### 3.4.2 Nomenclature Based Results.

Figure 3.12 shows the results of nomenclature based contouring of the dataset of subglacial bedforms. This reveals the group of small bedforms found in Section 3.4.1 to consistently plot separately to all other bedforms to be those commonly assigned the term “flute”. The distinguishing factor of flutes is their  $b$ -axis, which is much smaller than for all other subglacial bedforms, and has a narrow range and small measures of variance (Table 5). Overlap occurs between all other categories, as shown by the intersection of density contours belonging to adjacent categories (Figure 3.12). This overlap occurs between all neighbouring 95% density contours, and occurs between 95% and 75% contours with the exception of between quasi-circular forms and subglacial ribs.

The strongest overlap occurs between drumlins and MSGL, which for all parameter combinations occurs between adjacent 75% density contours. This area represents the densest portion of my dataset, as drumlins and MSGL are the highest sampled bedform type (Table 5) due to a higher frequency of occurrence within the literature and available datasets. The mean *b*-axis of the drumlin and MSGL categories is remarkably similar (Table 7), indicating a consistency between the two groups, and explaining why flow-aligned bedforms are detected as one single cluster in most analyses (Figure 3.10). The elongation ratio of ribbed moraines and mega-ribs is also similar, with low coefficients of variation (Table 7). This indicates a similar shape. The size range of quasi-circular bedforms is much narrower compared to all other subglacial bedforms, except for flutes. Additionally, the coefficient of variation for their size metrics is comparatively small, hence their selective positioning on Figure 3.9. The category of quasi-circular bedforms may contain bedforms some might categorise as either drumlins or ribbed moraines. However, the mean elongation ratio of 1.07 (Table 5), and the high density of points on Figures 3.9, 3.11 and 3.12 where the elongation ratio is 1, clearly indicates the existence of near-circular forms, despite their scarcity in the literature.

Figure 3.12. Contour plots to assess the degree of overlap between previously labelled bedform types. Flutes consistently plot separately to all other bedform types, whilst overlap between all other subglacial bedform types occurs. This overlap occurs between all neighbouring 95% density contours, and occurs between neighbouring 95% and 75% contours with the exception of quasi-circular forms and ribbed moraines.

		Range (m)	Minimum (m)	Maximum (m)	Mean (m)	Standard Deviation (m)	Coefficient of Variation
<b>Flute</b>	<i>a-axis</i>	138.1	6.5	144.6	36.7	22.6	0.6
	<i>b-axis</i>	5.6	0.3	5.9	2.3	0.9	0.4
	<i>Elongation</i>	41.0	5.19	46.18	15.96	7.10	0.44
<b>Mega-subglacial ribs</b>	<i>a-axis</i>	11765.4	393.6	12159.0	2317.1	1331.6	0.6
	<i>b-axis</i>	53940.1	2097.4	56037.4	10557.0	6239.7	0.6
	<i>Elongation</i>	0.55	0.07	0.62	0.24	0.10	0.40
<b>Ribbed Moraines</b>	<i>a-axis</i>	3683.6	9.7	3693.3	282.7	260.8	0.9
	<i>b-axis</i>	16749.8	30.6	16780.4	985.1	1006.7	1.0
	<i>Elongation</i>	0.75	0.06	0.81	0.29	0.11	0.37
<b>Circular Bedform</b>	<i>a-axis</i>	876.4	145.3	1021.6	434.8	134.3	0.3
	<i>b-axis</i>	1002.7	150.9	1153.5	422.8	133.3	0.3
	<i>Elongation</i>	2.64	0.39	3.03	1.07	0.29	0.27
<b>Drumlin</b>	<i>a-axis</i>	10602.1	99.3	10701.4	762.5	552.2	0.7
	<i>b-axis</i>	1509.7	35.7	1545.3	238.5	111.1	0.5
	<i>Elongation</i>	36.20	1.24	37.44	3.19	1.62	0.51
<b>MSGL</b>	<i>a-axis</i>	37268.2	177.4	37445.6	1795.51	2062.7	1.2
	<i>b-axis</i>	2725.8	38.94	2764.7	226.87	197.2	0.9
	<i>Elongation</i>	131.62	1.93	133.55	8.03	6.28	0.78

Table 7. Summary statistics of subglacial bedform categories.

### 3.4.3 Location Based Results

Figure 3.13 plots the outlines of the scatter clouds of each bedform locality shown in Table 5. No single location plots separately to all others, with all locations overlapping with locations which are adjacent on the plotting space. The abundance of overlapping areas within regions of the plot may explain many of the density variations visually apparent on Figure 3.9 (Section 3.4.1) as oversampling in these overlapping regions may have occurred due to two regions containing similar bedforms (i.e. Figure 3.5B).

Figure 3.13. Outlines of the  $a$ -axis and  $b$ -axis of bedform scatter plots grouped by location. Locations are listed in Table 5. Note the overlap between locations, such that data from no single location is found to be entirely unique.

### 3.5 Interpretation

Building on the definition provided at the start of Section 3.2, my interpretation of whether subglacial bedforms belong to a morphological continuum hinges upon whether a continuous sequence of size and shape measurements exists, or whether there is a perceptible difference between subglacial bedform morphology. In turn, this has implications for bedform formation theories.

#### 3.5.1 Flutes

Flutes are found to form a statistically distinct population to all other subglacial bedforms (Section 3.4.1; Figures 3.9, 3.11, 3.12). Given their smaller size, flutes were only visible on aerial photography (Tables 5 and 6). But, I do not believe the separation of flutes to be a consequence of higher resolution data being used for mapping. Instead, I interpret flutes to be morphologically distinct to all other subglacial bedforms. This interpretation is in line with other observations. Flutes are more narrow and elongate than other subglacial bedforms. They have been reported to reach over 1.5 km long, whilst maintaining their narrow width and thus achieving elongation ratios of  $> 500$  (Kjær et al., 2006). The juxtaposition in scale that flutes have with other subglacial bedforms is perhaps most apparent at the numerous localities they can be found superimposed on top of drumlins (e.g. van der Meer, 1983; Boulton, 1987; Hart, 1995; Rose, 1987, 1989; Schomacker et al., 2006; Waller et al., 2008). Furthermore, the scaling laws for drumlins show that they have a minimum bound of approximately 50-100 m wide (Clark et al., 2009; Figure 2.28), wider than any flute studied here. Thus, flutes are morphologically distinct from all other subglacial bedforms, and possess separate scale specificity (Evans, 2012). This interpretation quantitatively confirms the previous results of Rose (1987) and the interpretation of Clark (1993) (Figure 3.3A).

#### 3.5.2 Drumlins and MSGL

In contrast to flutes, the size and shape measurements of drumlins and MSGL overlap with each other. A lack of empirical data led Clark (1993) to differentiate drumlins and MSGL based upon a perceived difference in scale and frequency of occurrence (c.f. Figure 3.3). These flow-aligned bedforms are not separated by cluster analysis (DBSCAN) under any parameter combination tested (Figure 3.10). The geomorphological labels ‘drumlin’ and ‘MSGL’ show the greatest degree of

nomenclature overlap (Figure 3.12), and the  $b$ -axis and across-flow spacing of drumlins and MSGL is remarkably similar (Table 7; Spagnolo et al., 2014a). Figure 3.14A plots the  $a$ -axis and  $b$ -axis of drumlins and MSGL. A similar cone-shaped scatter cloud is found in comparison to Clark et al.'s (2009) plot of just drumlins, with MSGL merging into drumlins (Figures 3.11A and 20.24). Furthermore, the scale dependant maximum elongation limit reported for drumlins in Clark et al. (2009) is also apparent when MSGL are included, highlighting a further shared characteristic of drumlins and MSGL (Figure 3.14B; c.f. Stokes et al., 2013b). Thus, drumlins and MSGL are difficult to distinguish on the basis of  $a$ -axis,  $b$ -axis and elongation alone.

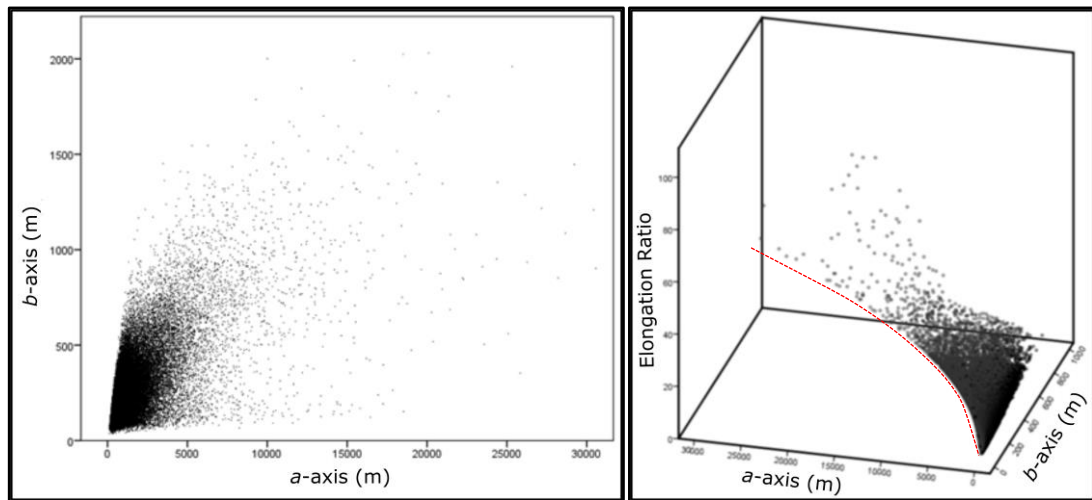


Figure 3.14. A) The  $a$ -axis and  $b$ -axis of drumlins and MSGL. Note the cone shaped distribution similar to Figure 20.24. B) The  $a$ -axis,  $b$ -axis and elongation ratio of subglacial bedforms. Red line highlights the size dependant elongation ratio limit of drumlins and MSGL, reported elsewhere (see text for references).

A second distinguishing factor proposed by Clark (1993) to differentiate MSGLs from drumlins was their straight parallel arrangement in a field. However, drumlins have been often noted to evolve spatially downstream into more parallel ‘MSGL-like’ forms (Aario, 1977; Briner, 2007; Graham et al., 2009), and features typically thought of as drumlin scale can be found in parallel alignment with much longer features (Stokes et al., 2013b), eliminating a distinction between drumlins and MSGLs. Instead, if I take the established relationship between subglacial lineation length and ice velocity (e.g. Hart, 1999; Briner, 2007) then perhaps their orientation and relative alignment mimics the direction of ice flow. Drumlins are more likely to be found under the converging flow of an ice stream onset-zone (e.g. Ó Cofaigh et al., 2002) and in fan shaped marginal settings (e.g. Greenwood et al., 2009a) where ice flow would be slower and radial. Conversely, longer ‘MSGL-scale’ subglacial lineations are more likely to be

found in the main ice stream trunk where ice flow is comparatively straight (e.g. Stokes and Clark, 2003).

The relief of drumlins and MSGL (not measured here, see Section 3.3), does differ if the two are considered as separate entities, with MSGL amplitude (mode = 2 m) being typically half that drumlin relief (mode = 4 m; Spagnolo et al., 2012; Spagnolo et al., 2014a). However, many drumlins also possess low amplitudes (Spagnolo et al., 2012), and features described as MSGL can be as much as 40 m in amplitude (e.g. Canals et al., 2000) and are commonly reported to be approximately 10 m (Clark et al., 2003; Heroy and Anderson, 2005; Ottesen et al., 2005; Graham et al., 2009). Given that the relief of a bedform may be a consequence of stochastic growth or shrinking (see Section 2.5.4 for discussion), the lower relief of MSGL could also be attributed to either a shorter duration of formation, or more erosional shrinking processes occurring during their development. Both of these interpretations complement the long-standing relationship between MSGL and palaeo-ice stream beds (Clark, 1993; Stokes and Clark, 1999; Margold et al., 2015), as the fast flow of ice streams means that bedform morphology may develop quickly, under conditions of high erosive potential and sediment transport rate. Overall, it is difficult to separate drumlins and MSGL purely on a morphological basis. Instead, I propose they form a larger population of subglacial lineations instead of being morphologically discrete entities. The implication this has upon deciphering their formation processes is discussed in Section 3.6.1.

### 3.5.3 Flow-transverse Bedforms

Subglacial ribs and mega-scale subglacial ribs also possess overlapping size and shape metrics (Figure 3.12), which are not separated by any of the tested DBScan parameters (Figure 3.10). Intriguingly, the most consistent metric within transverse scale bedforms is the elongation ratio of  $\approx 0.3$  with a small standard deviation and coefficient of variation for both 'normal-scale' and mega-scale subglacial ribs. Plots of length and width highlight this and the overlap that occurs between the two (Figure 3.15). The cone-shaped distribution of the scatter also highlights that scaling laws apply across the subglacial rib population in a similar manner to drumlins and MSGL (Section 3.5.2; Figure 3.11). Furthermore, there is a lack of a clear break or stepwise relationship in the metrics to suggest separate morphological populations. Thus, it is difficult to separate flow transverse bedforms based upon a purely morphometric basis.



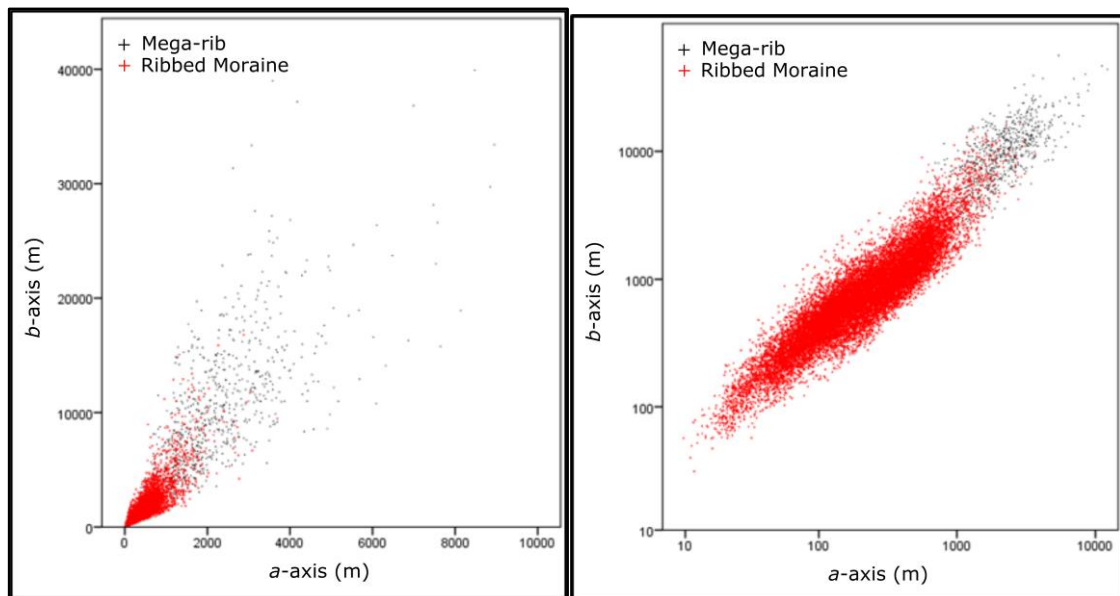


Figure 3.15. A)  $a$ -axis and  $b$ -axis of subglacial ribs. B)  $a$ -axis and  $b$ -axis of subglacial ribs with logarithmic axis to demonstrate the overlap of “normal-scale” and mega-scale subglacial ribs.

Spatially the relationship between mega-scale and ‘normal-scale’ subglacial ribs is more complex than that which occurs between drumlins and MSGL (Section 3.5.2). Mega-scale ribs have been observed in isolation (Klages et al., 2013). Transitions between different scales of transverse bedforms occasionally grade, but can also be abrupt, with superimposition of forms between the scales (Greenwood and Kleman, 2010). The lack of frequent observations of clear transitions may be a consequence of the relatively recent discovery of these features (Greenwood and Kleman, 2010), or their potential scarcity as their great size means that a large area of similar bedforming conditions is required to accommodate them. Elsewhere, subglacial ribs have been observed to occur in potentially evolutionary spatial sequences (Markgren and Lassila, 1980); arrangements reminiscent of transitions between drumlins and MSGL (see Section 3.5.2 and references therein).

Overall, subglacial ribs and mega-scale subglacial ribs are difficult to separate based upon their size and shape. Indeed, any subdivision of transverse subglacial bedforms based upon these factors is not apparent within my dataset (Figure 3.12). Yet further observations of subglacial rib morphology and relationship to other subglacial bedforms is required.

### 3.5.4 Quasi-Circular Bedforms

The existence of quasi-circular bedforms that overlap with drumlins and ribbed moraines (Figures 3.9, 3.10 and 3.12), raises the possibility of a single bedform

continuum comprising ribs to quasi-circular forms to lineations (e.g. Aario, 1977). All three are often categorised as one cluster by DBCAN (Figure 3.10B-J). When they are split into separate clusters by the quantitative analyses (Figure 3.10K-N) it may be a consequence of a genuine difference in the shape and scale of subglacial ribs and lineations (Figure 3.9D), and/or a small sample size of quasi-circular forms (Table 5). The bridging between ribbed moraines and drumlins provided by quasi-circular bedforms only occurs within a narrow range of length and width, centred around 450 m (Figure 3.9C). The existence of quasi-circular subglacial bedforms morphometrically links subglacial ribs and lineations, suggesting that the two could be linked forming a much larger morphological subglacial bedform population (Section 3.5.5).

Quasi-circular bedforms, such as the Blattnick moraine of Markgren and Lassila (1980), the mammillary hills of Aario (1977), the circular forms noted by Knight et al., (1999), and the ovoid forms noted by Smith and Wise (2007), are often reported in transition zones between ribbed moraines and drumlins. Quasi-circular forms were most notable in several locations across the bed of the Irish-Ice Sheet (Greenwood and Clark, 2008). Given their potential importance, further examples of quasi-circular bedforms were sought, and are shown in Figure 3.16. These examples illustrate how they occur in gradual downstream transitions between subglacial ribs and lineations, and sometimes super-imposed upon subglacial ribs. Since subglacial bedforms are often assigned a label based upon flow orientation, perhaps quasi-circular forms have been confusing to identify and classify and are more common than is reported in the literature. As they may form an important link between subglacial ribs and lineations, further work on quasi-circular bedforms is required.

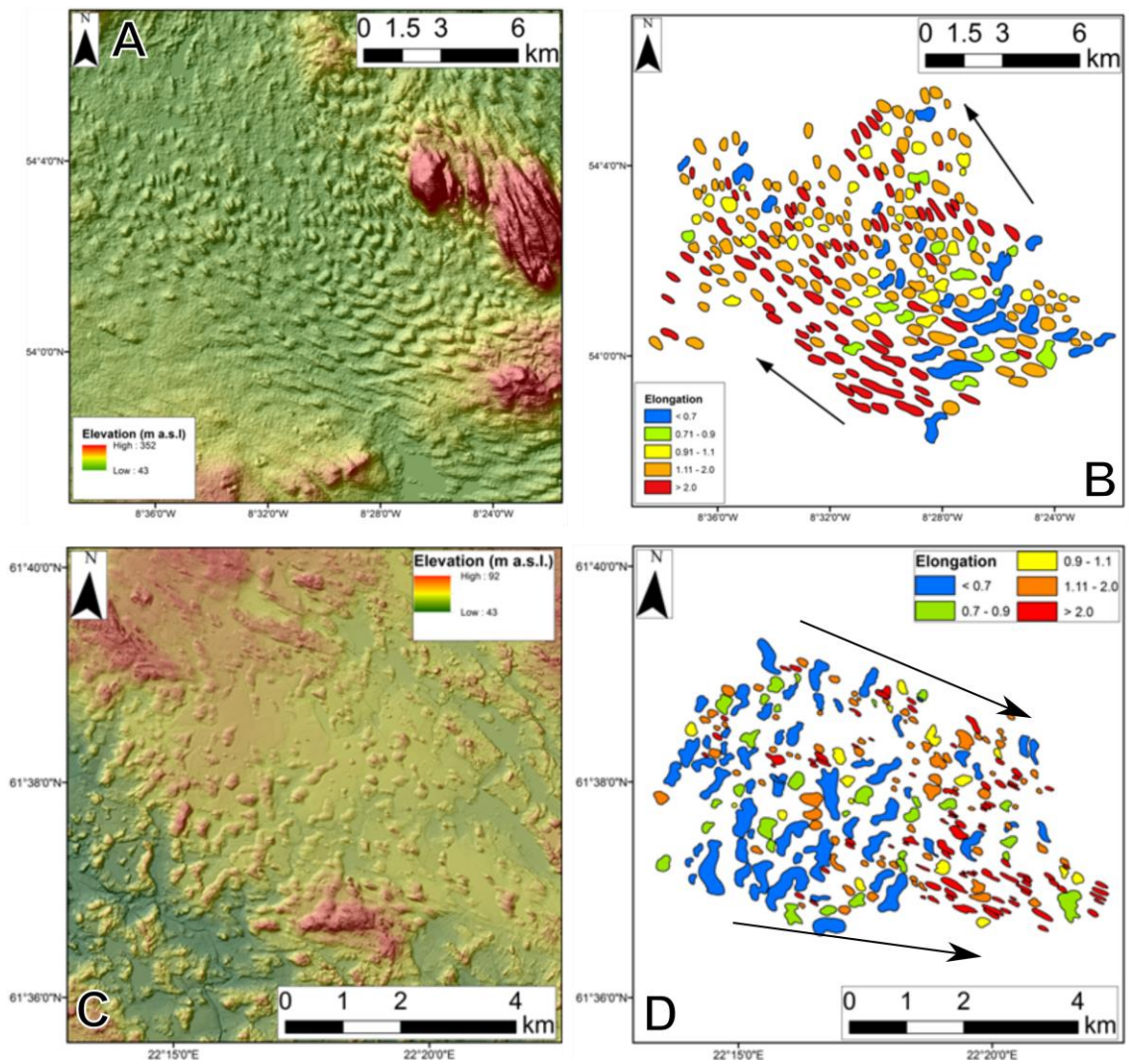


Figure 3.16. Examples of spatial transitions between ribbed moraines and drumlins. Arrows denote flow direction. Note how in each case, bedforms with no clear alignment to flow (elongation ratio of 0.9 to 1.1; yellow) were noted. A) Hill-shaded SRTM DEM (30 m) and mapping (B) of bedforms in County Roscommon, Ireland. C) 2 m LiDAR derived DEM and mapping (D) of bedforms near Harjavalta, Finland.

### 3.5.5 Subglacial bedform continua.

Returning to the definition at the start of this section (Section 3.5), two characteristics determine whether a continuum of morphology exists: i) whether the size and shape measurements collected were continuous, and ii) whether there is a perceptible difference between bedforms. Flutes clearly form a separate distinguishable morphological continuum to all other subglacial bedforms (Figure 3.12; Section 3.5.1), and thus do not belong to a morphological subglacial bedform continuum. Drumlins and MSGL represent the extreme ends of a morphological continuum of subglacial lineations (Section 3.5.2). In a similar manner, subglacial ribs also form a continuum (Section 3.5.2). These two are perceptibly different morphologically, divided by their alignment with flow direction. However, the presence of quasi-circular bedforms blurs this division. Many outputs from DBSCAN also connect subglacial ribs and subglacial lineations through quasi-circular forms (Figure 3.11), and the scatter clouds of quasi-circular forms also joins lineations and ribs (Figure 3.9). Yet, this morphometric realignment is abrupt, occurring at a specific scale, and not at one end of either the lineation or rib spectrum, retaining the perceivable distinction between the two.

Overall, I interpret my dataset of  $\approx 100,000$  subglacial bedforms size and shape to show there are three subglacial bedform continua: flutes, lineations and ribs. However, the latter two are linked by quasi-circular subglacial bedforms, creating a larger discernible population of subglacial bedforms. Further work is required to decipher the origin of quasi-circular bedforms and their role within a continuum.

The above interpretation has implications for the nomenclature used when referring to subglacial bedforms. The separate size and shape of flutes suggests that the term should specifically be applied to the narrow, elongate bedforms which often have a stoss-side boulder. However, the term flute (as well as ‘fluting’ or ‘mega-fluting’) is often misleadingly used to refer to bedforms of the same scale as drumlins and MSGLs (e.g. Colgan and Mickelson, 1997; Munro-Stasiuk and Shaw, 2002; Sutinen et al., 2010). As there is no distinction between drumlins and MSGL, or between ribs and mega-ribs, the continued utility of these terms is also questionable. I suggest that terms such as drumlins and MSGL should be referred to as subglacial lineations, but that the terms should be retained for descriptive and communicative purposes. By analogy, red

and orange are known to be colours arbitrarily placed upon a spectrum, but their use as terms is useful for describing and communicating.

## **3.6 Discussion and Implications**

### **3.6.1 Implications for Formation Hypotheses**

The literature on subglacial bedforms has led to a plethora of formation hypotheses (for reviews see Menzies, 1979; Shaw, 2010 and Clark, 2010). It is beyond the scale of this Chapter to review every hypothesis, but hypotheses can generally be placed into four categories: equifinite, bedform-specific, unifying and polygenetic (see Section 2). A complete bedforming hypothesis must account for both a bedform's morphology and the often complex array of internal structures (Patterson and Hooke, 1995; Stokes et al., 2011). Although the ultimate goal of any theory of subglacial bedforming would be to explain all facets of subglacial bedform formation, their morphological properties provide perhaps a more achievable first target. Thus, I focus upon the processes which give subglacial bedforms their size and shape, referring only passively to their internal composition.

The separate, statistically distinct (Figures 3.11 and 3.12), continuum formed by flutes suggests that a distinct bedforming process, or set of boundary conditions, is responsible for their genesis. Numerous bedform specific hypotheses exist for the formation of flutes. These broadly fit into the following categories: i) the lee-side cavity infill behind a lodged boulder (e.g. Hoppe and Schytt, 1953; Boulton, 1976; Morris and Morland, 1976; Eklund and Hart, 1996; Roberson et al., 2011); ii) lee-side cavity infill behind a boulder in a pervasively deforming till layer (Eklund and Hart, 1996; Hart, 1997; Hart and Smith, 1997); iii) deposition from a debris-rich basal ice layer (Gordon et al., 1992); iv) erosion by a ploughing till layer (Fuller and Murray, 2000); v) an instability in the coupled ice, sediment and water flow (Schoof and Clarke, 2008) or vi) cavity infill behind a stiff patch of sediment caused by differential frost heave (Baranowski, 1970).

The finding presented here, that flutes are much narrower than all other subglacial bedforms, suggests that the flute formation mechanism prevents flutes from growing wider. This scale specificity is most readily explained by lodged boulder often found on the stoss end of flutes, favouring hypotheses (i) and (ii) above which view flutes as a product of cavity development in the lee of this boulder. This is supported by measurements of flute morphology which show that flute metrics, especially width, are

often related to the size of a stoss-side boulder (e.g. Boulton, 1976, Åmark, 1980). However, such data are limited due to a lack of fieldwork and high resolution DEMs or aerial photography. It is harder to envisage how hypotheses (iii) and (iv), above, account for the scale specificity of flutes. Instabilities, invoked in hypotheses (v) and (vi) above, may have a preferential scale at which they form (see Section 2.2.1), accounting for flute scale-specificity. Currently, the hypothesis of Schoof and Clarke (2008) produces bedforms the scale of drumlins and MSGL, and therefore needs refinement to explain flute formation. Furthermore, the frost-heave instability infill mechanism (Baranowski, 1970) was created to account for flutes which lacked a stoss-side boulder. The prevalence of such flutes is currently unknown, and were not studied here. This hypothesis may be viewed as an extension of cavity infill mechanism, invoking stiff frozen sediment as an obstacle for cavity development instead of a boulder. Although further work is needed, I propose that the scale-specificity of flutes found here supports hypotheses of flute formation which invoke cavity infill behind a lodged boulder. Other obstacles may also create flutes where no boulder is present. As flutes likely form by processes separate to all other subglacial bedforms, the remainder of this discussion will focus upon the formation of all other subglacial bedforms.

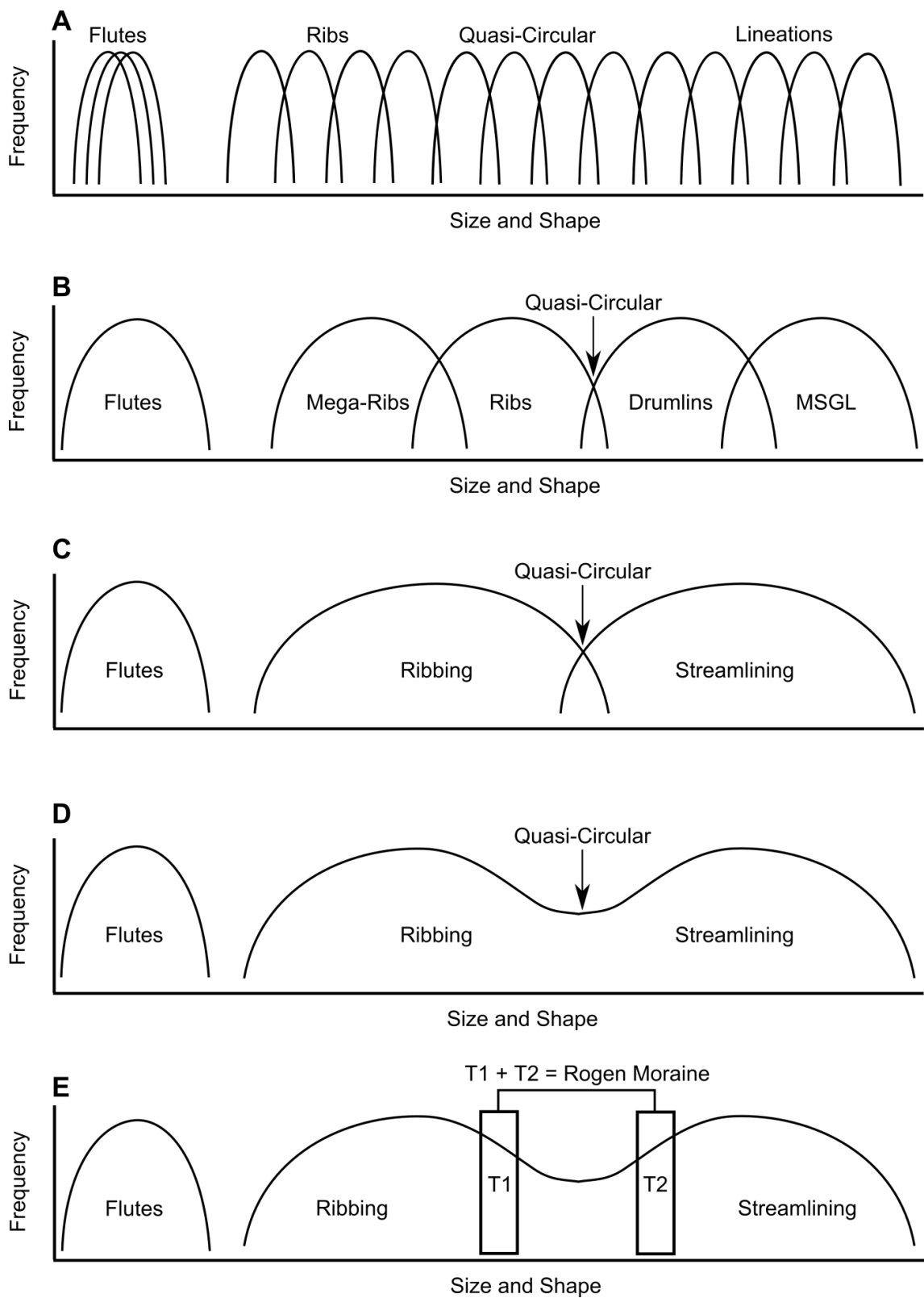


Figure 3.17. Schematic of how different types of bedform formation hypotheses may account for the subglacial bedform continua found here. (A) an equifinite interpretation. (B) a bedform specific interpretation. (C) an interpretation where ribbing and streamlining are separate. (D) a unifying hypothesis and (E) a polygenetic or polyphase hypothesis. See text for further details.

Under an equifinite interpretation, multiple processes (e.g. mega-flooding (Shaw, 2010), lee-side cavity infill (Dardis et al., 1984), thrust stacking (Bouchard, 1989)) could act to produce a continuum of ribs, circles and lineations (Figure 3.17A). Such a view is difficult to reconcile with the scale specificity displayed by subglacial lineation *b*-axis (Table 7), and the shape specificity of subglacial ribs. Equifinality would require each process to produce specifically scaled bedforms whose distribution of size and shape happen to overlap in order to replicate the observed results. As I view the continua of size and shape found here to represent commonality between my diversely located dataset of subglacial bedforms (Figure 3.13), I interpret my results to be least consistent with the equifinite category of subglacial bedform hypotheses.

A schematic of how a bedform-specific view could account for my findings is shown in Figure 3.17B. In addition to those which have been invoked for flutes, bedform specific views have tended toward explaining drumlins (e.g. Smalley and Unwin, 1968; Menzies, 1979; Boyce and Eyles, 1991; Hooke and Medford 2013), MSGs (e.g. Tulaczyk et al., 2001; Clark et al., 2003; Shaw et al., 2008) and ribbed moraines (e.g. Shaw, 1979; Aylsworth and Shilts, 1989; Bouchard, 1989; Hättestrand and Kleman, 1999) in isolation from each other. However, my results indicate that morphologically there is little distinction between most categories and transitions between clusters are often found, thus undermining the bedform-specific view. How can this justify the absence of stepwise changes in morphology that occur between different bedform ‘types’? For example, it is remarkable that *b*-axis would remain consistent between drumlins and MSG (Table 7) if formed by separated processes.

Under a unifying subglacial bedform formation hypothesis, the formation of all subglacial bedforms would be accounted for by the same process (e.g. a subglacial mega-flood (Shaw, 2010) or an instability in the coupled flow of ice-water and till (Fowler and Capwanya, 2014)), which produces different bedform sizes and shapes due to different boundary conditions. This unifying interpretation is consistent with the morphometric similarity of bedforms within a field, where one would expect similar glaciological conditions to have occurred. Formation by a single set of processes accounts for the similarity of bedforms found in diverse localities (Figure 3.13). Furthermore, observations of gradual spatial transitions in bedforms (Aario, 1977; Markgren and Lassila, 1980; Ó Cofaigh et al., 2002; Heroy and Anderson, 2005; Briner, 2007) suggests the evolution of a single process, rather than a jump between processes and bedform types.



Quasi-circular forms raise questions for the applicability of a hypothesis which seeks to explain the formation of ribs and lineations separately (e.g. Shaw, 2010; Fowler and Chapwanya, 2014). If we view the results of my cluster analysis (Figures 3.10 and 3.11) as showing that ribs and lineations are two separate continua (Figure 3.10 K-L), then quasi-circular bedforms could be the result of ribbing and lineating processes overlapping (e.g. Figure 3.17C). If this is the case, then a truly ‘unifying’ formation hypothesis (i.e. one that fully explains ribs, circles and lineations) is not required. Whilst overprinting and reconstitution of subglacial ribs by a later phase of drumlinsiation is clearly the case for some transition zones (e.g. Carl, 1978), others are more gradual (e.g. Dunlop and Clark, 2006b; Clark, 2010; Figure 3.16), suggestive of a progressive downstream evolutionary sequence. An alternative interpretation, which is more consistent with gradual transitions, is that the same bedforming process could manifest itself as both flow transverse and parallel bedforms in response to conditions at the ice-bed interface (e.g. Figure 3.17D). In this case, quasi-circular bedforms represent the transitory state of a single process, forming under the conditions where bedform realignment occurs. Further work is required to resolve whether a single formation mechanism can explain ribs, circles and lineations, or whether two are required.

Interestingly, circular forms of aeolian dunes have been observed on Earth and Mars (Figure 3.18) and were recreated in laboratory experiments. These forms also occur at a transition in bedform alignment. The fundamental process which governs the formation of these landforms (the movement of sand) does not change as bedform orientation changes. Rather, boundary conditions alter accordingly, for example wind direction (Rubin and Hunter, 1987) and formation time (Reffet et al., 2010). If these are analogous to subglacially produced quasi-circular bedforms, the fundamental process (the movement of sediment at the ice-bed interface) may not change between bedform reorientation, but boundary conditions may alter.

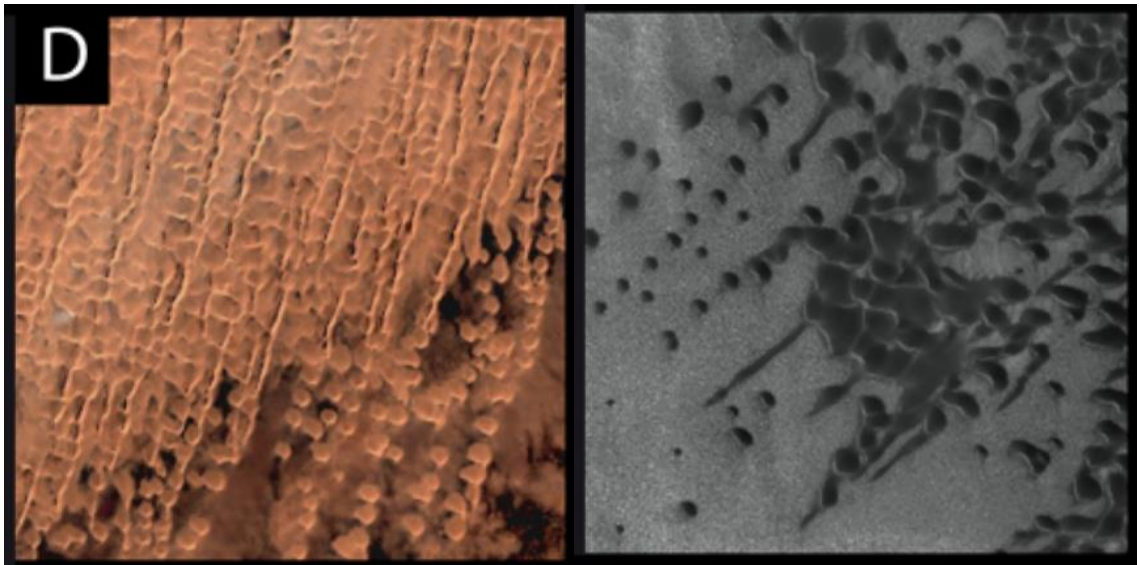


Figure 3.18. Satellite images of quasi-circular sand dunes on Earth (left) and Mars (right). Note the gradation from transverse to linear features. Adapted from Reffet et al. (2010) supplementary material item number 2010144 in the GSA Data Repository. Note the similarity of these images to Figure 3.2.

The nature of sediment at the ice-bed interface is undoubtedly a key parameter in ice-bed interaction (Alley, 1989; Piotrowski and Tulaczyk, 1999; Dunlop et al., 2008). A primary control upon bedform production is sediment supply, as without sediment bedforms cannot be created. However, the internal structure of subglacial bedforms can be entirely unrelated to the processes of bedform moulding (Patterson and Hooke, 1995; Stokes et al., 2011). Subglacial sediment movement is often confined to a layer that is less than a meter in thickness (Hooke et al., 1997; Kamb, 2001). Such minimal deformation thickness means that sediment formed prior to bedform formation can be preserved inside the bedform. Indeed, many drumlins display only a minimal veneer or carapace of deformed till (e.g. Whittecar and Mickelson, 1979; Boyce and Eyles, 1991; Menzies and Brand, 2007). Furthermore, sediment can be deposited and draped over bedforms subsequent to the processes that produced them (Finlayson, 2013; Spagnolo et al., 2014b). Hence, large proportions of the internal constituents of subglacial bedforms can be entirely unrelated to the processes of bedform moulding, recording instead the history of sediment deposition and erosion that has occurred in the area. Therefore, the vast array of internal constituents displayed by subglacial bedforms does not require that separate distinct processes produced the size and shape of the bedform that we observe today, indeed much of the inside of a bedform may be unrelated to the bedform moulding process. However, different sequences of events, occurring both before and after bedform shaping, could be preserved within a subglacial bedform, revealing a

history of processes at that locality, but not necessarily requiring a fundamentally distinct set of bedform shaping processes to have occurred. This is conceptually outlined in Figure 3.19. Stokes et al. (2013a) propose that sediment supply is a likely control upon whether erosional (Figure 3.19 B and D) or depositional (Figure 3.19 C and E) bedforms are created, but argue that this does not require a separate fundamental mechanisms. They propose that erosional bedforms occur where there is a net deficit of sediment into the system, and depositional forms occur when there is a net surplus. If the sediment budget at the ice-bed interface is negative for long enough (i.e. there is net transport of sediment out of the system), then sediment starvation may lead to exposed bedrock at the ice-bed interface, stopping subglacial bedform production. Therefore, the sediment budget may be an important control upon the sedimentology of subglacial bedforms, but erosional and depositional bedforms may not require separate bedforming mechanisms to explain their formation.

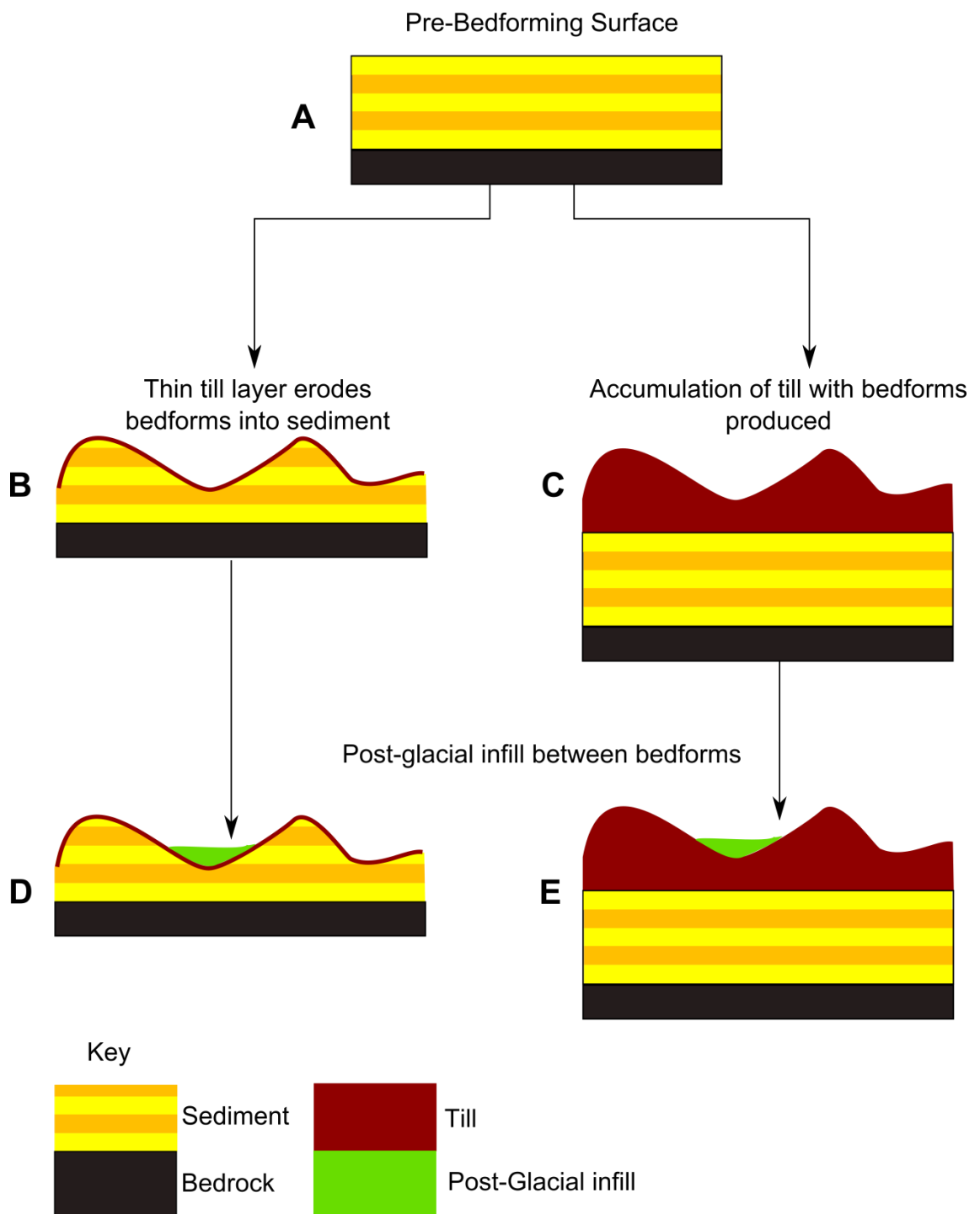


Figure 3.19. The relationship between sedimentology and bedform shaping processes. Based upon Stokes et al. (2013a). A) Initial surface and horizontally bedded structure. B) Erosional thin till later preserves pre-formational sediments, unrelated to the bedform formation process. C) Accumulation of till on top of preserved sediments. D) and E) post-glacial infill can also be added, unrelated to bedform shape defining process.

Often viewed as diametrically opposed to unifying formation hypotheses (e.g. Möller, 2006; Sutinen et al., 2010), polygenetic hypotheses require multiple phases of

bedforming to occur in order to account for the sequence of events recorded in the sedimentary archive of a subglacial bedform (Kurimo, 1980). However, I propose that such a view is not incompatible with a set of unifying processes from which the size and shape of subglacial bedforms originate (Figure 3.17E). Instead, polygenetic bedforms may be formed by a sequence of such processes, interrupted by non-bedforming phases and processes. This would explain the stratigraphic successions and hiatuses found within bedforms (e.g. Newman et al., 1990; Zelčs and Dreimanis, 1997), yet retain the simplest explanation for the morphological continua found here (Figure 3.9; Figure 3.17D). For example, Rogen moraines (a type of ribbed moraine which often transitions into drumlins (Lundqvist, 1969)) have been proposed to form via an initial stage of ribbing, then later streamlining (Lundqvist, 1989; Sarala, 2006). Such a history of development does not require a set of distinct bedforming processes to have occurred at this locality, but rather a different sequence of events caused by a change in boundary conditions at the ice-bed interface (e.g. Figure 3.17E).

The sediments which record the processes which gave the bedform its original size and shape may also be contaminated with subsequent deposition (e.g. Figure 3.19). For example, a bedform may be draped with melt-out till during deglaciation (e.g. Aario and Peuraniemi, 1992; Möller, 2010), or inter-bedform areas may be partially infilled with Holocene sediments (e.g. Spagnolo et al., 2014b). Both of these processes are unrelated to the processes which originally gave the bedform its size and shape, and are therefore unrelated to the phase of bedform genesis which initiated a subglacial bedform at the ice-bed interface. Furthermore, if a phase of bedforming does not reconstitute pre-existing sediment, pre-existing structures within subglacial bedforms may be preserved (c.f. Stokes et al., 2013a), such as stratified sediments (e.g. Boyce and Eyles, 1991; Jørgensen and Piotrowski, 2003) or pre-existing moraines (e.g. Möller, 2006); an interpretation which is consistent with a thin layer of mobile subglacial sediment (e.g. Hooke et al., 1997; Kamb, 2001). Thus, I propose that bedforms which record a history of development are more adequately described as polyphase, rather than polygenetic.

### 3.6.2 Controls on the Size and Shape of Subglacial Bedforms

A correspondence between bedform size and shape and the flow characteristics of the geomorphic agent is often invoked for aeolian, fluvial and marine bedforms (Allen, 1968; Rubin and Ikeda, 1990; Reffet, 2010). Similar links have been sought for subglacial bedforms (e.g. Rose and Letzer, 1977). There are several lines of evidence

that suggest that subglacial bedform size and shape is primarily determined by properties of the overlying ice mass. Firstly, bedforms within a flowset are usually morphometrically similar (Clark, 1999). Thus, different flow events, with different glaciological properties, produce different bedform morphologies. Secondly, bedforms are often observed to evolve gradually along former ice flow trajectories. Such evolutionary sequences can take the form of increases in the elongation of lineations (e.g. Ó Cofaigh et al., 2002; Stokes and Clark, 2002; Briner, 2007; Stokes et al., 2013b) or a switch from ribs to drumlins (e.g. Figure 3.16; Aario, 1977; Aylsworth and Shilts, 1989; Dyke et al., 1992; Knight et al., 1999; Dunlop and Clark, 2006b). Both of these situations have been interpreted to indicate ice acceleration along flow, particularly in ice stream settings (Aario, 1977; Hart, 1999; Ó Cofaigh et al., 2002; Stokes and Clark, 2002; Briner, 2007; Stokes et al., 2013a). Support for this is found from modern ice streams where drumlins have been observed beneath the onset zone of Rutford Ice Stream (King et al., 2007) and MSGs further down flow where ice velocity is higher (King et al., 2009). Subglacial ribs can also be found in evolutionary sequences (Markgren and Lassila, 1980; Greenwood and Kleman, 2010), suggesting a gradual change in boundary conditions, potentially induced by ice flow properties. Thirdly, bedform morphology conforms strongly to glaciological variables at the ice sheet scale, with factors such as lithological changes in the bed exerting a smaller and more localised influence (Greenwood and Clark, 2010). Therefore, the size and shape of subglacial bedforms in an area may be predominately determined by the properties of the ice under which they formed.

Sedimentological factors have been proposed to influence bedform morphology. At a local scale, abrupt changes in sedimentological properties have been shown to correspond to shifts in bedform morphology (Rattas and Piotrowski, 2003). Although sediment is required to form a subglacial bedform, the influence of sediment supply upon bedform morphology is difficult to discern. Often, where there is a boundary between thin till draped over hard bedrock and abundant soft deformable marine sediment, there is a corresponding increase in bedform elongation (e.g. Wellner et al., 2001, Ó Cofaigh et al., 2002). Given that deformable sediment can accommodate accelerated ice flow (Alley et al., 1986), this sedimentological property is hard to distinguish from palaeo-ice velocity, as the increase in elongation may also be interpreted as an increase in ice velocity (Stokes and Clark, 2002). Furthermore, both drumlins and MSGL record sequences of net till accretion (e.g. Newman and

Mickelson, 1994; Spagnolo et al., 2014b; Spagnolo et al., 2016) and erosion (e.g. Boyce and Eyles, 1991; Ó Cofaigh et al., 2013). This means that there is no simple link between bedform morphology and sediment supply.

The most commonly invoked glaciological control on subglacial bedform morphology is ice velocity. Ribbed moraines are typically found near ice divides or cold based regions (Hättestrand, 1997), or on ice stream beds where they have been inferred to record deceleration immediately prior to ice stream shutdown (Stokes et al., 2008). This suggests slower ice flow is associated with their formation, even if the precise mechanisms are unknown. Drumlins are found further away from ice divides, and in the onset zones of palaeo (Stokes and Clark, 1999; Anderson and Fretwell, 2008) and contemporary (King et al., 2007) ice streams, whereas more elongate subglacial lineations (MSGs) have been associated with ice streams (Clark, 1993; 1994; Stokes and Clark, 1999; King et al., 2009; Spagnolo et al., 2014a). Therefore, ice velocity seems to be a primary influence upon bedform orientation and elongation within and between ribs and lineations.

### 3.6.3 Comparison to the Instability Hypothesis

Although the mega-flood hypothesis can explain the three subglacial bedform continua found here, it has been widely discredited (Evans, 2000; Clarke et al., 2005; Evans et al., 2006; Ó Cofaigh et al., 2010; Livingstone et al., 2013). My interpretation also finds it highly unlikely that a plethora of separate processes act to initiate the formation of subglacial bedforms (Section 3.6.1). Therefore, a non-equifinite interpretation of the results presented here is arguably most compatible with the Hindmarsh-Fowler instability hypothesis of subglacial bedform formation (Hindmarsh, 1998b; Fowler, 2000). Additionally, the instability hypothesis is the only theory which produces testable predictions of bedform size and shape.

Rather than being the consequence of separate processes, the instability hypothesis views the range of subglacial bedforms produced to be a combination of different instabilities in the coupled flow of ice, water and sediment (Fowler, 2000). Subglacial ribs are hypothesised to form as fluctuations in the deformation of subglacial till develop (Hindmarsh 1998a, 1998b and 1998c). Numerical modelling of this instability already successfully replicates the array of subglacial rib sizes found here (Dunlop et al., 2008). Subglacial ribs are produced only when a static, background hydrological system is considered (Chapwanya et al., 2011). Conversely, MSGs are

thought to form under a more dynamic subglacial hydrological system, with higher water fluxes and the formation of subglacial streams between subglacial bedforms (Fowler, 2010b). Modelling of this system again produces results consistent with MSGL morphology (Stokes et al., 2013b; Spagnolo et al., 2014a). Between these two extremes, the formation of subglacial ribs would provide a barrier to water flow (Fowler, 2010a), which when intersected by subglacial streams or areas of wetter till would cause the formation of drumlins.

Recently, Fowler and Chapwayna (2014) combined the subglacial ribbing and MSGL forming instabilities to model three dimensional subglacial bedforms (i.e. drumlins). Here, the dominant wavelength of the instability produced at the ice-bed interface (or the type of bedform) is a function of subglacial conditions, particularly the distance between supporting clasts within the sediment matrix, a function of subglacial water thickness and sediment granulometry (Creys and Schoof, 2009). Remarkably, the results of Fowler and Chapwayna (2014) predict subglacial bedform morphologies similar to that of the measured subglacial bedforms here (Figure 3.20). Since the amount of water and the form of the subglacial hydrological system is a key determinant of ice velocity (Alley, 1989; Piotrowski and Tulaczyk, 1999), it is plausible that future research may be able to link the modes of subglacial drainage proposed by the instability hypothesis and ice velocities in the manner postulated in Section 3.6.2.



Figure 3.20. Predicted growth rates of bedforms for different subglacial conditions by the instability theory. Note the similar positioning of maximum growth rates to the size and shape of bedforms on Figure 3.9. From Fowler and Chapwanya (2014). Darker (redder) colours are higher predicted growth rates.

In its current form, the instability hypothesis does not account for the clear separation of flutes from other subglacial bedforms (Figure 3.12). If flutes form under thinner ice than all other subglacial bedforms (see Section 3.6.2), then perhaps lower overburden pressures and less pervasive deformation result in the formation of flutes. Otherwise, additional instabilities, or modes of sediment transport under other subglacial boundary conditions may have to be incorporated acting under other subglacial conditions in order to account for this (e.g. Schoof and Clarke, 2008).

The current instability hypothesis model has yet to be solved numerically in a manner in which it can make full predictions of ice-bed interface evolution (e.g. Chapwanya et al., 2011). Once this step has been achieved, the model should then consider the role of stationary objects, such as stiff till or bedrock, and how both erosional and depositional bedforms can be built, potentially by altering sediment

supply. Then the model will both account for the morphological and sedimentological properties of subglacial bedforms.

### **3.7 Summary and Conclusions**

The size and shape of  $\approx 100,000$  subglacial bedforms reveals there to be three main subglacial bedform continua. Flutes are much narrower than all other subglacial bedforms, forming a distinct size and shape continuum. Subglacial ribs and subglacial mega-ribs merge to form a size and shape continuum which is distinct in orientation from the continuum of subglacial lineations displayed by drumlins and MSGL. These latter two continua, ribs and lineations, are bridged by the presence of quasi-circular subglacial bedforms which tend to occur spatially between subglacial ribs and subglacial lineations. Subglacial ribs have a preferred shape, whilst subglacial lineations have a preferred width. The spatial distribution of subglacial bedforms and the morphological similarity of bedforms within a field is interpreted as evidence against equifinite interpretations of subglacial bedform formation. Furthermore, bedform specific hypotheses fail to account for these aspects of bedform size and shape. Unifying hypotheses, such as the Hindmarsh-Fowler instability hypothesis, may be more fruitful for explaining the subglacial bedform continua discovered here. However, future work should reconcile morphological and theoretical considerations of subglacial bedforms with sedimentological studies.

## Section B: Insights into the Characteristics and Formation of Ice Sheet Surface Flow Signatures.



Section B: Landsat ETM+ mosaic image of the surface of Byrd Glacier, West Antarctica. Ice flow is toward the bottom left of the image. Note the structures aligned with and transverse to flow direction.

Source: <http://lima.usgs.gov/>

# Chapter 4 Antarctic Surface LSSs: Insights into their formation arising from analysis of their morphology and glaciological context

## 4.1 Introduction

The surface of an ice sheet is covered in morphological features which are the result of ice flow (Section 1.2.2. and Table 1). Perhaps the most pervasive of these features are longitudinal surface structures (LSSs); flow parallel curvilinearities that persist for great distances along ice flow. Often, LSSs are also referred to or distinguished as flowstripes, foliations, streaklines, flow-bands or flow-lines (Crabtree and Doake, 1980; Fahnestock et al., 2000; Merry and Whillans, 1993; Reynolds and Hambrey, 1988; Swithinbank et al., 1988). Since LSSs are associated with fast flowing ice, and ice streams (Fahnestock et al., 2000), their formation is pertinent to understanding fast glacial regimes, and may be able to tell us about conditions at the ice-bed interface (Gudmundsson et al., 1998). Furthermore, LSSs observed on the interior of the Antarctic ice sheet (Conway, et al., 2002) and on ice shelves (Catania et al., 2012) have been used to infer previous switches in ice flow direction. Their origin remains debated (Glasser and Gudmundsson, 2012).

Whilst LSSs have been considered theoretically (e.g. Gudmundsson et al., 1998) and are frequently included in structural maps (e.g. Glasser and Scambos, 2008; Holt et al. 2013a), little work has been conducted to define their morphology, the conditions under which they form and how their properties change spatially. Such a task is important as it provides constraints for any model of LSS formation, and may provide further insight into their formation. Here I adopt a remote sensing and GIS-based approach to the study of LSSs. I create a database of mapped LSSs from which I study the morphology of LSSs and the glacial conditions under which they form. This enables testing of current formation hypotheses of LSSs and to suggest a model for their formation.

## 4.2 Background

The ubiquity of LSSs on the ice streams, outlet glaciers and ice shelves of the Antarctic ice sheet was first evident from Landsat imagery and aerial photography (e.g. Crabtree and Doake, 1980; Dowdeswell and McIntyre, 1987; Reynolds and Hambrey, 1988; Ferrigno et al., 1994). LSSs over 100 km in length have been mapped on satellite



imagery (Glasser and Scambos, 2008) and can occasionally start at the ice stream onset zone and reach the calving front (Glasser et al., 2015). Thus, LSSs can persist for long distances along ice flow, crossing the grounding line and continuing upon the ice shelf (e.g. Figure 4.1).

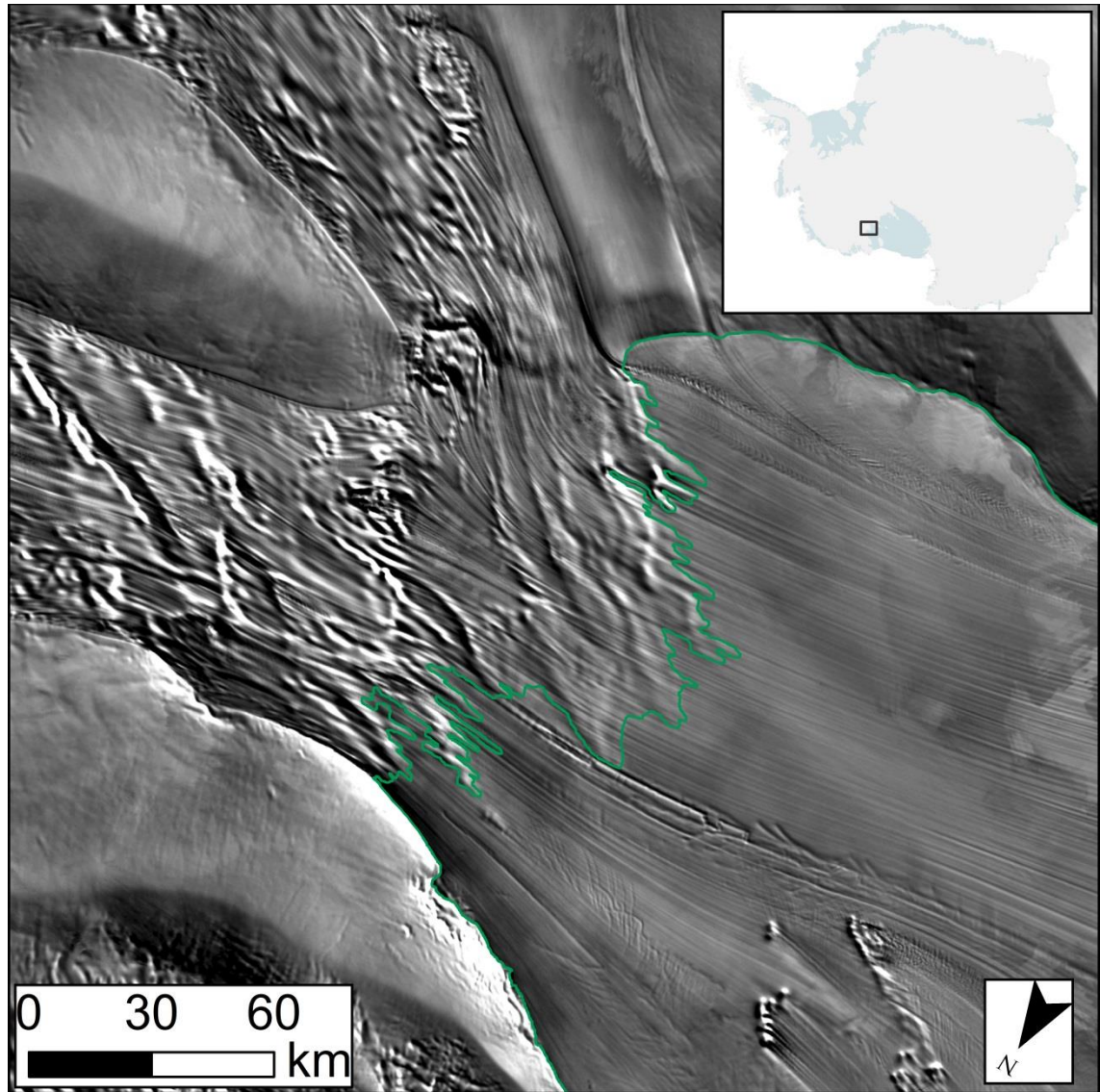


Figure 4.1. MODIS image of LSSs crossing the grounding line (green) at the mouth of the confluence between the Bindschadler (upper) and MacAyeal (lower) ice streams. Ice flow towards the lower right.

The along flow persistence and long residence time on the ice (Casassa and Whillans, 1994) makes LSSs useful tools for deciphering palaeo-ice flow regimes. On grounded ice, relict LSSs exist as muted expressions of previous rapid flow, documenting palaeo ice flow configurations (e.g. Conway et al., 2002). Thus, LSSs have been used to identify a relict tributary to the Kamb Ice Stream (Jacobel and Gades, 1995), are evident on the stagnant Kamb Ice Stream itself (Scambos and Nereson, 1995;

Anandakrishnan et al., 2001) and have been used to infer flow across the Bungenstock ice rise during the last glacial maximum (Siegert et al., 2013). As LSSs cross the grounding line, they are advected along with the ice shelf parallel to flow direction (e.g. Figure 4.1) where they can persist for hundreds of years (Casassa and Whillans, 1994). Thus, where deviation from this flow parallel configuration occurs, a corresponding change in the stress patterns during the residency of the LSSs upon the ice shelf must have occurred (Fahnestock et al., 2000). Using this principle and ice flow velocity data, Fahnestock et al. (2000) were able to reconstruct the variability of flow from ice streams flowing into the Ross Ice Shelf. LSSs upon the Stancomb-Wills Ice Tongue have also been used to infer flow direction and corresponding grounding line shifts (Wuite and Jezek, 2009). Contrary to the above changes to ice flow configuration inferred from LSSs, elsewhere the long residence time of undisturbed LSSs has been used to argue that the flow configuration of the Antarctic ice sheet has remained unchanged for several thousand years (Glasser et al., 2015). However, since the formation of LSSs is as yet an unresolved topic, the assumptions of reconstructions based upon LSSs may be invalid.

Two main hypotheses have been proposed regarding the formation of LSSs. The first views LSSs as the product of stresses imposed on ice, mainly by lateral variations in ice flow geometry (Reynolds and Hambrey, 1988; Hambrey and Dowdeswell, 1994; Hambrey and Glasser, 2003); the second sees LSSs as the transmission of basal bumps to the ice surface (Gudmundsson et al., 1998). Under the first hypothesis, the main mechanism via which LSSs are formed is analogous to that of longitudinal foliations found on valley glaciers (Figure 4.2). Foliations form where ice convergence causes lateral compression and longitudinal extension of glacier ice (Figure 4.3). This causes the ice to fold exposing pre-existing inhomogeneity's, such as primary stratification (e.g. Hambrey, 1975; Hooke and Hudleston, 1978; Hambrey and Lawson, 2000, p.70). Importantly, this creates three dimensional features within the ice. Thus, only where the three-dimensional nature of LSSs can be demonstrated (i.e. bare ice regions) can a LSS be labelled as a foliation (e.g. Dowdeswell and McIntyre, 1987; Hambrey and Dowdeswell, 1994; Glasser et al., 2015). Once formed, foliations advance down ice, such that their morphology reflects cumulative strain (Hambrey and Milnes, 1977; Hudleston and Hooke, 1980). This process is the same as that responsible for the formation of foliations in rock, arguably making glacier surfaces the ideal place to study such deformation features as they evolve on a much shorter timescale (Hudleston and

Hooke, 1980; Hambrey and Lawson, 2000). The compression hypothesis predicts that regions of high lateral compression to have more LSSs which are tightly spaced, producing variability between different flow units (Jennings et al., 2014). Furthermore, since higher compression would occur, more LSSs are expected where two glacier tributaries converge and at the edges of a flow unit (Glasser and Gudmundsson, 2012).

Figure 4.2. Longitudinal foliations on the surface of Comfortlessbreen, Svalbard. Photo M.J. Hambrey (1978). Note the juxtaposition between these meter-scale features and those on Figure 4.1. Source: <http://www.swisseduc.ch/glaciers/glossary/foiliation-en.html>

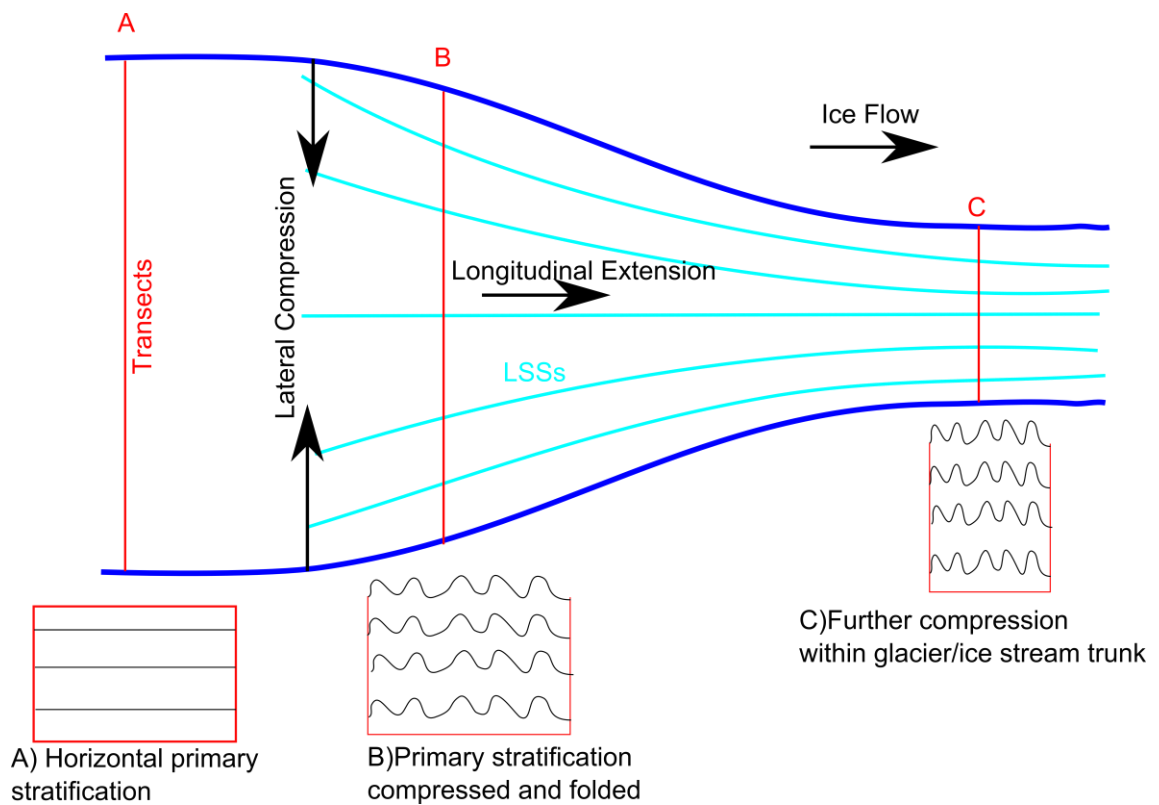


Figure 4.3. The lateral compression hypothesis of LSS formation. The squeezing of ice into an ice stream or outlet glacier causes topographic perturbations through folding of the ice. Upper portion of figure shows the surface of the ice, with lower panels showing hypothetical cross sections through the ice. At (A), ice layers from primary stratification are horizontal. These become folded (B) as the ice stream or glacier narrows (C). N.b. other inhomogeneities may also be modified to create foliations.

Two further mechanisms by which LSSs can form as a response to ice stress have also been proposed. Firstly, Glasser and Gudmundsson (2012) suggest that a separate type of LSS forms where either two glacier tributaries converge or in the lee of nunataks. Here there is longitudinal extension in the horizontal plane, and shear between ice masses flowing at different speeds (Figure 4.4). They argue that these LSSs are morphologically distinct as they are narrower and more clearly delineated than other LSS features, and bear no relationship to ice thickness (Glasser and Gudmundsson, 2012). Secondly, Merry and Whillans (1993) propose that LSSs are caused by localised high shear strain rates at the onset zone of an ice stream can also cause LSSs to form, so that they may form by acceleration and attenuation independent of convergence.



Figure 4.4. Development of a LSS at the confluence of two ice masses. A surface depression is created due to lateral shear between the two differentially moving ice masses. Figure from Glasser and Gudmundsson (2012).

Another mechanism for the formation of LSSs was proposed by Gudmundsson et al. (1998) who viewed LSSs as the result of rapid basal sliding across uneven topography (Figure 4.5). Here, the ice acts as a band-pass filter selectively transmitting bumps with a wavelength comparable to that of ice thickness to the surface of the ice (Gudmundsson et al. 1998; Schoof 2002). Undulations with a wavelength 3-10 times the ice thickness are most effectively transmitted to the surface (Gudmundsson et al. 1998; Gudmundsson et al., 2003). According to this theory, this process only occurs where there is a high ratio of sliding to internal deformation, as expected within an ice stream. The corresponding undulation that is transmitted to the surface is then attenuated downstream to form a LSS. Therefore, under this hypothesis, LSSs should only occur in regions of rapid basal sliding and their presence or absence should relate to variations in bed topography.

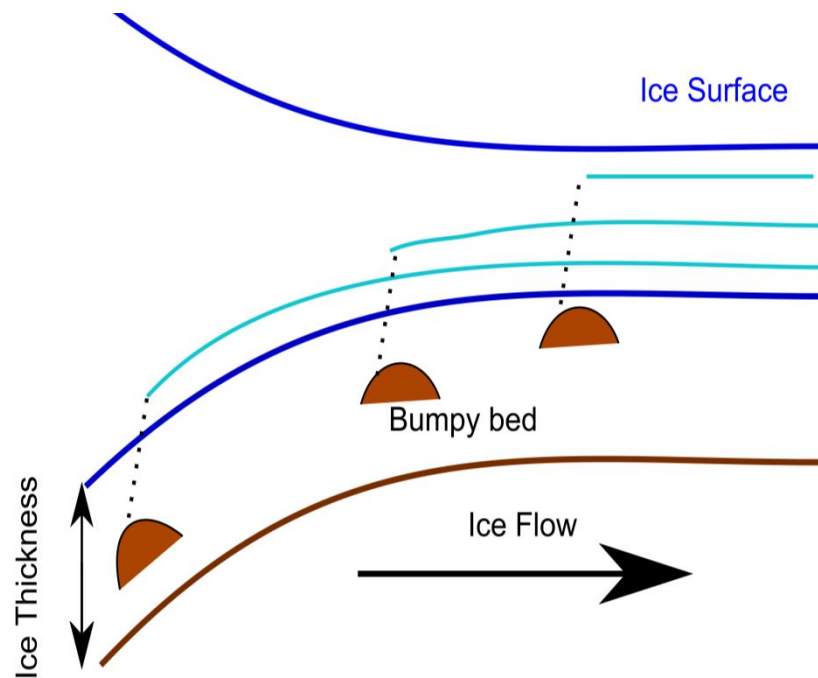


Figure 4.5. The basal transmission hypothesis of LSS formation. Bumps of a certain wavelength are transmitted to the surface of the glacier as the ice slides over them. This produces an ice surface bump which is translated downstream.

Beyond the two main mechanisms proposed for LSS formation, a further hypothesis is that LSS represent vertical bands of aligned crystal fabric (Hulbe and Whillans, 1997; Whillans and Van der Veen, 1997). Such changes in ice crystal fabric would introduce spatial variations in velocity (e.g. the “shear zones” of Raymond, 1996). However, velocity data of Byrd Glacier found no discontinuities between different LSS structures (Casassa and Brecher, 1993). Furthermore, LSSs do not narrow downstream (Glasser and Gudmundsson, 2012), as is predicted by Hulbe and Whillans (1997). Therefore, the lateral compression hypothesis (Hambrey and Dowdeswell, 1994; Hudlestone and Hooke, 1980) and the basal transfer hypothesis (Gudmundsson et al., 1998; Schoof, 2002) are the most feasible current hypotheses to explain LSS formation.

## 4.3 Methods

### 4.3.1 Mapping

LSSs were mapped via on-screen digitisation at multiple scales. Cloud-free Landsat ETM+ pan sharpened images of the Antarctic ice sheet are freely available for the region of Antarctica north of 82.5°S, and possess a pixel resolution of 15 m

(<http://lima.usgs.gov/>). Multiple band combinations were used in this study, adjusted in order to maximise feature identification. RADARSAT Antarctic Mapping Mission-2 SAR images have a slightly lower resolution of 25 m, but are freely available for the entire continent (<http://bprc.osu.edu/rsl/radarsat/data/>). Additional mapping was conducted on the MODIS Mosaic of Antarctica (<http://nsidc.org/data/nsidc-0280.html>). The multiple illumination angles composited into the mosaic allow for greater identification of subtle features. However, MODIS data have lower spatial resolution (250 m), meaning smaller features, typically found on valley glaciers, are unidentifiable in the data. Additionally, the oblique look angle of the MODIS satellite precludes mapping in valleys, as imagery is often obscured by valley walls. Although the resolution and sensor properties of the three sources of data all vary, in many places across Antarctica the images show high levels of agreement in terms of number of identifiable features, their distribution and alignment (e.g. Figure 4.6).

The subtlety of LSSs makes their identification problematic. Adaptive contrast stretching (i.e. using local image statistics) was utilised in order to enhance the satellite images. Longitudinal surface structures were mapped along their perceived crest (i.e. the point of highest reflection or backscatter values). Often, features were interrupted by crevassing or by other surface features, only to reappear down-stream (e.g. Figure 4.7). On ice shelves, this included disruption by features which have been interpreted to be the surface manifestation of subglacial channels (LeBrocq et al., 2013; Figure 4.7C). Along their great length, occasionally features would also fade out. Frequently, a second feature may reappear aligned with the original downstream, giving the impression of longitudinal surface structures fading in and out of focus. As it would introduce ambiguity into my mapping, features were not joined across such interruptions. Whilst the higher resolution datasets (Landsat and RADARSAT) were preferred for mapping, all three sources were used to increase the likelihood of identifying features. My map is genesis blind, labelling features as only LSSs, rather than classifying into separate groups.

Figure 4.6. Comparison of the three sources of data used for mapping. Images of Ice Stream D, ice flow is from the top left of the image to bottom right. A) Landsat ETM+ image (15m resolution). B) RADARSAT SAR image (25m resolution). C) MODIS mosaic image (125m resolution). Features in this area are possibly clearest upon the MODIS imagery. However, there is a high level of agreement between all the images.

Figure 4.7. Examples of disrupted longitudinal surface structures. Disruptions labelled with arrows. A) Landsat image of crevassing disrupting longitudinal surface structures as ice flows from Lepekhin Glacier towards the top right of the image onto the Amery Ice Shelf. B) Landsat image of transverse waves (see Chapter 6) interrupting longitudinal surface structures on Recovery Glacier. Ice flow is toward the bottom left of the image. C) MODIS image an ice shelf surface channel emanating from Slessor glacier, disrupting longitudinal surface structures on the Filchner Ice Shelf (formation discussed in Le Brocq et al. (2013)).

The subtlety of longitudinal surface structures may preclude their identification in the field, which makes ‘ground-truthing’ problematic. An alternative approach is to compare the satellite data in which I perceive a map-able relief to high resolution elevation models of relief. Figure 4.8 shows a comparison between Landsat data and a 2 m resolution LiDAR derived DEM of Taylor glacier (downloaded from [http://nsidc.org/data/antarctic\\_dem.html](http://nsidc.org/data/antarctic_dem.html)). Figure 4.8 also presents a comparison between mapping from the two data sources. Visually, LSSs on the Landsat image (Figure 4.8A) and the hill-shaded digital elevation model (Figure 4.8B) are similar. When the two are mapped, LSS distribution, number and location are similar (Figure 4.8C). The changes in elevation and reflectance were compared across 3 transects (Figure 4.8 X, Y and Z). Values were normalised by a 100m running mean in order to remove any larger slope. For transects X and Y there is a reasonable, but out of phase, correspondence between the largest LSSs. This out of phase relationship may be due to the sun angle on the Landsat imagery causing the peak in reflectance to be offset from the elevation peak, or georectification error. The subtlety of LSS on Landsat imagery makes comparisons with elevation data across transects difficult. This is especially the case for the subtle LSS of transect Z. LSSs are easier to identify in an aerial view, as the continuity of a subtle change can be traced. This provides us with some confidence that the satellite images are representative of the glacier surface at an appropriate scale for identifying longitudinal surface structures, although small details may be missed. However, to my knowledge, this is the only freely available high resolution DEM covering Antarctica which contains longitudinal surface structures.

Multiple passes were made over each area in order to maximise the number of features identified. However, the large scale of the task may mean that some individual features may be missing from the final map. Additionally, subtle features that were undetected here may require more sensitive satellite instruments to detect.

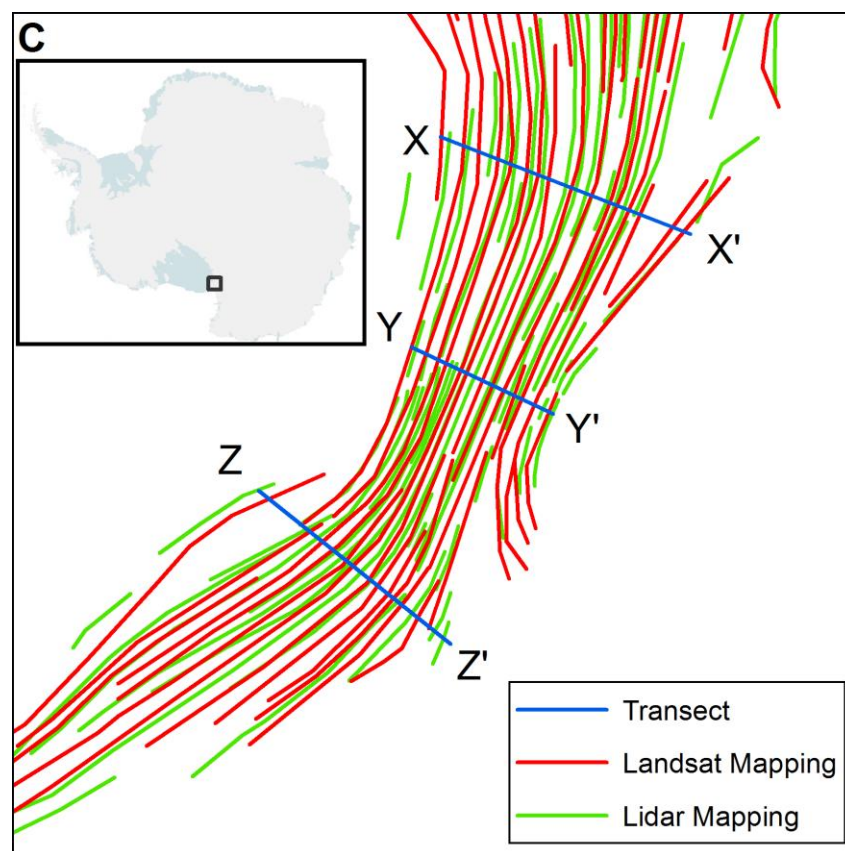


Figure 4.8. Visual comparison between a Landsat image (A), a hill-shaded high resolution (2m) LiDAR DEM (B) and mapping (C) of longitudinal surface structures on Taylor Glacier from both data sources. Mapped LSSs agree in terms of distribution and roughly the number of features mapped. Slight differences in location are unsurprising given the different data sources, resolution, georectification and sensor properties. Continued overleaf.

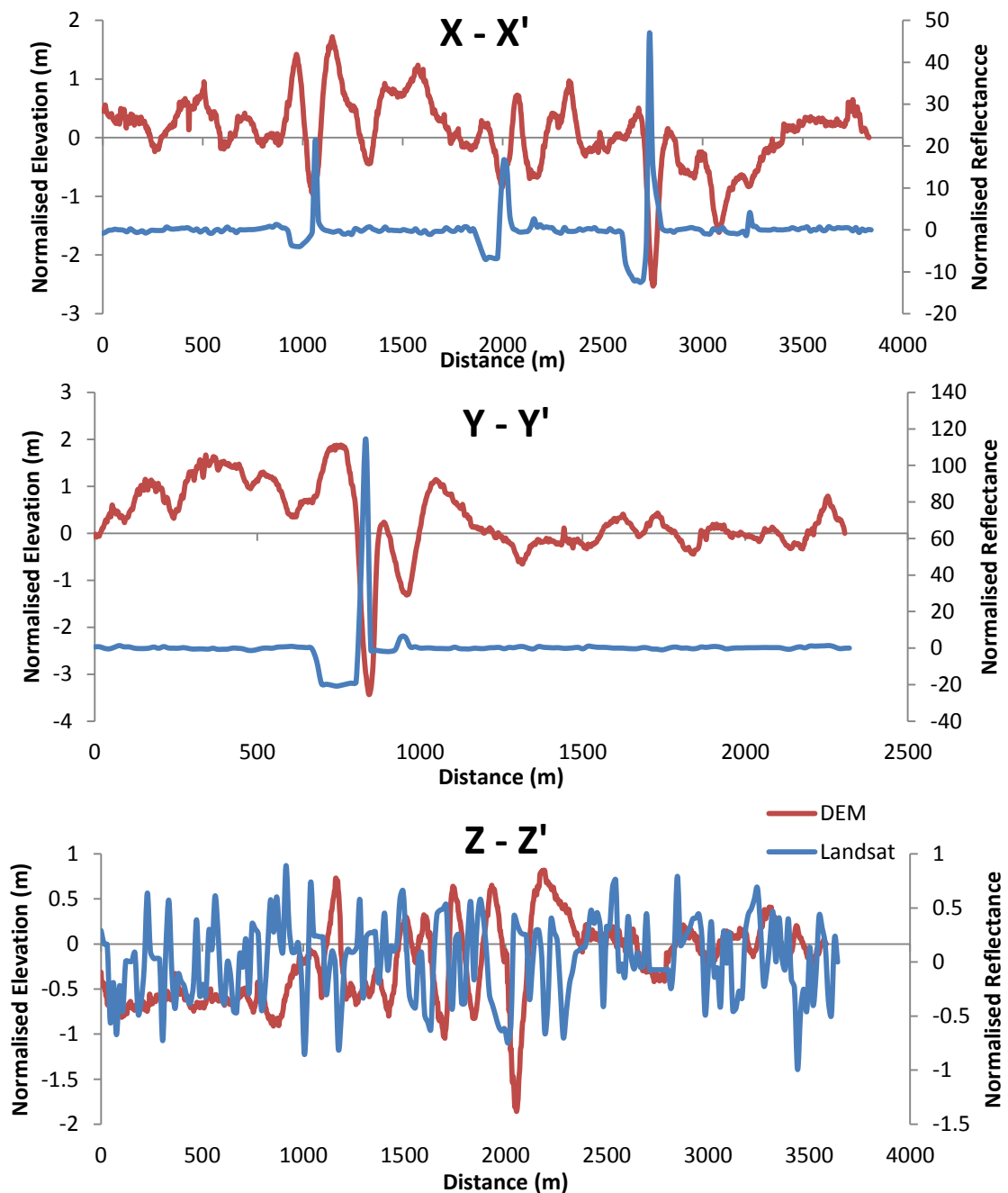


Figure 4.8 (continued). Comparison between normalised elevation and reflectance across transects X, Y and Z, located on Figure 4.8C. For transects X and Y, there is a clear correspondence between the largest LSSs on both sources of data. Smaller LSSs may not be as easy to detect in 2D given their subtlety on Landsat imagery. The out of phase relationship between the large LSSs and Landsat imagery may either be a georectification error, or a consequence of image sun angle. LSSs across transect Z are more subtle (hence the lower range of normalised reflectance), making comparison difficult.

#### 4.3.2 The Spatial, Morphological and Glaciological Characteristics of LSSs

The morphology of LSSs can be derived from the mapping conducted in Section 4.3.1. As highlighted above (Section 4.2), a systematic study of the morphological



parameters of LSSs has yet to be conducted, and would provide a test for models of LSS formation. Such an approach has proven insightful for the formation of subglacial bedforms (e.g. Clark et al., 2009; Spagnolo et al., 2014a). However, unlike for subglacial bedforms, glaciological data (Rignot et al., 2011; Fretwell et al., 2013) can be used to directly define the glaciological environmental parameters under which LSSs are found, and will be utilised here.

LSSs were grouped into glacier or ice stream flow units (e.g. Jennings et al., 2014). Each flow unit was defined by tracing ice structural and textural expressions. Features such as shear margins (Merry and Whillans, 1993) and depressions formed between converging flow units (e.g. Figure 4.5), as well as patterns within the LSSs themselves, were used to delineate the edges of each flow units.

LSS length was calculated within the GIS for each polyline. In order to determine LSS spacing a series of transects were placed across each glacier or ice stream flow unit, perpendicularly crossing LSSs. Then the distance between points created at the intersection of these transects and an LSS was calculated. Transects were strategically spaced downstream according to locations where there were no regions of obviously disturbed LSSs (e.g. Figure 4.7), and in accordance with LSS length so that repeat measurements were not made. In total, 2027 transects were placed (Figure 4.9). Analysis of spacing was restricted to the grounded portion of ice, defined by a dataset of grounding line position (Scambos et al., 2007). This procedure is similar to that used to determine of the spacing of MSGLs (Spagnolo et al., 2014a).

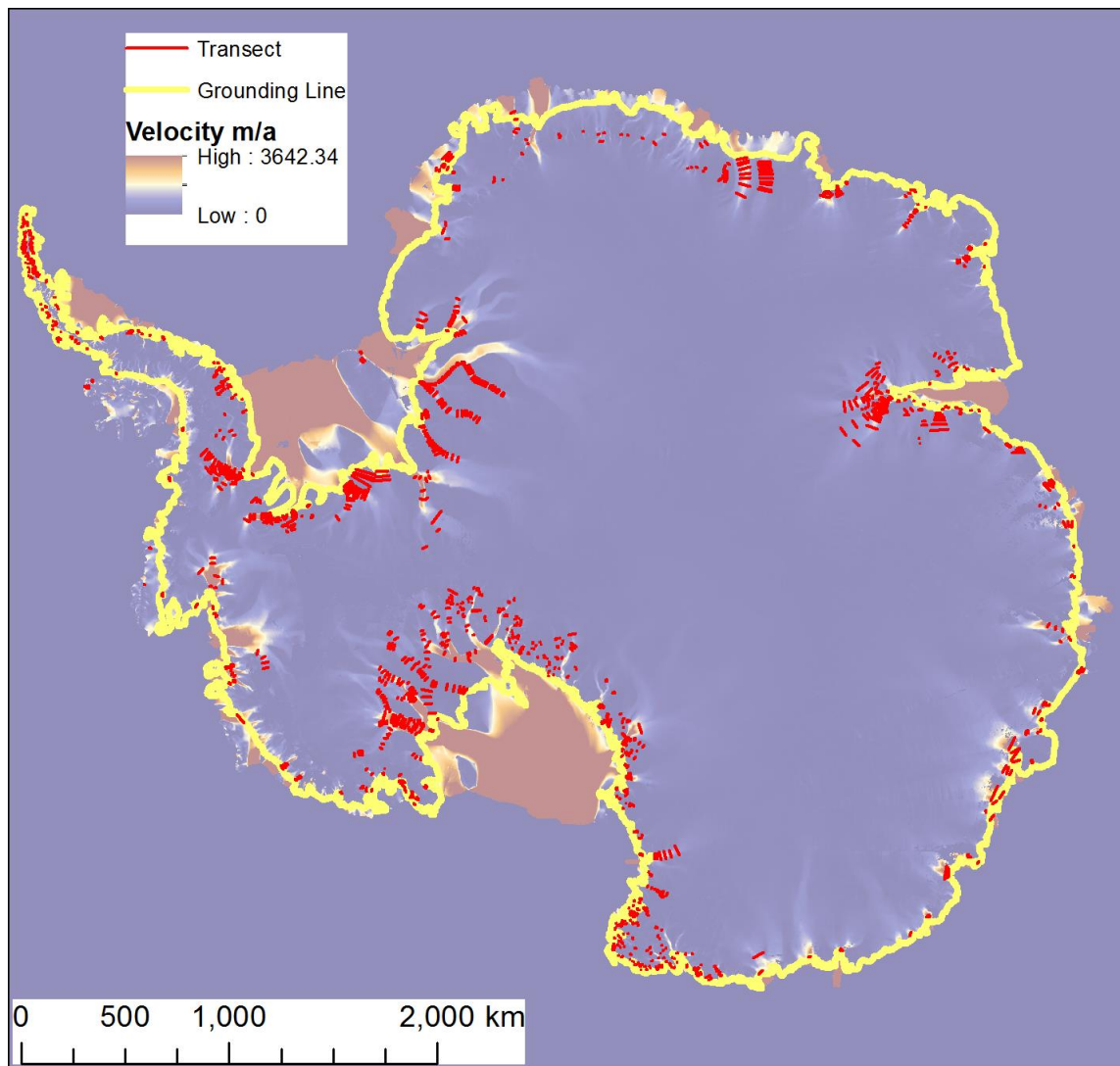


Figure 4.9. Locations of transects for measuring LSS spacing. Transect length is limited by flow-unit geometry.

Glaciological parameters for each LSS were derived from three datasets: ice velocity data derived from interferometric synthetic-aperture radar satellite data (Rignot et al., 2011), ice thickness data derived from ice penetrating radar and collated for the BEDMAP-2 project (Fretwell et al., 2013) and also ice surface slope derived from an elevation model of the ice surface (Fretwell et al., 2013). Both datasets contain regions of large measurement error, usually due to instrument error or large interpolation distances, which were discounted for this study. For the velocity data, regions where errors were highest were excluded, as defined by Rignot et al.s' (2011) error estimation. For the thickness data of Fretwell et al. (2013), regions where the uncertainty in bed elevation is greater than 300 m were not considered. Where combinations of the two parameters were considered (See Section 4.3.3), both error filters were applied.

Substantial errors still remain from both datasets. Where a measurement pertains to a single LSS (e.g. minimum values), then the error at this point is reported. Where a measure of average is reported (e.g. mean ice velocity), then the mean of all measurements is reported. Measurements were taken at the start point of each LSS, defined by the point of each feature closest to an ice divide. These glaciological parameters were also restricted to the grounded portion of the ice sheet, as this is the considered to be the region where the features are formed.

#### 4.3.3 Testing Formation Hypotheses

Both the lateral compression and the basal transfer hypotheses of LSS formation provide predictions pertaining to the spatial, morphological and glaciological characteristics of LSS. These predictions, and the procedures employed here to test them, are outlined below. Foliations on glaciers are commonly reported to be stronger, or more pronounced, at the lateral edges of flow units (e.g. Allen et al., 1960; Hambrey and Müller, 1978; Hambrey and Lawson, 2000, P.70; Hambrey et al., 2005). If the lateral compression hypothesis holds, the same may be true of LSSs. This increased pronunciation at flow unit boundaries may in turn correspond to increased spatial frequency of LSSs, and therefore a closer spacing of LSSs at the flow unit boundary. To test this prediction a second order polynomial taking the form of:

$$y = ax^2 + bx + c \quad \text{Eq.13}$$

was forced to fit a plot of the distance of each LSS along a transect (Figure 4.9) against the change in distance between neighbouring LSSs. If LSSs along a transect are concentrated (closely spaced) at the edges of a flow unit, coefficient  $a$  in Equation 13 would be negative. Conversely, if LSSs are concentrated in the centre of the transect,  $a$  is positive (Figure 4.10). Therefore, if the majority of flow unit transects to have a negative value of  $a$ , this is would partially support the lateral compression hypothesis.

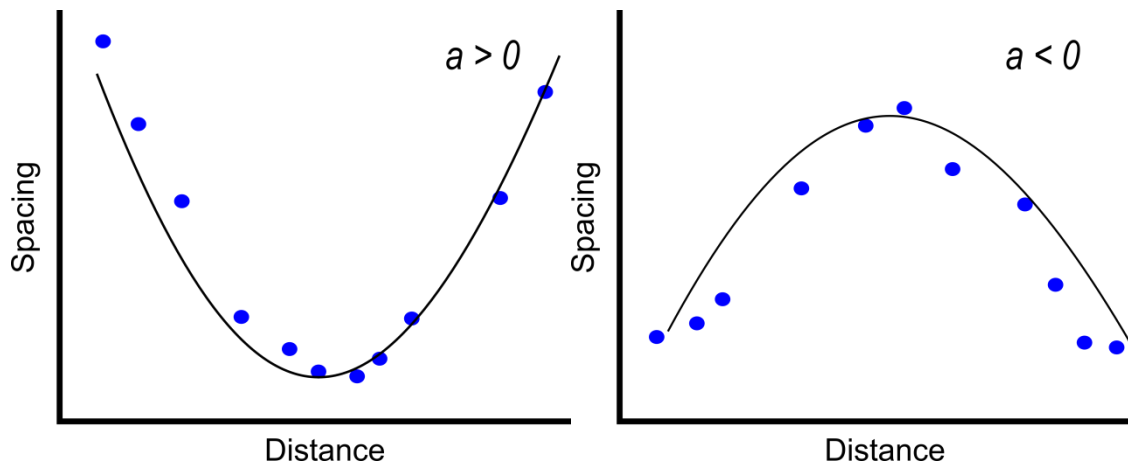


Figure 4.10. Expected outcomes of fitting polynomials to the spacing of LSS along an across flow transect.

The width of a flow unit may also be important for determining LSS spacing. Under the compression hypothesis, one might also expect the wavelength of LSSs to respond to changes in the width of a flow unit, whereby narrower flow units would have closer LSSs (Figure 4.11A). This is due to LSSs being created up-ice flow and advected downstream (Figure 4.11A). A relationship between flow unit width and LSS spacing may also occur due to basal transfer hypothesis. As more bumps are encountered, LSSs continue to form and are advected downstream (Figure 4.11B).

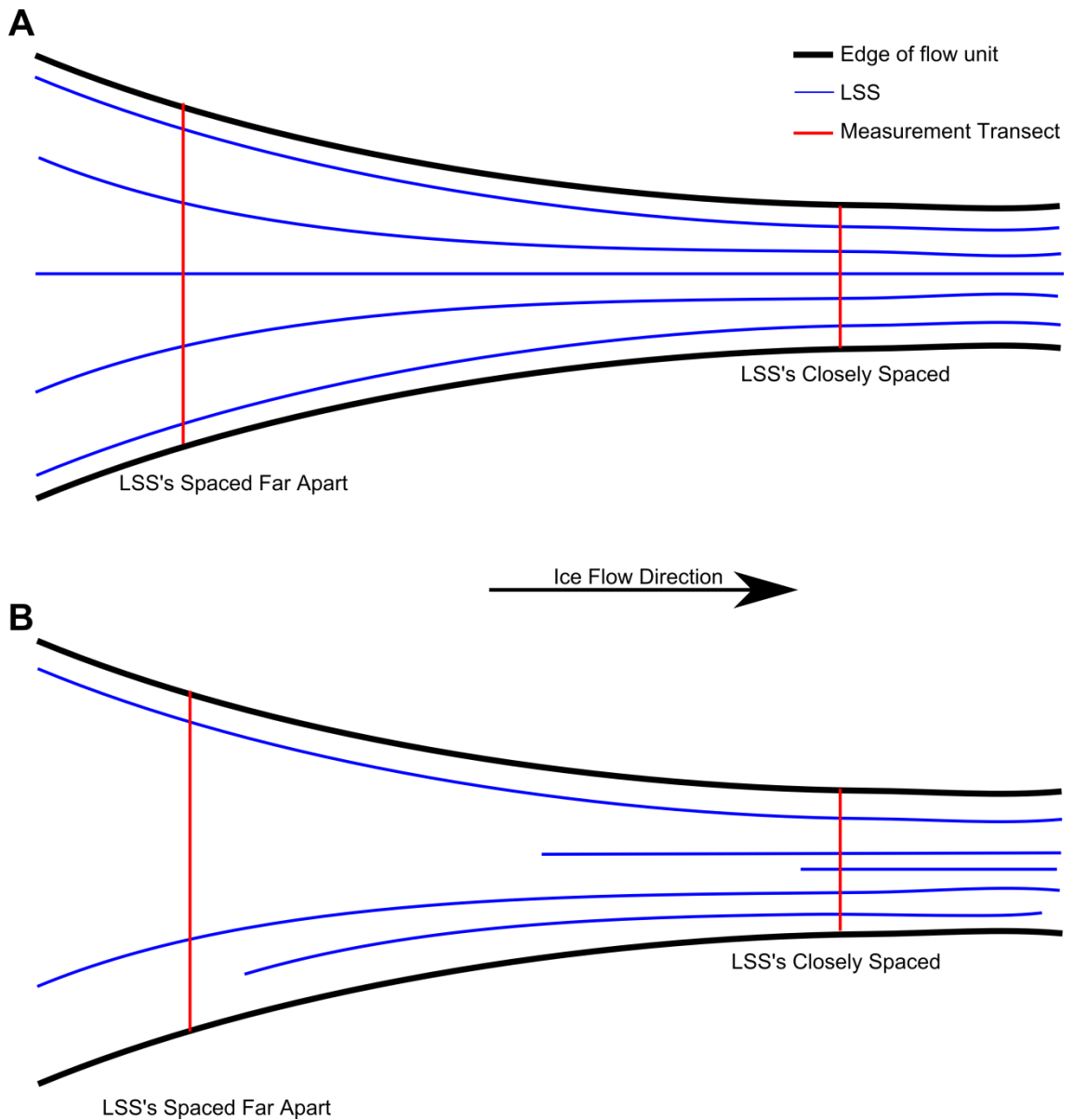


Figure 4.11. Hypothetical relationship between LSS spacing and changes to flow unit width under A) The compression hypothesis, and B) The basal transfer hypothesis. A) LSSs are created by compression and longitudinal extension. As they flow into a confined channel or outlet, the spacing of LSSs decreases. B) LSSs begin at points located within the flow unit. Both the accumulation of LSSs down-flow, and the flow of LSSs into a confinement, causes spacing to decrease.

If LSSs are formed by the transmission of basal bumps to the surface of an ice mass, there are two further intuitive expectations. Firstly, one would expect LSSs to be closer under thinner ice, as transmission through thinner ice would be easier. Secondly, where ice is flowing faster one would expect more LSSs and thus a closer spacing between them, as faster flow permits more bumps to be transmitted to the surface. Here I use regression analysis to see if there are relationships between these variables. However, the analyses of Gudmundsson (2003) showed that undulations with a

wavelength 3-10 times the ice thickness are most effectively transmitted to the surface of an ice sheet. Therefore, a third expectation of the basal transfer hypothesis is that most LSSs should be spaced 3-10 times further apart than the thickness of the ice at the point of initiation.

The above expectations of the basal transfer hypothesis assume that the bed is uniformly rough across the whole of Antarctica. Unfortunately a high resolution DEM of the bed of Antarctica does not exist. However, in Chapter 2 we saw that subglacial bedforms, an abundant roughness element of the beds of ice sheets, are regularly spatially distributed. Yet, other studies into ice stream bed roughness have shown spatial variability in bed roughness across Antarctica (e.g. Siegert et al., 2004; Rippin et al., 2011). Therefore, a fourth expectation of the basal transfer hypothesis is that LSSs should be concentrated in regions of high roughness. In order to test this expectation, here I compare the distribution of mapped LSSs to published roughness indices (e.g. Bingham and Siegert, 2007; 2009). During the course of my mapping qualitative observations of possible rough portions of the bed that have been transmitted to the surface were made. Table 8 provides a summary of the above expectations and analyses.

Hypothesis	Expectation	Parameters Measured
Compression	More pronounced LSSs at the edge of a flow unit.	Second order polynomial a coefficient between LSS distance along transect and spacing.
Compression	Flow unit width controls LSS spacing due to the degree of ice compression.	Flow unit width and spacing of LSSs.
Compression/Basal Transfer	LSSs within a flow unit will respond to changes in width.	Flow unit width and spacing of LSSs.
Basal Transfer	LSSs are closer where ice is thinner.	Spacing and ice thickness.
Basal Transfer	LSSs are closer where ice is faster.	Spacing and ice velocity.
Basal Transfer	LSSs should be most commonly spaced 3-10 times the ice thickness apart.	Spacing and ice thickness.
Basal Transfer	There should be more LSSs where the bed is rougher.	Published roughness indices and the spatial distribution of LSSs.

Table 8. Tested expectations of the compression hypothesis (e.g. Hambrey and Dowdeswell, 1994) and the basal transfer hypothesis (Gudmundsson et al., 1998).

## 4.4 Results

### 4.4.1 Mapping

In total 42,311 LSSs were identified and mapped. A map of all of these features is included on Plate 1. In general, LSSs conform to arborescent pattern, feeding into the main ice streams and outlet glaciers across the Antarctic Ice sheet (Plate 1). LSSs tend

to start at the onset of ice streams and tributary glaciers, and converge into the main trunks of flow (Plate 1). Good examples of this arrangement can be seen in the Siple Coast region (Figure 4.12A), and the Byrd Glacier catchment (Figure 4.12B). However, it is not only the largest or fastest flowing portions of the ice sheet which have LSSs, as can be seen of the Antarctic Peninsula (Figure 4.12C), where numerous LSSs occur on much slower flowing outlet glaciers. Indeed, LSSs are nearly ubiquitous to all glaciers of the Antarctic continent (Plate 1). Thus, it is surprising that LSSs were infrequently observed on Thwaites Glacier (Figure 4.12D), especially as it is one of the largest and fastest flowing Antarctic outlet glaciers (Rignot et al., 2011). Those that were observed appear infrequently, or further up the system. This may be due to observational limitations due to the numerous other features found on the surface of this main outlet of Thwaites limiting identification of features (Figure 4.12D; Chapter 5).

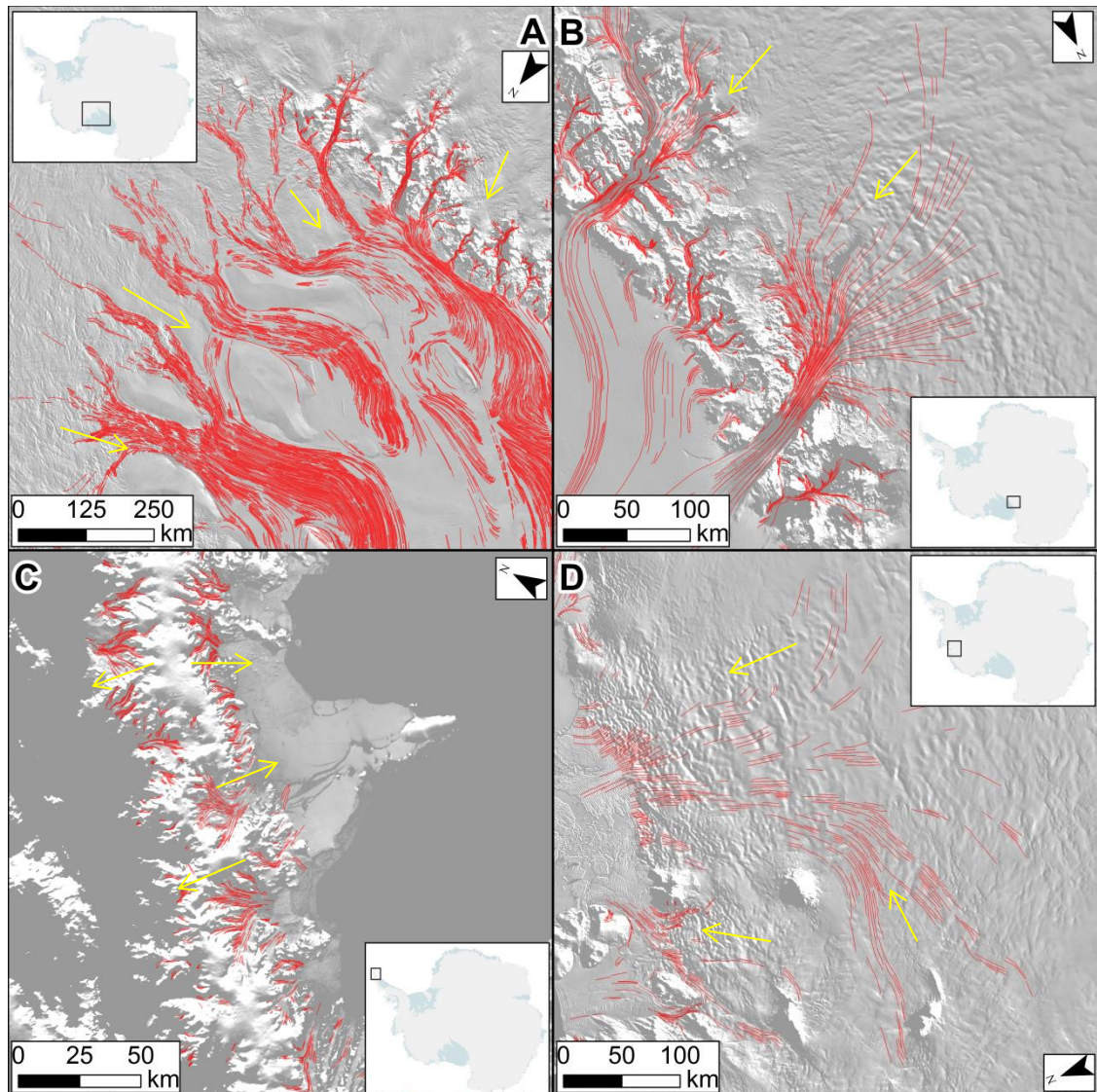


Figure 4.12. Examples of mapped LSSs (red). Background is MODIS mosaic. Yellow arrows denote approximate ice flow directions. A) The arborescent pattern of the Siple Coast Ice Streams. B) Byrd Glacier. C) Outlet glaciers of the Antarctic Peninsula. D) Relatively few LSSs on the surface of Thwaites glacier, due to disruption by other surface features.

#### 4.4.2 LSS Morphological and Glaciological Characteristics

Figure 4.13 displays the length of all the mapped polylines of LSSs shown in Plate 1. Typically, features were traceable for a distance of less than 50 km, with a mean value of 15.7 km and a median of 8.7 km. The abundance of smaller features is surprising, given the often reported great length of LSSs. This may be due to several reasons. Firstly, my mapping technique did not join together LSS polylines across interruptions (e.g. Figure 4.7), perhaps recording segments of LSSs instead of whole features. Secondly, my mapping includes a wide scale range of glacier and ice stream systems (Figure 4.12), whereas previous studies have tended to focus on larger ice



shelves and ice streams (e.g. Hambrey and Dowdeswell, 1994; Holt et al., 2013b). Finally, previous work has tended to only report exceptionally long features (e.g. Glasser and Scambos, 2008), whereas I report the whole distribution of features (Figure 4.13; Table 9). On the other hand, as the distribution of the histogram is positively skewed (Figure 4.13), much longer features were also noted, but less frequently. The longest single traceable feature was found on the Ronne Ice Shelf, and is 450 km long (Table 9).

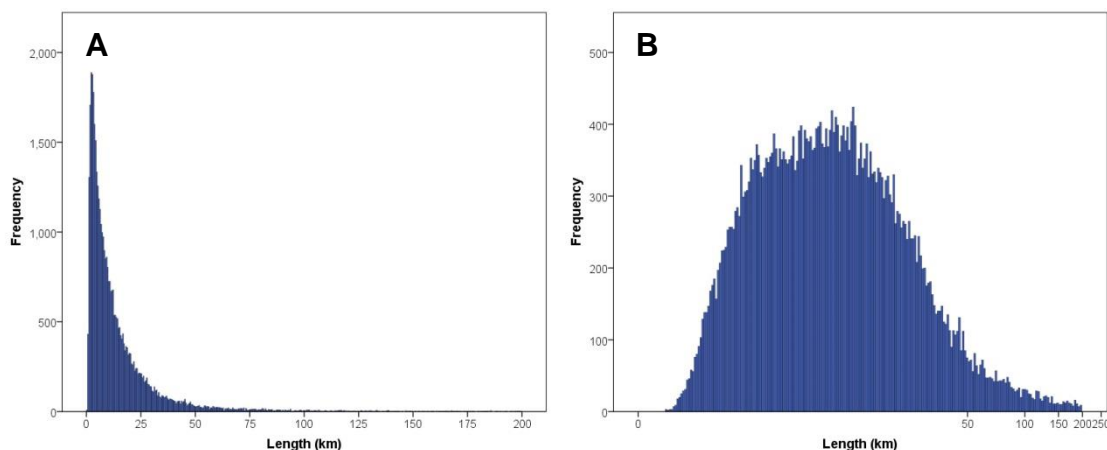


Figure 4.13. The length of mapped LSS polylines. N = 42,311. A) The histogram shows a highly positively skewed distribution, with a distinct modal peak at approximately 10 km. B) The same histogram, but with a log<sub>10</sub> scale. This highlights how the majority of LSSs are shorter than 50 km.

	Length (km)	Spacing (m)	Velocity (m/a)	Thickness (m)
<b>Mean</b>	15.62	1248.4	109.7 (+/- 3.2)	912.5 (+/- 195)
<b>Median</b>	8.64	865.1	50.9 (+/- 3.2)	796.0 (+/- 195)
<b>Mode</b>	9.57	1193.7	38.7 (+/- 3.2)	341.0 (+/- 195)
<b>Skewness</b>	5.9	5.2	5.5	1.0
<b>Kurtosis</b>	52.3	49.9	59.6	1.1
<b>Minimum</b>	0.38	0.6	0.11 (+/- 1)	51.0 (+/- 59)
<b>Maximum</b>	451.9	28073.9	3503.3 (+/- 2)	3949.0 (+/- 200)

Table 9. Descriptive statistics of measured LSS variables.

The spacing between mapped LSS polylines is plotted in Figure 4.14. Almost all LSS spacing measurements were less than 4,000 m, and the majority were less than 2000 m. In a similar manner to the length measurements (Figure 4.14), the histogram is highly peaked, reflected in the high kurtosis value (Table 9), suggesting a strong tendency for LSSs to be a specific distance apart. Measures of average show this to be

between approximately 850 m and 1250 m (Table 9). However, much larger measures of spacing were also recorded (maximum 28,073 m; Table 9), creating a positively skewed histogram. Again, this could be an artefact of my mapping technique, recording an area along a transect where an absence of polylines representing LSSs occurs due to surface disruptions. A similar explanation also explains the small minimum value of spacing recorded in Table 9. This and similar small values were taken where LSSs were perceived to merge together. However, I believe the effects of any of these anomalous values to be negligible as due to my sampling technique purposefully avoiding disturbed or interrupted regions (Section 4.3.2; Figure 4.9) and due to the high number of measurements taken ( $N = 14,758$ ). Thus, the majority of my measurements, and the averages derived from them, are reflective of LSS spacing.

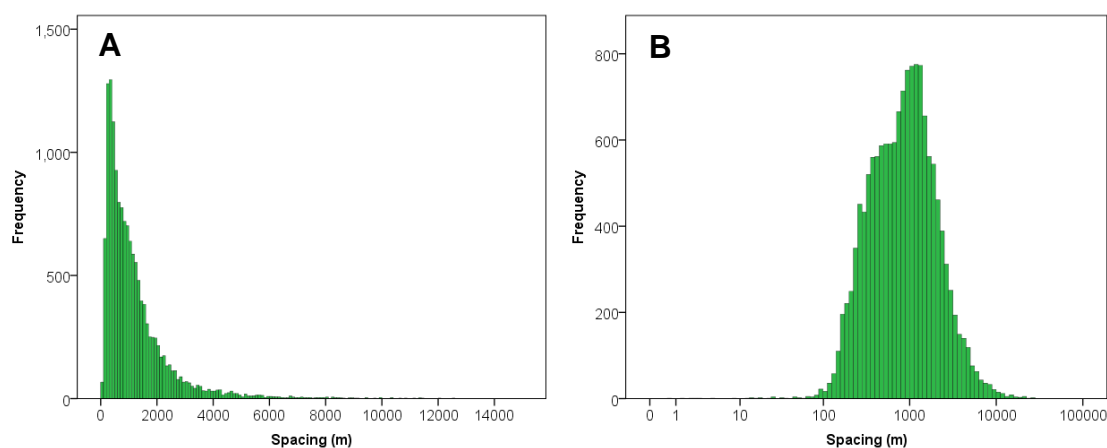


Figure 4.14. The spacing of mapped LSS polylines.  $N=14,758$ . A) A highly positively skewed distribution, but with a strong tendency for LSS spacing to be between 100 and 2000 m. B) The same histogram, but with a log<sub>10</sub> scale.

Figure 4.15 shows the distribution of LSS start point ice velocity measurements. Surprisingly, given the association that is sometimes made between LSSs and fast ice flow or ice streams (e.g. Swithinbank et al., 1988; Stephenson and Bindschadler, 1990; Campbell et al., 2008), rather than being restricted to only the fastest flowing portions of the ice sheet, LSSs were observed to begin at low ice velocities, and were even observed in regions of the ice sheet flowing at approximately 1 m/a (Figure 4.15; Table 9). The majority of LSSs originate at ice velocities lower than 500 m/a (Figure 4.15A). The match between the arborescent pattern of ice flow and that of the LSSs themselves is demonstrated in Figure 4.16. This figure also shows that the majority of LSSs coincide with the 20 m/a contour. Three regions of palaeo-ice flow were also identified from the literature, where relict LSSs exist (Figure 4.16). Exclusion of the LSSs in these regions from my analyses did not significantly change the result. It is concluded

that, contrary to established wisdom that LSSs represent fast ice flow, they actually frequently initiate in ice velocities below 20 m/a (mean error is +/- 2 m for these measurements).

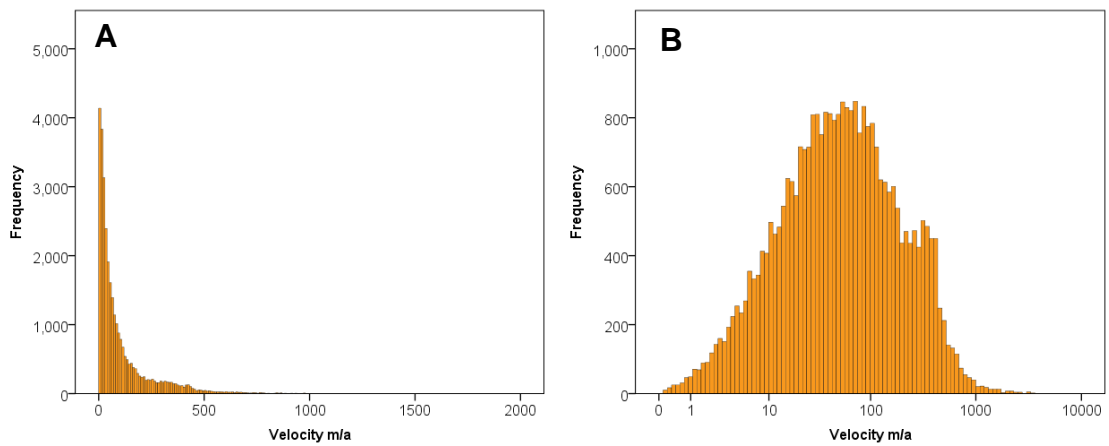


Figure 4.15. The velocity of LSS start point. N = 31,148. A) The majority of LSSs form in ice flow below 500 m/a. B) Log10 scale reveals the multitude of LSSs that occur in ice velocities below 10 m/a. Mean error for these measurements is +/- 3.2.

Figure 4.16. The correspondence between ice velocity and LSSs. Velocity data from Rignot et al., 2011. Areas labelled are those previously identified in the literature as recording palaeo-ice flow configurations. K) Kamb Ice Stream (Catania et al., 2005). S) Siple Ice Stream (Conway et al., 2002). B) The Bungenstock Ice Rise (Siegert et al., 2013).

Figure 4.17 shows the distribution of ice thickness measurements at which LSSs begin. These histograms have the lowest kurtosis value (Table 9), reflecting the large range of ice thickness at which LSSs are formed. The observed peaks at approximately 300 m and 900 m (Figure 4.17A) are also evident within the thickness dataset itself. This histogram is also the least positively skewed described thus far (Table 9). Therefore, LSSs occur at a range of ice thicknesses. The minimum value of 51 m (Table 9) is within the error bounds stated by Fretwell et al. (2011) (minimum uncertainty is +/- 59 m). In reality, LSSs are observed at thin ice areas such as glacier margins, and are therefore likely to survive on thin ice. The large number of measurements means that a

better resolved bed is unlikely to change the overall broad distribution of ice thickness measurements (Figure 4.17).

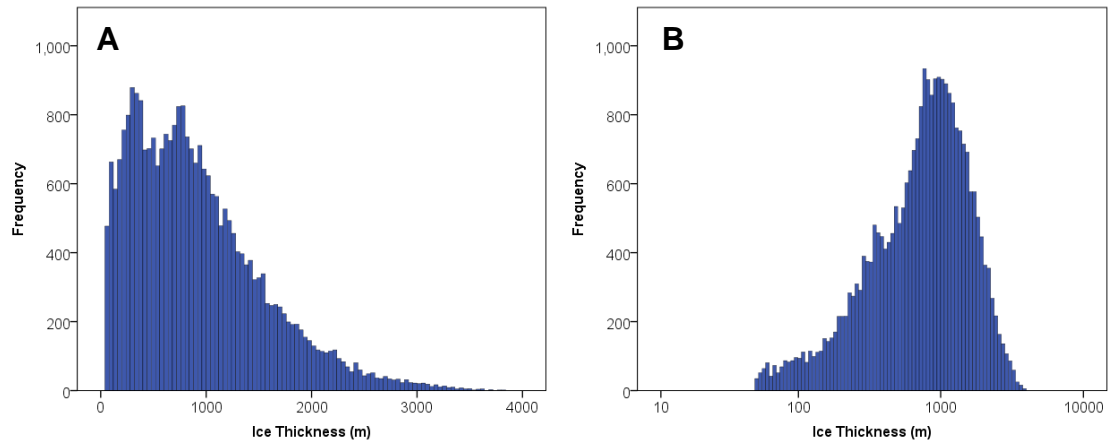


Figure 4.17. LSS start point ice thickness. Data from Fretwell et al. (2013). A) LSSs were observed to occur on thin and thick ice. B) The same histogram but with a log10 scale.

#### 4.4.3 Testing Formation Hypotheses

The tested expectations of the compression and the basal transfer hypotheses are listed above in Table 8. Here I present the results of these tests. The value of the  $a$  coefficients between spacing and distance along a transect, in order to test the compression hypothesis, are plotted in Figure 4.18. The distribution of  $a$  seems to be near symmetrical. Only a slight majority of 62.4% of the transects tested conform to this hypothesis, displaying an  $a$  coefficient which is less than 0. In some cases, LSSs at the edge of a flow unit were qualitatively more pronounced than toward the middle (Figure 4.19). Often, in situations similar to that described by Gudmundsson and Glasser (2012), the convergence of flow units led to the development of a depression (Figure 4.4) which was bordered by several pronounced LSSs (e.g. Figure 4.20B). To account for Figure 4.18, these LSSs are either a similar wavelength to the majority of LSSs across the ice stream, or do not occur frequently enough to cause the statistics to be more bias towards a negative  $a$  coefficient.

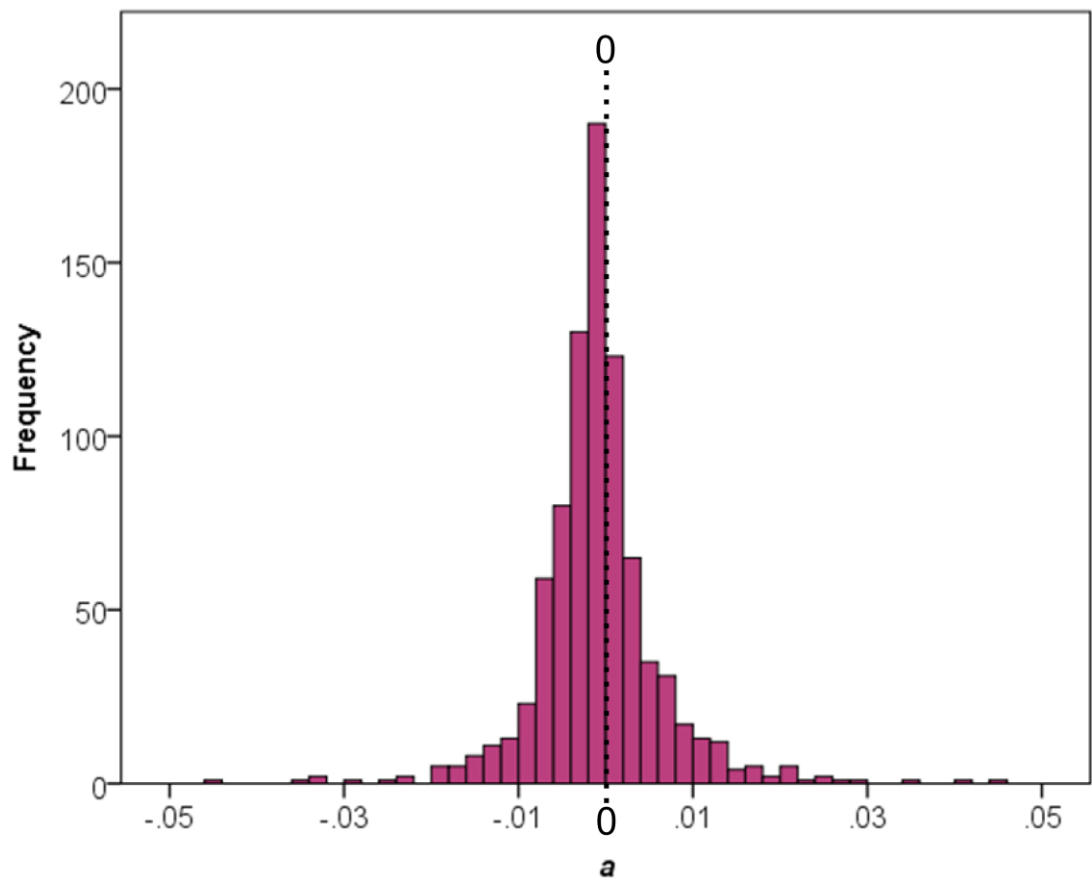


Figure 4.18. Histogram of the coefficient  $a$  for fitting a second order polynomial between distance along a transect and spacing.

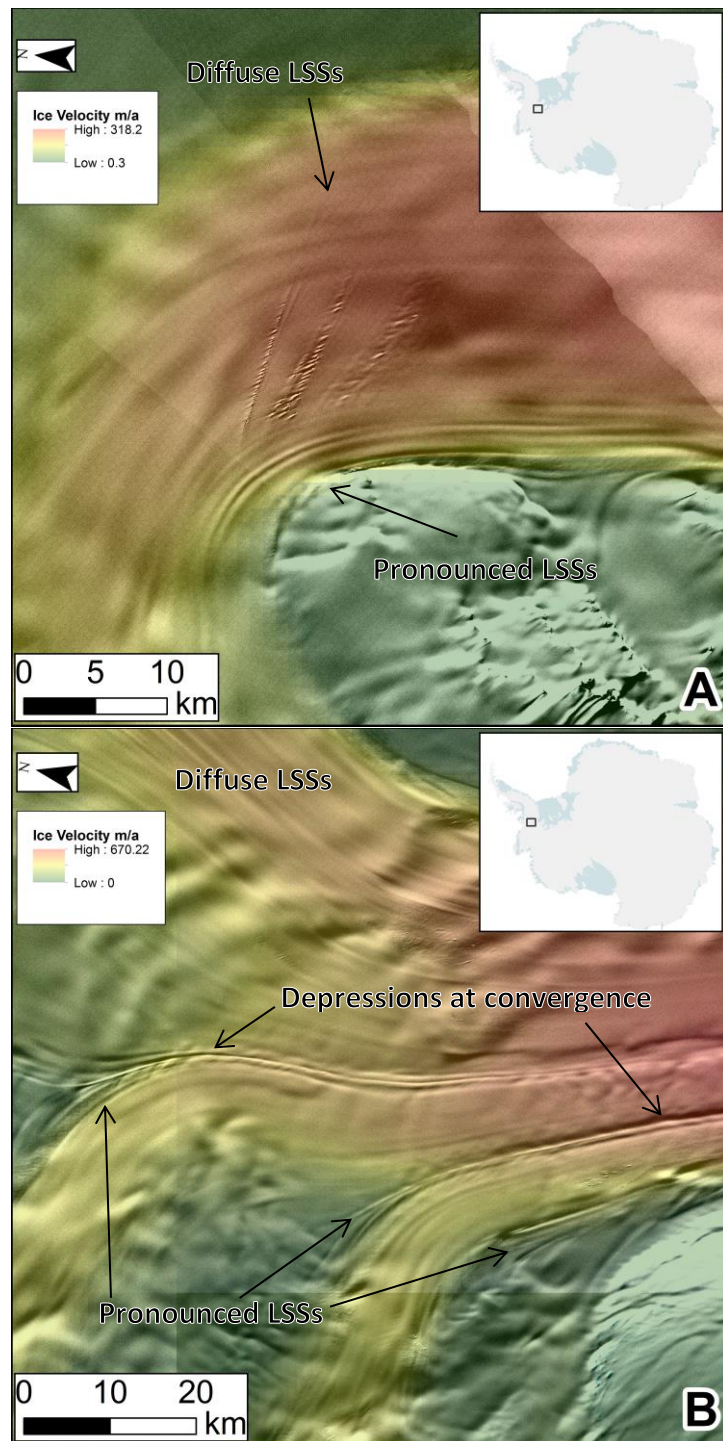


Figure 4.19. Qualitative observations of pronounced LSSs at flow unit boundaries. All images are from Landsat data with superimposed velocity data (Rignot et al., 2011). A) LSSs at the edge of the Rutford Ice Stream are more pronounced than those in the centre. B) Evans ice stream. Note the depressions where flow units converge, as described by Glasser and Gudmundsson, 2012, bordered by more pronounced LSSs. LSSs within the main ice stream are more diffuse.

Figure 4.20 shows the relationship between flow unit width and mean LSS spacing. There is a strong positive correlation between the two variables, such that the wider the flow unit the further apart on average the LSS were. The highest  $R^2$  value was

found when a power law was fitted to the data. A possible explanation for this is that the wider the transect the more likely that a region of “no data” would be included, leading to greater spacing measurements. However, transects were specifically positioned to avoid such areas (Section 4.3.2). Due to the high number of transects and spacing measurements ( $N = 14,758$ ), I believe that it is unlikely that this contributed to the overall trend in the data. Data are more concentrated for narrower flow units (Figure 4.20). This could be explained by spatial inhibition; a 3 km wide flow unit cannot have a mean LSS spacing of 3 kms. This may have contributed to the high correlation between the two variables. However, this effect does not explain why LSS spacing increases so much for wider flow units. LSS spacing could have remained at a set spacing regardless of flow unit width (e.g. in a similar manner to drumlins and MSGL, see Section 2.2.2).



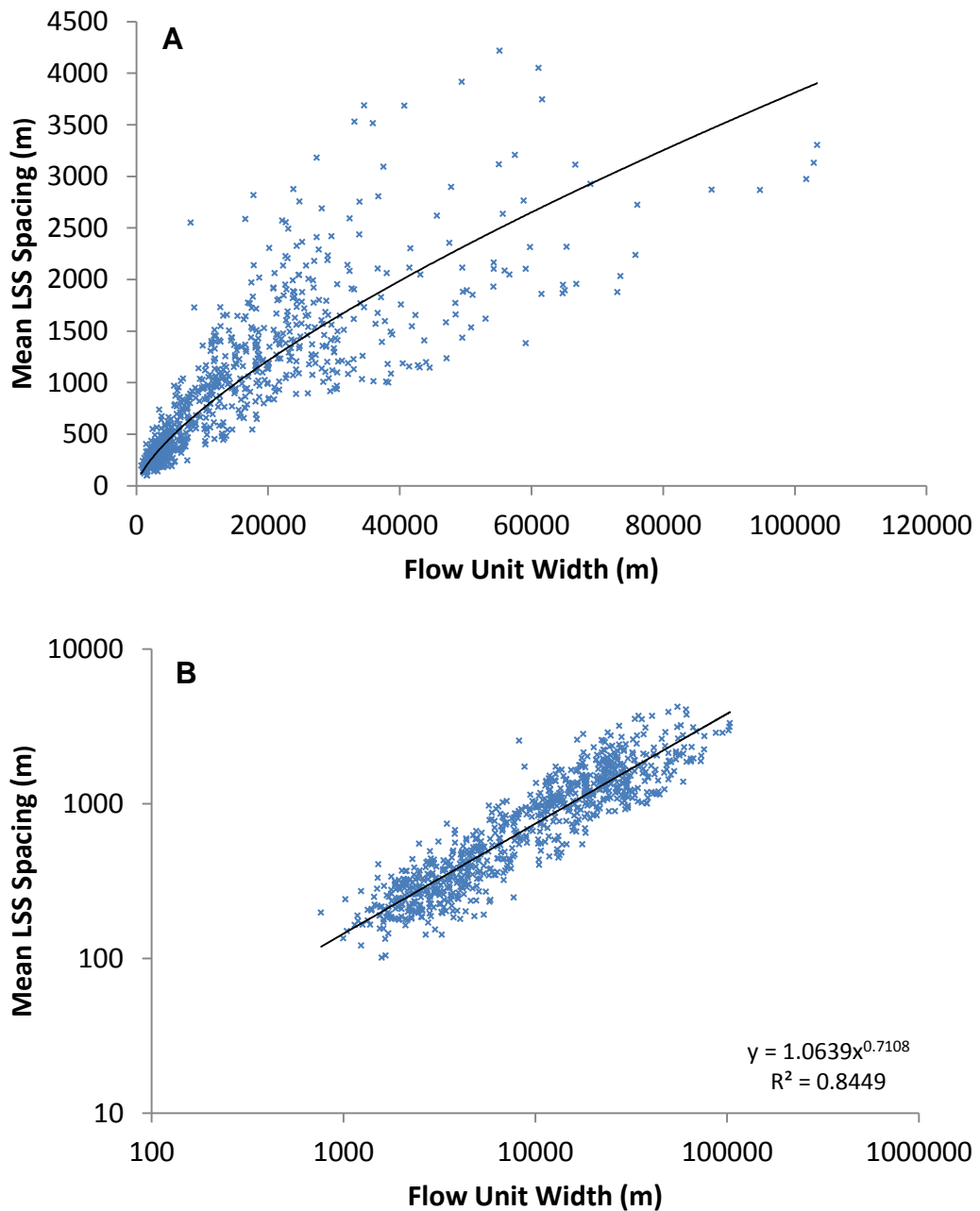


Figure 4.20. The relationship between flow unit width and mean LSS spacing. A) A strong positive correlation taking the form of a power law. B) The same graph but with log<sub>10</sub> axes.

Where there were sufficient transects and spacing measurements in a single flow unit, transects could be grouped together and the change of mean spacing against width along a flow unit could be plotted (Figure 4.21). Of the 46 flow units on outlet glaciers or ice streams measured only 8 (17%) displayed negative correlations, with the majority displaying a positive correlation. Those that display a negative correlation tend to be flow units whose width has changed little downstream. A mean  $R^2$  relationship for each regression line on Figure 4.21 of 0.61 is lower than when all transects are considered

together (0.84; Figure 4.20). Thus, it seems initial flow unit width is a more important control upon LSS spacing.

Under the basal transfer hypothesis (Gudmundsson et al., 1998), one would expect more basal bumps to be transmitted to the surface of an ice mass where the ice is thinner, and flowing faster (Table 8). Figure 4.22 shows a weak positive relationship between ice thickness and LSS spacing. Thus, a simple relation does not exist between ice thickness and the features observed at the surface of the ice stream. Secondly, Figure 4.23 displays a lack of a relationship between LSS spacing and ice velocity. Thus, neither of these simplistic expectations of the basal transfer hypotheses are met.

Figure 4.24 shows the ratio of LSS spacing to ice thickness. Under the basal transmission hypothesis (Gudmundsson et al., 1998), bumps underneath an ice mass should be most efficiently transmitted at a wavelength of 3-10 times the ice thickness. Therefore, LSSs should be spaced 3-10 times the ice thickness apart. However, the mean value of 1.8 and the median value of 1.1 fall well below this. Given that LSS spacing is typically between 850 and 1250 m, and mean ice thickness is 950 m at LSS start positions (Table 9), mean ice thickness errors of 195 m, a reduction in data uncertainty would not shift the peak of Figure 4.24 into this 3-10 times ice thickness window. Therefore, LSSs are generally spaced closer together than is predicted by the basal transfer hypothesis when compared to ice thickness. This could be viewed as an expected consequence of inheritance of LSSs from upstream. Indeed, a more worrying result for the transfer hypothesis would be a peak on Figure 4.24 after the 3-10 times ice thickness range.

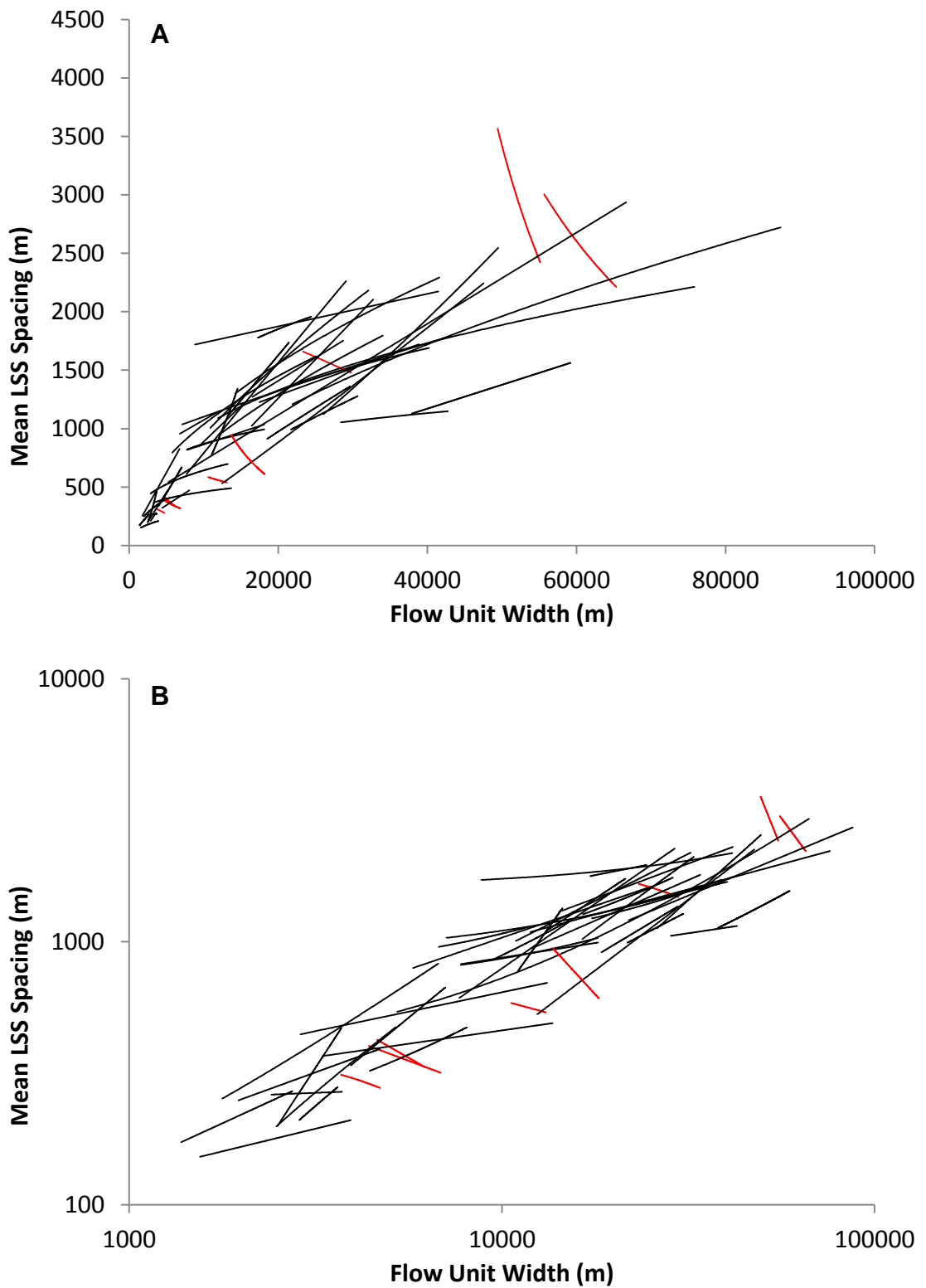


Figure 4.21. Regression lines between flow unit width and mean LSS spacing for 46 outlet glaciers and ice streams. Negative correlations are highlighted in red. A) Most flow units displayed a positive correlation as unit width changed. B) The same plot but with log<sub>10</sub> axes. Note that in general flow units tend to narrow downstream, making ice flow direction broadly from the right to the left.

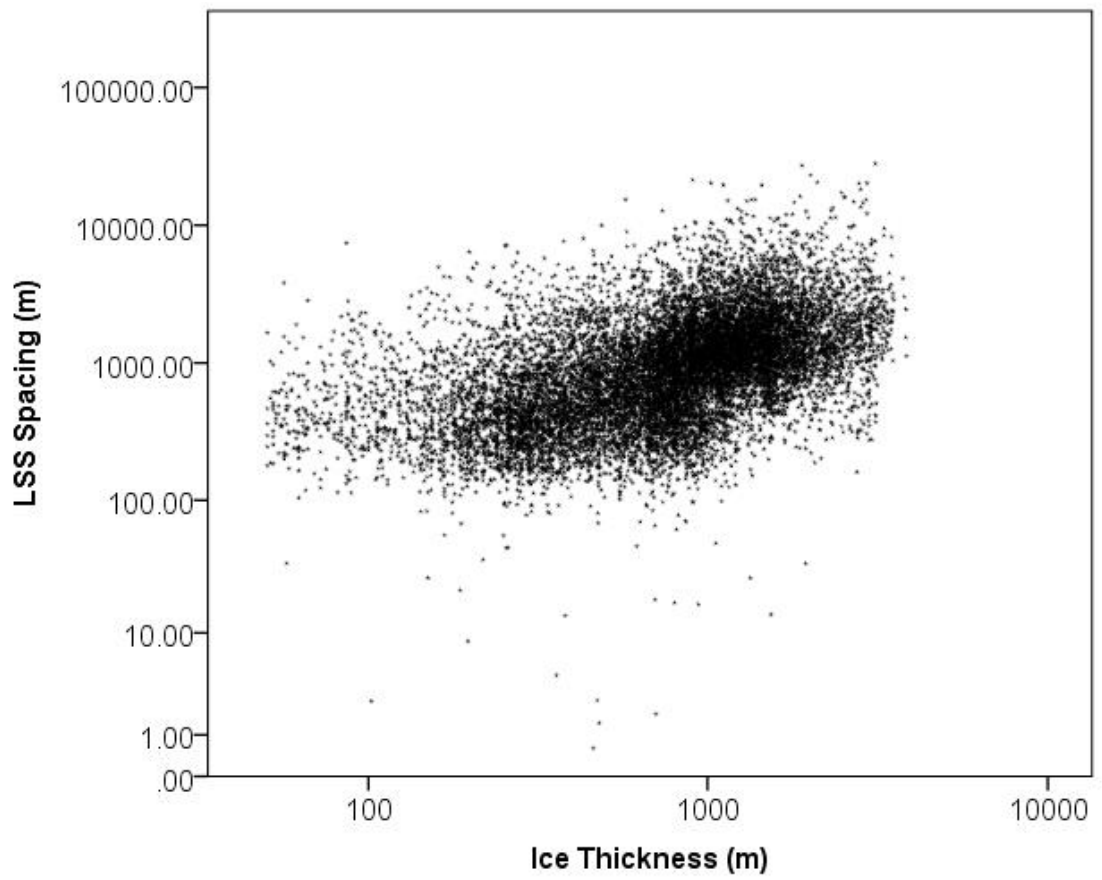


Figure 4.22. The relationship between ice thickness and LSS spacing. A weak positive relationship was found, with an  $R^2$  of 0.23. Note the log10 axes.

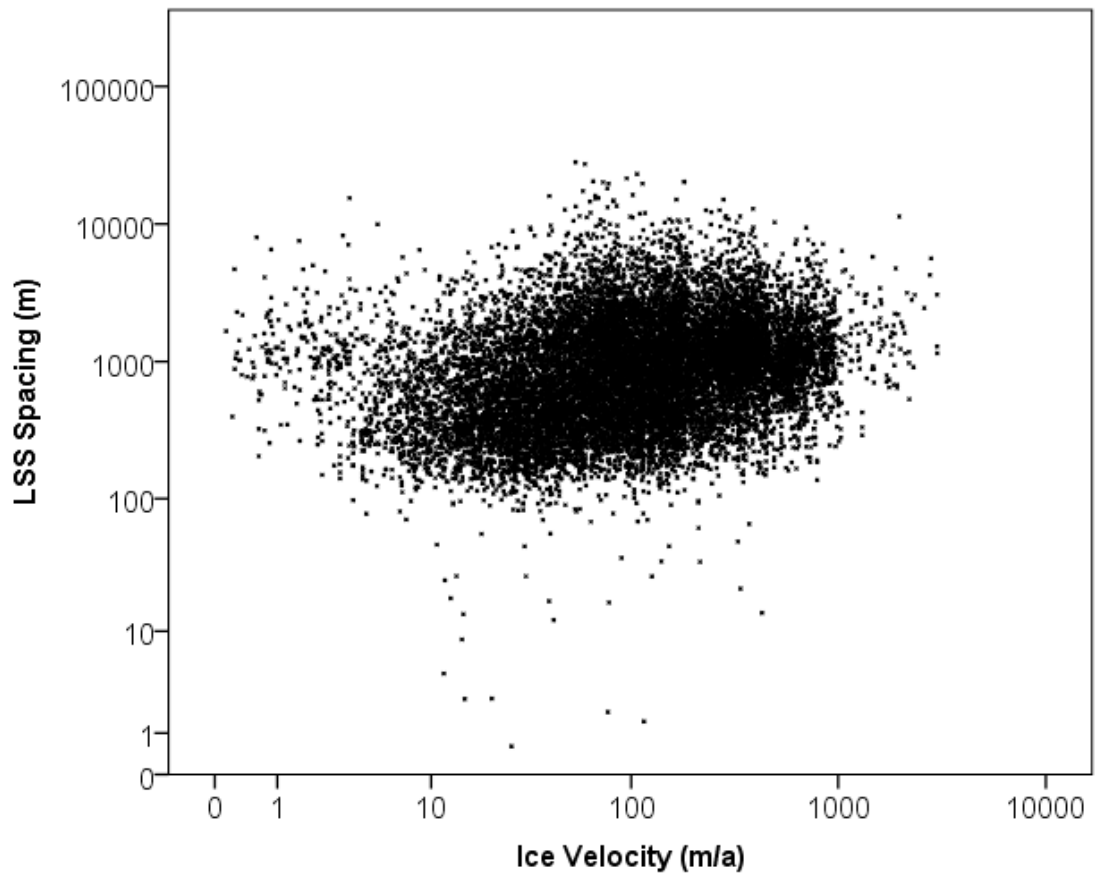


Figure 4.23. The relationship between ice velocity and LSS spacing. No relationship ( $R^2 = 0.01$ ) was found between these variables.

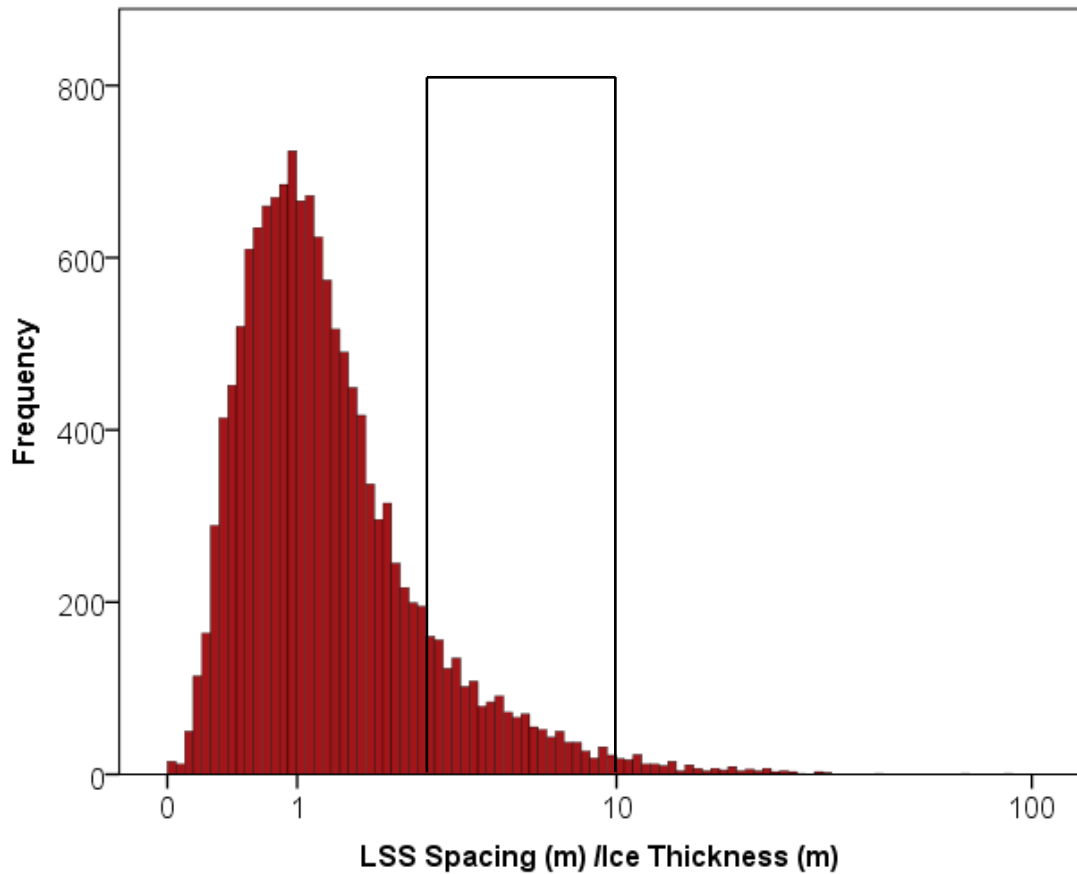


Figure 4.24. Histogram of the ratio between LSS spacing and ice thickness.  $N = 14,041$ . The modal bin occurs at approximately 1. Boxed area highlights the 3-10 values proposed by Gudmundsson et al. (1998).

Five basal roughness maps were georeferenced and analysed (two from Bingham and Siegert, 2009 and one each from Callens et al., 2014, Rippin et al., 2006 and Rippin et al., 2014) in order to test the prediction of the basal transfer hypothesis that there should be more LSSs emanating from rougher portions of the bed. These display different roughness metrics ranging from 0 (smooth) to 1 (rough), typically visualised on a colour scale. Mapping of LSSs (Section 4.4.1) was superimposed upon these for visual comparison. As ice streams are typically positioned where the bed is smoother, LSSs are typically located in regions of comparatively smooth bed (e.g. Figure 4.25A; B; Rippin et al., 2006; 2014). Occasionally LSSs were concentrated at regions higher basal roughness (Figure 4.25C). However, as individual bumps are not resolved by these datasets it is difficult to attribute LSSs to such regions. Furthermore, comparison is severely limited by the sparse spacing of the radar lines used to derive the roughness indices as well as the lack of a common roughness index. Therefore, links between basal roughness and LSS location by this technique were not reached.

Qualitative observations made during mapping may be more encouraging for the basal-transfer hypothesis. Ice rumples, regions of locally grounded ice within an ice shelf, may provide a more direct test for any possible link between basal roughness and LSS origin. This is because they are regions where basal roughness locally increases from 0 in the surrounding floating area. Figure 4.26 shows three examples of ice rumples where LSSs which were observed to begin on ice rumples. These LSSs must either be the consequence of a bump in an ice rumple being transmitted to the surface of the ice (Gudmundsson et al., 1998), or increased shear strain rates as ice passes over the surface of an ice rumple. More tentatively, satellite images may also show regions where a flow around a sticky-spot or bedrock bump leads to the development and attenuation of a LSS (e.g. Figure 4.27). Such regions generally show crevassing around a bump and the development of a LSSs downstream. Perhaps the clearest example of this occurs on the Rutford Ice Stream (Figure 4.27C), over an area known to be a bedrock high (Spagnolo et al., 2014a). However, such features appear to be the exception for LSSs rather than the norm, and are difficult to delineate from the overall pattern of LSSs. Overall, it is difficult to assign roughness variations broadly to the development of LSSs. Yet, isolated occurrences of LSSs may be related to increased basal friction.

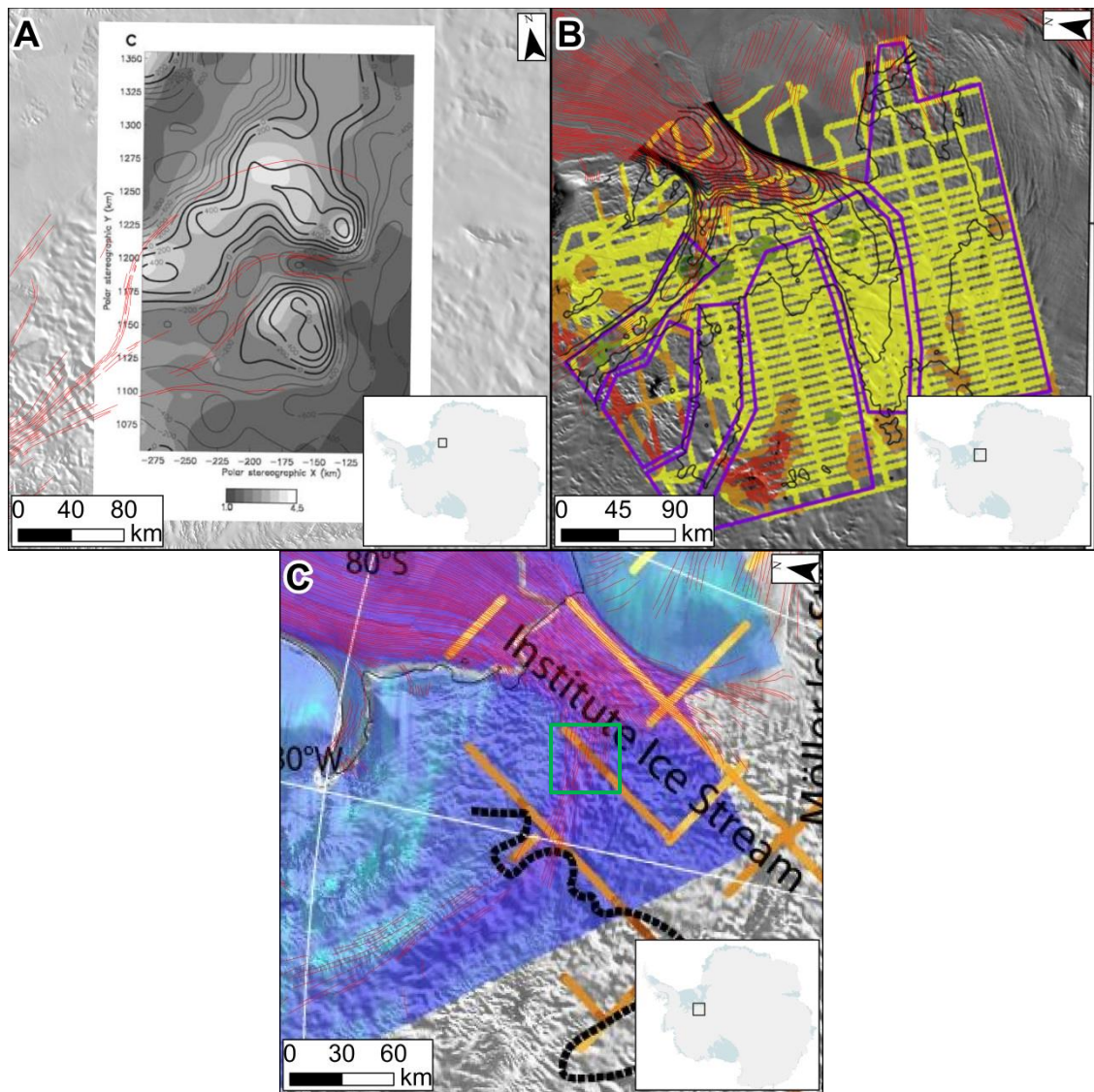


Figure 4.25. Examples of basal roughness indices compared to LSS mapping (red). Background is MODIS composite mosaic. A) Roughness of the bed of a tributary of Slessor Glacier from Rippin et al. (2006). Darker colours on grey-scale are smoother. LSSs are located along ice stream flow lines, where the bed is smoother. B) Roughness of the beds of Institute and Möller Ice streams from Rippin et al. (2014). Red regions are roughest, through orange, yellow and green as the smoothest regions. LSSs are typically located in regions of yellow and green, where the bed is smoothest. C) Roughness of the Institute Ice Stream bed, from Bingham and Siegert (2009). Lines of yellow (smooth) through to dark brown (rough) denote roughness. Light blues denote slow ice velocity, purple denotes high. Green box indicates a potential area where more LSSs coincide with a rougher bed.



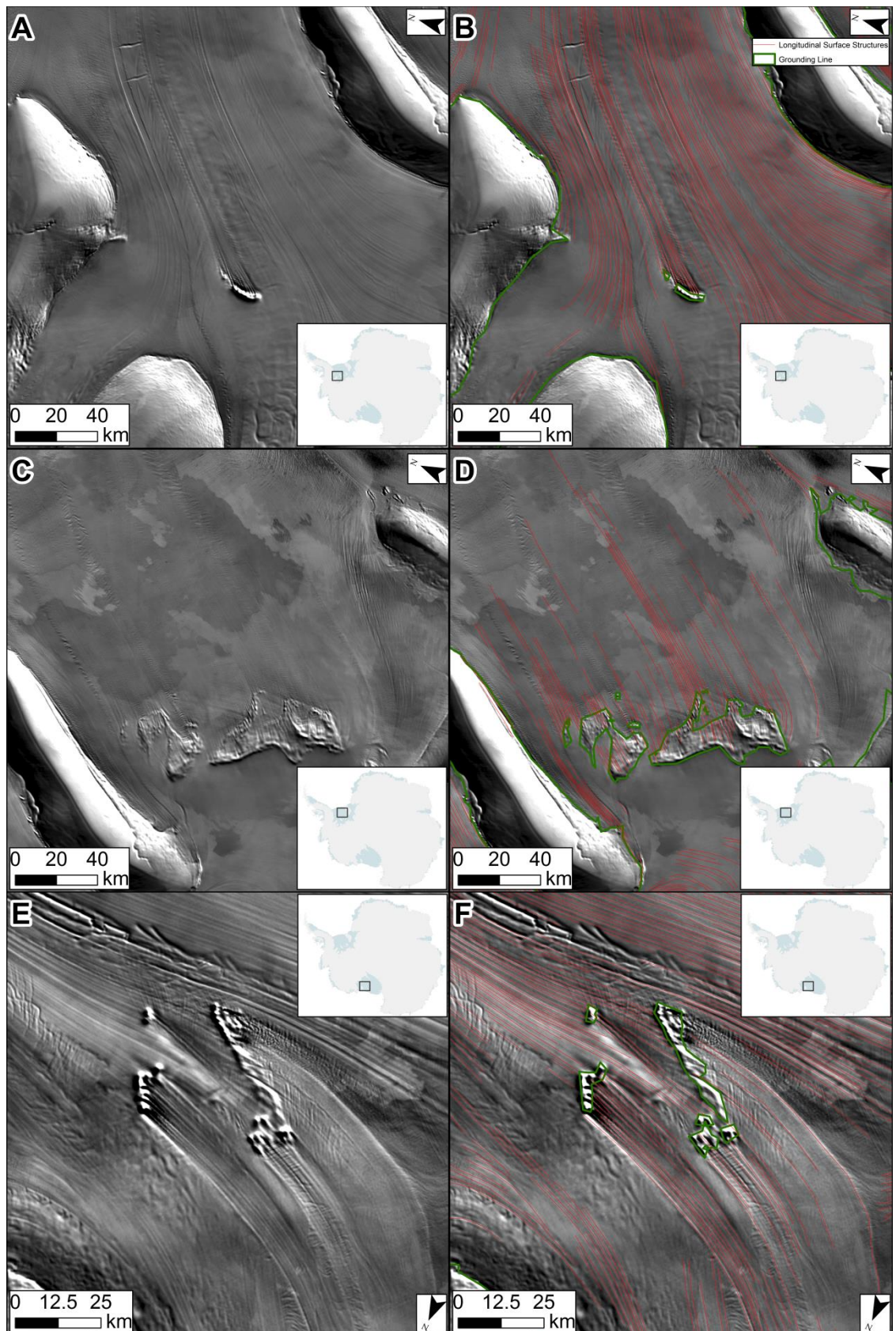


Figure 4.26. MODIS images (left) and mapping (right) LSSs observed to begin at ice rumples. A) and B) The Kershaw Ice Rumples, the Ronne Ice Shelf. C) and D) The Doake Ice Rumples, The Ronne Ice Shelf. E) and F) Ice rumples at the mouth of the MacAyeal Ice Stream, Ross Ice Shelf.



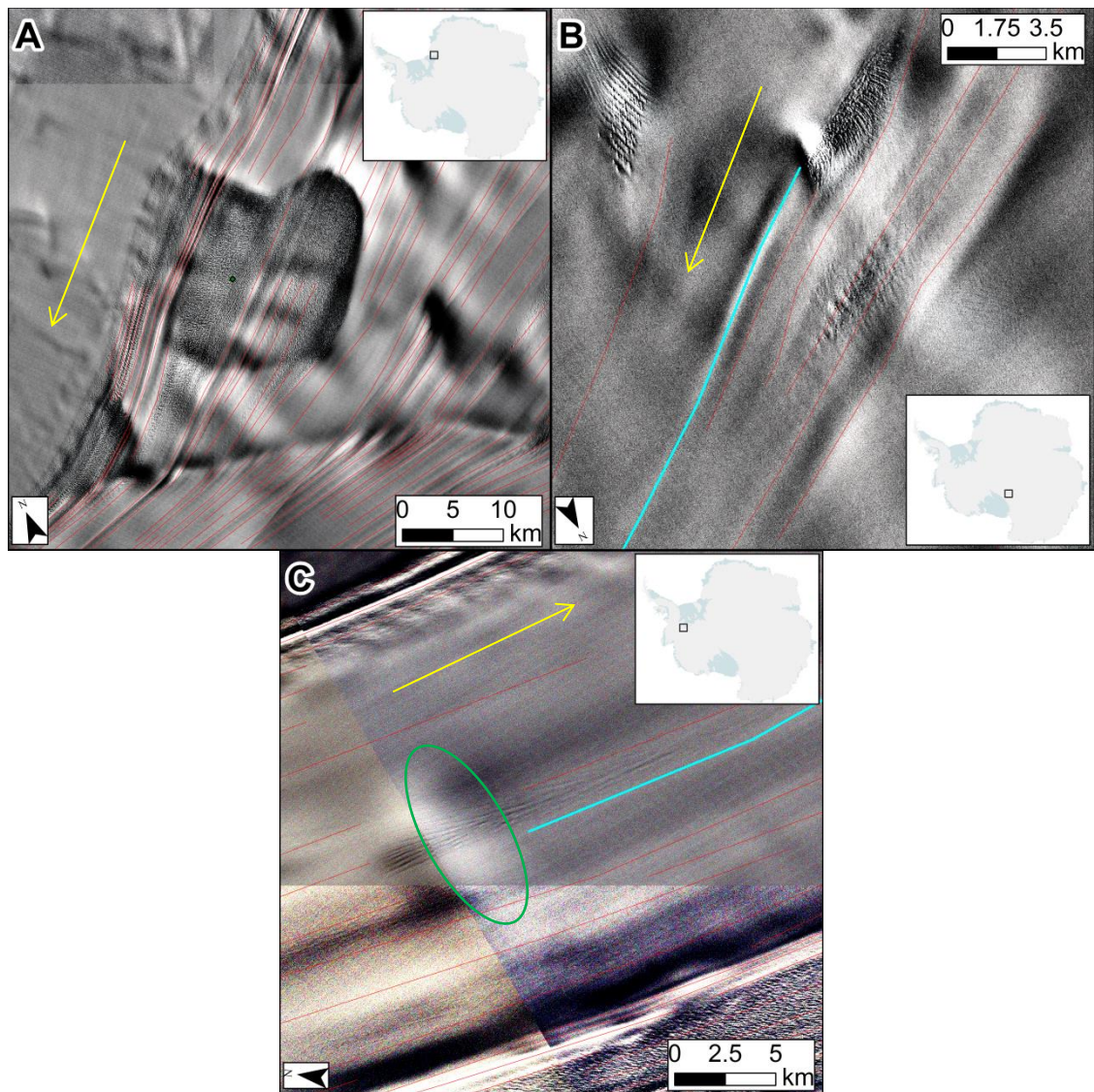


Figure 4.27. Landsat images and mapping of LSSs emanating from possible sticky spots. Yellow arrows denote ice flow direction. A) Ice flow over a bedrock ridge on Slessor Glacier. Note the intense crevassing in the lee of the ridge, and the development of multiple LSSs. However, LSSs are also observed upstream of this ridge. B) An LSS, highlighted in turquoise, emanating from a possible sticky spot at the onset of Byrd Glacier. Note the intense crevassing prior to the LSS. C) An LSS emerging from a known bedrock bump of the Rutford ice stream (highlighted in turquoise). Bedrock bump location is beneath the green oval.

#### 4.4.4 Summary of Results.

Due to the multitude of variables measured, it is useful to summarise the results. Thus far, my results show the following:

- 42,311 polylines representing LSSs were mapped across the Antarctic Ice Sheet at a variety of glaciological settings (Figure 4.12).

- LSSs are typically less than 50 km long, with a median value of 8.7 km. The longest single traceable feature is 450 km long.
- The majority of LSSs are spaced less than 2,000 m apart, with a strong preference between 850 and 1250 m.
- LSSs can begin at low ice velocities, including regions of the ice sheet flowing at approximately 1 m/a, with the majority occurring in regions flowing less than 500 m/a.
- LSSs occur at a wide range of ice thicknesses.
- Only a slight majority of transects showed a negative  $a$  coefficient for a polynomial fit between spacing and distance along a line, representative of a slight preference for more features occurring at the edges of a flow unit.
- There is a strong positive correlation between flow unit width (Figure 4.20) and mean LSS spacing. This relationship is reduced at the individual flow unit scale.
- LSS spacing displays only a weak relationship to ice thickness (Figure 4.22) and velocity (Figure 4.23).
- The ratio between LSS spacing and ice thickness is on average approximately 1; less than the range of 3-10 proposed by Gudmundsson (2003).
- A relationship between LSS occurrence and basal roughness is difficult to derive. However, LSSs were frequently observed to occur at ice rumples, where basal roughness increases (Figure 4.26). More tentatively, LSSs may occasionally also be related to sticky spots (e.g. Figure 4.27).

## 4.5 Discussion

### 4.5.1 Implications for LSS Formation Hypotheses.

The morphological and glaciological properties should provide insight into the formation of LSSs. In Section 4.4.3 I listed several predictions of the basal transfer hypothesis and the compression hypothesis. Table 10 re-reports these predictions and comments on how they were met in my results. These results form the basis of my following discussion regarding the two main formation hypotheses.

Hypothesis	Expectation	Comparison to Results	Expectation met?
Compression	More pronounced LSSs at the edge of a flow unit.	A slight majority (62.4%) of flow units displayed this characteristic. However, some qualitative examples show more pronounced LSSs at flow unit edges.	Partially
Compression	Flow unit width controls LSS spacing due to the degree of ice compression	There is a strong positive correlation between the spacing of LSSs and the width of a flow unit.	Yes
Compression/Basal Transfer	LSSs within a flow unit will respond to changes in width.	The majority of flow units show that as ice converges, the spacing between LSSs gets smaller.	Yes
Basal Transfer	LSSs are closer where ice is thinner.	No significant relationship between ice thickness and LSS spacing.	No
Basal Transfer	LSSs are closer where ice is faster.	No significant relationship between ice velocity and LSS spacing.	No
Basal Transfer	LSSs should be most commonly spaced 3-10 times the ice thickness apart.	LSSs are spaced closer together than expected, typically 1 times the ice thickness.	No
Basal Transfer	There should be more LSSs where the bed is rougher.	Insufficient resolution of bed to highlight individual bumps/roughness areas. But ice rumples are a clear example of increased roughness leading to LSSs.	Partially

Table 10. Expectations of the two main LSS formation hypotheses and comparison to results.

#### 4.5.1.1 Are LSSs a response to basal perturbations?

Table 10 shows that some of the expectations of the basal transfer hypotheses of Gudmundsson et al. (1998) were not supported by my data and analysis. The mechanism proposed by Gudmundsson et al. (1998) requires there to be a rapid basal velocity through slip compared to that achieved by internal ice deformation. Figure 4.16 and Plate 1 show that LSSs typically conform to the arborescent pattern of ice streams and outlet glaciers which achieve their enhanced velocity either through basal sliding or till deformation (e.g. Engelhardt and Kamb, 1998). Figure 4.16 shows that LSSs generally occur where ice velocity is above 20 m/a, which given the low surface profile of many of these regions is higher than could be achieved by internal deformation alone (Glasser et al. (2015) propose sliding must occur above 15 m/a). However, Figure 4.15 shows that many LSSs actually form at velocities much lower than this (as low as 0.11 m/a). These LSS formed in slower ice areas are not limited to small, slow flowing glaciers (e.g. Figure 4.28A, B), but LSSs can also be seen to occur at the onsets of many of the largest ice stream systems (Figure 4.28C-D) (Merry and Whillans, 1993). LSSs can also form in thick ice (Figure 4.17), where transmission of a bump may be difficult. Therefore, it is difficult to explain the formation of all LSSs via the mechanism proposed by Gudmundsson et al. (1998).



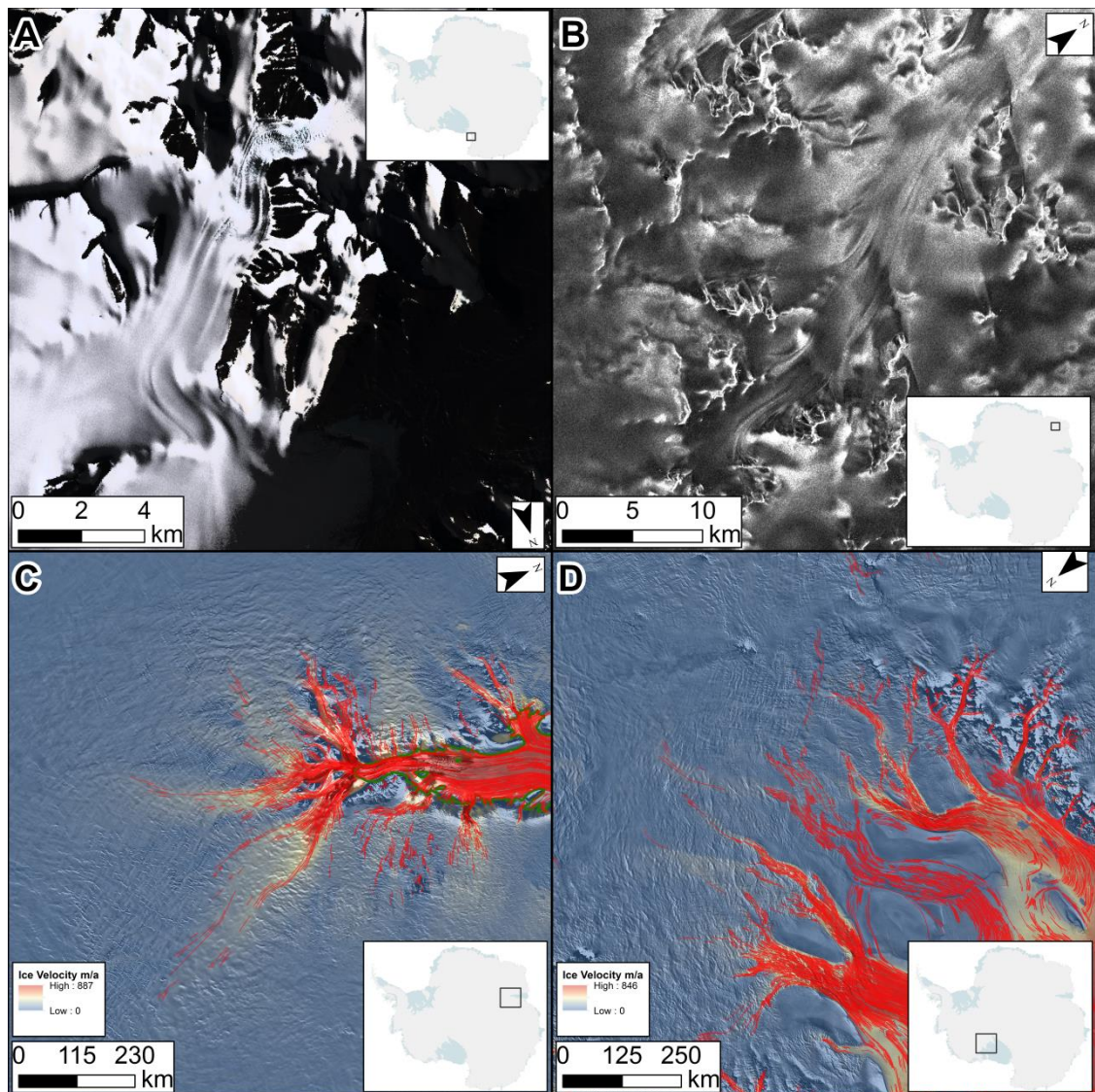


Figure 4.28. Examples of LSSs formed in low ice velocities. A) Landsat image of LSSs on the surface of Commanada glacier, which flows at 4 m/a. B) Radarsat image of Sørhøfjell, which reaches a maximum velocity of 17 m/a. C) The onsets of the Lambert Amery systems shows LSSs in slow flowing ice regions. D) A similar pattern of LSSs in slow flowing onset zones in the Siple Coast region.

In contradiction to the above, it is difficult to explain the formation of LSSs at ice rumples (Figure 4.26) without invoking a connection to an increase in basal roughness. The LSSs that originate from ice rumples are typically spaced 1 km apart (Figure 4.26). However, the ice thickness here is approximately 700m, with uncertainties of +/- 150 m. Therefore, the spacing of LSSs emanating from ice rumples is below Gudmundsson et al.'s (1998) proposed ratio of 3-10 times the ice thickness. LSSs that form by the sudden increase in basal friction presented by an ice rise may therefore form by a different mechanism, most likely as a response to increased strain, rather than a correspondence

to individual bumps. Grounded LSS spacing was also less than predicted by Gudmundsson et al. (1998), which typically have the same spacing as the ice thickness (Figure 4.24). However, on grounded ice this may be the consequence of inherited LSSs from upstream, which would act to reduce the spacing of LSSs (e.g. Figure 4.11 B). Whereas, no inheritance of LSSs was observed on the Kershaw and Doake ice rumples (Figure 4.26 A-D).

Overall, the mechanism proposed by Gudmundsson et al. (1998) is not applicable for the formation of many LSSs. However, isolated occurrences of LSSs emanating from possible bedrock bumps or sticky spots were noted (e.g. Figure 4.27). Therefore, it does appear that increased resistance at the ice-bed interface can lead to the formation of LSSs. However, I propose that a minority of LSSs are formed by this mechanism.

#### *4.5.1.2 Do LSSs form by lateral compression and longitudinal extension?*

Many of the expectations of the compression hypothesis were met in this study. A slight majority of flow units had more LSSs at the edge of the flow unit (Table 10). However, examples of more pronounced LSSs at flow unit boundaries were noted (Figure 4.19). Occasionally, these bordered the troughs described by Glasser and Gudmundsson (2012). These are regions where there is strong lateral convergence and accelerated longitudinal extension (Glasser and Gudmundsson, 2012). These enhanced conditions may explain why LSSs in these regions have a more pronounced morphology. Such a distribution has been noted for foliations formed by lateral compression (Allen et al., 1960; Hambrey et al., 2005). Further examples of LSSs forming where ice is laterally compressed can be seen in Figure 4.29A and B. Therefore, the compression hypothesis is at least applicable in certain situations.

For individual flow units, both the compression hypothesis and the basal transfer hypothesis can explain the correlation found between flow unit width and LSS spacing (Figures 4.11 and 4.21). However, the compression hypothesis may also be able to explain why this occurs across multiple flow units. (Figure 4.20). On a narrow ice mass, compressional stress will cause strain across the whole ice mass, leading to folding of the ice which manifests itself as LSSs on the surface. On a wider ice mass, the same compressional stress would be spread across a greater distance, creating LSSs that are further apart due to an increased amount of accommodation space. Therefore, the compressional hypothesis is the most applicable to explain the bulk characteristics of LSSs.

Despite the above, instances of LSSs occurring that are difficult to reconcile with the compression hypothesis were also noted. LSSs were observed to occur where little convergent streaming flow has occurred (Figure 4.29 C), and to begin before ice stream onset zones (Figure 4.28 C and D; Figure 4.16). These LSSs must either form through flow convergence and lateral compression before the start of streaming flow, or begin due to localised high shear strain at an onset zone (Merry and Whillans, 1993). Additionally, the LSSs which begin at ice rumples (Figure 4.26) and sticky spots (Figure 4.27) are difficult to reconcile with the compression hypothesis. Although the compression hypothesis may be applicable to some LSSs, like the basal transfer hypothesis it is unable to explain the formation of all LSSs. However, as a majority of flow units conform to the expectation of the compression hypothesis, and it is able to explain the relationship LSSs have with flow unit width, I propose that most LSSs form in this way.

Interestingly, LSSs flowing into the Helle Slope piedmont appear to disappear once flow divergence onto the piedmont begins (Figure 4.29 D). This is perhaps due to a relaxation of surface topography by lateral extension within the ice. This suggests that LSSs can disappear due to flow divergence, as well as form by flow convergence.

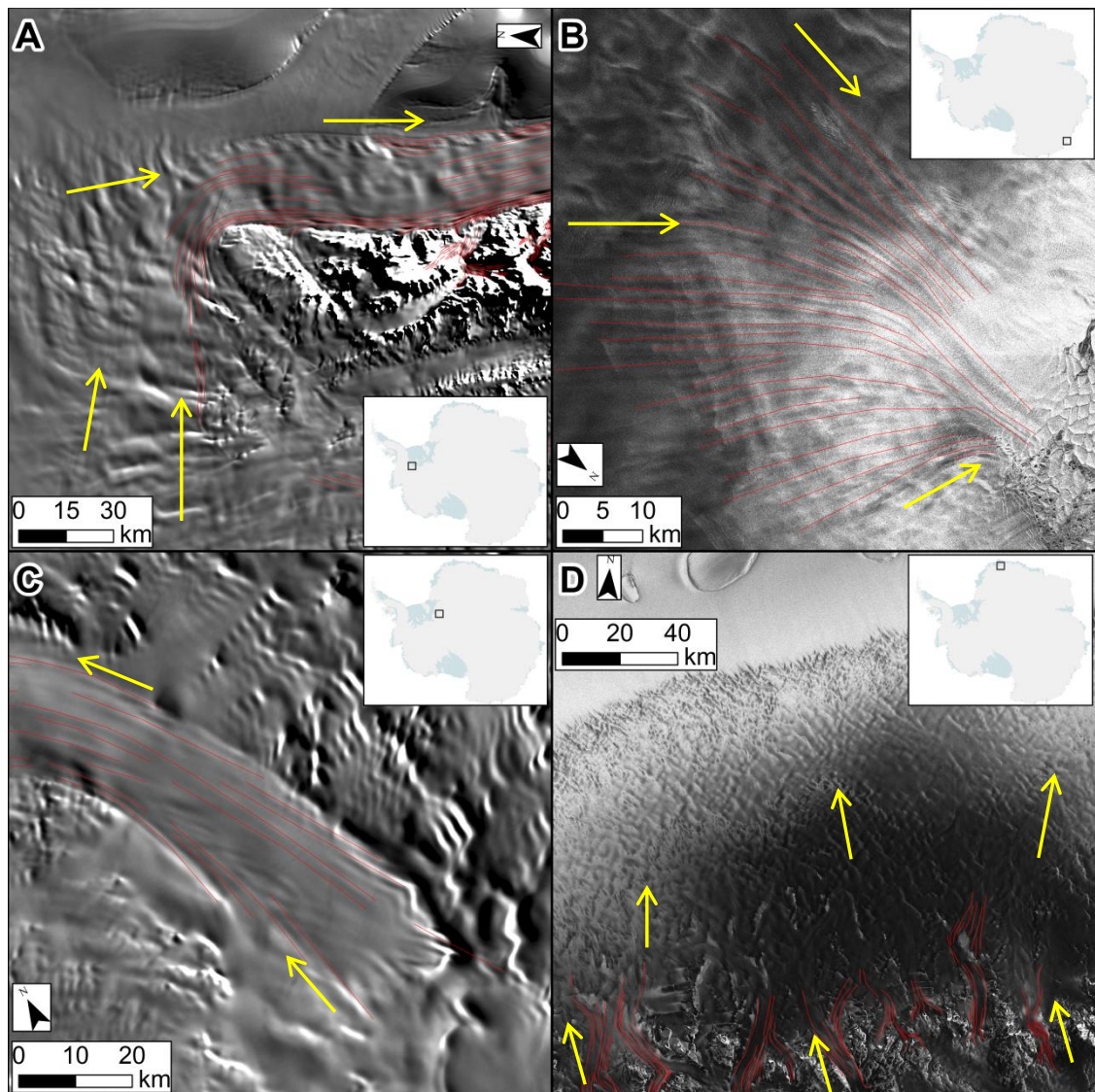


Figure 4.29. A) MODIS image and mapping of LSSs on the Rutford Ice Stream. LSSs are concentrated where ice is flowing around the Ellsworth Mountains, and where tributaries join the ice stream. These are the regions of highest compression. B) RADARSAT image and mapping of LSSs on Frost Glacier. This shows a clear convergent flow pattern. C) MODIS image and mapping of LSSs at the onset of Blackwell ice stream. Flow here shows only a weakly convergent pattern. D) RADARSAT image and mapping of LSSs flowing onto the Helle Slope piedmont. These LSSs seem to disappear on the piedmont, where ice flow is divergent. Yellow arrows denote approximate ice flow directions.

#### 4.5.2 Hybrid Model of LSS Formation

From the above discussion (Section 4.5.2) it is clear that a single formation mechanism cannot explain all LSSs. Therefore, I propose a hybrid model of LSS formation, invoking multiple formation mechanisms. In order to explain the formation of LSSs, the following main characteristics and situations must be explained:

1. The relationship between LSS spacing and flow unit width.



2. LSSs that form at the onset of enhanced flow.
3. LSSs at the boundary of flow units.
4. The formation of LSSs at regions of increased basal friction, such as ice rumples.

As discussed above, the compression hypothesis is the best suited to explain the relationship LSSs have with the width of a flow unit. Therefore, I propose that the majority of LSSs are formed by the strain of ice under lateral compression and longitudinal extension (e.g. Hambrey and Dowdeswell, 1994). This accounts for factor 1. Similarly, LSSs at onset zones can be seen as the consequence of increased shear strain at these locations (e.g. Merry and Whillans, 1993), accounting for factor 2. Thin LSSs which form due to lateral shear between two ice masses have been accounted for by the mechanism proposed by Glasser and Gudmundsson (2012), whereby the differential strain between two converging ice masses leads to a surface depression (Figure 4.7). On satellite imagery, these features appear as depressions, with distinct features either side (Glasser and Gudmundsson, 2012). Here, the feature itself was not mapped, only the high points in reflection either side. These are also regions of localised ice strain, accounting for factor 3. Finally, increased regions of basal shear stress, from sliding over bed bumps, may also lead to the development of LSSs (e.g. Figure 4.27, Merry and Whillans, 1993), but to a lesser extent than was proposed by Gudmundsson et al. (1998). Such regions are more likely to be isolated, and include sticky spots, and ice rumples, accounting for factor 4. Thus, I propose these 4 mechanisms combine to produce the LSSs we observe on the surface of the ice. A summary of my hybrid model of LSS formation is provided in Figure 4.30. Therefore, my hybrid model views LSSs as an expected consequence of strain, induced by stresses encountered by ice in multiple situations (Figure 4.30).

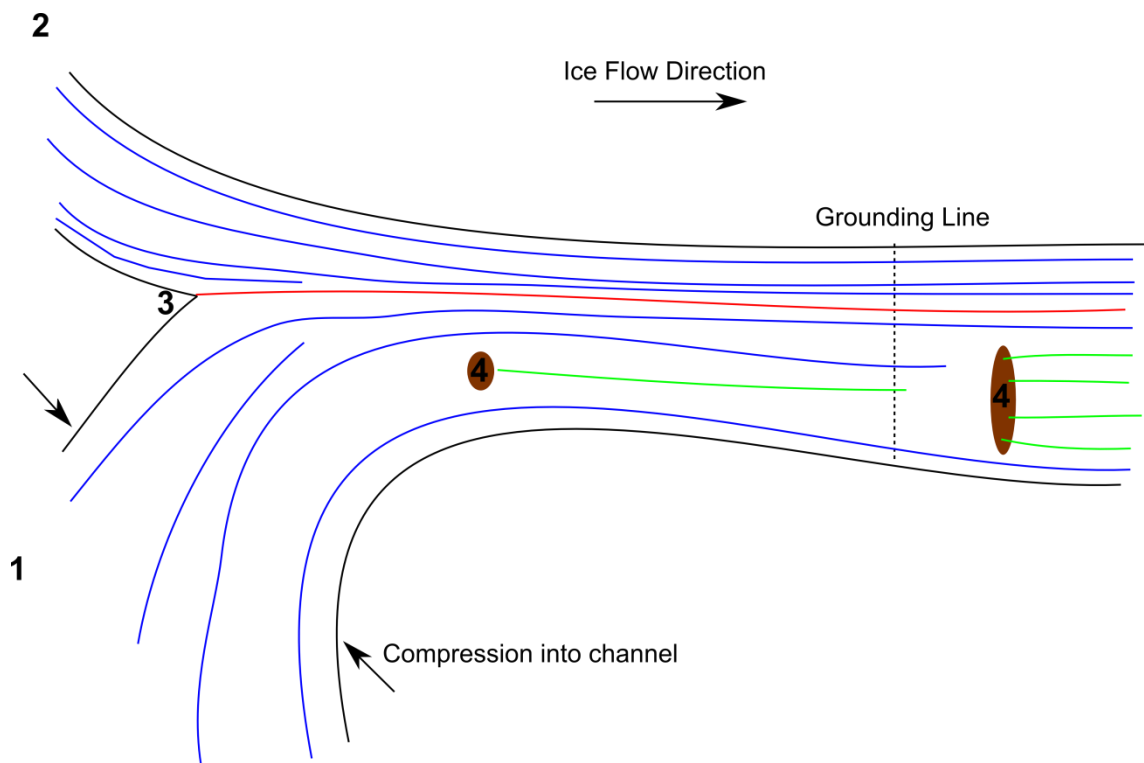


Figure 4.30. A hybrid model of LSS formation. LSSs are the consequence of strain in 4 different situations. Black lines denote flow unit boundary. 1) LSSs formed by the lateral compression and longitudinal extension of ice. 2) LSSs formed at the onset of fast ice flow, leading to increased shear strain. 3) LSS formed at the convergence between two ice channels, distinguished in red. 4) LSSs formed by flow over a sticky spot (left), and an ice rumple (right), these are coloured green.

#### 4.5.3 Flow Stripes or Foliations?

LSSs are often placed into two categories; foliations and flow stripes, the key distinguishing feature being the three dimensional structure to foliations. Above I propose the compression hypothesis, which is based upon the formation of foliations found on valley glaciers (e.g. Hambrey, 1977; Hambrey and Lawson, 2000, p.70; Figure 4.3), is applicable to the majority of LSSs. Whilst here I only have an aerial view of LSSs, distinguishable populations were not found in my analysis of length, spacing, ice velocity or ice thickness. Perhaps the most remarkable of these metrics is spacing, which has the highest kurtosis value (Table 8), and is therefore the most consistent metric. Within a flow unit, LSSs tend to be regularly spaced (e.g. Figure 4.31), and it is thus difficult to ascribe different genetic origins for LSSs based upon satellite imagery and morphometrics alone. Furthermore, the similar behaviour found in the spacing metric between different flow units points to a common origin for LSSs between flow units.

Figure 4.31. Examples of regularly spaced LSSs. LSSs are marked in red, background is MODIS imagery. A) LSSs on Byrd Glacier occur at regular intervals in the onset zone. This regular spacing is changed as they converge into the main trunk of the glacier. B) Regularly spaced LSSs of the Institute Ice Stream (I), Bugenstock ice rise (B) and Foundation Ice Stream (F). Note the regularity is modulated by the size of the flow unit.

Whilst I find common properties between LSSs when viewing them as two dimensional objects in satellite images, the three dimensional structure of LSSs may be observed in ice penetrating radar. Therefore, it is apt to briefly review the previously published literature concerning ice penetrating radar images of isochrones. Campbell et al. (2008) found the folds in isochrones of the Kamb ice stream to be a similar wavelength to that of the LSSs at the surface. Although isochrone wavelength changes with depth, potentially due to different patterns of surface accumulation and strain history (Grey et al., 2008). Interestingly, like LSSs the wavelength of isochrone folds also decreases as the ice stream converges (Campbell et al., 2008; Figure 4.20). Isochrone folds have also been found under other regions where LSSs are situated. King (2011) observed folded isochrones within a portion of the Rutford Ice Stream that flows at 250 m/a, which has surface LSSs. Conversely, the isochrones of the slower Carlson inlet (5 m/a), which does not display surficial LSS, were not folded (Figure 4.33). Furthermore, the neighbouring Talutis Inlet (180 m/a), which again has LSSs, also contains folded isochrones (Figure 4.32). Finally, a third example of folded isochrones and LSSs coexisting occurs on the Bugenstock Ice Rise (Siegert et al., 2009). Here, the relict LSSs at the surface correspond with a buried buckled, or folded, layer of isochrones. Whilst far from a comprehensive survey, it appears that all three examples

where radar images and LSSs coexist reveal folded isochrones and thus fully three-dimensional features in the ice.

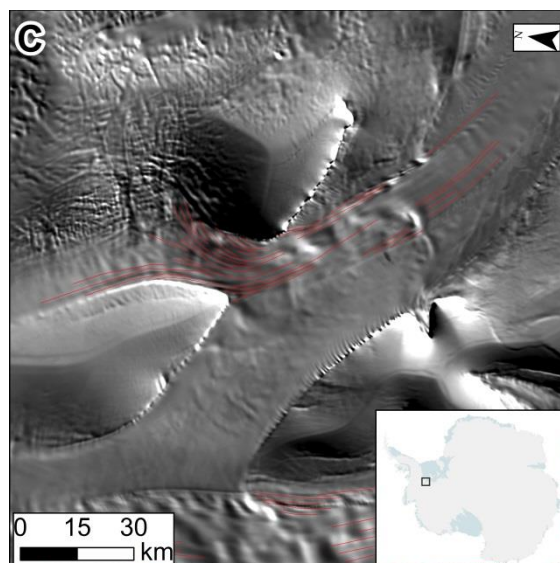


Figure 4.32. The relationship between LSSs and isochrone folding on the Talutis inlet and Carlson inlet. A) A three dimensional view of an isochrone, note the folding of isochrones on the Talutis Inlet, but lack of folding within the Carlson Inlet. B) Location of A is shown by labels. A and B from King et al., 2011. C) Modis image of the area and mapping of LSSs. Note the lack of LSSs on the Carlson Inlet, yet their presence on the Talutis Inlet. This corresponds with the pattern of isochrones folds seen in A.

Despite the possible three dimensional structure of LSSs, there is a jump in scale between the longitudinal foliation commonly reported on valley glaciers and LSSs visible on satellite imagery. Longitudinal foliations tend to be in the order of millimetres in amplitude and spaced meters apart (e.g. Figure 4.2; Allen et al., 1960; Lawson et al., 1994; Appleby et al., 2010; Jennings et al., 2014). Whilst LSSs in Antarctica have been reported to be meters in relief, with spacing's typically in the order of a kilometre (Dowdeswell and McIntyre, 1987; Fricker et al., 2000; Raup et al., 2005; Figure 4.14). Therefore, whilst the radar data suggest that many LSSs are three dimensional, perhaps they are separate phenomena to foliations, forming at a much larger scale.

Overall, the similar behaviour of LSSs between different flow units, and their often observed three dimensional structures suggests that the distinctions placed between LSSs may not be justifiable. However, the term 'foliation' has genetic connotations (e.g. Hambrey and Lawson, 2000, P.70), and is more often reserved for the

much smaller phenomena found in field studies of glacier structure (e.g. Figure 4.2). LSSs can form in a variety of situations, and therefore a non-genetic term is required. I therefore retain the term LSS due to its non-genetic connotations and its association with features of this scale.

#### 4.5.4 Implications for Reconstructing Palaeo-Ice Flow.

One of the main utilities of LSSs is their ability to inform us about palaeo-ice flow conditions (e.g. Fahnestock et al., 2000; Hulbe and Fahnestock, 2007; Glasser et al., 2014, Section 4.2). However, these reconstructions are based on an incomplete knowledge of the formation of LSSs, and thus the utility of LSSs are re-evaluated here in light of my results (Section 4.4) and my new model of LSS formation (Section 4.5.3). Firstly, LSSs are often associated with fast flow (e.g. Campbell et al., 2008; Swithinbank et al. 1988; Stephanson and Bindschadler, 1990). This means that where relict LSSs are found, these regions are often interpreted as palaeo-regions of fast ice flow (e.g. Conway et al., 2002; Sigert et al., 2014). However, I find that LSSs are formed in a range of ice velocities, including slow flowing ice regions (Figure 4.15 and 4.16). Thus, whilst the regions where relict LSSs have been found are prone to contemporary ice streaming, the presence of relict LSSs should not be taken as evidence for ice streaming or high velocity ice flow on its own. The assumption that these features represent palaeo-ice flow direction remains valid.

LSSs have also been used to argue for regions of flow stability (Glasser et al., 2015). Here, the length of an LSS is thought to be related to its age. However, such an assumption is only valid where LSSs form at a stationary point source (e.g. a basal bump or ice rumple). Therefore, only where such features can be identified should this technique be used to date the age of an LSS. As I propose that the majority of LSSs are formed by lateral compression of the ice (e.g. Figure 4.30), such a technique is not valid as under this model features do not emanate from a clearly identifiable start point. LSSs emanating from ice rumples provide the strongest case for applying this technique. Interestingly, LSSs from both the Kershaw ice rumples (Figure 4.26A and B) and the Ice Rumples on the Ross Ice Shelf (Figure 4.26 E and F) reach the calving front of the ice shelf, suggesting a consistent flow configuration. However, LSSs emanating from the Doake Ice Rumples (Figure 4.26 C and D) do not propagate to the calving front. This agrees with the interpretation that ice flow has switched direction in this region (Siegert et al., 2014).

## 4.6 Summary and Conclusions

Here I present mapping of 42,311 polylines representing LSSs observed on satellite imagery of the Antarctic Ice Sheet. Analysis of the morphological and glaciological properties of the mapped LSSs reveals that the majority of LSSs are spaced between 850 m and 1250 m apart. LSSs spacing changes between ice flow units, and has a strong positive correlation with flow unit width. LSSs occur at a wide range of ice thicknesses, but can form where ice is flowing at approximately 1 m/a. My observations are incompatible with any single pre-existing hypothesis of LSS formation. However, the majority of LSSs conform to the hypothesis that they are the result of lateral compression and longitudinal extension of ice. LSSs were also observed to occur in 4 situations of increased strain; as ice converges into a channel, at the onset to ice streaming, between flow unit boundaries and as ice flows over a basal bump or ice rumple. I thus propose a hybrid model of LSSs formation to account for these situations, whereby the majority of LSSs form by lateral compression and longitudinal extension, but isolated examples also form via three other mechanisms. My model and findings have implications for deciphering ice sheet history from LSSs.

# Plate 1

Map of LSSs.





# Chapter 5 Transverse Surface Structures on the Antarctic Ice Sheet

## 5.1 Introduction

Compared to the surrounding slow-flowing domes, ice stream surfaces have a complex morphology (Figure 5.1). Many aspects regarding this “texture” remain unresolved (Hindmarsh, 1998c). In Chapter 4 I analysed the morphological characteristics of the features belonging to this texture that are aligned with the direction of flow (LSSs). Here I take a similar approach to the study of transverse surface structures (TSSs), examples of which can be seen in Figure 5.1C. Elsewhere, these features have previously been named mottles, lumps and warps (Casassa and Whillans, 1993). However, the non-genetic term transverse surface structures (TSSs) is preferred here.

TSSs (Figure 5.1) are thought to be caused by localized thickening and thinning of ice, with corresponding variations in ice velocity (e.g. Bindschadler and Scambos, 1991; Sergienko and Hulbe, 2011). These features would not occur if conditions within the ice or at the ice-bed interface were homogenous (Bennet, 2003). Therefore, their origin is thought to be a consequence of either: i) variations in ice rheology (Whillans and van der Veen, 1993; Hulbe and Whillans, 1994); ii) flow over basal topographic perturbations (McIntyre, 1986; Bindschadler and Scambos, 1991; DeRydt et al., 2013); or iii) variations in basal lubrication and sliding (Bindschadler et al., 1996; Hindmarsh, 1998c; Whillans and Johnsen, 1983). The latter two of these explanations would mean that TSSs are the surface manifestation of ‘sticky spots’ (Alley, 1993; Stokes et al., 2007), isolated regions of high basal drag. They therefore would represent significant components in the force budgets of ice streams, inducing lateral variations in ice flow which the latest versions of numerical ice sheet models need to incorporate (e.g. Sergienko, 2012). Furthermore, it is unclear whether these features are static (i.e. standing waves), migrate or a combination of the two (Hindmarsh, 1998c; Hulbe and Whillans, 1994; Reusch and Hughes, 2003). Elucidating this may provide clues for deciphering TSS genesis, and is important for their incorporation into our understanding of ice sheet flow.

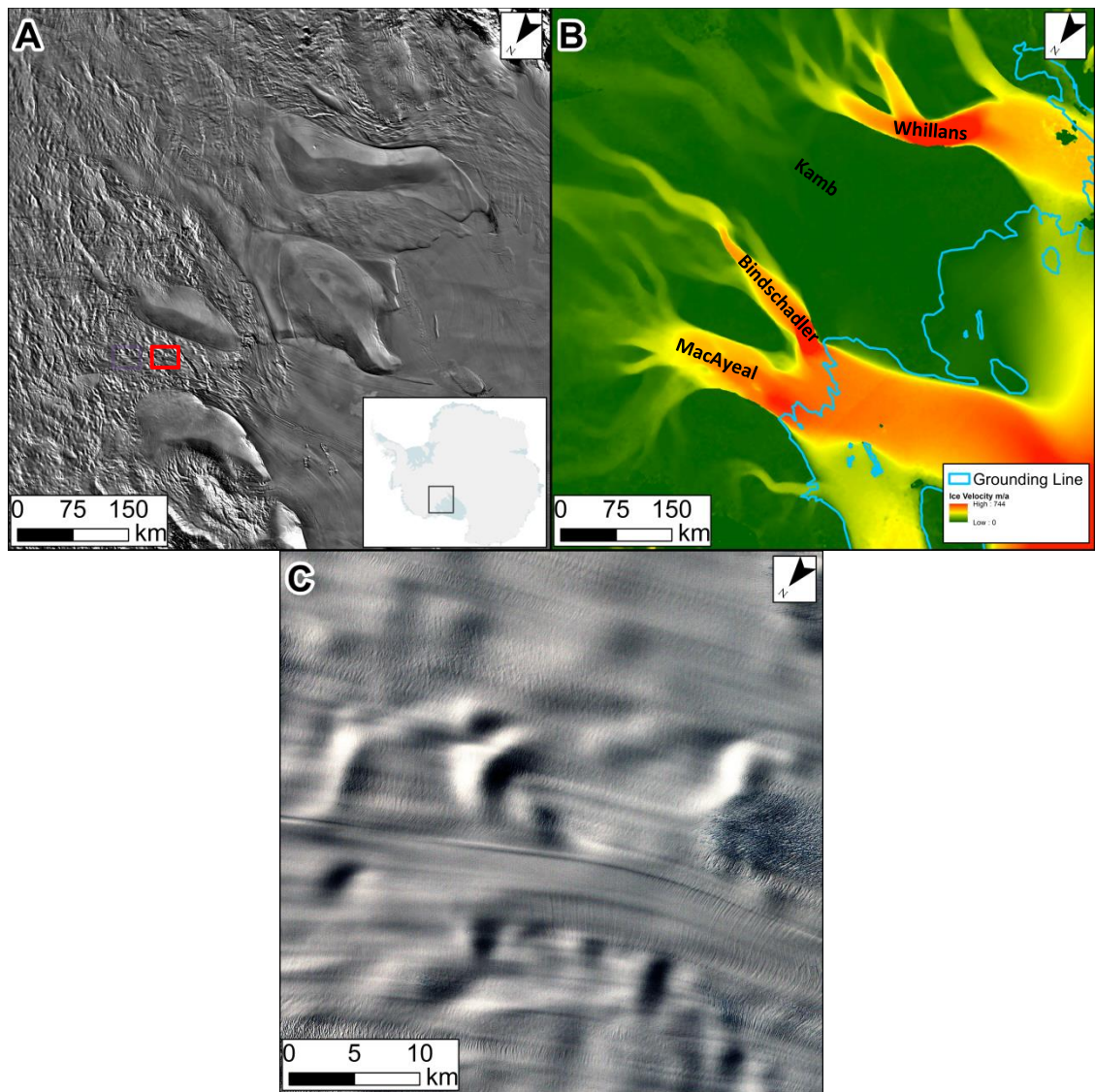


Figure 5.1. MODIS imagery of the surface of the Siple Coast ice streams shows the distinction between the textured ice streams, and the smooth inter-ice stream ridges (A). This texture roughly corresponds with regions of fast flow on grounded ice (B). These ice streams are labelled on (B). Features are also evident, but more subdued, on the now relict Kamb Ice Stream. This texture is composed of surficial wave-like features which are broadly transverse to flow direction, as seen on the Landsat image (C), ice flow is to the right. (C) is located within the red box drawn on (A).

Although TSSs are a common feature of ice stream surfaces (Figure 5.1A), previous work on TSSs and sticky spots has been limited to small study areas typically within a single ice stream (e.g. Bindschadler and Scambos, 1991; Merry and Whillans, 1993; Hulbe and Whillans, 1994). Thus, differences and similarities in the manifestation of TSSs between ice streams is unknown. Whilst ice penetrating radar has the potential to reveal much about sticky spots (Ashmore et al., 2014), this requires costly field campaigns or airborne geophysical surveys, limiting the spatial and temporal

distribution of such data. Furthermore, regions of high basal drag are usually located by inversions of ice thickness and velocity measurements (e.g. Thorsteinsson et al., 2003). Such inversions are computationally expensive and limited in resolution by the available thickness and velocity data (Sergienko et al., 2014). Here I utilise satellite imagery of the ice surface to give us full spatial coverage of the ice sheet, and a temporal record of how the surface may have evolved. This enables us for the first time to derive the morphological properties and distribution of TSSs which can be compared to available glaciological data (e.g. Rignot et al., 2011; Fretwell et al., 2013). Furthermore, the multi-temporal record that satellite images provide, should provide insight into whether or not TSSs migrate.

## 5.2 Previous Work

Flow transverse variations in the surface of an ice mass were first revealed by detailed topographic and altimetric surveying (e.g. Budd, 1970; McIntyre, 1986). However, the extent and abundance of this texture was only appreciated when sufficient satellite imagery became available (Swithinbank et al., 1988; Merry and Whillans, 1993). Based upon a perceived variation in scale, Merry and Whillans (1993) divided the flow-transverse features (TSSs) on the surface of Whillans Ice Stream into three categories; lumps, mottles and warps. Mottles are the largest and most common of these, and are typically spaced 10 km apart. Whilst warps may be a more pronounced version of mottles (spacing  $\approx$  8 km). Lumps appear to be much smaller ( $\approx$  600 m spacing), and may be related to the specific history or shear margin migration that has occurred at the Whillans Ice Stream (Price et al., 2001). Here the term transverse surface structures (TSSs) is preferred, as my intention is to study the origin of ice surface texture (e.g. Figure 5.1), rather than study individual features such as lumps that may be specific to just the Whillans Ice Stream.

The origin of TSSs has been attributed to three different variations in ice flow properties. Budd (1970) was the first to propose that TSSs are the result of flow over bed undulations. His model predicted that undulations with a wavelength 3.3 times that of the ice thickness would be preferentially transmitted to the ice surface, with shorter wavelength features being dampened out and thus not creating a surface expression. Subsequent modelling highlights that ice only acts as a band-pass filter in this manner where the rate of basal slip is high compared to ice internal deformation (Gudmundsson, 2003), explaining the selective location of TSSs upon ice stream surfaces. Furthermore,

bed to surface transmission is modified by vertical variations in the temperature of the ice sheet (McIntyre, 1986), such that surface expressions should be weaker where the temperature gradient in the ice is higher (Schoof, 2002). Models of basal transfer produce an output that looks similar to that observed on the ice surface (Sergienko, 2012; Figure 5.2). These modelling studies are supported by both radar profiles of the ice sheet comparing the bed to the surface (e.g. McIntyre, 1986; DeRydt et al., 2013), and observations of increased transmission during surge events where the component of basal sliding drastically increases (Gudmundsson et al., 2003). The hypothesis of transmission from basal bumps would require all TSSs to be spaced 2-10 times the ice thickness apart, with a strong preference around 3, and their wavelength to be modified by the ratio of sliding to internal deformation. Furthermore, different bodies of ice, with different properties such as viscosity should have selected different wavelengths for TSSs.

m

m/yr

Figure 5.2. From Sergienko (2012). Modelling of flow over bumps in the bed of an ice stream. Ice flow is from left to right. Bed topography is pictured in (a). Ice surface height variations are plotted in (b) and (d). Ice velocity is plotted in (c) and (e). Flow produces surface elevation perturbations (b and d) that are similar in appearance to TSSs. Furthermore, these features induce variations in ice velocity (c and e).

A deficiency of the bed undulation mechanism is its inability to explain TSSs where no clear relationship exists between surface and basal topography (Hindmarsh, 1998c; Whillans and van der Veen, 1993). Whillans and Johnsen (1983) noted distortions in radar layering at a wavelength of 10 km with corresponding surficial features, occurring over regions of flat basal topography. Instead, variations in basal radar return power were interpreted to show variation in the amount of basal water, and hence basal coupling. Whillans and Johnsen (1983) added to the model of Budd (1970) to propose that variations in basal coupling or sliding could also produce TSSs (Figure

5.3). Similar to the bed undulation hypothesis, slip variations spaced 2-10 times the ice thickness apart should be preferentially displayed at the surface (Gudmundsson, 2003).

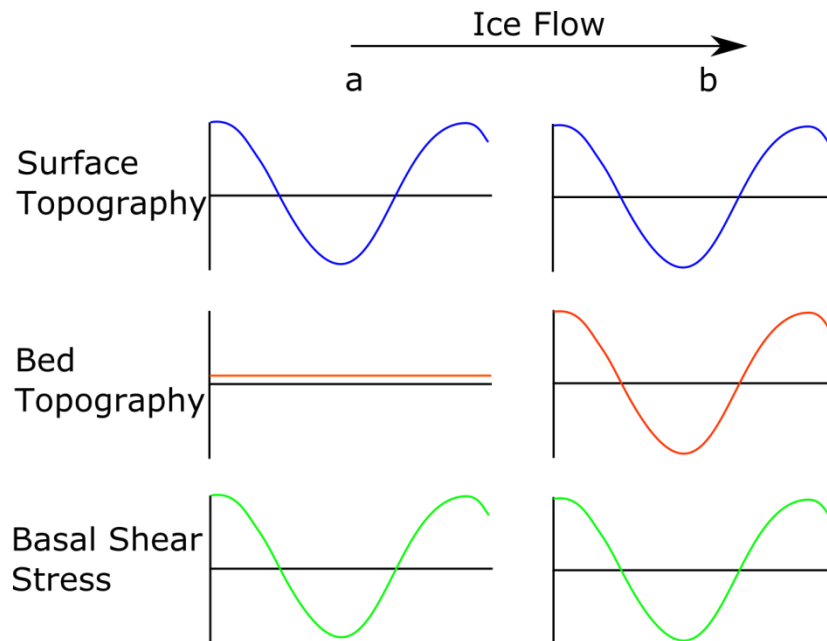


Figure 5.3. Schematic of Whillans and Johnsen's (1983) model for the formation of TSSs. TSSs were modelled as a response to longitudinal variation in either the basal shear stress alone, caused by differential water pressure (a), or bed topography (b).

Both basal perturbations and regions of no sliding act as sticky spots; localised patches of high basal drag surrounded by low well lubricated low shear stress regions (Alley, 1993). In a review of both contemporary and palaeo-ice sheets, Stokes et al. (2007) found four types of sticky spots: bedrock perturbations; till-free areas; areas of well-drained till; and regions of basal freeze-on. Thus, TSSs may be the surface manifestation of sticky spots. Under contemporary ice sheets, variations in basal stress are revealed by inversions from surface data (e.g. MacAyeal, 1992; Joughin et al., 2004, 2009; Sergienko et al., 2008). The latest generation of such models reveal regular patterns in the spatial distribution of basal shear stresses (Sergienko and Hindmarsh, 2013; Sergienko et al., 2014), the appearance of which are strikingly similar to that of TSSs (e.g. Figure 5.4). Thus, the formation of both sticky spots and TSSs may be linked, and require a mechanism which produces a regular pattern. Sergienko and Hindmarsh (2013) propose that an instability, similar to that which forms subglacial ribs (Dunlop et al., 2008), could explain the formation of such patterns, pointing to their similarity to mega-ribs (Greenwood and Kleman, 2010; See Chapter 3). Thus, TSSs may be the surface manifestation of subglacial ribs.

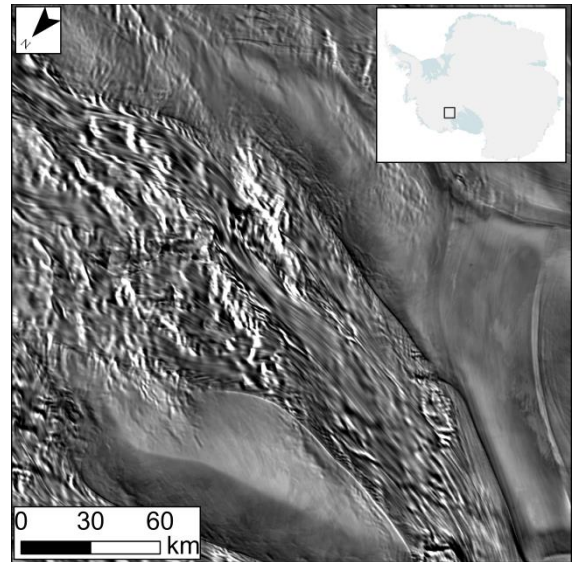


Figure 5.4. Sergienko et al.s' (2014) inversion reveals regular patterns in basal shear stress of the Bindschadler Ice stream (A). These are qualitatively comparable to patterns observed in (B), a MODIS image of the ice surface.

A third explanation for TSSs requires no basal variation. Instead, others have proposed that TSSs represent bands of different ice properties. One proposed mechanism by which alternate bands of ice can be incorporated into ice stream flow is by head-ward expansion of an ice stream incorporating discrete bodies of cold based ice, termed ice rafts, into the flow (Shabtaie et al., 1987; Merry and Whillans, 1993). However, the abundance of such features is questionable, as they have only been observed on Whillans Ice Stream, which has a complex history of widening and expansion (Catania et al., 2012). Hulbe and Whillans (1997) proposed that differential crystal fabrics within ice would lead to bands of aligned crystal fabric which create bands of horizontal ice strength. Therefore, the strain rate of the ice varies due to contrasts in ice strength, creating topographic perturbations in the ice surface. In contrast to the bed undulation and slipperiness mechanisms, these mechanisms require no relation to underlying basal properties or ice thickness.

Intriguingly, it is unclear whether TSSs form standing or migratory waves on the surface of an ice sheet (Reusch and Hughes, 2003), or whether both co-exist (Hulbe and Whillans, 1994). Yet, both mechanisms which appeal to variations in basal lubrication (Hindmarsh, 1998c; Sergienko et al., 2014) and variations in ice strength (Hulbe and Whillans, 1994) predict that features could migrate. The direction of travel for some features is unknown, with some features having been observed to migrate upstream and

others downstream (Hulbe and Whillans, 1994). For the lubrication mechanism, migration should occur on a decadal to centurial timescale (Sergienko et al., 2014), whereas variations in ice properties would be advected with ice flow (Shabtaie et al., 1987).

The differential strain at a TSS creates perturbations to measured velocity fields (Bindschadler and Scambos, 1991; Sergienko, 2012). When attempting to model ice streams in an ice sheet model, the effect of such variations is often averaged across the flow, as the drag imposed by a shear margin is often considered more important (e.g. Raymond, 1996; Whillans and van der Veen, 1997; Schoof, 2012). However, modelling of grounding line evolution is extremely sensitive to conditions such as ice velocity and basal drag (Favier et al., 2012; Pattyn et al., 2013; Walker et al., 2013). Therefore, understanding the spatial scale of these features, and the magnitude of the perturbation in ice flow that they induce is important for how ice sheets flow. If the morphology and perturbation of these features is regular, this may allow for simple parameterisation within an ice sheet model.

Thus far, a morphological study of TSSs across different ice stream surfaces and from imagery at different time periods has not been undertaken. Thus, the morphology, spatial characteristics and velocity variation of TSSs is poorly defined. This chapter aims to:

- Define the length and spacing of TSSs
- Assess the regularity of TSSs
- Ascertain their relationship to ice thickness and velocity measurements, to test the basal transfer hypothesis
- Compare their morphology between different ice streams, to elucidate any controls on TSS morphology
- Observe whether features migrate or not
- Define the magnitude of the perturbation in ice velocity that TSSs represent.

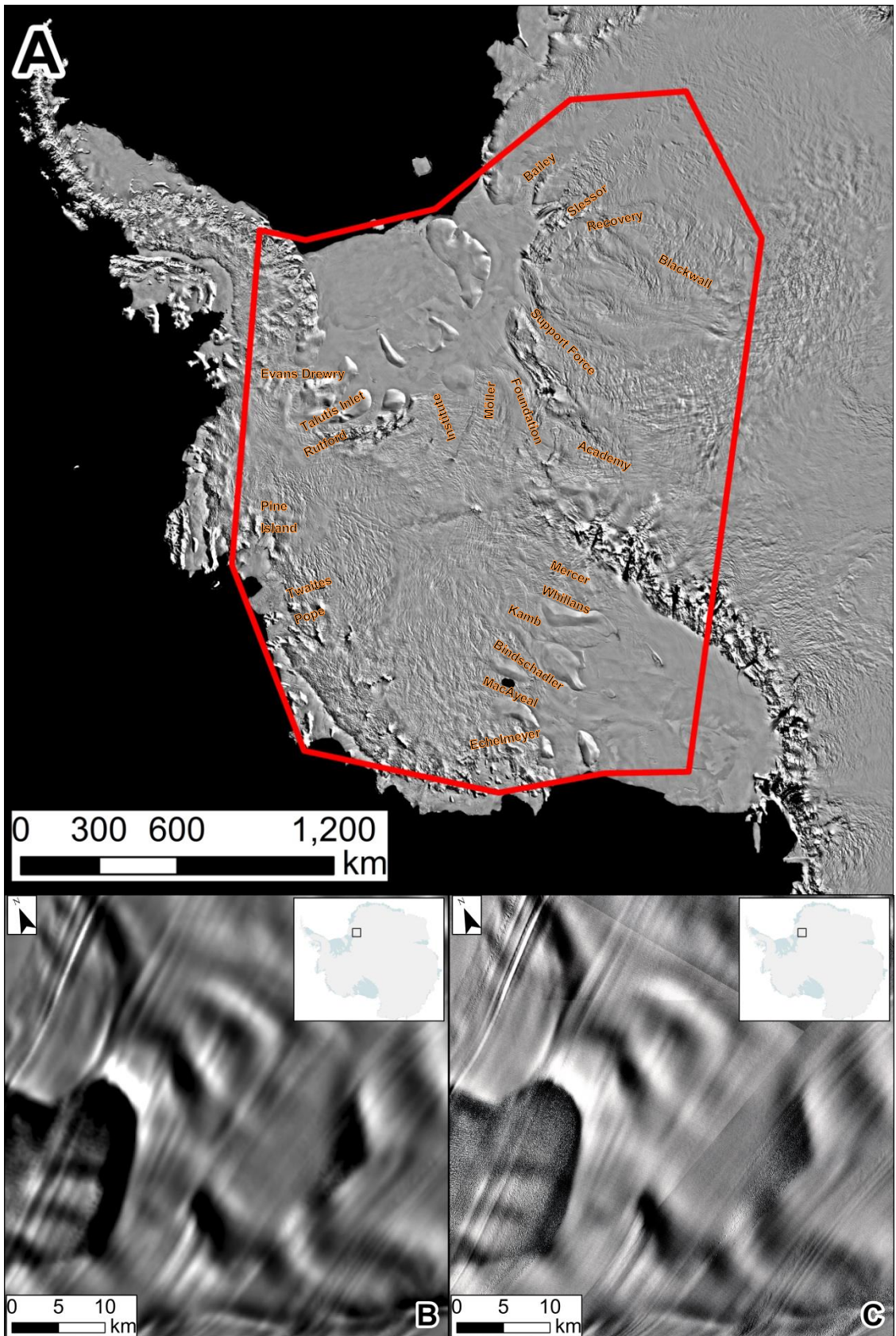
Thus, for the first time I will define the morphology of TSSs and examine the spatial distribution of their characteristics. This will help test models of their formation.



## 5.3 Methods

### 5.3.1 Mapping

Two sets of mapping were conducted in this study. Firstly, a static map of TSSs was created by digitising features visible on the MODIS Mosaic of Antarctica (<http://nsidc.org/data/nsidc-0280.html>). As TSSs are subtle, the multiple illumination angles in the images composited into the mosaic allowed for greater identification of subtle features. TSSs were mapped along their highest reflectance value. This was termed the TSS ‘crest line’, but in reality this may not be the highest topographic region. Mapping was restricted to the region in Figure 5.5A, as this was the area identified to have the most prominent TSSs, possibly due to the abundance of flat ice stream surfaces upon which subtle topography could be identified. TSSs were grouped by location according to the labels on Figure 5.5A. Although the MODIS mosaic is of a lower resolution (125 m) to the available Landsat imagery (15-30 m), a similar number and orientation of features are visible on both datasets in many regions (Figures 5.5 B-G). However, slight differences may be apparent due to the differing sensor properties and sun angles of the imagery (Figures 5.5 F and G).



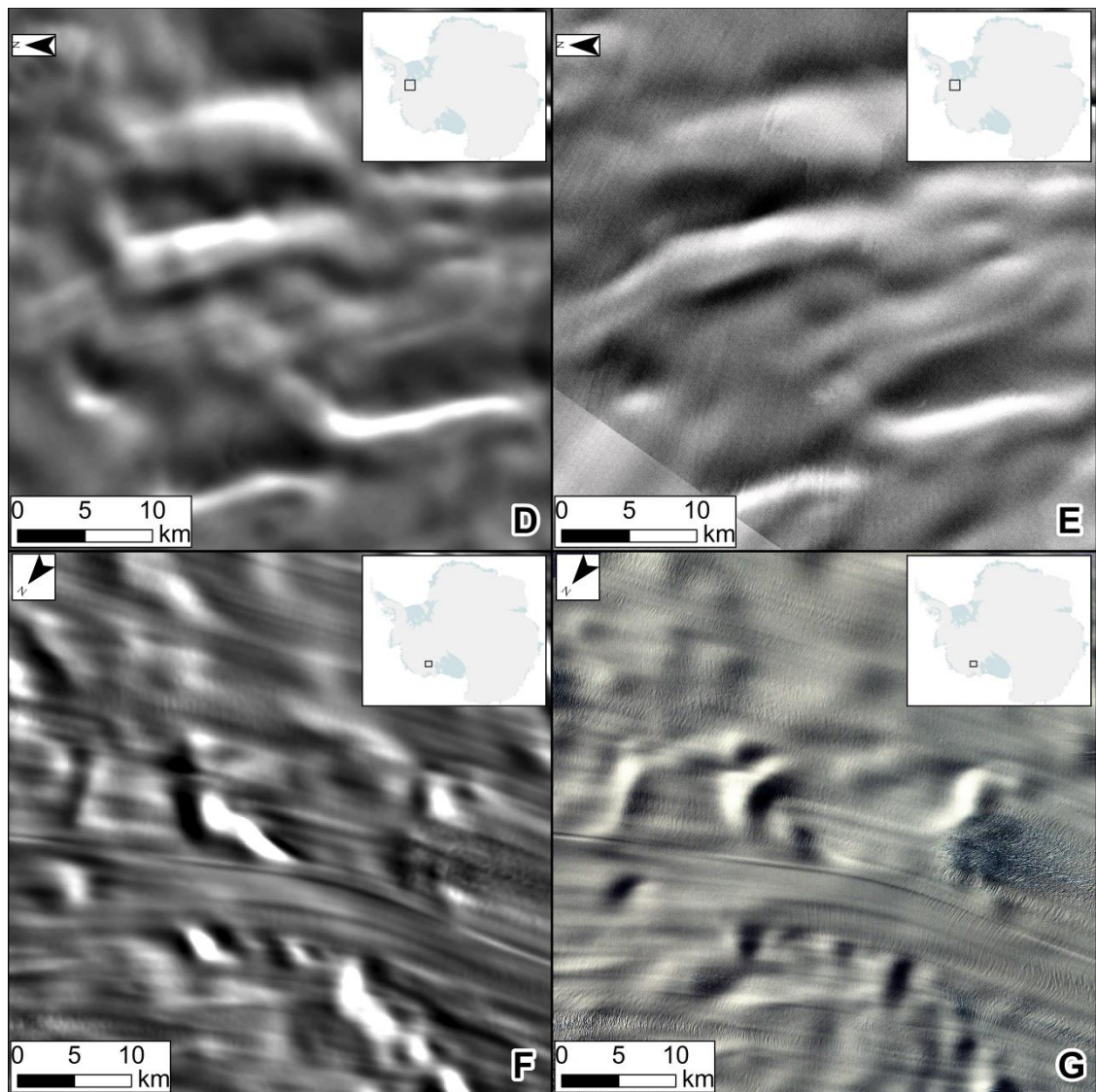


Figure 5.5. TSSs were mapped across West Antarctica, in the area shown in (A). In many places MODIS (left) and Landsat (right) images agree on the location and orientation of TSSs. Examples shown are Slessor Glacier (B and C) and the onset to Rutford Ice Stream (D and E). Occasionally, for example on the MacAyeal Ice stream (F and G), the apparent orientation of features changes between the imagery.

In order to ascertain whether TSSs migrate, three multi-temporal maps were also made by examining Landsat images from multiple dates (Table 11). This allowed for repeat measurements near decadal intervals across approximately 4 decades. Evans Ice Stream, Slessor Glacier and MacAyeal Ice Stream were chosen due to their prominent TSSs (Figure 5.6). Furthermore, these are some of the fastest flowing regions of the ice sheet, and therefore locations where one would intuitively expect the most migration to occur. The images were mapped independently of each other, in order to avoid biasing the results. Again, TSSs were mapped along their perceived crestlines. Locational differences may occur due to mapping error, sun illumination angle and slight locational differences in the satellite imagery. These factors limit the identification of any subtle ( $\approx$

1 km) migration of features which may have occurred. Mapping from different dates was then superimposed on top of each other in order to assess whether features had changed location.

Satellite	Evans	Slessor	MacAyeal
Landsat 8	December 2014	January 2015	December 2014
Landsat 7	December 2002	January 2001	December 2002
Landsat 5	March 1997	December 1996 March 1986	January 1987
Landsat 1	February, 1974	January 1974	November 1973

Table 11. Location and date of imagery studied.



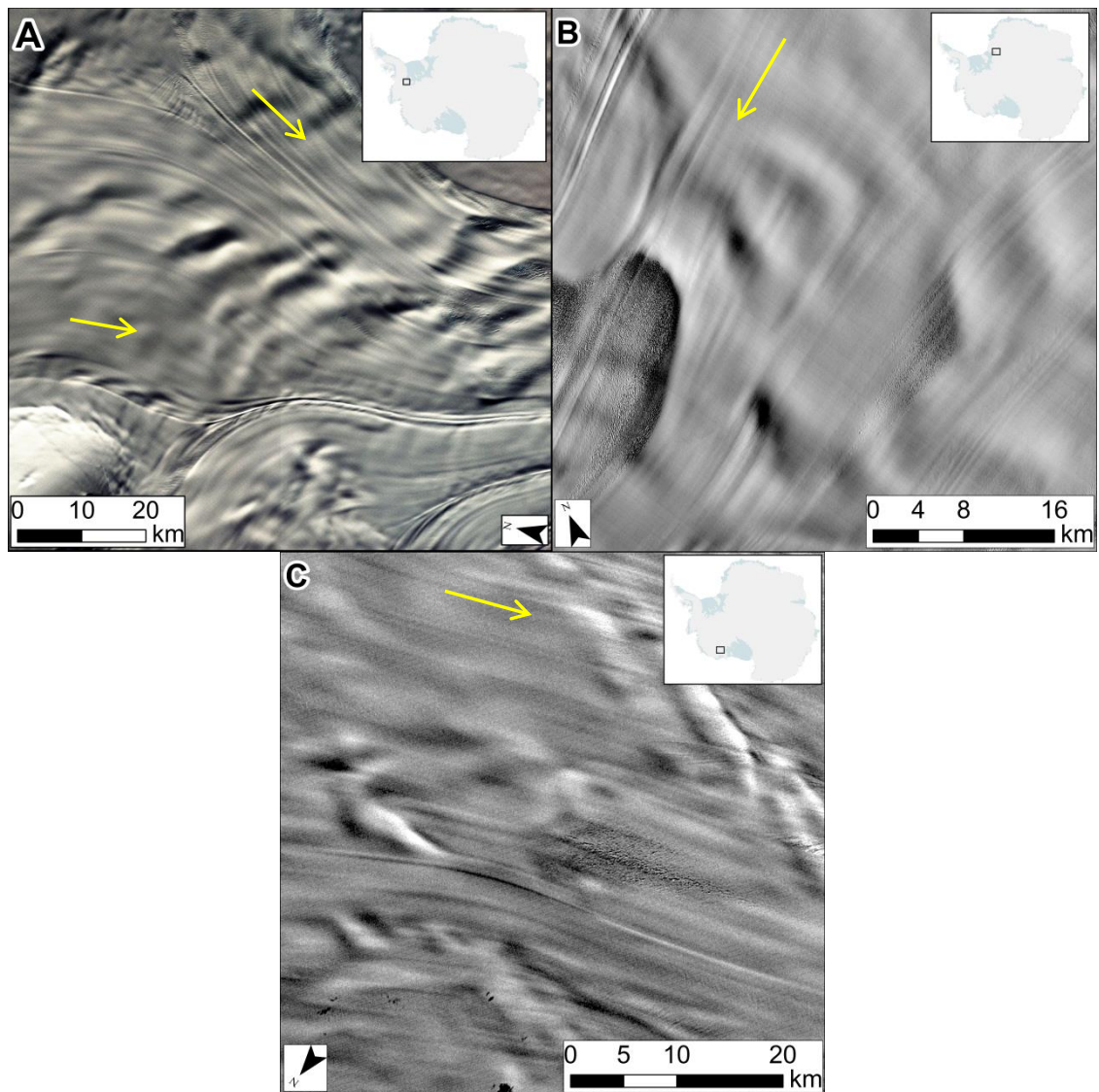


Figure 5.6. TSSs on the ice streams studied at multiple time slices. A) Landsat 8 image of Evans Glacier in December 2014. B) Landsat 5 image of Slessor Glacier, December 1996. C) Landsat 5 image of MacAyeal Ice stream, December 1984. Yellow arrows denote approximate ice flow directions.

### 5.3.2 TSS Morphological and Glaciological variables

The crest-line length of each mapped TSSs was calculated within the GIS. Downstream transects were created in order to define TSS spacing. The orientation and placement of these was guided by the map of LSSs which are aligned in the direction of ice flow (Chapter 4: Plate 1). These transects were then split within the GIS into separate polylines in order to define the spacing distance. 295 transects were placed in order to capture as many TSSs as possible (Figure 5.7). Repeat measurements were avoided using the ID number of the mapped TSSs. The velocity and ice thickness for each TSS was defined by measurements of the Rignot velocity dataset (Rignot et al., 2011) and BEDMAP 2 (Fretwell et al., 2013). The mean value was taken for the

crestline of each TSS. The same measurements were also taken across the spacing polylines, in order to determine any relationship between these variables. Both sets of measurements disregarded regions where measurement error was high, in the same manner as was conducted in Chapter 4 (Section 4.4.2). Uncertainties are also reported in the same manner (mean value for measures of average, specific value for individual measurements). In order to calculate the difference in ice velocity at each TSS, a ‘velocity anomaly’ raster was created (Figure 5.8). This was created by taking a mean local velocity, over a distance of 5 km, and subtracting this from the original dataset. Velocity change was then defined as the difference between the minimum and maximum velocity along a spacing polyline. Regions where other features dominate the velocity anomaly map, such as shear margins and tributary glaciers (Figure 5.8F), were avoided when taking measurements.

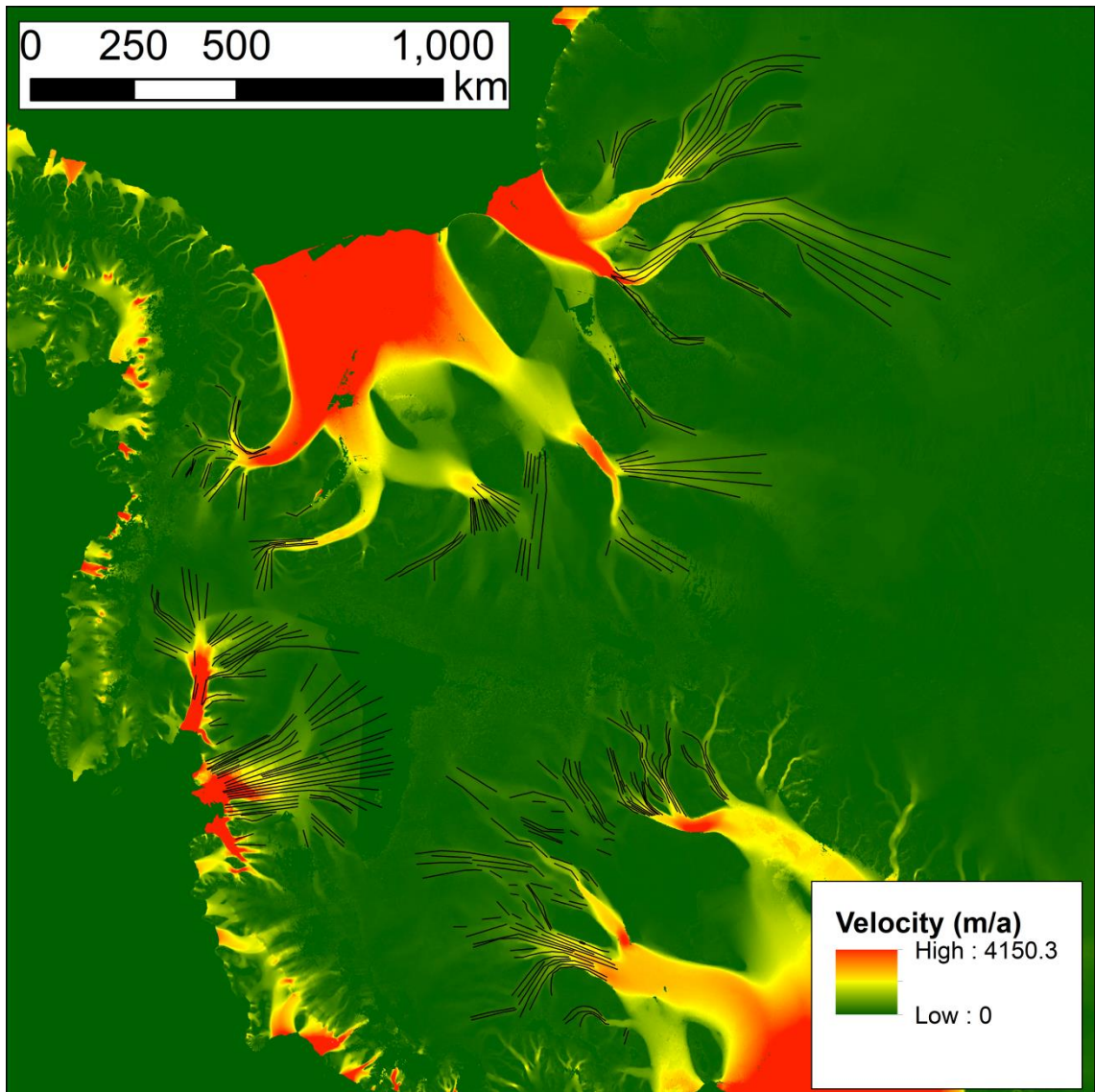


Figure 5.7. Location of TSS spacing measurement transects. 295 downstream aligned transects were placed in regions where there were sufficient TSSs.

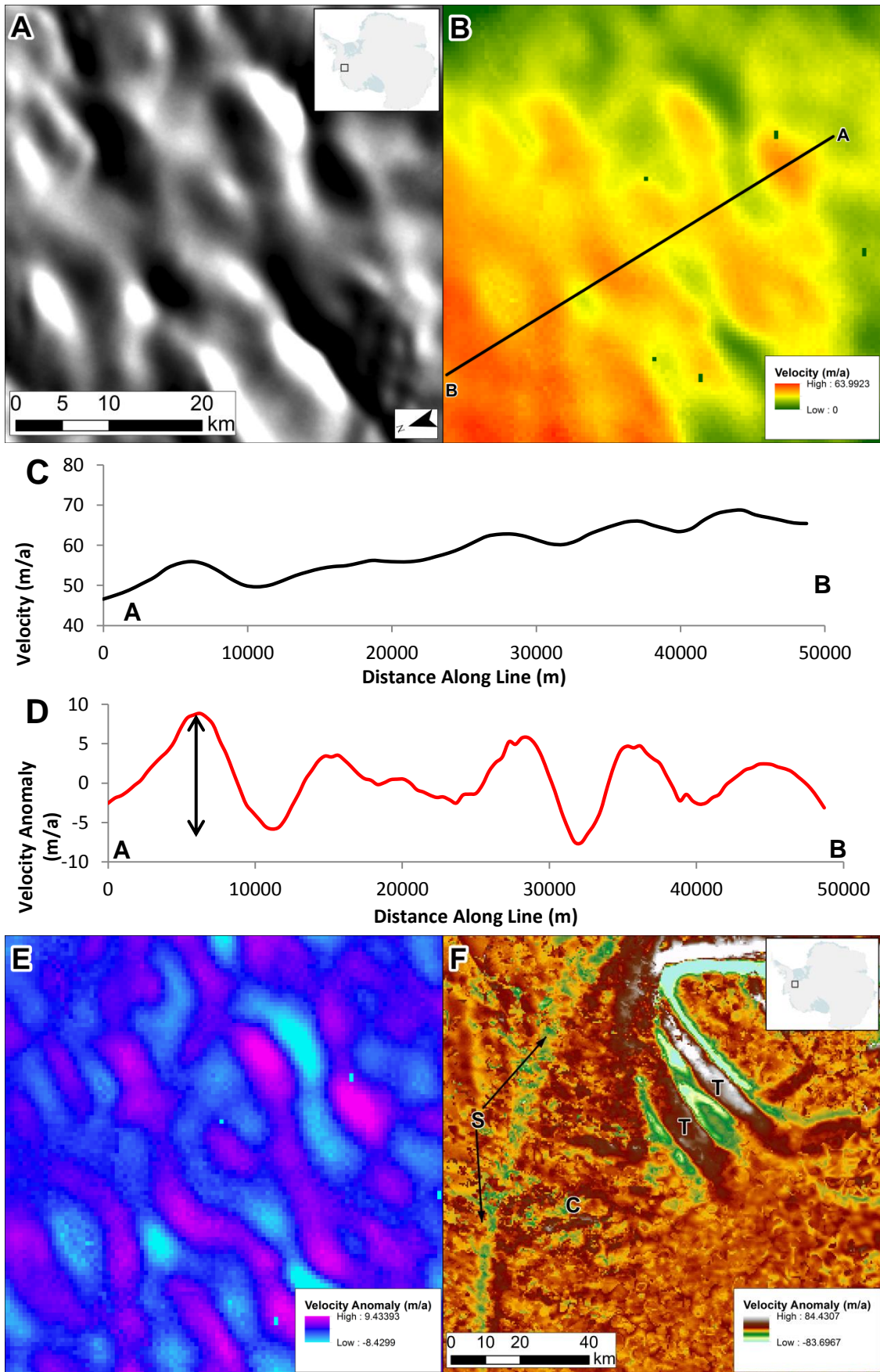


Figure 5-8. Figure caption overleaf.



Figure 5.8. Ice flow is from upper right to lower left in (A). Regular surface waves are visible on MODIS imagery of the upstream portion of Thwaites Glacier (A). These correspond to fluctuations in ice velocity (B), as can be seen along the transect line A-B (C). These fluctuations are normalised in the velocity anomaly raster (E), as can be seen along the transect A-B in (D). The arrows denote a single measurement (D), the amplitude of a velocity anomaly fluctuation. However, in other regions, such as the onset to Rutford, noise from other features is introduced into the velocity anomaly raster (F). On (F), there are regular waves in the main channel labelled C. These are pictured in Figures 5.5 D and E. However, other features such as a shear margin, labelled S, and tributary glaciers, labelled T, introduce larger fluctuations into the velocity anomaly raster. Such regions were avoided when sampling.

## 5.4 Results

### 5.4.1 Static Mapping

4,234 TSSs were mapped within the study area (Figure 5.5A). Their distribution is shown on Figure 5.9A. The pattern of TSSs is arborescent, following the flow of ice streams (Figures 5.9B-D). TSSs are not restricted to the fastest flowing portions of ice streams, but were also observed on upstream tributaries (Figures 5.9B-D). Often, TSSs were aligned roughly transverse to flow direction. However, some features which were more oblique to flow were also noted. On the Kamb ice stream, TSSs were only obvious where ice streaming is still occurring in its onset zone (Figure 5.9B). In the now stagnant main channel of the Kamb ice stream, the texture and any potential TSSs are much fainter. This gives the impression that TSSs on the surface of the Kamb ice stream have relaxed since ice stream shutdown. Unlike LSSs (Chapter 4), TSSs were not observed on ice shelves. Instead, TSSs are restricted to the grounded portion of the ice sheet, suggesting that coupling to the bed is necessary for a TSS to be sustained. Thus, from qualitative observations of the distribution of TSSs, it appears that ice streaming and transmission from the bed are required for them to form and be sustained.

### 5.4.2 Multi-Temporal Mapping

Figure 5.10 shows the results of the multi-temporal mapping. The most striking aspect of these three maps is the consistency in the positioning of the TSSs. Some slight locational differences may be due to different interpretations during mapping, or shifting of the perceived crestline due to different sun angles. A feature may appear separated into two on a subsequent image, only to be perceived as a single feature again on a later image. Although images with the lowest cloud cover were chosen, occasionally this obscured TSSs on some images. Furthermore, images did not perfectly overlap, meaning that the region of TSSs mapped do not coincide perfectly between different dates. However, where TSS were mapped at different times, none significantly change position. The general pattern is that of a consistent positioning of TSSs on the ice stream surface. Overall, for all three studied examples (Evans, Slessor and MacAyeal) no significant migration of features was detected. Therefore, at the timescale (40 years) and localities studied here, TSSs do not migrate.

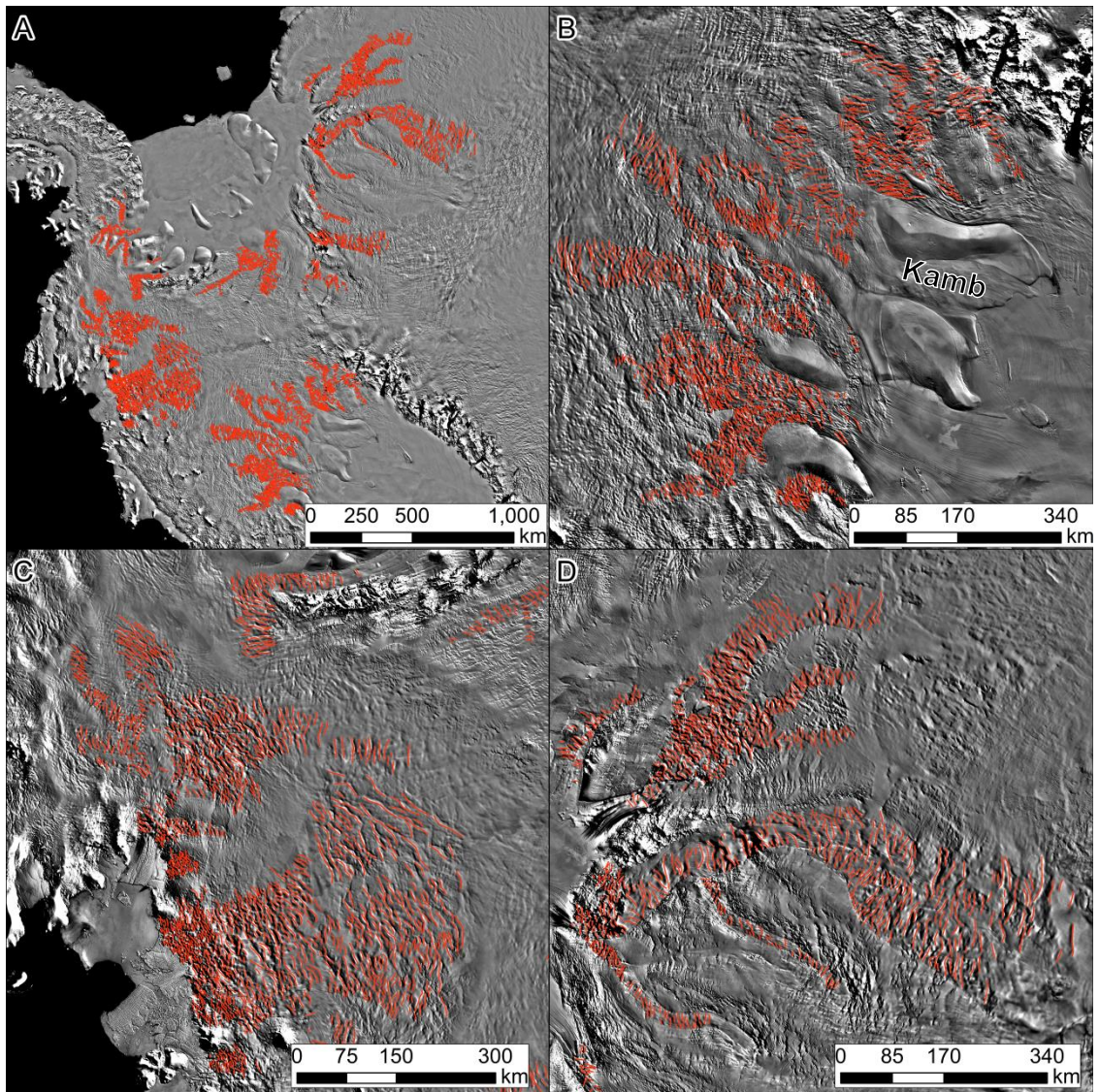


Figure 5.9. The distribution of mapped TSSs across the study area (A). Examples of TSSs in the Siple Coast (B), Thwaites and Pine Island (C) and Slessor and Recovery regions.

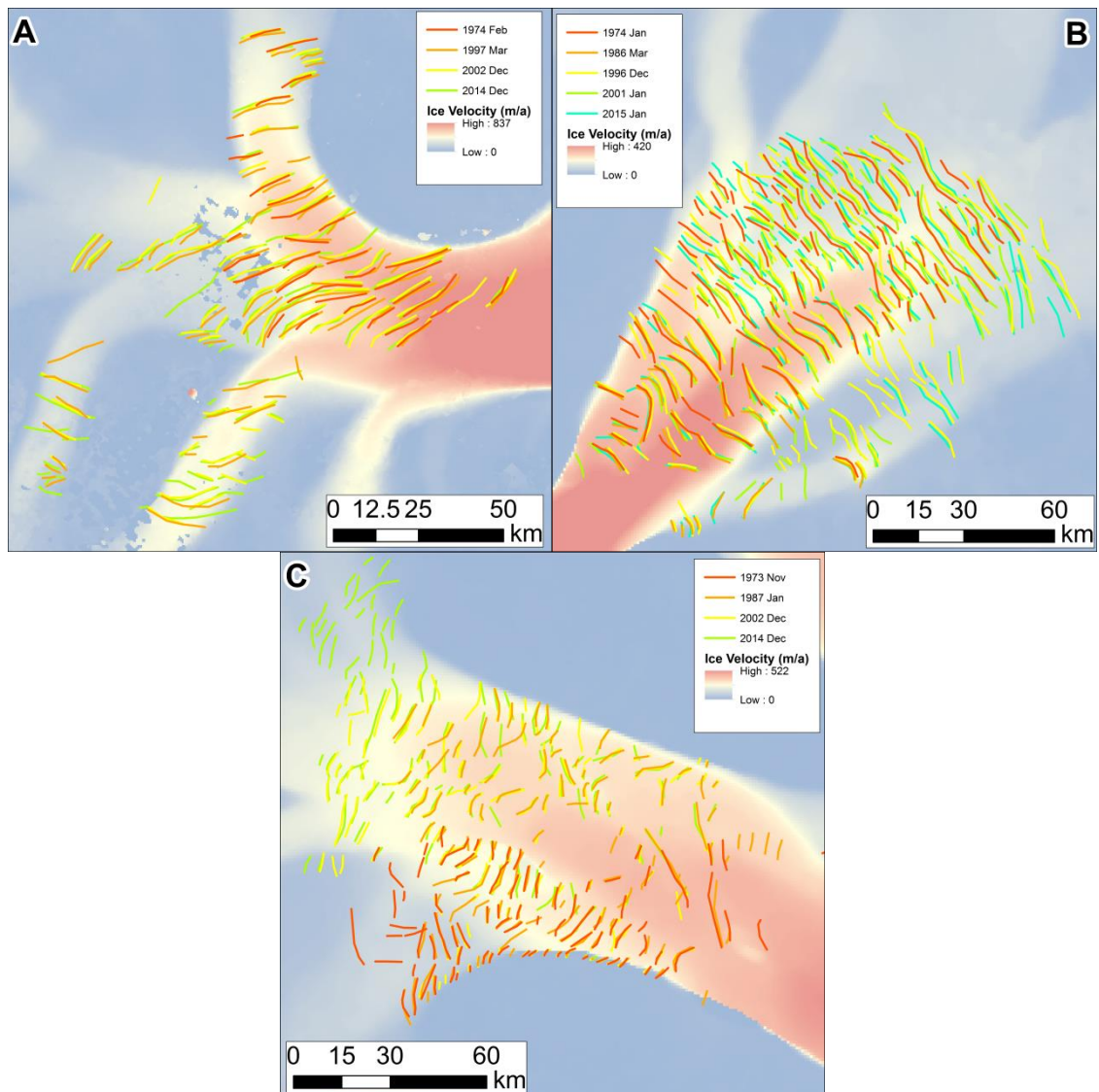


Figure 5.10. Maps of TSSs from satellite images at different time periods. A) Evans Ice stream. B) Slessor Glacier. C) MacAyeal Ice Stream. Note the agreement between mapping of different dates, and general lack of change in TSS position or size. Differences in cloud cover and image placement restricted complete overlap in mapping between different dates.

#### 5.4.3 TSS Morphology

A histogram of the length of all 4,234 mapped TSSs is shown in Figure 5.11. A distinct modal peak of  $\sim 12$  km is evident, similar to that of the measures of average (Table 12). The dataset contains some much larger features (maximum 91 km; Table 12). However, 80% of the features are between 6.1 km and 26.3 km long. This is an indication that TSSs have a selective size range. Between ice streams there are only slight differences between the mean lengths of features (Figure 5.12). Generally, longer features were found on wider ice streams, perhaps due to space constraints. More

remarkable is the similarity in TSS length between the different ice streams (Figure 5.12).

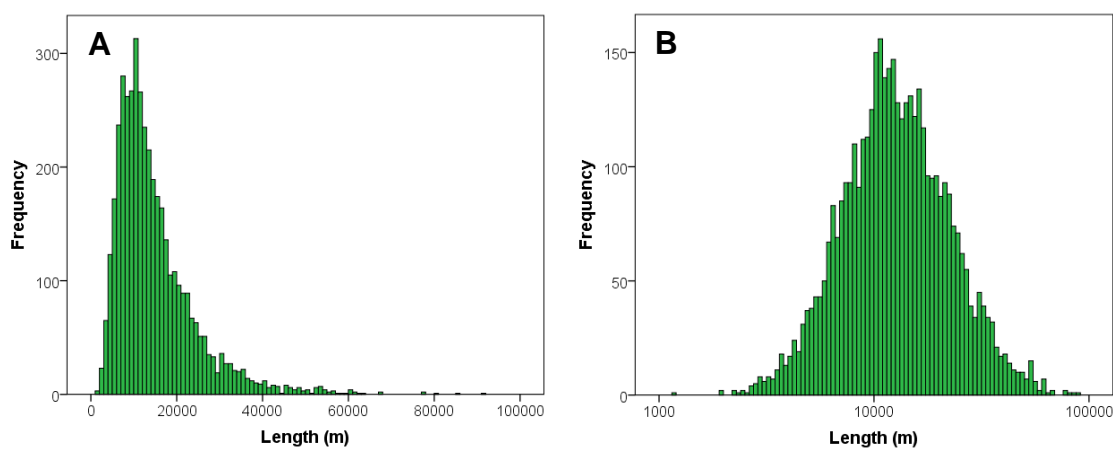


Figure 5.11. The length of all TSSs (A), plotted on a log scale on (B). Note the prominent peak at approximately 12 km.

	Length (m)	Spacing (m)	Velocity (m/a)	Velocity Anomaly (m/a)	Thickness (m)	Spacing (m)/Ice Thickness (m)
Mean	14,903	9499	137 (+/- 2.9)	7.1 (+/- 2.6)	1817.5 (+/- 135)	5.66
Median	12,392	7456	78 (+/- 2.9)	3.7 (+/- 2.6)	1765 (+/- 135)	4.15
Standard Deviation	9419	7448	202	13.7	561.3	5.47
Minimum	1190	165	1.4 (+/- 1)	0.2 (+/- 1.1)	469 (+/- 83)	0.6
Maximum	91,069	91322	3053.8 (+/- 2)	314 (+/- 3.2)	3501 (+/- 149)	142.8

Table 12. Descriptive statistics of TSS variables.



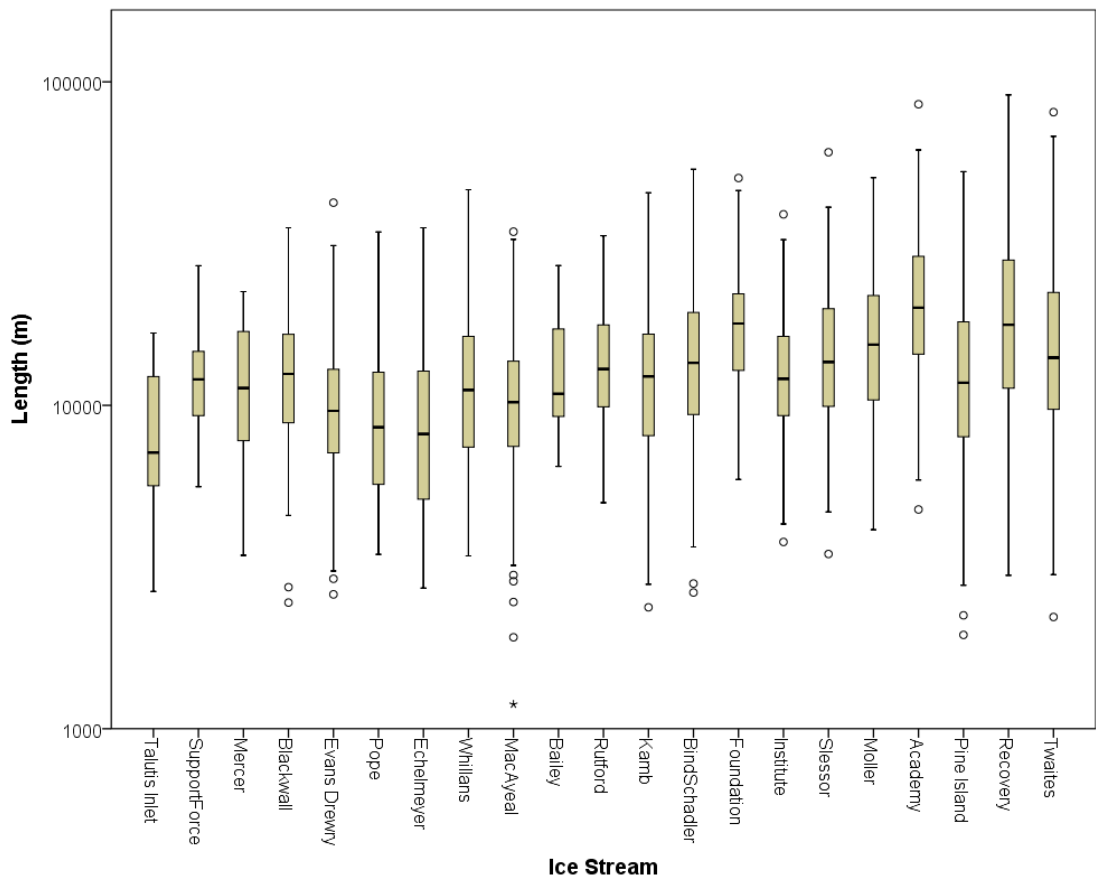


Figure 5.12. Boxplot of TSS length grouped by location. Ice streams are ordered by approximate size, based on maximum and minimum width. The smallest ice streams are to the left, the largest to the right. Note the weak trend in TSS length, increasing with ice stream size.

The spacing measurements of TSSs are plotted in Figure 5.13. The modal peak occurs at  $\sim 9$  km, with the vast majority of measurements (80%) lying between 3.7 km and 16.9 km. This is consistent with Merry and Whillans (1993) approximation that TSSs (mottles) are spaced roughly 10 km apart, Reusch and Hughes' (2003) observations on Byrd glacier, and Whillans and Johnsens' (1983) observations of internal radar layer folding spaced 10 km apart. In a similar manner to their length, TSS spacing does not vary much between ice streams (Figure 5.14). Such consistency between locations suggests a common origin for TSSs between ice streams. This selective spacing is common with other patterned phenomena, such as subglacial bedforms (Chapter 2).

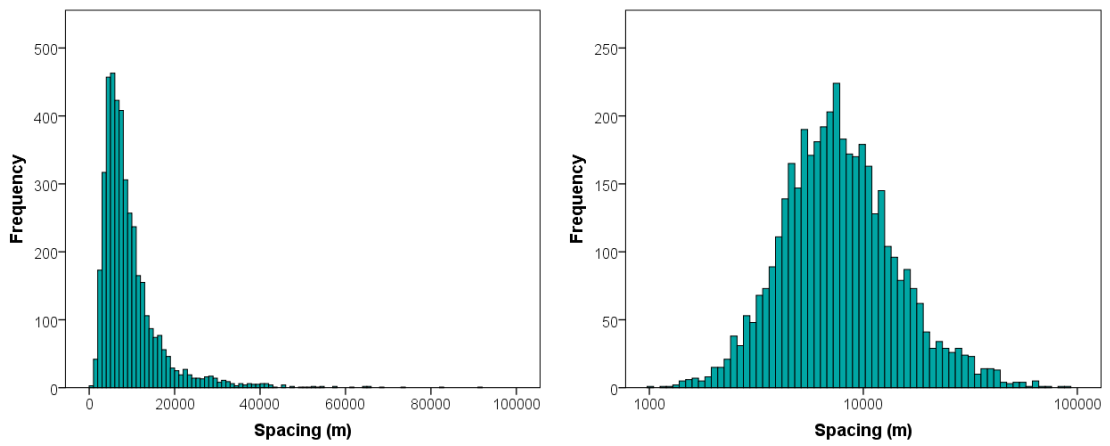


Figure 5.13. Histograms of TSS spacing. Plotted on linear (A) and log (B) scales. Note the peak at approximately 9 km.

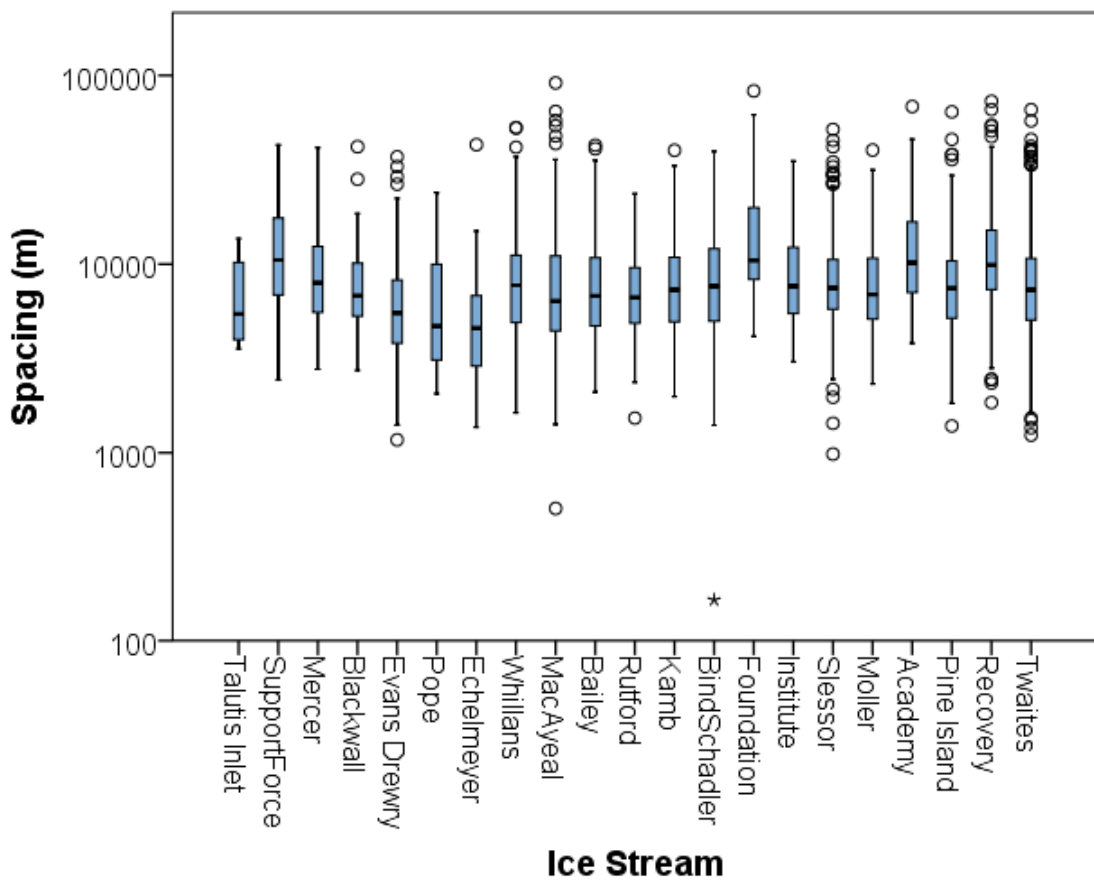


Figure 5.14. Boxplot of TSS spacing grouped per ice stream. Note the consistency between different locations.

#### 5.4.4 Glaciological Characteristics

Figure 5.15 plots the mean ice velocity across the crestline of each TSS. Perhaps most interestingly, TSSs can occur at relatively slow ice velocities ( $> 10$  m/a). However, the majority (90%) occur where ice is flowing above 27.5 m/a. Therefore, TSSs are not just restricted to the fastest flowing portions of ice streams, as is also shown in their spatial distribution (Figure 5.9). Indeed, the majority of TSSs occur on ice flowing below 289 m/a. This lack of TSSs at the highest ice velocities (1,000s of m/a) is possibly due to their absence on ice shelves (e.g. Figure 5.9). Figure 5.16 plots the velocity anomaly between each TSS. The tail in this skewed distribution is most likely a consequence of measurements taken in regions of high noise (Figure 5.8F). Therefore, many of the high values (maximum = 314 m/a  $\pm$  3.2, Table 11) may be erroneous. Interestingly, there is a strong peak in velocity anomaly at  $\sim 7$  m/a (c.f. Table 11), with the majority (80%) of TSS velocity anomalies recorded to be between 1.3 and 13.6 m/a. This indicates a narrow range of velocity fluctuation that is attributable to TSSs. However, smaller velocity anomalies may be predominated by uncertainty in the dataset, as mean uncertainty across TSS velocity anomaly measurements was 2.6 m/a.

The mean ice thickness across each TSS crestline is plotted in Figure 5.17. Compared to all previous distributions (Figures 5.11, 5.13, 5.15, 5.16), the distribution is broad and spread, with less of a distinct peak. This shows that TSSs can occur in a wide range of ice thicknesses. However, the distribution of the ratio of TSS spacing to ice thickness is much narrower and more peaked (Figure 5.18). There is a modal bin of approximately 4.5, with 80% of the TSS spacing to thickness ratios lying between 2.2 and 10.6. Mean thickness errors of  $\pm 185$  m (Table 12) would not significantly change this result. The long tail is most likely a consequence of sampling across regions where TSSs were not detected. Therefore, my data suggests that TSSs are actually spaced 4.5 times the ice thickness apart, as opposed to the 3.3 originally proposed by Budd (1970). However, my data is remarkably consistent with subsequent estimates of 2-10 times the ice thickness (McIntyre, 1986; Gudmundsson, 2003; De Rydt et al., 2013), although they do exist outside this preferred range.



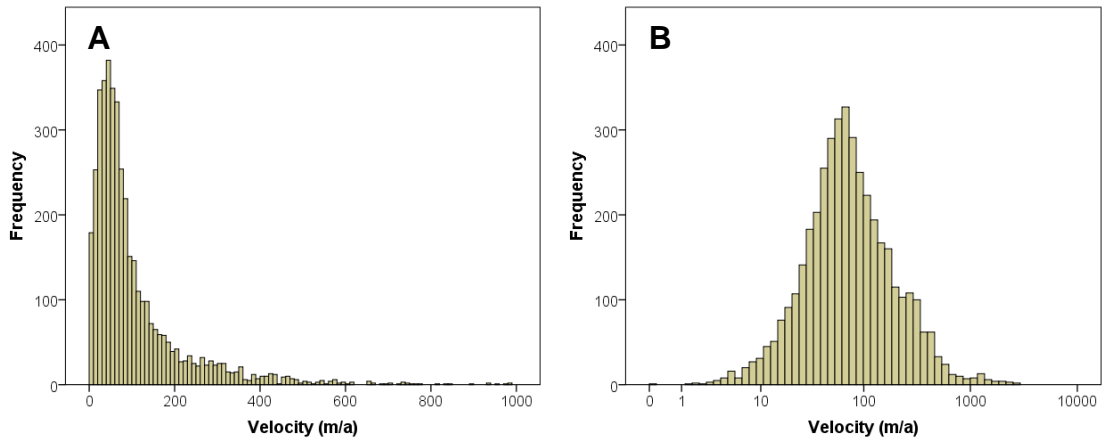


Figure 5.15. Mean velocity across the crest-line of TSSs on (A) a linear and (B) a log scale. Note the low minimum velocity at which these features occur.

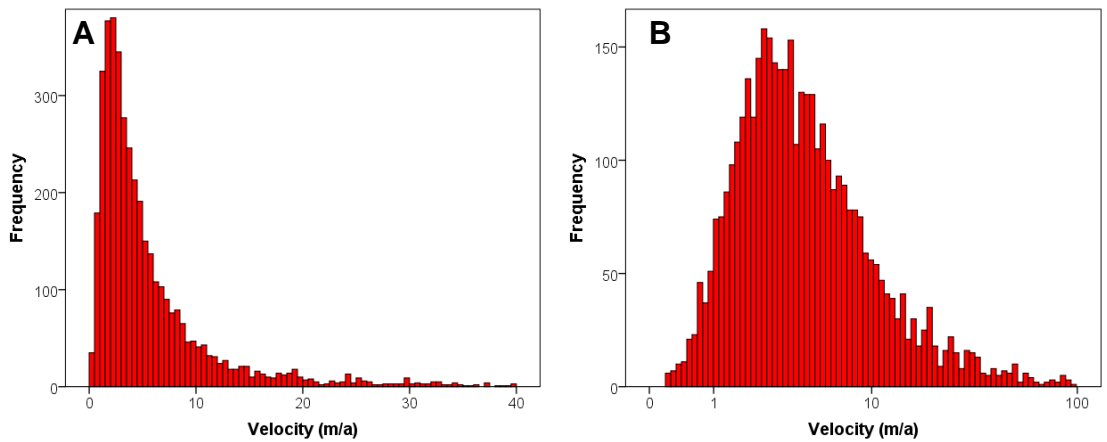


Figure 5.16. Velocity anomaly across the gap between TSSs on (A) a linear and (B) a log scale. Note the distinct peak at 7 m/a, and the vast majority of measurements between 1-15 m/a.

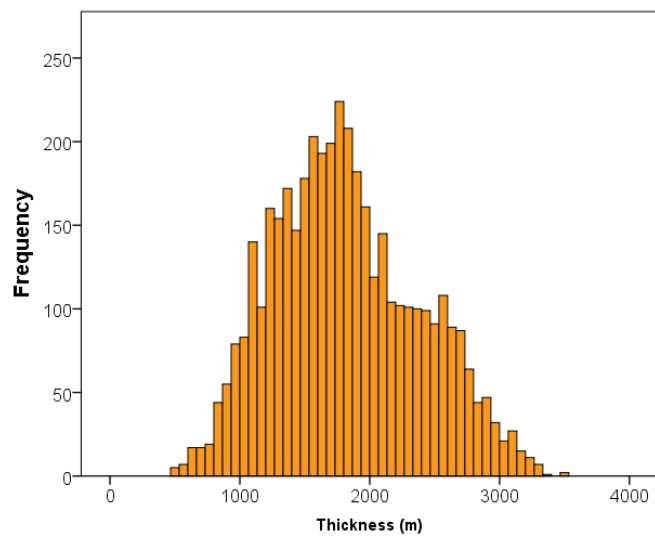


Figure 5.17. Distribution of ice thickness measurements across the crestline of TSSs.

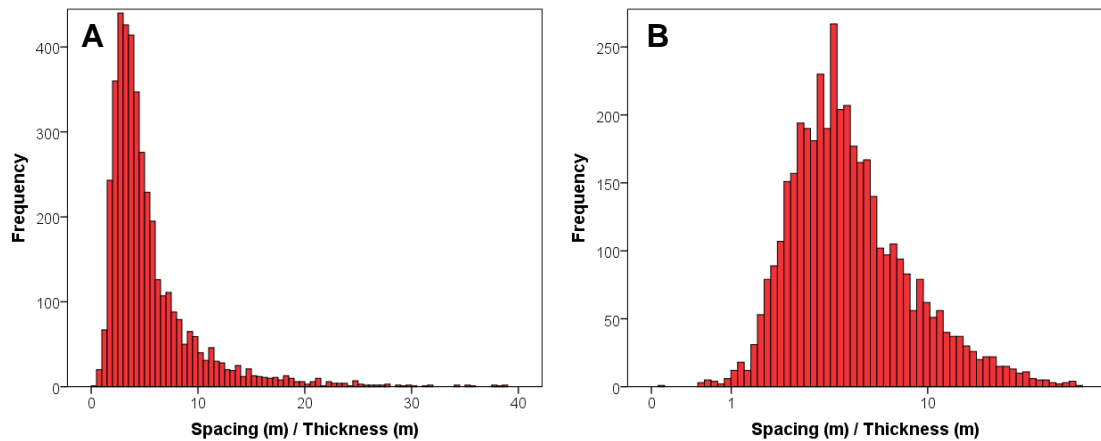


Figure 5.18. The distribution of the ratio between TSS spacing and ice thickness, plotted on a linear (A) and a log (B) scale). Note the distinct peak at  $\sim 4.5$ , and the majority of measurements between 2 and 10.

## 5.5 Discussion

TSSs are thought to be the consequence of either the transmission of bed perturbations to the surface, variations in the strength of the bed or variations in ice strength. Any model for TSS formation should account for their morphometric and glaciological properties as found in my results (Section 5.4). My finding that 80% of TSSs are spaced between 2.2 and 10.6 ice thicknesses apart (Figure 5.18) is consistent with both the bedrock and the bed strength hypotheses (Gudmundsson et al., 2003; Whillans and Johnson, 1983). Conversely, there is no apparent reason why this should be the case for the ice strength hypothesis. Thus, this characteristic of TSSs, and their restriction to the grounded portion of the ice sheet (Figure 5.9), is taken to indicate that they are a consequence of basal variability, rather than a property of the ice itself.

No TSSs were detected to migrate in my study areas (Figure 5.10). This is interpreted as further evidence against the ice strength hypothesis, as one would expect variations in ice rheology, or “ice rafts” (Merry and Whillans, 1993), to be transported at the same velocity as ice flow and be visible on ice shelves. Features observed to migrate elsewhere (Hulbe and Whillans, 1994; 1997) may be a localised phenomenon. The lack of detected migration implies that the features at the bed which cause TSSs are static, rather than migratory (Reusch and Hughes, 2003). This could be interpreted as support for the bedrock transmission hypothesis, as one would expect bedrock features to remain static. Some variations in bed strength would also be expected to remain

static. For example, sticky spots created by well drained till located over more permeable bedrock (Ashmore et al., 2014).

Some models for bed strength variation have predicted that features grow and then migrate (Hindmarsh, 1998c; Sergienko et al., 2014), in a similar manner to instability based hypotheses of subglacial bedforms (Section 3.6.4). Whilst such migratory behaviour was not noted here, such instability based hypotheses do overcome a major deficiency in a purely bedrock transmission view. The regular spacing of TSSs (typically 9 km apart, Figure 5.13), which varies little between ice streams (Figure 5.14), is difficult to reconcile with a bedrock only origin. Indeed, in order for there to be a 1 to 1 relationship between bedrock bumps and TSSs the geology underneath Antarctic ice streams would have to vary little across the entire study area and be aligned roughly transverse to ice flow in a radial pattern. This further rules out a purely geological control on patches of sticky and soft sediment by basal dewatering (e.g. the sticky strings of MacAyeal et al. 1995). On the other hand, if the positioning of TSSs were controlled by an instability, this would account for the regular spacing and patterning of TSSs. Therefore, the bedrock bump transmission hypothesis is unlikely to account for the formation of every TSS.

Sergienko and Hindmarsh (2013) observed variations in basal shear stress that formed a rib-like pattern, similar to that of TSSs (e.g. Figure 5.4). These ‘traction ribs’ are similar in scale to subglacial mega-ribs (e.g. Greenwood and Kleman, 2010; see Chapter 3). Similar traction ribs were subsequently found in additional localities (Sergienko et al., 2014). If traction ribs correspond to subglacial mega-ribs then one would expect mega-ribs to be more abundant on palaeo-ice sheet beds. Such inversion techniques are limited in the spatial resolution that is achievable due to ice filtering out smaller scale information (Gudmundsson and Raymond, 2008). Therefore, Sergienko and Hindmarsh’s (2013) technique is unable to find smaller subglacial bedforms and may produce only larger variations in subglacial coupling. The regions where traction ribs were found may actually contain the more abundant smaller scale subglacial bedforms. Perhaps these bedforms, and smaller bedrock perturbations, are regularised by the effect of ice acting as a band-pass filter before information is transmitted to the surface, in order to create TSSs. Therefore, a 1:1 relationship between the surface of an ice stream and the bedrock topography or basal slipperiness is unlikely.

Despite the above, observations of a few TSSs suggest that they are produced as ice flows over a bedrock bump. Qualitatively, features that appear more prominent than the surrounding TSSs were noted (e.g. Figure 5.19A). These features frequently had significant bed elevation differences when transects were run across the BEDMAP 2 dataset (Fretwell et al., 2013; Figure 5.19). Therefore, these more prominent TSSs are likely to be the consequence of flow over a bedrock perturbation. However, occasionally there were no traces of bed elevation controls of TSS, suggesting here that variability in basal resistance is more likely. The abundance of bedrock transmitted TSSs, as opposed to those formed by another source, remains unknown. Furthermore, a false dichotomy between the two may exist, as variations in till slipperiness may produce topographic bedforms. Overall, a mixed origin for TSSs is likely, with some being the product of bedrock features, whilst others formed by a patterning process which produces regular variations in bed strength, which may also be topographic.

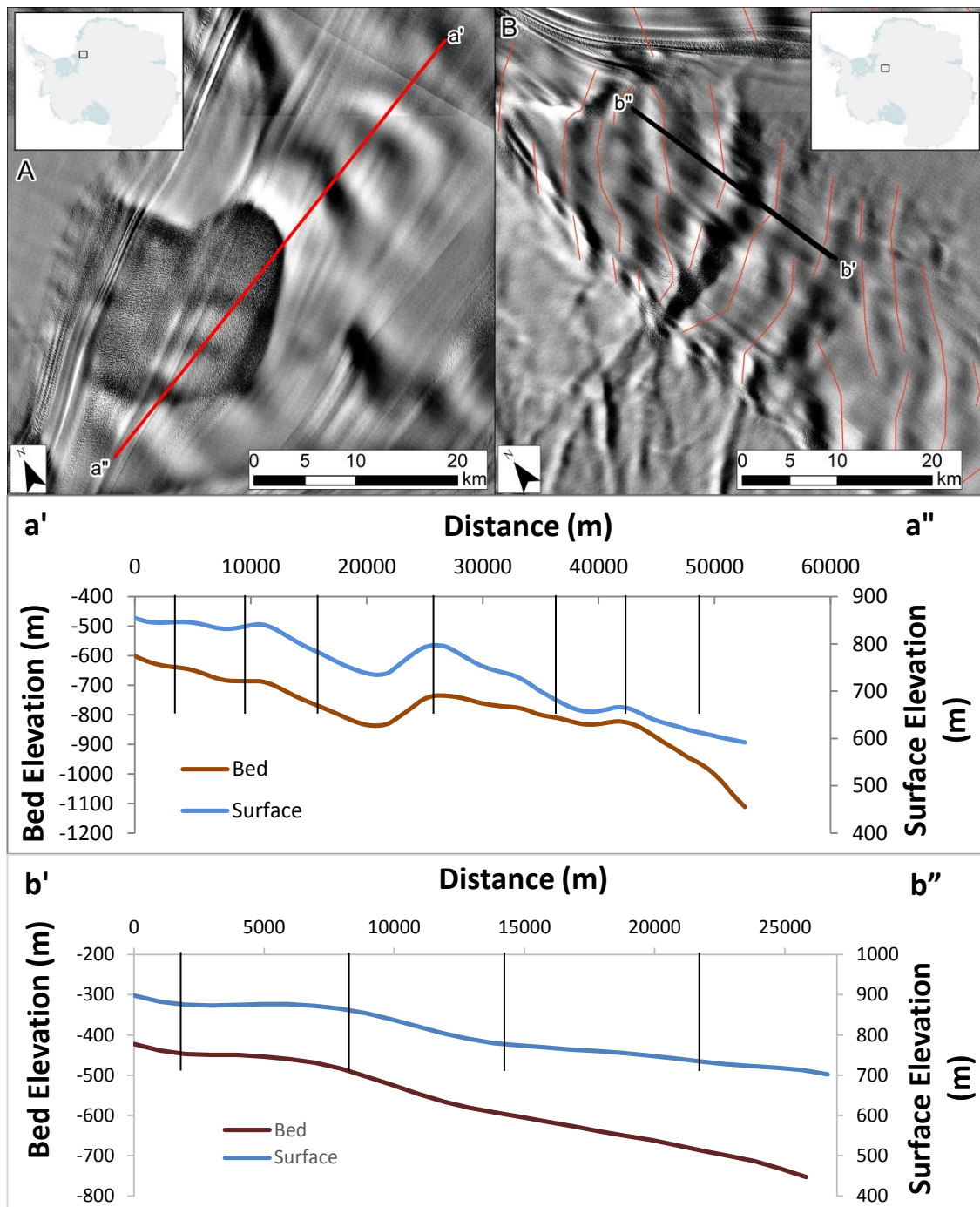


Figure 5.19. Bed and surface topography profiles across particularly prominent TSSs. Black vertical lines are mapped TSS crestline locations. A) across distinct features on Slessor Glacier, which show good relation to the bed in many instances. However, note that a few features have no bed expression. B) Across features on Blackwall glacier, which have no bed expression in the Bedmap 2 dataset.

## 5.6 Summary and Conclusions

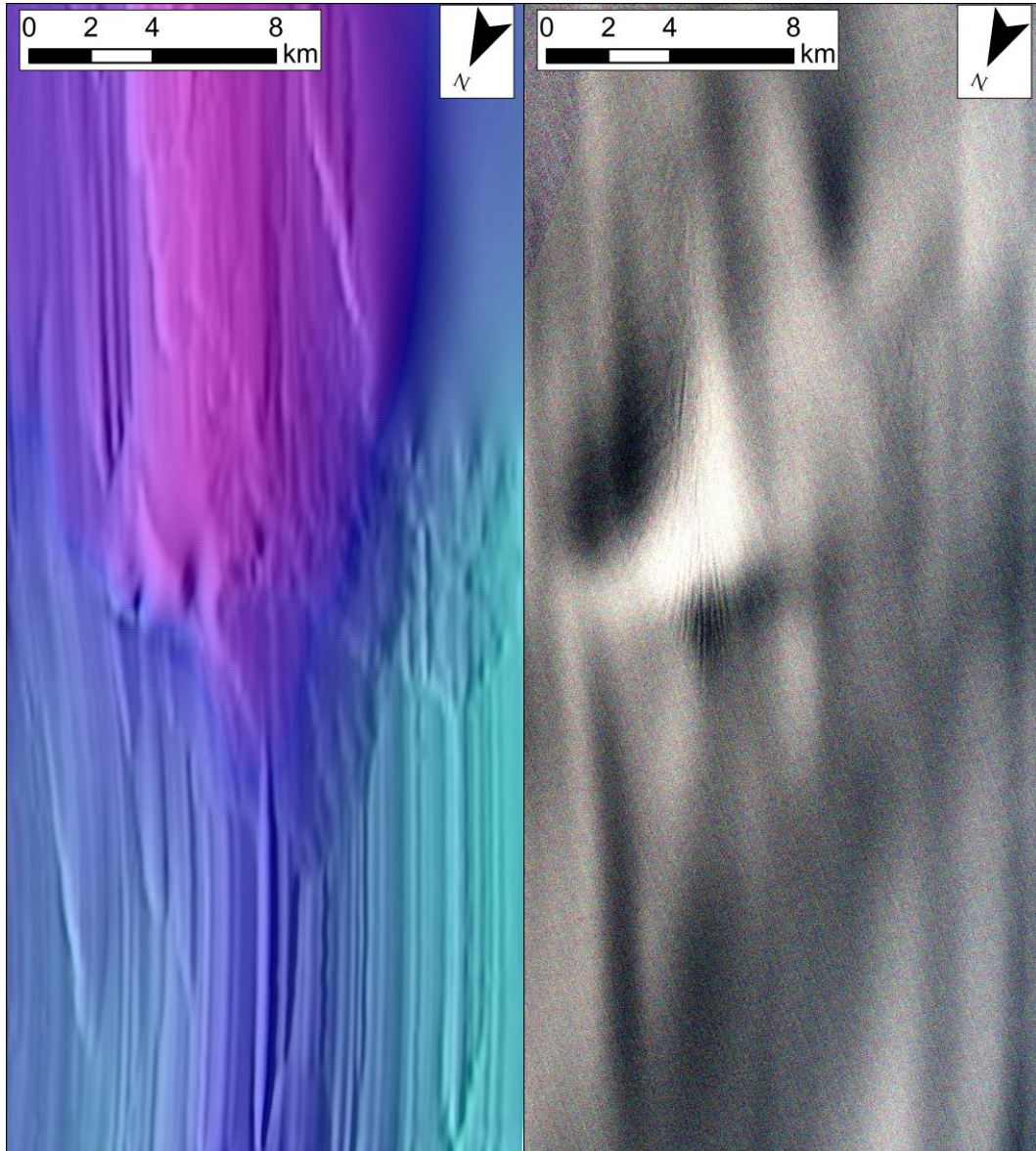
The surface texture of an ice stream is composed of numerous transverse surface structures (TSSs), previously referred to as mottles. The formation of TSSs has been linked to i) the transmission of basal bumps to the surface of the ice; ii) the transmission

of variable basal slipperiness to the surface of the ice; iii) variation in the ice strength itself. Here I examine the morphological and glaciological characteristics of TSSs on the surface of the Antarctic ice sheet through GIS and remote sensing observations. I find that TSSs:

- Are restricted to the grounded portion of the ice sheet (Figure 5.9)
- Occur within ice streams or outlet glaciers and their tributaries (Figure 5.9).
- Are static within the observed timeframe ( $\approx 50$  years) upon Evans, Slessor and MacAyeal Ice streams (Figure 5.10).
- Are typically 6.1 – 26.3 km long across their crestline with a modal peak of 12 km (Figure 5.11), with mean values only slightly changing between ice streams (Figure 5.12).
- Have a modal spacing of 9 km, with most TSSs occurring 3.7-16.9 km apart (Figure 5.13), a value which does not change significantly between ice streams (Figure 5.14).
- Can occur where ice is flowing relatively slowly (less than 10 m/a), but the majority occur at ice velocities above 27.5 m/a (Figure 5.15).
- Have a modal velocity anomaly of 7 m/a ( $\pm 2.6$  m/a), with the majority of TSSs representing ice velocity fluctuations between 1.3 m/a and 13.6 m/a. The smallest of these may be unresolved due to uncertainty in the ice velocity measurements.
- Occur in a range of ice thicknesses, from 500 to 3500 m (Figure 5.17).
- Have a modal spacing to ice thickness ratio of 4.5, but with a majority between 2.2 and 10.6.

I refute the ice-strength hypothesis as being able to explain the vast majority of TSSs. This is because they were not observed to migrate, and this hypothesis provides no explanation for the narrow range of ice thickness to spacing ratios under which they occur. My results are most consistent with hypotheses which see them as the transmission of basal variability to the surface of an ice stream. Sources for this are either bedrock bumps or variations in the basal shear stress. I suggest that a combination of the two is required to account for my observations. The pattern of TSSs is reminiscent of basal instabilities in coupled sediment, water and ice flow, suggesting that such a mechanism may be a more common cause than from bedrock features alone.

## Section C: Comparing Basal and Surficial Ice Sheet Flow Signatures



Section C: Digital elevation model of the bed (left) and Landsat ETM+ image of the surface (right) of the Rutford Ice Stream, West Antarctica. Ice flow is toward the top of the page. Bed elevation model supplied by Ed King. Surface image from <http://lima.usgs.gov/>



# Chapter 6 Discussion: Connections between flow signatures on the base and the surface of an ice sheet.

## 6.1 Introduction

Both the beds (Section A) and the surfaces (Section B) of ice sheets display features that relate to ice flow; flow signatures. Previous work has hinted at links between these two sets of patterns. Modelling studies show that surficial flow signatures are an inevitable consequence of the flow of ice over an uneven bed (Gudmundsson et al., 1998; Schoof, 2002; Gudmundsson, 2003). Elsewhere, it has also been suggested that uneven topography at the ice surface can influence the formation of flow signatures at the bed (Clark et al., 2003; Section 6.2). However, basal and surficial ice flow signatures are rarely considered together. Thus far, the two sets of features have been considered in isolation in this thesis. The aim of this discussion chapter is to bring together our knowledge of basal and surficial flow signatures in order to elucidate whether links between them exist.

In order to compare basal and surficial flow signatures I adopt several approaches. Firstly, I compare the size and morphology of subglacial flow signatures (bedforms) of palaeo-ice sheets with the surface features of the Antarctic ice sheet (Section 6.3). I then present a case study of the flow signatures of the Rutford Ice Stream, Antarctica; a location where sufficient data regarding both the bed and the surface of the ice sheet exist (Section 6.4). In order to make further direct comparisons, in Section 6.5 I examine bed sounding radar data, and compare this to the surface observed in satellite imagery. Finally, preliminary modelling of the flow of ice over subglacial bedforms is examined (Section 6.6), a field which needs much further work. No single approach is designed to provide the definitive answer. Instead, the combination of these approaches allows me to discuss whether interactions between basal and surficial flow signatures occur (Section 6.7).

## 6.2 Background

Models of ice flow over uneven topography predict that ice acts as a band-pass filter, selectively transmitting basal perturbations to the surface depending upon the ice thickness and the amount of sliding that occurs (Gudmundsson et al., 1998; Gudmundsson, 2003; De Rydt et al., 2013; Sergienko, 2014). In these models,



perturbations that are comparable in wavelength to ice thickness can be effectively transmitted to the surface as perturbations or flow signatures. Schoof (2002) specifically considered a basal perturbation the size and shape of a drumlin. His model showed that the flow of ice over a drumlin would have a corresponding surface undulation (Figure 6.1). However, observational validation of this model has yet to be conducted. It may be likely, as Schoof (2002) notes, that much larger wavelength undulations dominate ice surface expression.

Figure 6.1. Schoofs' model of ice flow over the drumlin in (e). Ice flow is from left to right and ice thickness is 1 km. b to d show the changes in surface elevation (d(m)) at different points in model time. Each simulation has a different ice rheology and ice temperature gradient, but each results in a surface bump. a is the normal stress distribution at the bed at the end of a simulation.

Whilst most attention has focussed on how undulations on the bed are transmitted to the ice surface, there have also been suggestions that the surface can influence processes occurring at the bed. The groove-ploughing model for the formation of MSGL's invoked LSSs as a means of isostatically compensating for basal 'keels' ploughing into underlying till, allowing them to persist for greater distances downstream (Figure 6.2). Whilst some of the predictions of the groove-ploughing model

have been falsified (Dunstone, 2014; Spagnolo et al., 2014a), the prediction that the spacing of LSSs should match that of MSGL (and by extension drumlins, see Chapter 3), has never been tested. Even if the groove-ploughing hypothesis is incorrect (see Chapter 3), the modelling in Clark et al. (2003) highlights how surface topography can help to preserve basal ice roughness downstream. Therefore, the attenuation of subglacial bedforms may be linked to surface morphology.

Figure 6.2. Simulations of subglacial bedforms caused by a groove-ploughing mechanism (from Clark et al., 2003). Darker colours in the grey scale denote positive topography, whilst lighter indicate negative. Ice flow is from left to right, with bedrock bumps placed to the left of the images. (a) and (c) show simulations without LSSs developing on the ice surface. The bedforms produced in (b) and (d) are much longer as the keels in these experiments are isostatically compensated by LSS development on the ice surface.

Surface topography also has other important influences upon subglacial processes which may influence the formation of subglacial bedforms. Ice thickness is a key determinate of subglacial hydraulic pressure (Shreve, 1972). Thus, if morphological features on the surface are topographic, then they may induce subtle changes in the subglacial hydrology. In turn this may spatially alter the sliding rate (Sergienko et al. 2014). Over a deformable bed, changes in the amount of available water may also alter the rate of till deformation (Iverson, 2010). As till deformation is dependent upon the effective pressure at the ice bed interface (Fowler, 2010b), then changes to this property induced by surface topography (which changes overburden pressure) may feedback upon the morphology and location of subglacial bedforms. The hypothetical influence that LSSs and TSSs may have on a pervasively deforming till layer are summarised in Figure 6.3. Here, surface bumps cause a hydrological gradient, causing water to collate between them and thus causing differential rates of deformation leading to subglacial bumps.

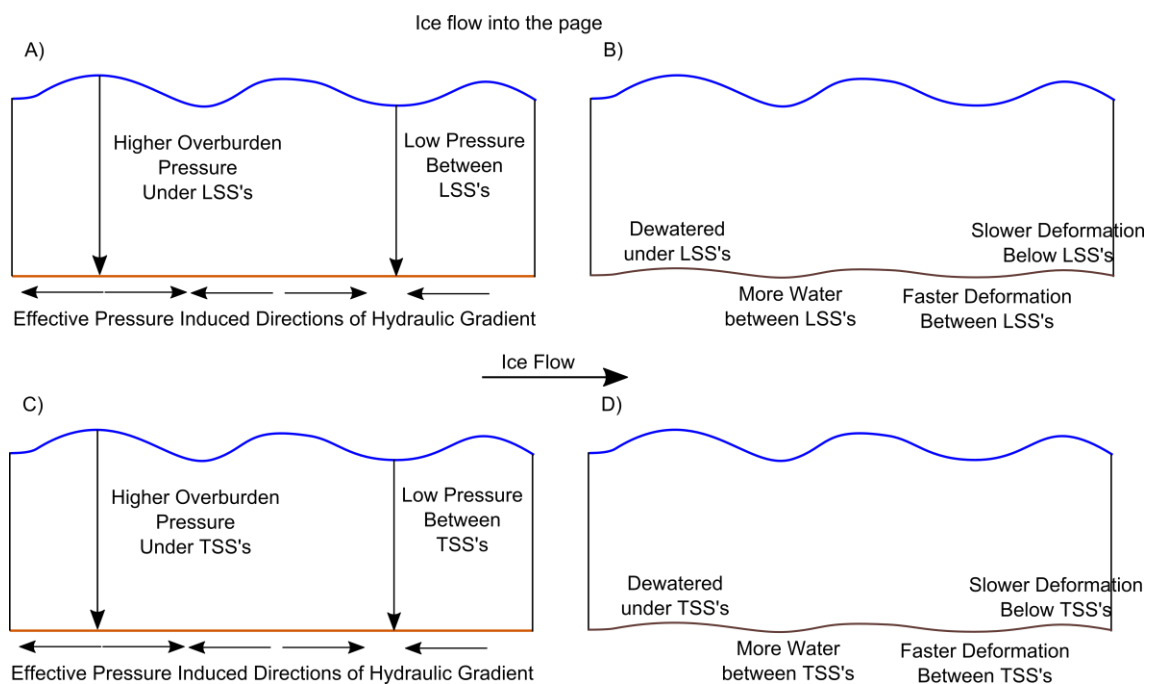


Figure 6.3. The effect of LSSs and TSSs on hydraulic gradients, and thus deformation rates where the bed is pervasively deforming. A) and C) Undulations in the surface create overburden pressure variations at the bed, creating hydrological gradients. This leads to dewatering underneath either the LSS B) or TSS D), creating regions of differential deformation rates. Essentially water movement away from the surface topographic highs creates regions where water is concentrated and till can become more like a slurry. Note that the small topographic height of LSSs and TSSs may mean that this effect is minimal.

### 6.3 Morphological Comparison Between Basal and Surficial Flow Signatures

If surficial and basal flow signatures are linked, then one might expect their morphological properties to be related. Both surface and bed flow signatures can be divided in terms of their orientation to ice flow direction (although note circular bed features as discussed in Chapter 3). Therefore, I make morphological comparisons between features of the same orientation (i.e. between ribs and TSSs and between lineations and LSSs). At a very basic level, both surficial and basal flow signatures have preferred wavelengths (e.g. subglacial bedforms in Figure 2.3; LSSs in Figure 4.14; TSSs in Figure 5.13), a common characteristic of phenomena which are formed by patterning processes (Chapter 2). Therefore, one generalisation is that the flow of an ice sheet creates patterns which appear both at the bed and the surface. This section aims to see whether the scale of these patterns is similar

A width measurement of LSSs is hard to derive, as they have no clear break of slope. However, the metrics of length and spacing can be compared to that of subglacial lineations. Figure 6.4 compares the length of all subglacial lineations measured in Chapter 3, and all grounded LSSs from Chapter 4. In general LSSs are much longer than subglacial lineations. Even if I consider just MSGs, Spagnolo et al. (2014a) report a median length of  $\approx 2900$  m compared to  $\approx 8600$  m for LSSs (Table 8). As palaeo-ice streams tend to be bigger than contemporary ice streams (Winsborrow et al., 2004; Margold et al., 2015), this cannot be attributed to a control by the size of the glacier or ice streams studied. On average LSSs can be traced for longer distances than subglacial lineations. This is either a true characteristic of the two features, or the surface of an ice sheet enables us to trace features further than on their beds. Measurements of spacing show a similar result to length data (Figure 6.5), with LSSs (mode  $\approx 9600$  m) typically being spaced more than an order of magnitude further apart than drumlins and MSGs (mode  $\approx 250$ ). Furthermore, LSS spacing is strongly related to the width of a flow unit (Figure 4.20), whilst lineation spacing is remarkably similar between flow units (Spagnolo et al., 2014a; Section 2.5.2). Therefore, there is a difference in the scale of LSSs and subglacial lineations.

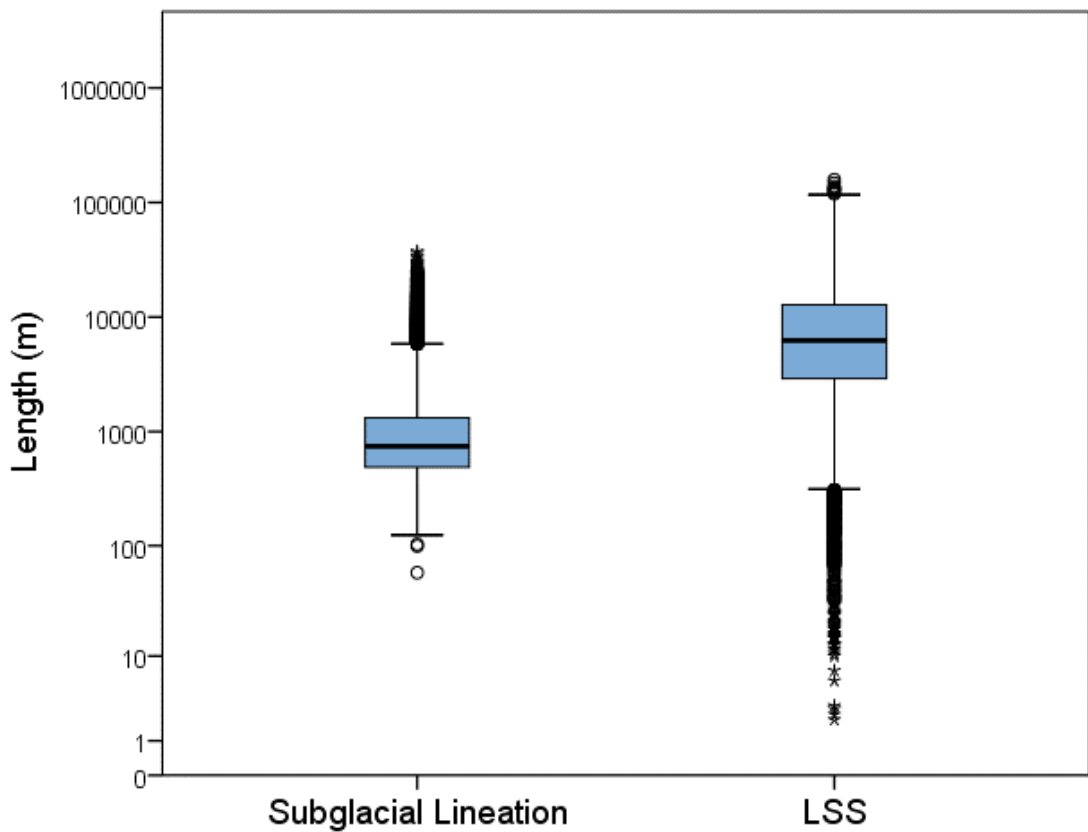


Figure 6.4. Comparison between subglacial lineation and LSS length. LSSs are generally much longer than lineations. Note the log-scale.

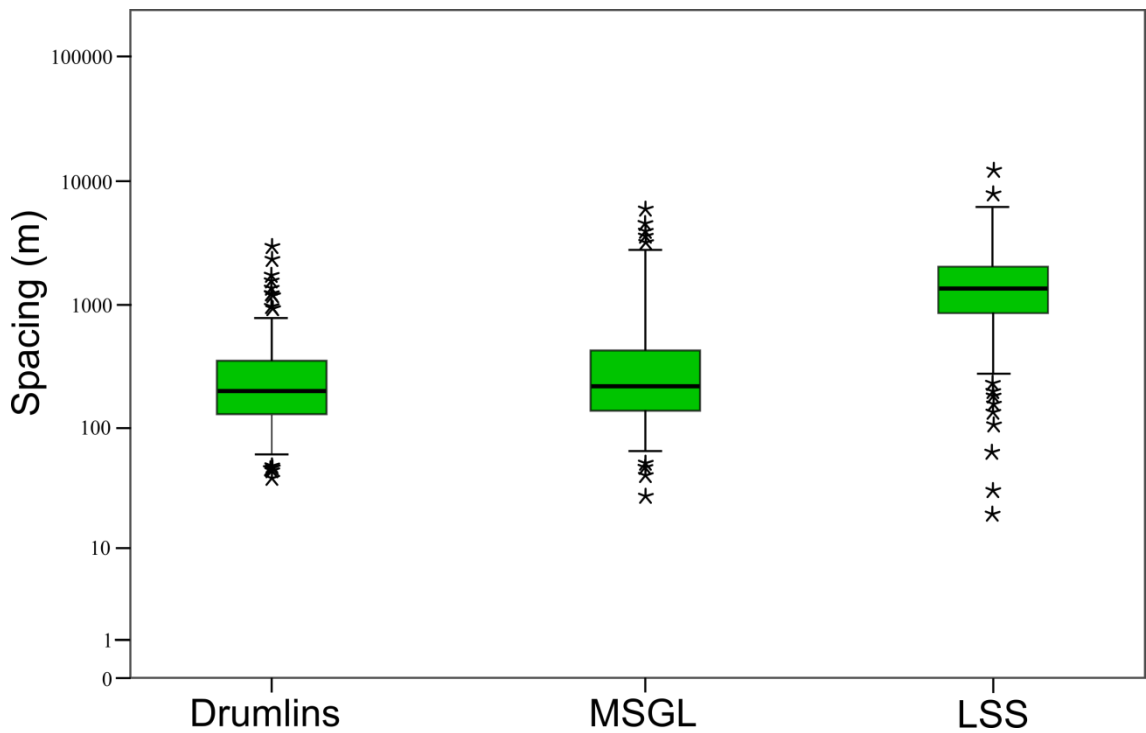


Figure 6.5. Comparison between the spacing of subglacial lineations (A and B) and LSSs (C). LSSs are spaced further apart than subglacial bedforms. Note the log-scale.

A similar comparison can be made between flow signatures aligned transverse to flow direction. Figure 6.6 compares the across flow length of TSSs and subglacial ribs (i.e. the width in Chapter 3). TSS length only overlaps with the extreme end of the subglacial rib continuum. Thus, when I consider the “mega-ribs” of Greenwood and Kleman (2010) alone, the length of these is much closer to that of TSSs (Figure 6.6). The same picture is revealed when I compare the spacing of transverse bedforms. “Normal-scale” subglacial ribs only slightly overlap with TSSs (Figure 6.7). When mega-ribs are considered alone their spacing is closer, but does not exactly match that of TSSs. Thus, there is a difference in scale between surficial and basal flow signature of both alignments, with surficial features tending to be spaced further apart and be larger than their basal counterparts. This is to be expected if ice acts as a bandpass filter when transferring basal variability to the surface (e.g. Gudmundsson, 2003). In other words, the high frequency bumps of subglacial bedforms may have been filtered into lower frequencies to form surface features. However, this mis-match also suggests that little surface-bed transfer is occurring (e.g. Figure 6.3). Only mega-ribs and TSSs are near to matching in terms of metrics, partially supporting a surface control upon their formation (e.g. Sergienko et al., 2014). However, the expectation that there is a match between surficial and basal topography ignores the selectivity of bed-surface ice transmission (e.g. Gudmundsson, 2003). Therefore, the closer match of mega-ribs and TSSs may be coincidental.

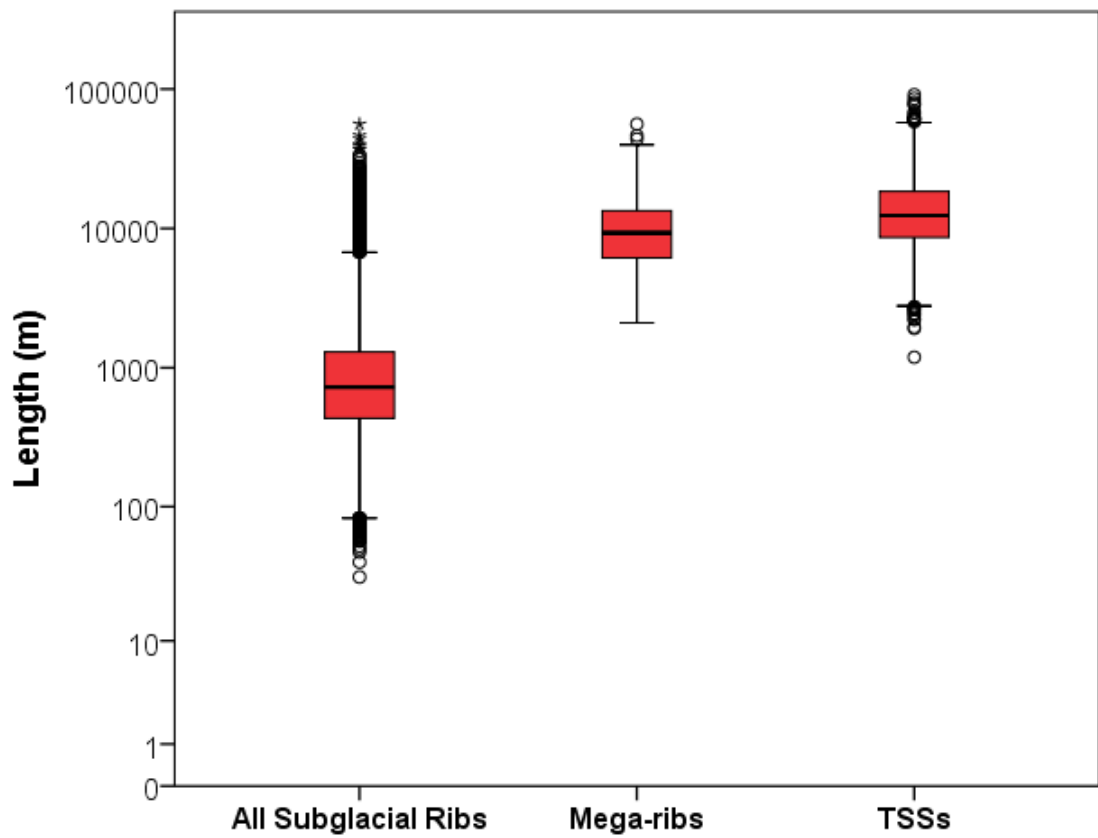


Figure 6.6. Comparison of the across-flow length of transverse flow signatures. Note the log-scale.

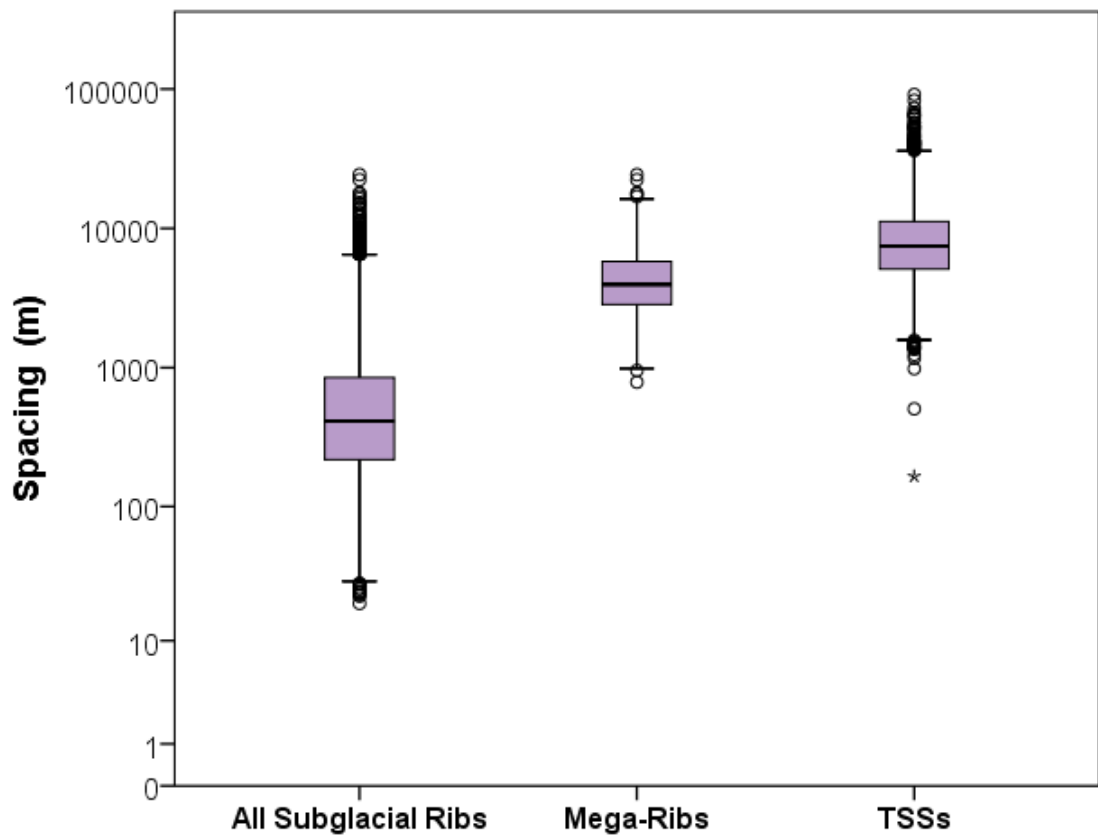


Figure 6.7. Comparison between the spacing of transverse flow signatures. Note the log-scale.

## 6.4 The Bed and the Surface of the Rutford Ice Stream

The Rutford Ice Stream presents the opportunity to study both the surface and the bed of an ice stream at an adequate resolution for comparing flow signatures. Several geophysical surveys have revealed subglacial bedforms beneath Rutford Ice Stream. They have revealed drumlins which rapidly form and migrate downstream (Smith, 1997; Smith et al., 2007), a series of ribbed moraines and drumlins in the onset zone (King et al., 2007), a field of MSGL in the fast flowing ice stream trunk (King et al., 2009) and a bedrock bump downstream of these MSGL (Spagnolo et al., 2014a). These findings are summarised in Figure 6.8 which also outlines the surface features of the Rutford Ice Stream. TSSs originate in Rutford's onset zone and continue throughout the main channel of the ice stream. LSSs occur slightly further downstream, and are concentrated to the sides of the channel, where tributaries feed into the ice stream. Potentially, there is a correspondence between flow signature alignment as subglacial ribs and TSSs occur upstream, with MSGLs and LSSs occurring further downstream (Figure 6.8), although further bed data are required to confirm this partitioning.

Between 1997 and 2004, Smith et al. (2007) detected the migration of a drumlin across their study area (Figure 6.5A). The newly created drumlin also corresponded with a switch from deforming bed conditions to sliding (Smith and Murray, 2009), which one might expect to cause a difference in basal coupling. To analyse whether there are corresponding changes in the surface of the ice stream, Landsat images from different dates were analysed. The failure of the scan line corrector on Landsat 7 limited image acquisition during this timeframe so further scenes before and after were also examined. Landsat images do not detect any significant change in the positioning of surface structures within this time period (Figure 6.9). There are several possible explanations for this: i) there is no relationship between surface and basal flow signatures; ii) surface features react slowly to basal changes; iii) the change in basal conditions was too small to influence the surface. Minor changes may be detectable on Figure 6.9, but these may be consequences of georectification or sun-angle changes. Further work, using a more sensitive satellite instrument or ground-based surveying, should be conducted in order to determine whether ice surface elevation changes occur during a period of drumlin migration.





Figure 6.8. Summary of surficial and basal flow signatures of the Rutford Ice Stream. Central figure has location of subsequent figures and surficial flow signatures from Chapters 4 and 5. A) Smith et al., 2007 detected the migration of a drumlin shaped object from repeat seismic surveying. B) These features were later revealed to be a field of MSGL (King et al, 2009; Spagnolo et al., 2014a). C) Further upstream a series of drumlins have also been imaged, as well as D) a drumlinised subglacial rib (King et al., 2007).

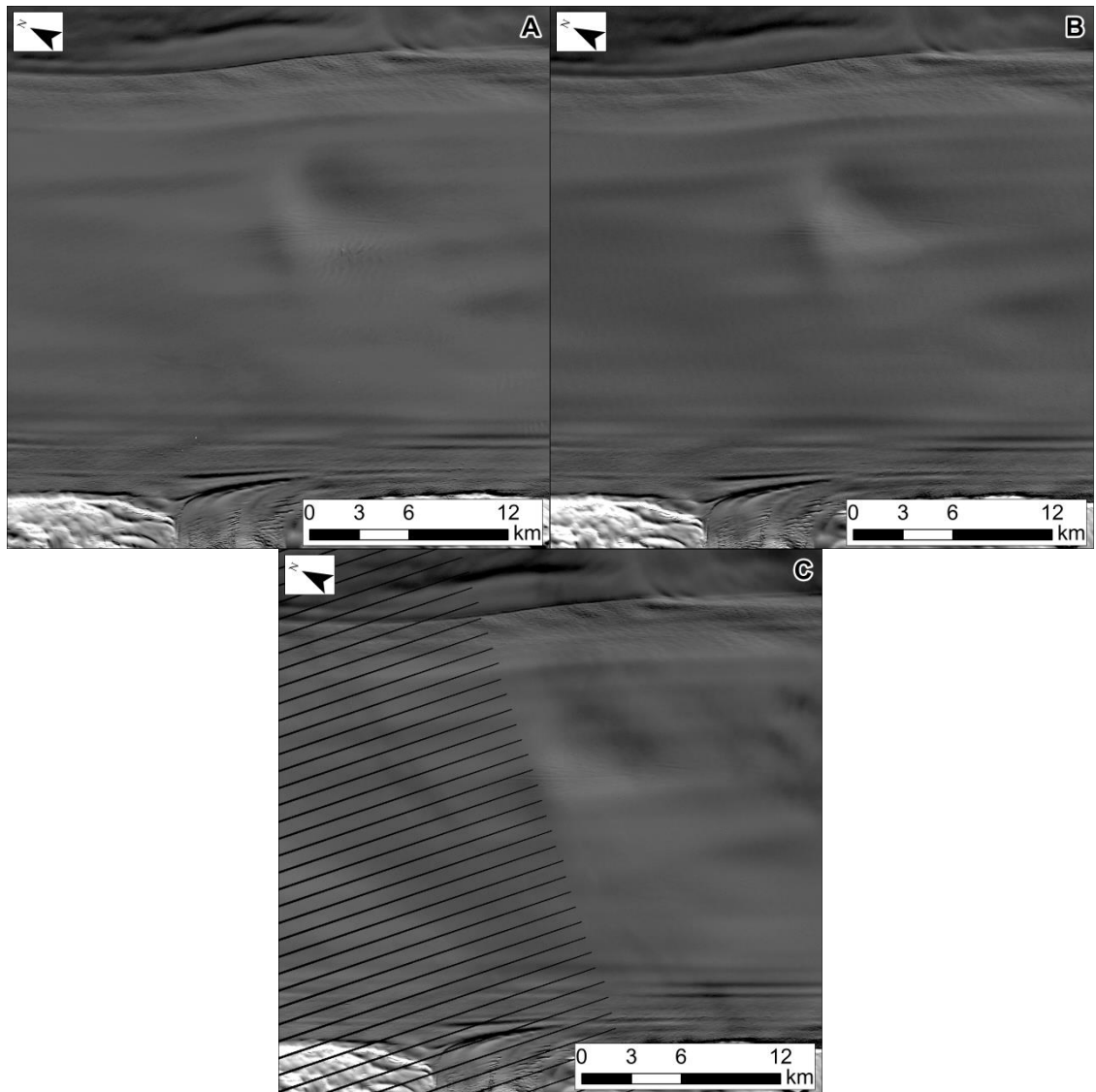


Figure 6.9. Landsat images of the surface of Rutford Ice Stream. A) March 1997. B) January 2003. C) March 2004. Note the lack of surface change during a period of rapid basal evolution (Smith et al., 2007). Slight changes may be the consequence of sun-angle or georectification.

High resolution elevation data of the bed of Rutford have revealed multiple subglacial bedforms and a bedrock bump (King et al., 2009; Spagnolo et al., 2014a). Using these bed data, surface elevation data collected during surveying, and Landsat images, basal flow signatures can be compared with surficial ones. Positional uncertainties are below the scale of both the lineations and LSSs. For the bed data, these were located using a dGPS, and are therefore below a meter (King et al., 2015). The geometrical accuracies of the Landsat images are subpixel (30 m, [limg.usgs.gov/access.php](http://limg.usgs.gov/access.php)). Figure 6.10 collates mapping of surficial flow signatures (Chapters 4 and 5) with mapping of the basal flow signatures. For aligned flow

signatures (MSGSL and LSSs), there is a discrepancy in the frequency of features between the two: MSGSL's are more closely spaced than LSSs. Furthermore, LSSs were mapped to start in the area, with no direct correspondence to an MSGSL's (Figure 6.10). Conversely, the TSS mapped in this area corresponds well with the bedrock bump in the middle of the study area (Figure 6.10). To confirm this pattern a series of transects were placed along and across the study region, comparing bed elevation to surface elevation and reflectance (Figures 6.11 to 6.13). The position of the bedrock bump corresponds with a region of both raised elevation and reflectance (6.11; Line A to A'). Across-flow bed elevations show little if any correspondence to surface elevation or reflectance at the kilometre or so scale of flow signatures (Figures 6.12 and 6.13, lines B to B' and C to C'). It is worth noting that surface reflectance from Landsat images is dominated by noise, making individual LSSs difficult to discern on transects (Figures 6.12B and 6.13B).

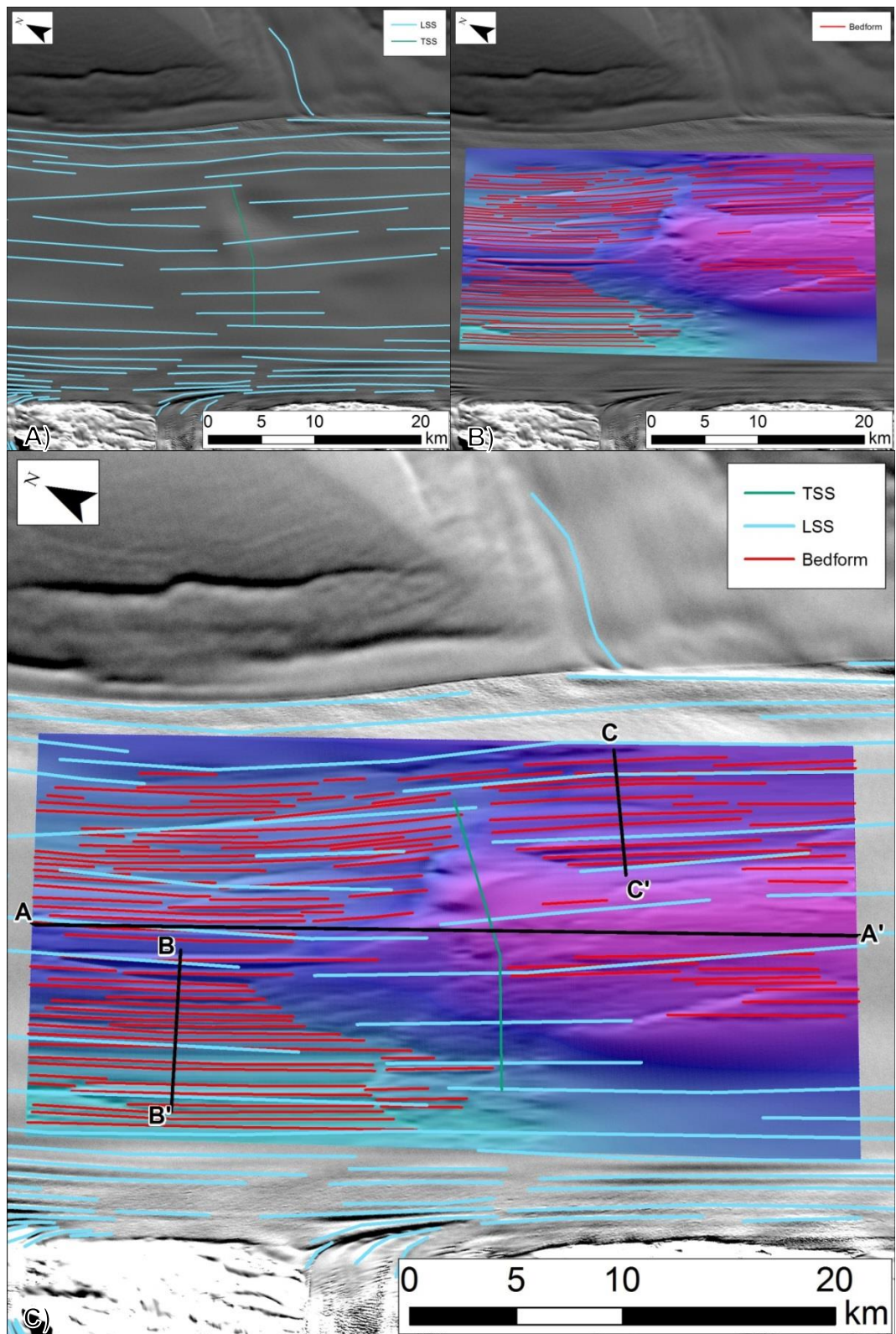


Figure 6.10. Comparison between surficial and basal flow signatures of the main channel of the Rutford Ice Stream. A) Mapping from previous chapters shows numerous LSSs and one TSS in the area. B) Elevation data of the ice stream bed show MSGLs and a bedrock ridge. C) Combining the two sets of mapping shows little to no spatial co-location between MSGLs and LSSs, but a clear correspondence between the bedrock ridge and the TSS. Location of subsequent profiles are shown here.

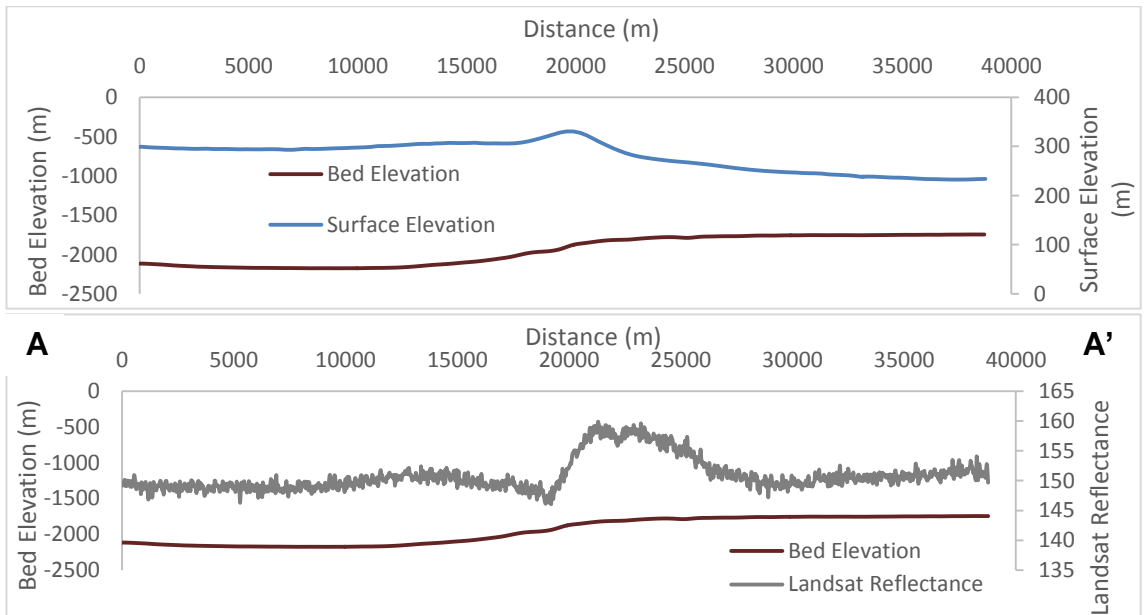


Figure 6.11. Along-flow transect of the bed of the Rutford Ice Stream, compared to surface elevation and Landsat reflectance. The TSS is expressed as an increase in elevation and Landsat reflectance. This coincides with the start of the bedrock bump visible in Figure 6.10.

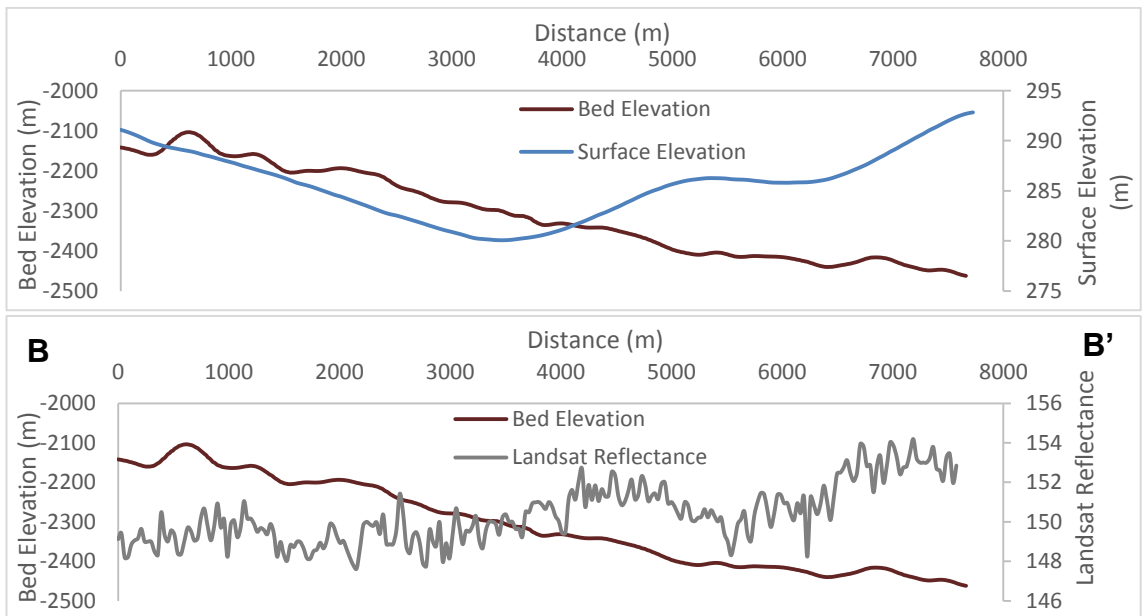


Figure 6.12. Comparison between surface and bed for across-flow transect B. Neither the surface DEM nor the Landsat reflectance values display correspondence to the underlying topography. Note that the Landsat profile is dominated by small noise fluctuations, across a relatively homogenous surface.

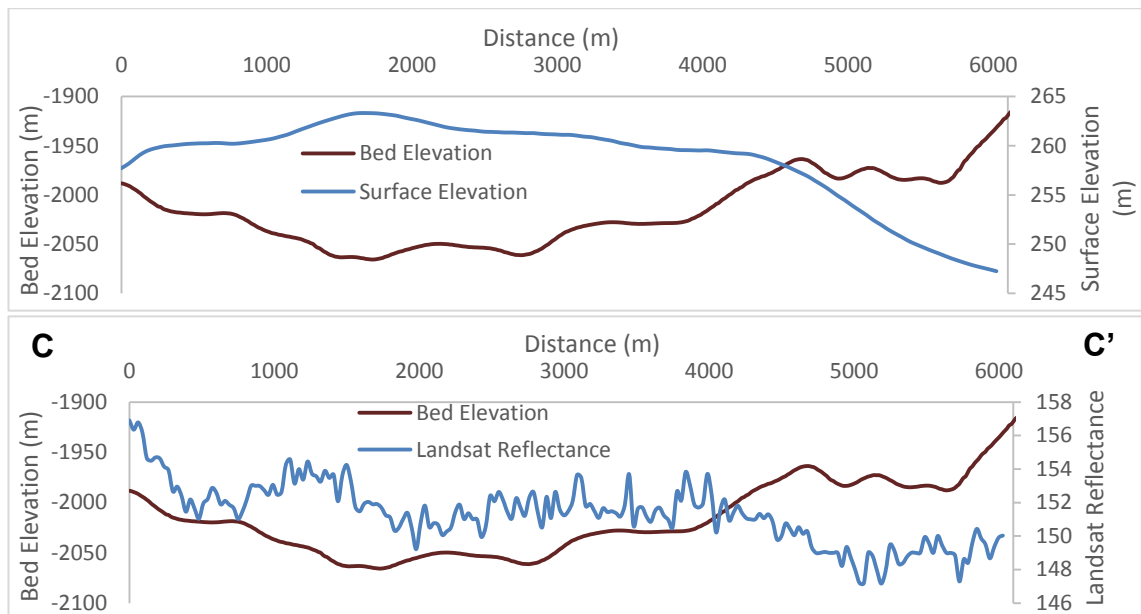


Figure 6.13. Comparison between the bed and the surface of the Rutford Ice Stream across transect C. In a similar fashion to Figure 6.12, there is no correspondence between the bed DEM and the surface DEM (above) or Landsat reflectance (below) at the scale of flow signatures (100s of m to kms).

At the Rutford ice stream, flow-aligned flow signatures are spaced further apart than MSGL (Figure 6.5). This agrees with the previous morphometric comparison of flow-aligned flow signatures (Section 6.3). Only one TSS occurs in the region where high resolution data are available. This corresponds to a bedrock bump. TSSs are more abundant further upstream (Figure 6.8), occurring in a region where ribbed moraines and drumlins are thought to occur. I cannot rule out a bedrock control on these TSSs. However, a second possibility remains that they are the result of the flow of ice over a subglacial bedform, transferring some information to the surface. Further geophysical data are required in order to resolve this.

## 6.5 Airborne Radar

Whilst ground based seismic and radar surveys have given us detailed insight into the subglacial bedforms of the Rutford ice stream (Section 6.4), a broader coverage can be obtained using airborne radar. Airborne radar has a lower resolution than its ground based equivalent, but it has been used previously to identify subglacial bedforms (Schroeder et al., 2014). The wide spacing of flight lines means that elevation models similar to that examined above (e.g. King et al., 2009; Figure 6.10), cannot be made from airborne radar, providing instead two dimensional images of the bed. Therefore, I am unable to say without further analysis (e.g. Schroeder et al., 2014) whether the

features I observe are subglacial bedforms. However, the data do provide us with an idea of the shape of the bed, and will reveal bumps of a similar scale to subglacial bedforms.

Here I analyse freely available radar data obtained by the Center for Remote Sensing of Ice Sheets (CREGIS, <https://data.cresis.ku.edu/>), collected over numerous campaigns by their radar depth sounders. The data were processed and visualised by creating a custom MATLAB script. Here the radar propagation delay ( $u_s$ ) was transformed into a depth measurement via the equation:

$$d = (u_s - h_s) * \left(\frac{c}{2\sqrt{\epsilon_i}}\right) \quad \text{Eq. 14}$$

whereby  $d$  is depth,  $h_s$  is the ice surface height,  $c$  is the speed of light and  $\epsilon_i$  is the dielectric constant of ice, here a value of 3.15 was used in accordance with the Looyenga model for dealing with a heterogeneous density mixture (Looyenga, 1965; Kanagaratnam et al., 2001). Measurements of depth agree well with the Bedmap 2 dataset (Fretwell et al., 2013). I split my analysis into across-flow and along-flow radar in order to study any possible relationship between basal and surficial linear and transverse flow signatures respectively. Locations were chosen in places with clear examples of surficial flow signatures in satellite imagery.

Approximately 750 km of across-flow radar data, distributed across three ice streams (Pine Island, Foundation and Recovery; Figure 6.14), were analysed and interpreted. Figures 6.15 to 6.17 show examples of the data and interpretation of the radargrams. In general there is little correspondence between the location of undulations in the bed and mapped LSSs. This is confirmed with analysis of further radar lines, and holds even if only bumps greater than 50 m in amplitude, which one might expect to be more readily transmitted to the surface, are considered (Figures 6.18 to 6.20). Ice sheet surface undulations visible in the radar data also do not line up with basal undulations (Figures 6.15 to 6.17). Often, these are spaced roughly the same distance ( $< 1$  km) apart as subglacial lineations (Figure 6.15, 6.17). Therefore in an across flow direction, there is little correspondence between basal and surficial topography and it is unlikely that bumps with the same dimensions as subglacial bedforms are related to LSSs.

The mismatch could be caused by positional errors between the radar data and satellite data. Furthermore, there may be inheritance of features formed by upstream bumps that were not detected by the radar data as flight lines were not positioned at the



origin of the features. Thirdly, the location of LSSs is altered by surficial processes (e.g. Campbell et al., 2008). However, this does not explain the difference in frequency between basal bumps and LSSs (e.g. Figures 6.18 to 6.20). Additionally, LSSs are likely influenced by secondary factors such as the location of tributary convergence (e.g. Figure 6.16). Whilst no obvious relationships are apparent between the surface and the bed in this analysis, it is far from a perfect technique. Instead this is taken as a first pass in order to ascertain whether an obvious relationship between the surface and the bed exists, and should be considered with my other results. This mismatch between the bed and the surface in an across flow direction is concurrent with my previous results (Sections 6.3 to 6.4), and LSSs within the Rutford ice stream which started within the study area did not correspond to basal topography (Figure 6.10). Further work on radar lines, potentially showing how internal reflectors vary with depth, is required.

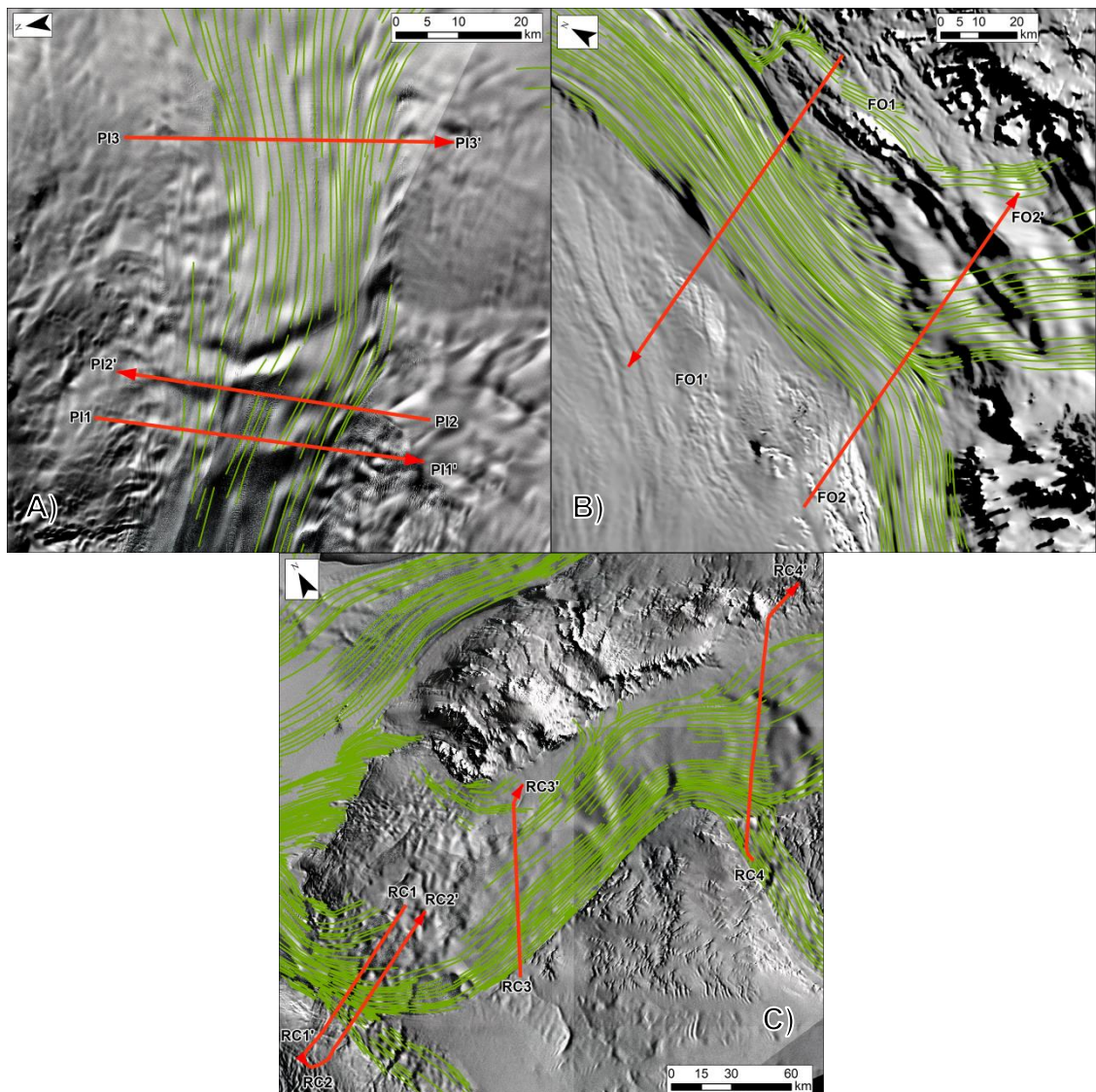




Figure 6.14. Locations of studied across-flow radar profiles. Red arrows denote flight direction. Green lines are mapped LSSs. A) Pine Island Glacier. B) Foundation Ice Stream. C) Recovery Glacier.

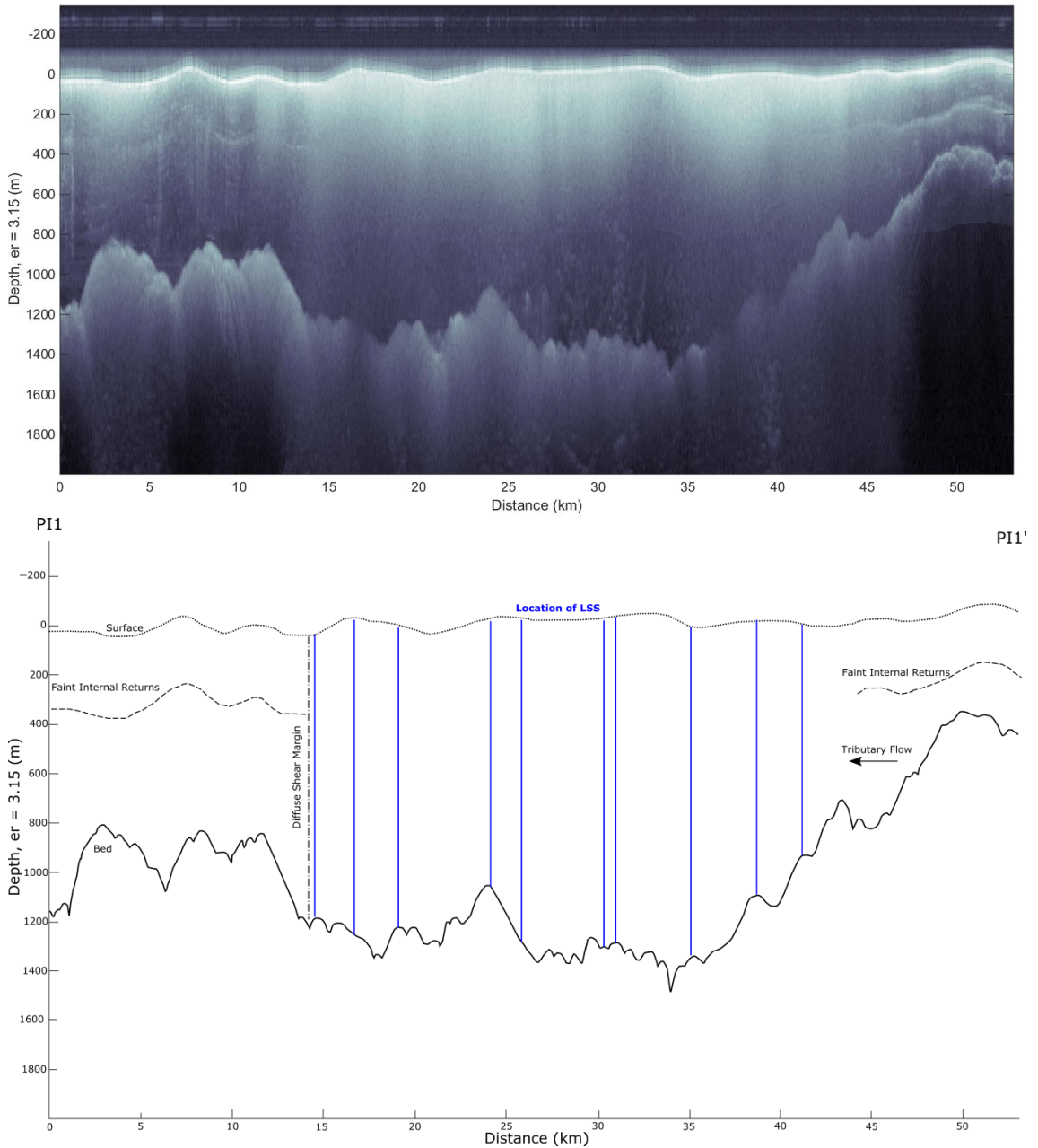


Figure 6.15. Radargram (above) and interpretation (below) of line P11 (location on Figure 6.14). Blue lines are locations of mapped LSS's (see Figure 6.14). Note the numerous bumps in the bed compared to the frequency of LSSs. Some of these basal bumps may be subglacial bedforms. Faint internal returns may be echoes of the surface reflection, rather than distinct isochrones.

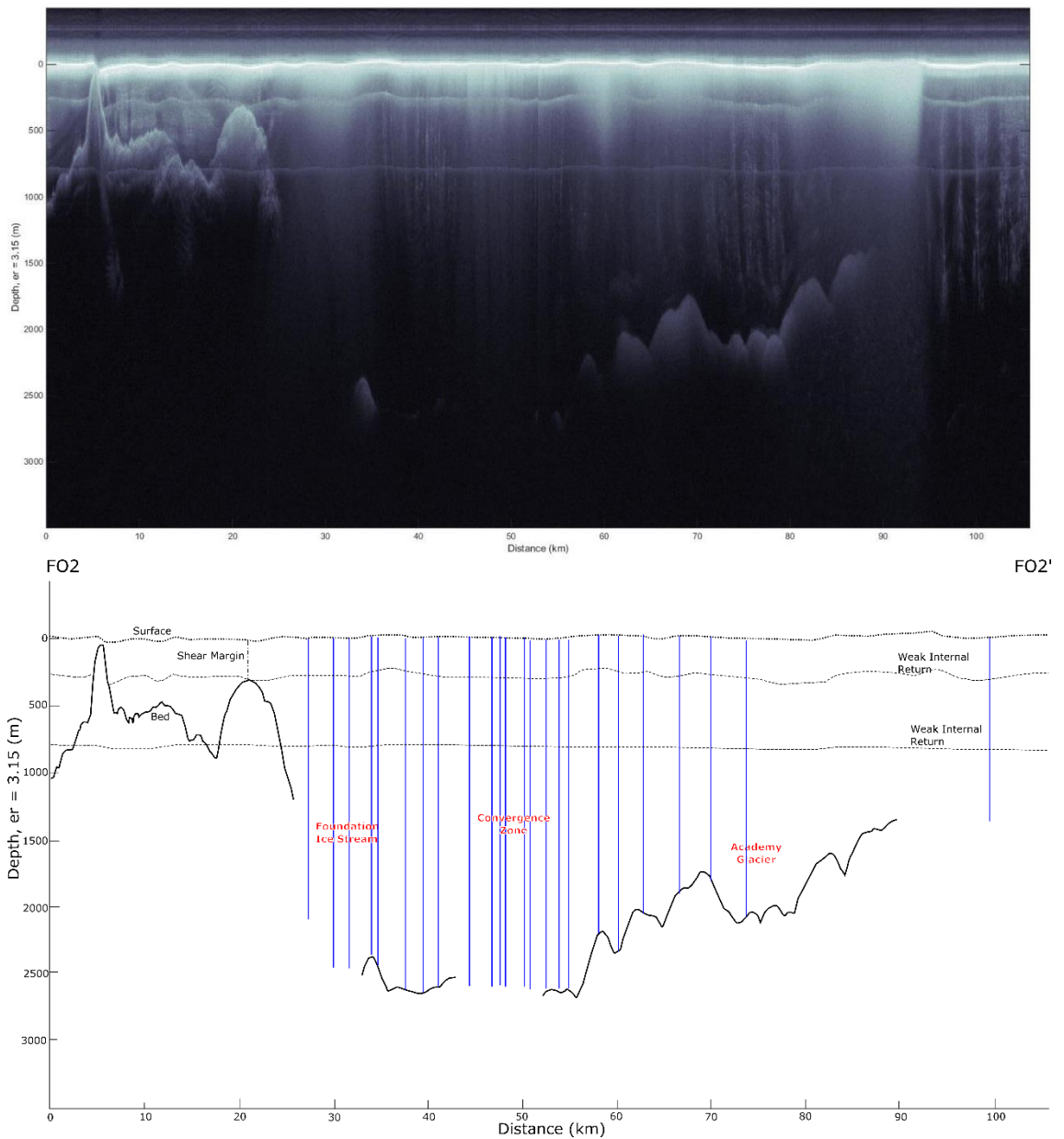


Figure 6.16. Radargram (above) and interpretation (below) of line FO2 (location on Figure 6.14). Blue lines are locations of mapped LSS's (see Figure 6.14). Weak internal returns are likely echoes of the return from the surface. Note the concentration of LSSs in the convergence zone between the Foundation Ice Stream and Academy Glacier. Whilst some bumps coincide with LSSs, the pattern and ubiquity of this is unclear.

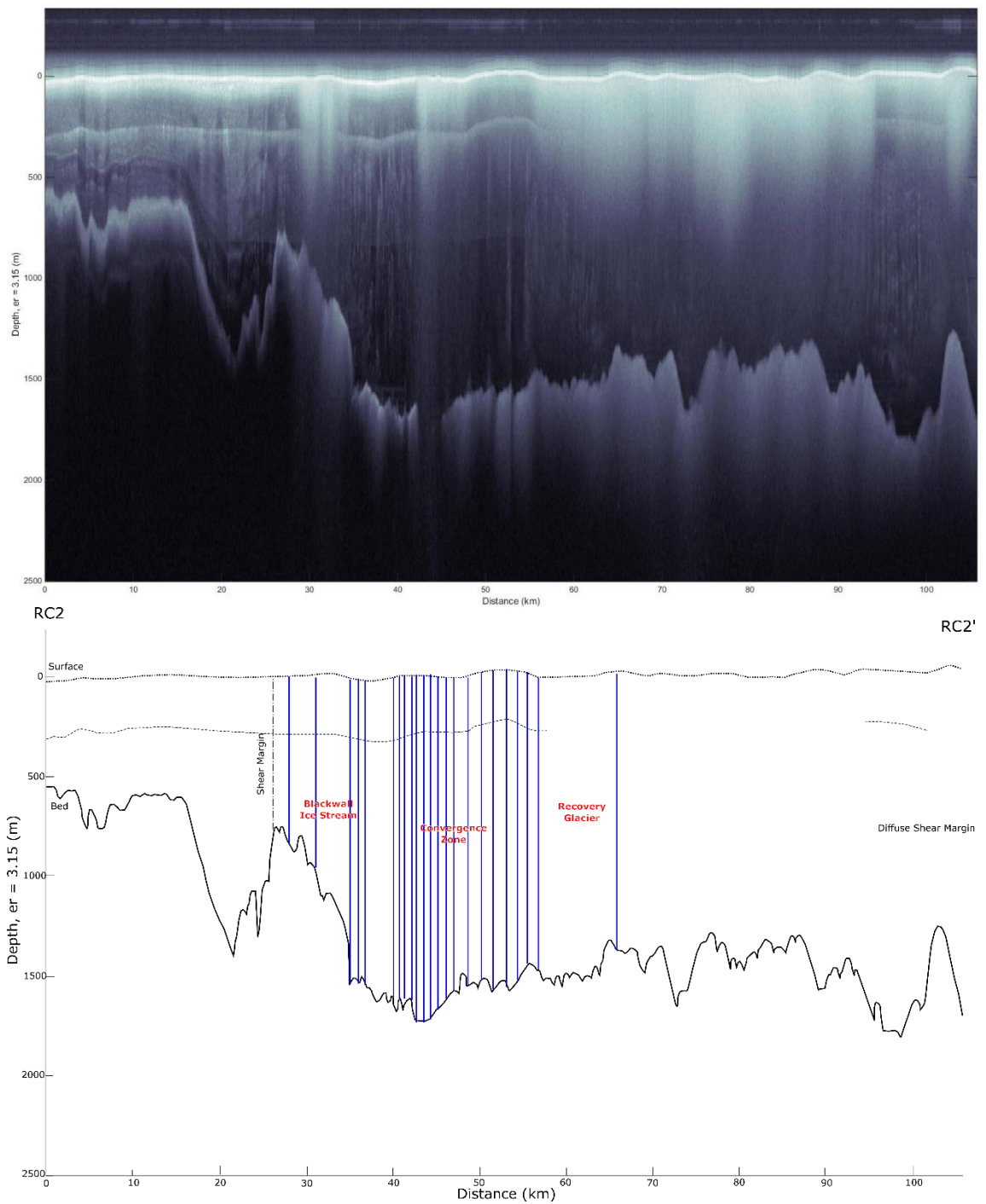


Figure 6.17. Radargram (above) and interpretation (below) of line RC2 (location on Figure 6.14). Blue lines are locations of mapped LSS's (see Figure 6.14). Note the frequent bed bumps which are spaced a similar distance to subglacial bedforms. LSSs are concentrated in the convergence zone between Blackwall Glacier and Foundation Ice Stream.

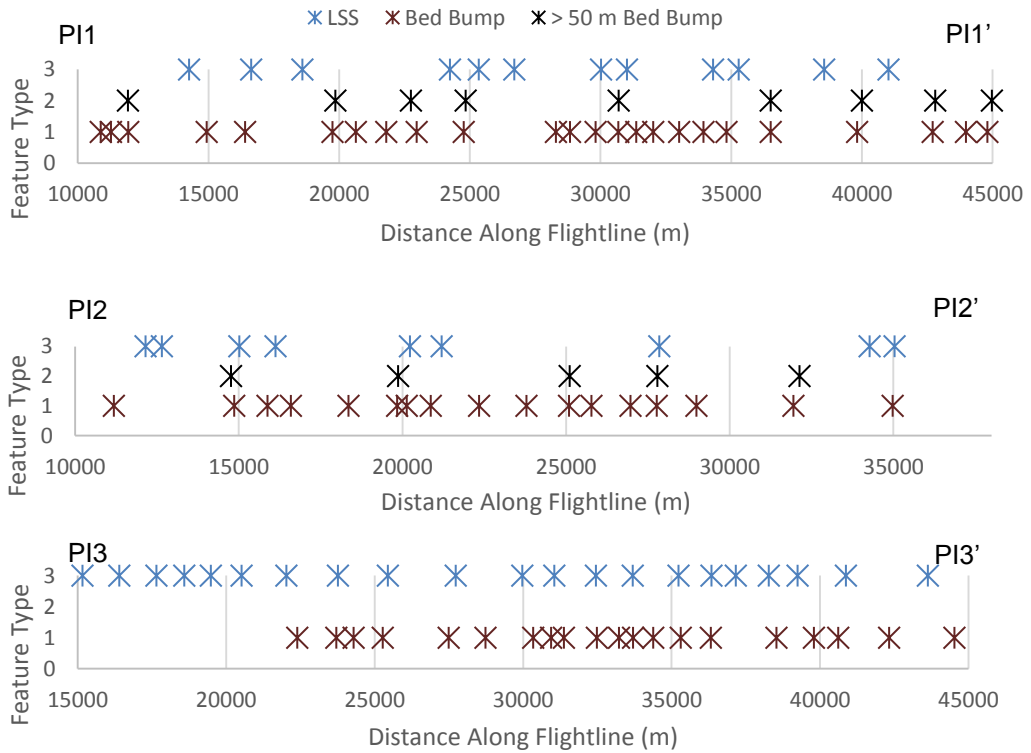


Figure 6.18. Location of bed bumps and LSSs along flightlines on Pine Island Glacier (locations on Figure 6.14). Note the lack of correspondence, and mismatch in frequencies, between the surface and the bed. Only regions where LSSs are present are displayed. Features are 1 = bump in the bed, 2 = bump greater than 50m in amplitude and 3 = LSS.

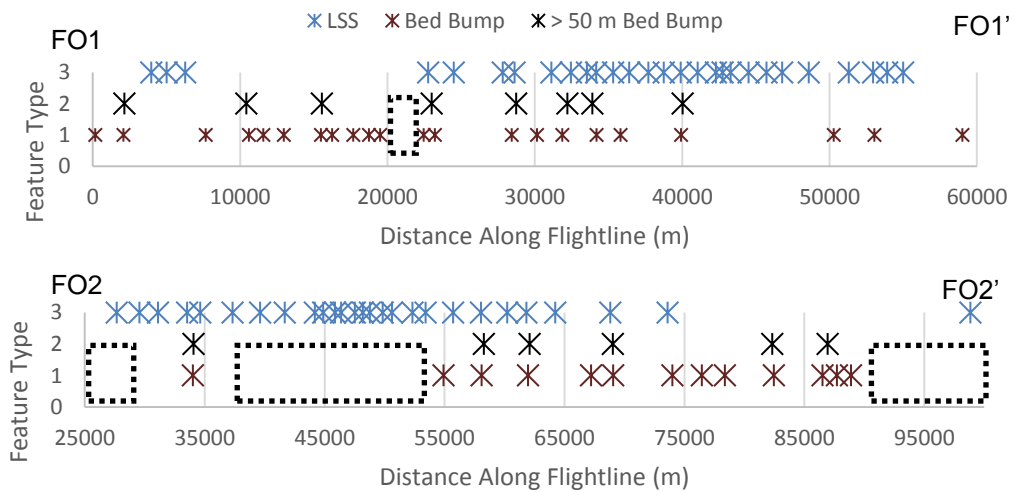


Figure 6.19. Location of bumps and LSSs along flightlines on Foundation Ice Stream (locations on Figure 6.14). LSSs again show a lack of correspondence with basal bumps. Features are 1 = bump in the bed, 2 = bump greater than 50m in amplitude and 3 = LSS. Dashed boxes indicate no bed data regions.

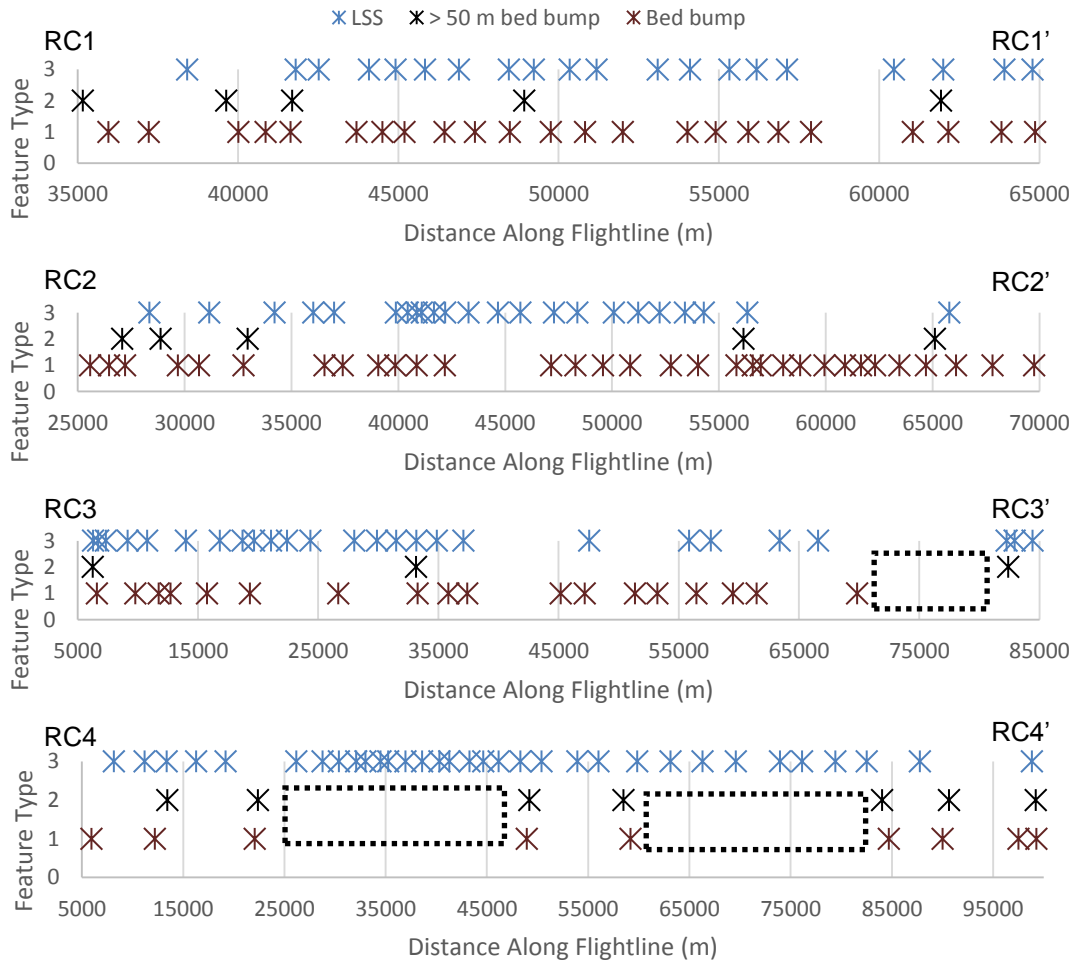


Figure 6.20. Location of bumps and LSSs along flightlines across Recovery Glacier (locations on Figure 6.14). Features are 1 = bump in the bed, 2 = bump greater than 50m in amplitude and 3 = LSS. There is a lack of correspondence between the bed and surface in terms of feature spacing and frequency. Black dashed boxes indicate no bed data regions.

Along-flow direction radar from Academy, Support Force, Slessor, Recovery and Thwaites glaciers (locations on Figure 6.21), stretching across approximately 2,500 km, were also analysed. Figures 6.22 to 6.27 show the results of this analysis. A mixture of TSSs controlled by bed features and those which show no correspondence to the bed was found. This is epitomised at Academy Glacier, where TSSs occur both on a smooth upstream slope without bed undulations and in a region where they are controlled by bed undulations (Figure 6.22). A similar pattern is found at Slessor Glacier (Figure 6.24). A likely source for TSSs not controlled by bed undulations is a variation in bed slipperiness (e.g. Sergiekno et al., 2014). However, higher resolution radar and further analysis (e.g. Ashmore et al., 2014) is required to study this further. The highest correspondence between the bed and the surface occurs at Thwaites Glacier (Figures

6.25 and 6.28). Across the flightline depicted in Figure 6.25, TSSs do not occur where ice is thickest, perhaps due to an inhibited surface transfer due to thick ice. Features which resemble isochrones were also noted during my analysis (e.g. Figures 6.22 to 6.24). These potentially show how high frequency bed undulations, of a similar scale to “normal-scale” subglacial bedforms (<1 km), are smoothed out at depth into a single fold in the ice. However, I was unable to trace the evolution of any folds to the surface in a similar manner to Campbell et al. (2008). Furthermore, no surface expression of subglacial mega-ribs (e.g. Greenwood and Kleman, 2010), was observed in my analysis. This suggests that at these localities that TSSs are unlikely a consequence of flow over subglacial mega-ribs as suggested by Sergienko and Hindmarsh (2013) and Sergienko et al. (2014). The above mentioned caveats of along-flow radar analysis (inheritance of features from up-flow and positional errors) should be considered with this along-flow radar. However, the overall picture of a mixed origin for TSSs, some features controlled by bed undulations and others without a bed undulation, is consistent with my analysis in Chapter 5 (Section 5.5.1).



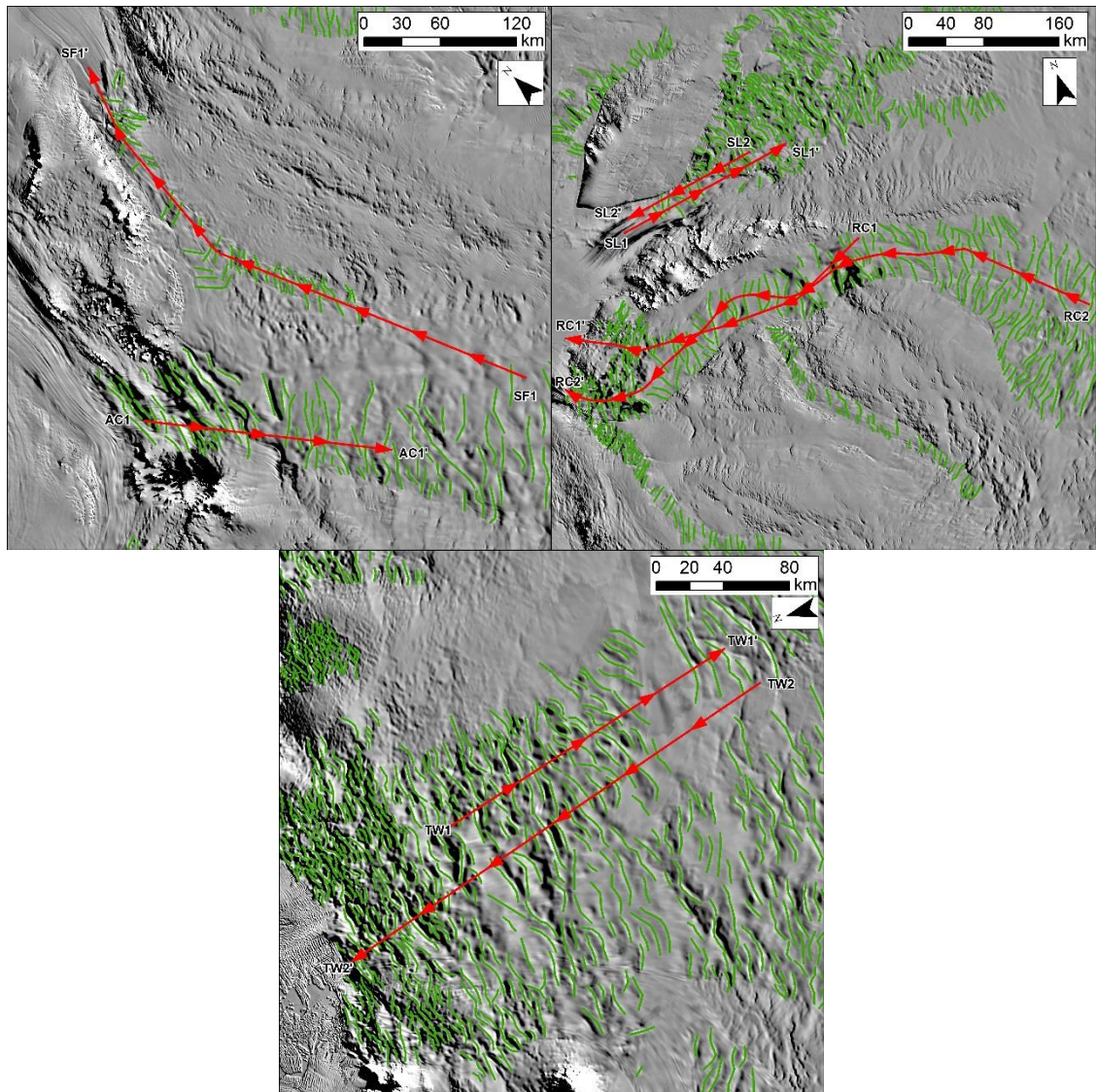


Figure 6.21. Location of studied along-flow radar lines (red) and TSSs (green). Arrows denote flight direction. A) Support Force (upper) and Academy (lower) glaciers. B) Slessor (upper) and Recovery (lower) glaciers. C) Thwaites Glacier.

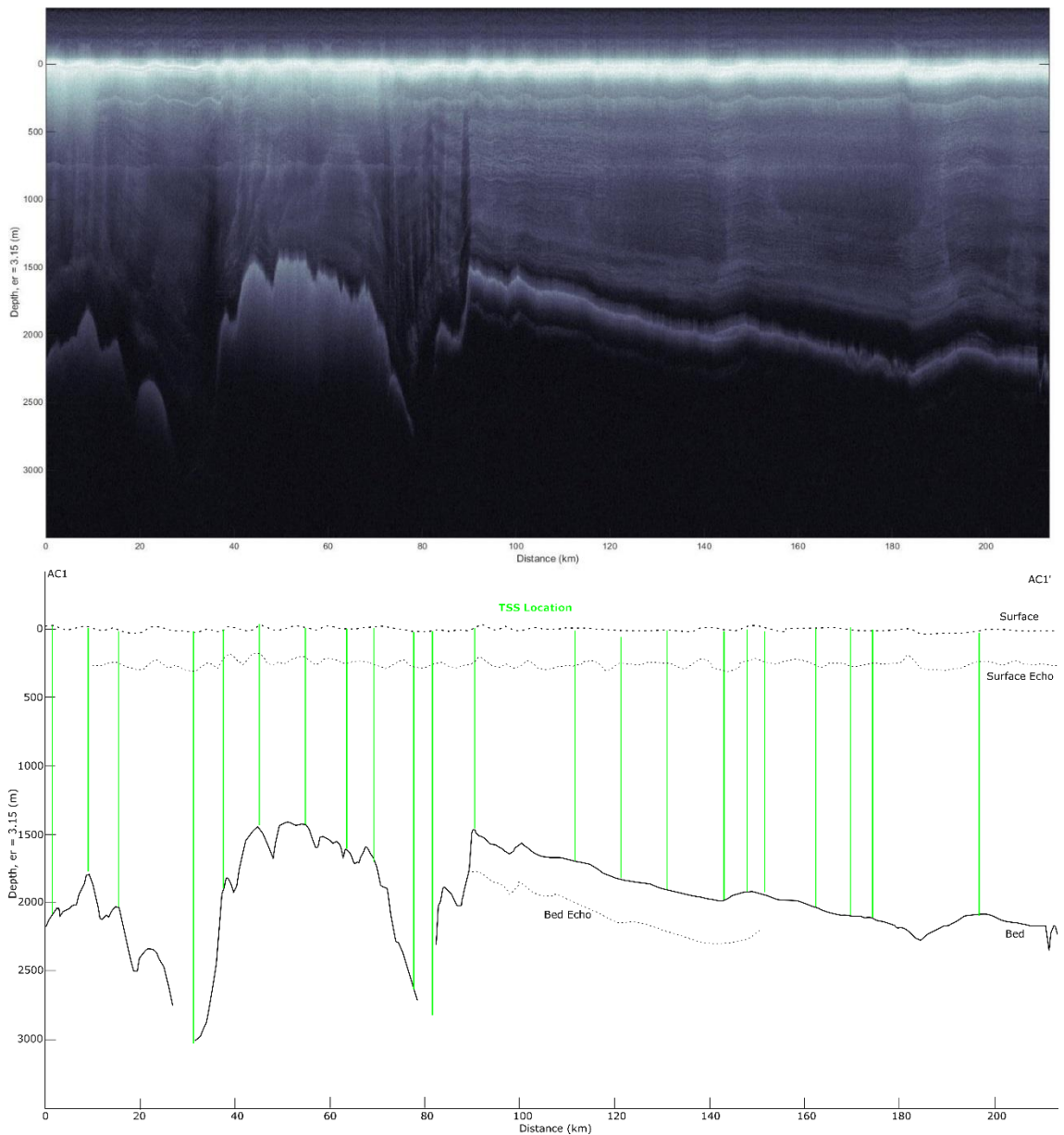


Figure 6.22. Radargram (above) and interpretation (below) of line AC1 (location on Figure 6.21). Note that TSSs match bed variability reasonably well to the left of the image. The slope to the right of the image is comparatively flat, yet TSSs were still observed in this area. One return appears to be an echo of the surface return. However, more internal structures (possibly isochrones) are evident in places.



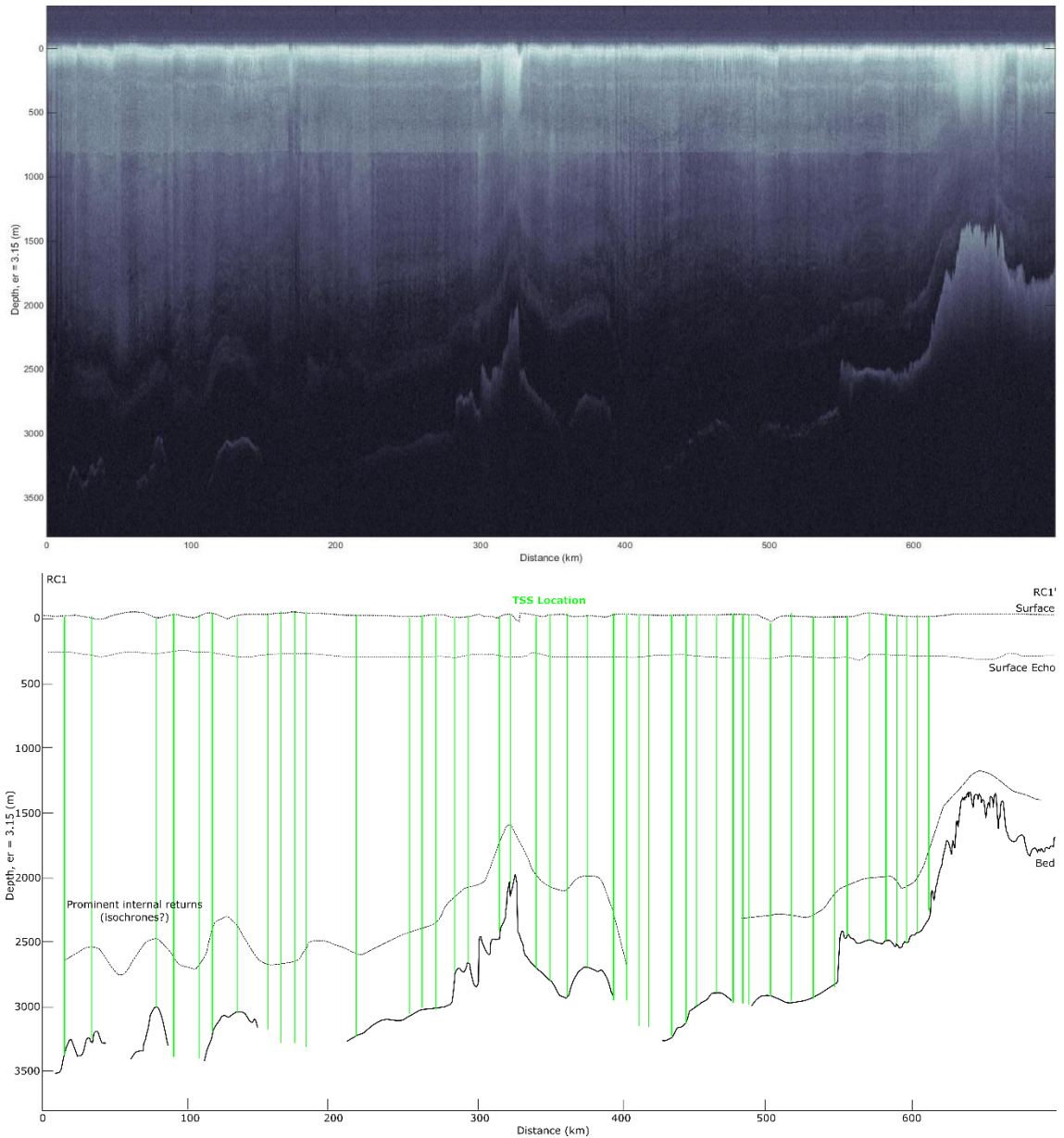


Figure 6.23. Radargram (above) and interpretation (below) of line RC2 (location on Figure 6.21). Note the mixture between TSSs that are controlled by bedrock topography, and those which are not. The potential deep radar returns (more evident in the radargram than depicted in the interpretation) may highlight initial smoothing from the bed upward of basal topography.

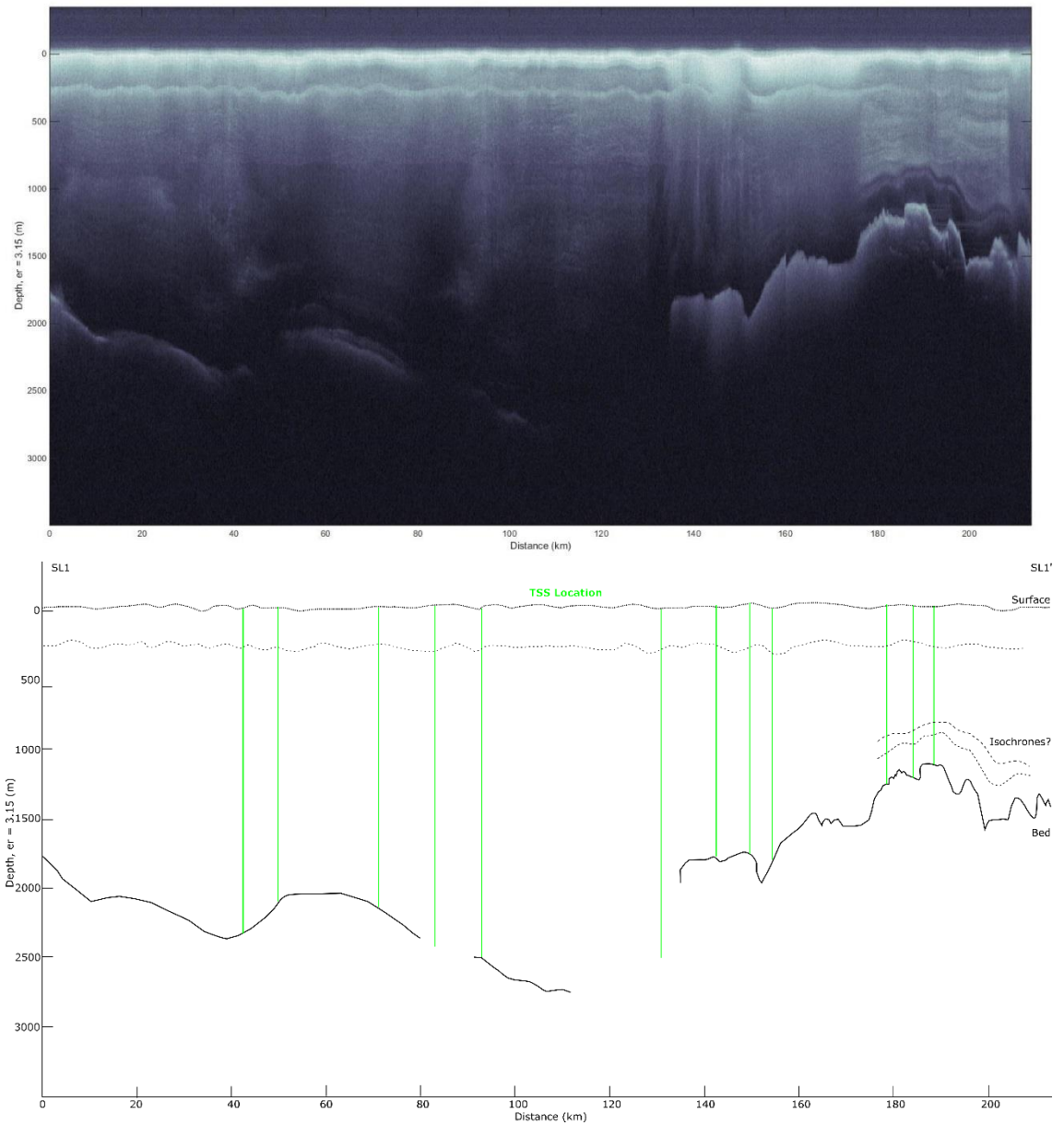


Figure 6.24. Radargram (above) and interpretation (below) of line SL1 (location on Figure 6.21). Note the lack of correspondence between TSSs and basal topography to the left of the image, where the bed is comparatively smooth. Potential isochrones to the right of the show how high frequency wavelengths of bumps are filtered out close to the bed.

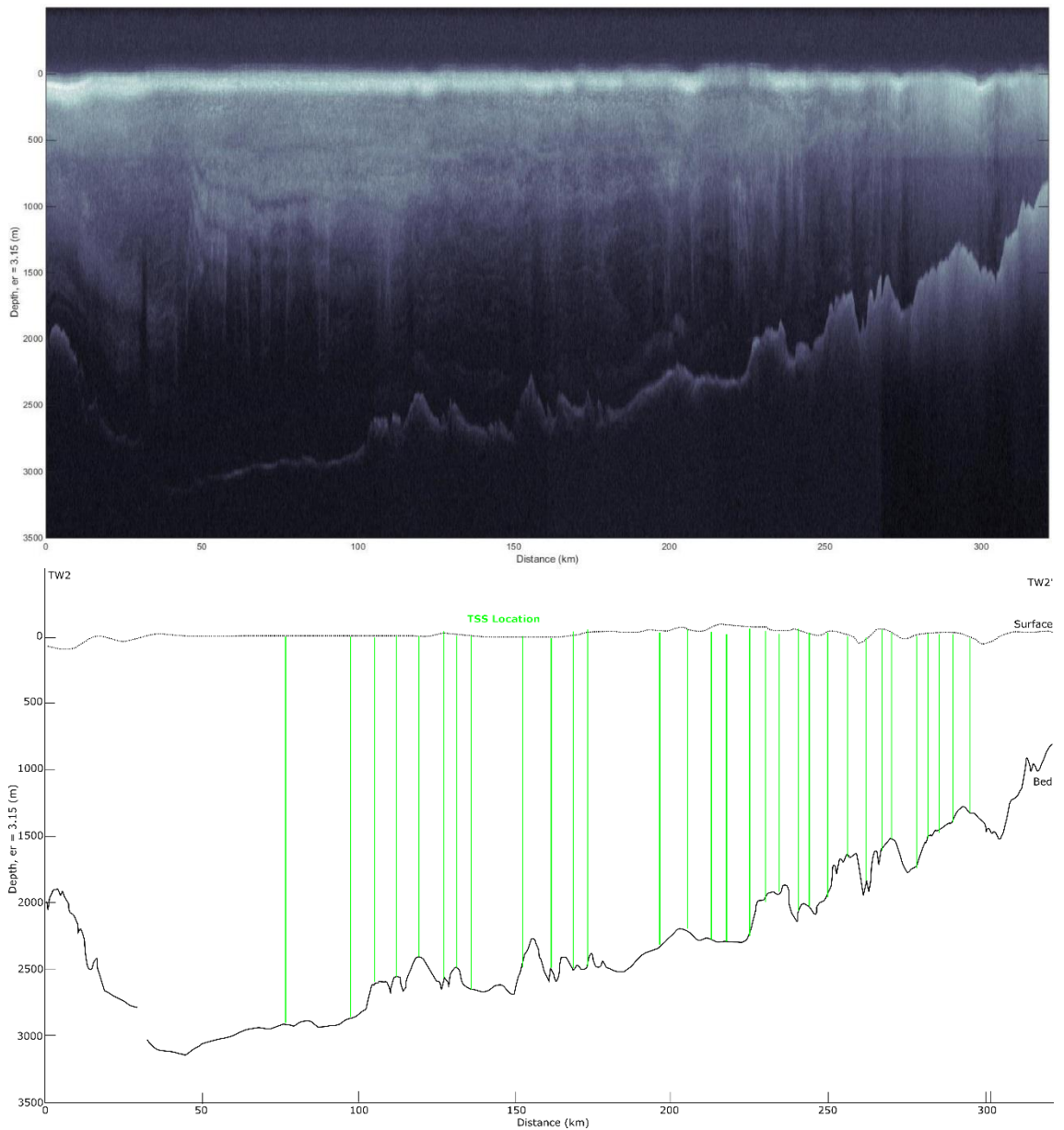


Figure 6.25. Radargram (above) and interpretation (below) of line TW2 (location on Figure 6.21). Note the lack of TSSs to the left of the image, where ice thickest. More TSSs are observed to the right of the image as ice gets thinner and bedrock bump frequency increases.

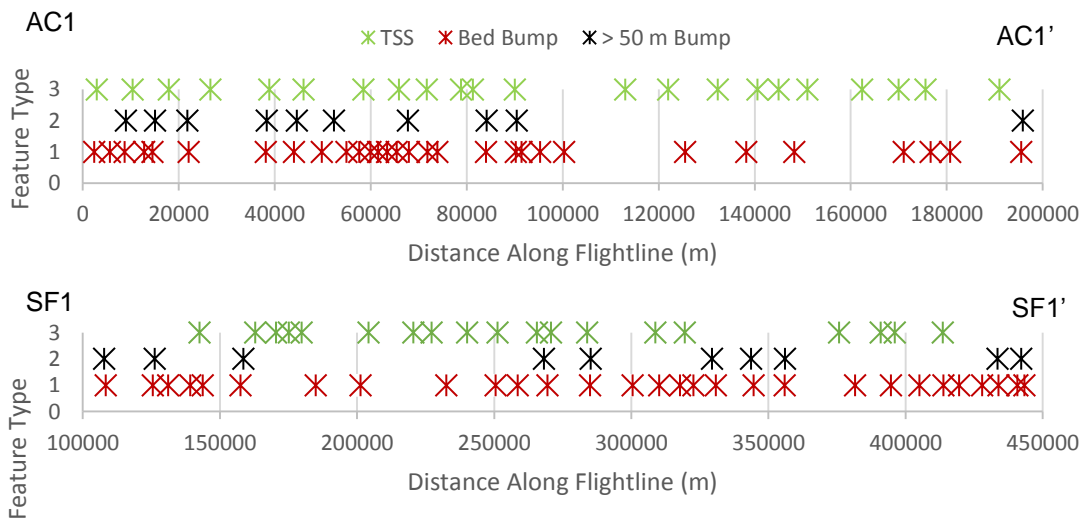


Figure 6.26. Location of TSSs and bed bumps across flightlines over Academy and Support Force glaciers (see Figure 6.21 for locations). Note that for both examples, the location of TSSs is not purely controlled by the location of bedrock bumps.

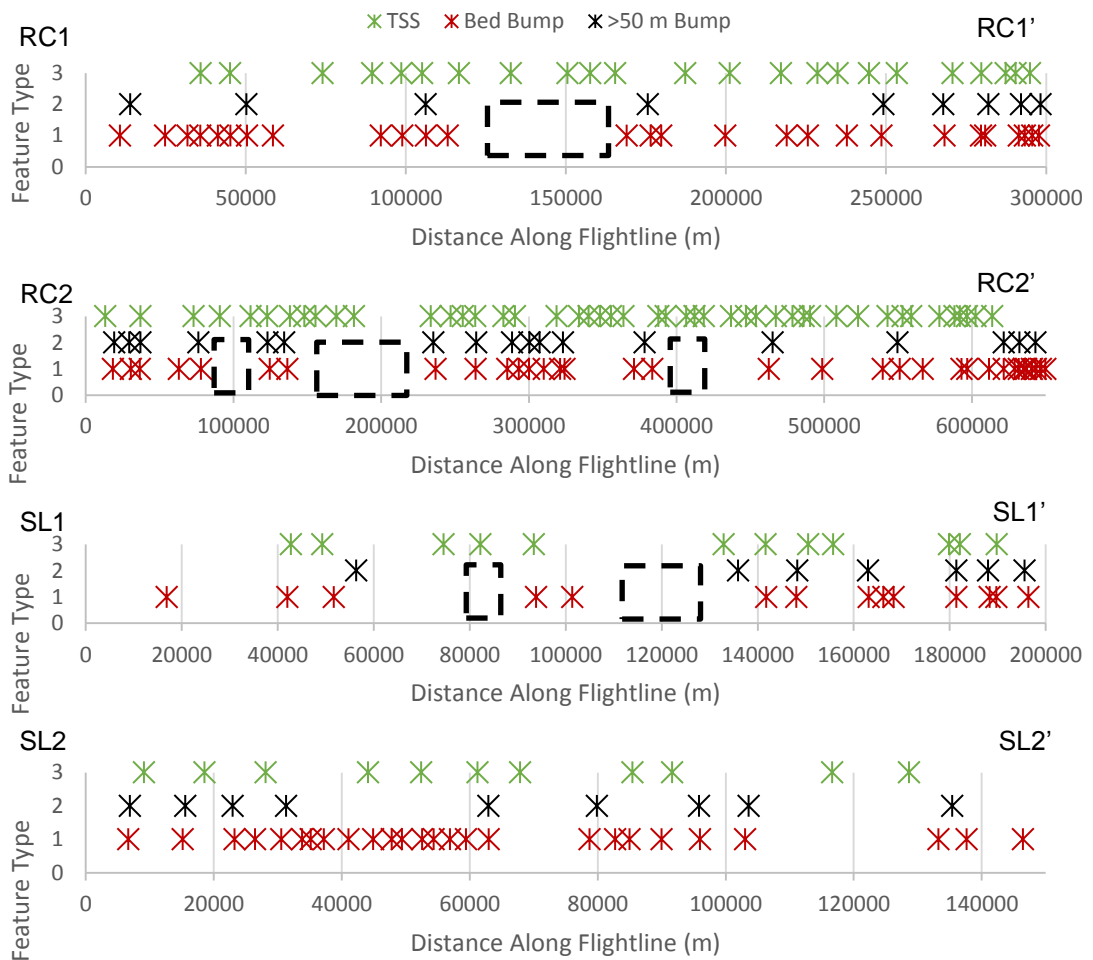


Figure 6.27. Location of TSSs and bed bumps across flightlines over Recovery and Slessor glaciers (see Figure 6.21 for locations). Black boxes indicate no bed data regions. Note again how only some TSSs correspond to bedrock bumps.

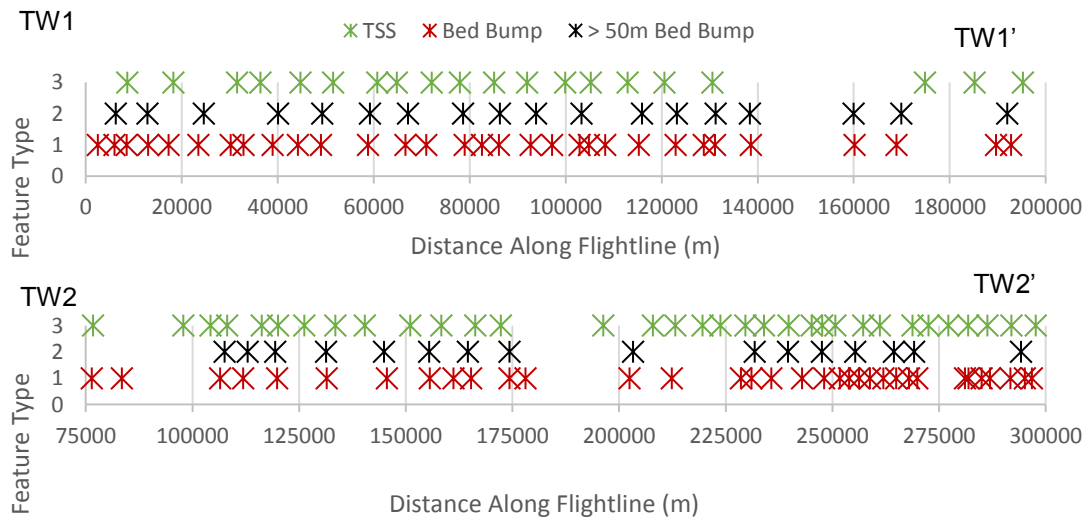


Figure 6.28. Location of TSSs and bed bumps across flightlines over Thwaites glacier (see Figure 6.21 for locations). TSSs show the highest, but still not perfect, correspondence to bed bumps on Thwaites glacier.

## 6.6 Modelling of the Flow of Ice Over Subglacial Bedforms

Thus far, I have undertaken an observational approach to the study of ice flow over subglacial bedforms. This has numerous limitations; comparisons between the flow signatures of palaeo and contemporary ice sheets have limited utility (Section 6.3), there is a lack of coincidental high resolution data of both the bed and the surface of contemporary ice sheets (Section 6.4) and radargrams only provide a two dimensional view of the bed (Section 6.5). However, the biggest drawback is that observational comparisons cannot isolate the effect of subglacial flow signatures on ice flow alone, due to the occurrence of larger bed undulations that also exist. Therefore, modelling provides us with an opportunity to run a controlled experiment of the flow of ice over subglacial bedforms alone, and further examine whether they have any relationship to surface flow signatures. Here I examine previous attempts at modelling ice flow over subglacial bedforms, and then show preliminary results of full-stokes modelling of ice flow over bedforms.

Schoof (2002) considered the flow of ice over a single drumlin (Figure 6.1). Although this predicted that bedforms should limit the sliding velocity of an ice stream and have corresponding surface expression, Schoof (2002) notes that longer wavelength bed undulations will be more readily transmitted to the surface and therefore dominate the surface signal. The drumlin incorporated into Schoofs' (2002) model has a asymmetric longitudinal profile and is 40 m in amplitude, a geometry which subsequent morphometric studies have shown to possible, but uncommonly large (Spagnolo et al.,

2011; 2012). Although studying flow over much larger features (20 km in diameter, 100s of meters in height), Sergienko (2012) showed that 2-D models overestimate the amplitude of a surface perturbation as ice cannot flow around a bump, only up and over. Thus, it is likely that if Schoofs' (2002) model was extended to 3-D, the amplitude of the surface bump produced would be reduced further. Therefore, 3-D modelling is required to more accurately simulate the flow of ice over subglacial bedforms.

A version of the instability hypothesis for subglacial bedform formation incorporated a finite-depth solution (Fowler, 2010a), thus enabling computation of the surface response to subglacial bedforms. Chapwanya et al. (2010) solved for this surface evolution in their model of subglacial rib formation. Figure 6.29 shows time-steps from an output of this model. This output is from a model run which enabled the produced subglacial ribs to migrate. The surface perturbations produced also migrated at a similar velocity. Model runs where migration of ribs does not occur also produced similar surface perturbations which remained stationary. The variation in ice surface topography was deemed largely inconsequential by Chapwanya et al. (2010) due to their minimal amplitude (approximately 5 cm). It is worth noting that the model produced comparatively small (maximum of 1 m) subglacial ribs (Figure 6.29). Intuitively, if the model produced greater amplitude subglacial ribs, corresponding greater amplitude of surface topography would be expected. The surface perturbations created by this model (Figure 6.29) are qualitatively similar in appearance to TSSs. They have a similar size shape and appearance. This is apparent when comparing Figure 6.29 to the real TSSs on Figure 5.1C. This model therefore demonstrates how flow over modelled subglacial ribs can produce variations in surface topography at a much larger scale. This suggests that 'mega-scale' subglacial ribs are not required to produce a TSS (e.g. Sergienko and Hindmarsh, 2013), instead the cumulative effect of numerous subglacial ribs may produce a TSS.



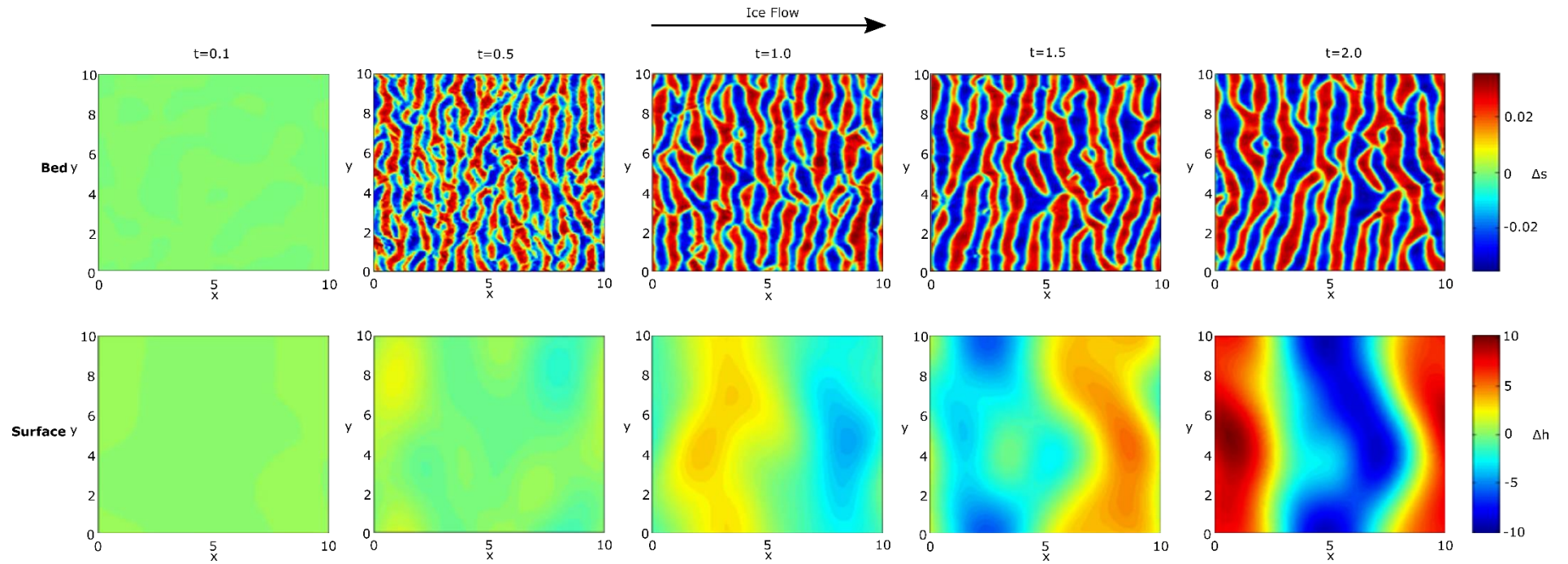


Figure 6.29. Bed and ice surface output from the model of Chapwanya et al. (2010) of a co-evolving field of subglacial ribs and ice surface TSSs. From an initially flat state, both subglacial ribs and surface expressions resembling TSSs are produced and migrate with ice flow. Time ( $t$ ) refers to arbitrary model units such that  $t = 2$  is approximately 60 years. Length ( $x$ ) and width ( $y$ ) units are also arbitrary, such that 1 unit on here is approximately 280 m. The model domain is therefore approximately 2.8 km by 2.8 km. The change in bed elevation ( $\Delta s$ ) corresponds to a maximum of approximately 1 m. The surface elevation change ( $\Delta h$ ) is in the order of a maximum of 5 cm.

In order to evaluate the effect of appropriately proportioned subglacial bedforms upon ice flow, “real” subglacial bedforms from a digital elevation model (STRM) of Ireland were imported into an ice flow model (Figure 6.30A). Unlike the model of Chapwanya et al. (2010), this is not a model of subglacial bedform formation. Therefore, features are static and remain the same size. The digital elevation model was de-trended to remove any slope and long wavelength features ( $> 10$  km) were removed from the data (Figure 6.30B). The data was imported into Elmer-Ice, a 3-D full-Stokes ice flow model. Ice 1 km thick was then modelled to flow over the subglacial bedforms approximately in the direction of palaeo-ice flow at 1000 m/a (Martin, 2015, pers. comm.). The results of this can be seen in Figure 6.30. The model shows transverse undulations in surface topography which I interpret as TSSs. These are greater in amplitude ( $\sim 3$ m) than those modelled by Chapwanya et al. (2010); an expected outcome of larger bed undulations. This model therefore further highlights how numerous small bumps are filtered out into longer wavelength topography on the surface of the ice. Near the base of the ice, subglacial bedforms induce variations in vertical ice velocity  $\sim 4.5$  m/a. These preliminary results prompt the need for further modelling experiments to be conducted. For example, would the ice surface be flat if the bed was flat? What happens if a field of MSGL or drumlins is input into the model?



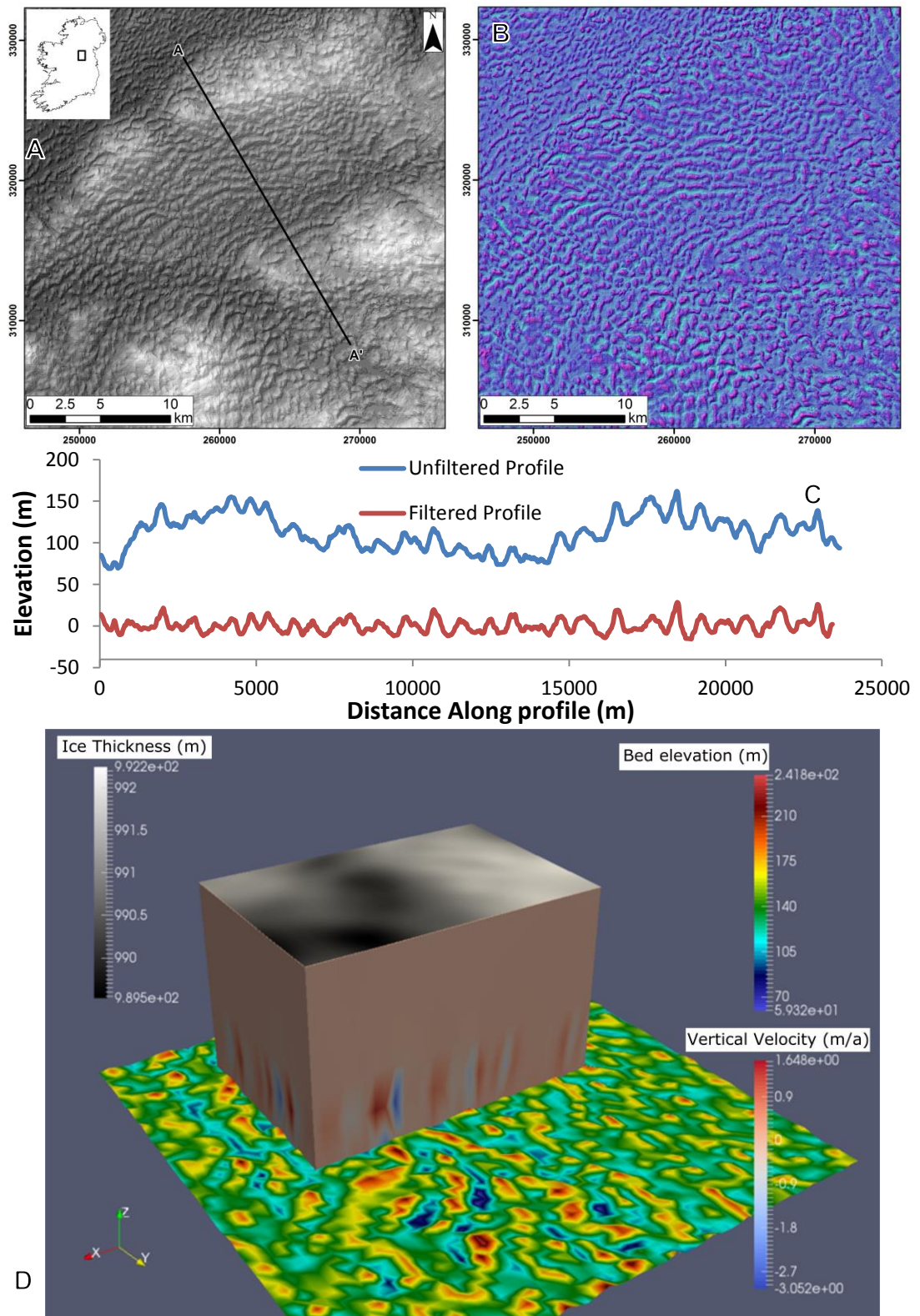


Figure 6.30. Initial results of full-stokes modelling of ice flow over subglacial bedforms. A) Hill-shaded SRTM digital elevation model of subglacial bedforms in Meath County, Ireland. B) Hill-shaded detrended surface DEM. C) Transects across the DEMs in A) and B). This highlights how the long-wavelength topography has been removed in B), leaving only the bedforms. D) Modelling results. Ice flow is toward

the bottom left of the image. Subglacial bedforms cause fluctuations in vertical velocity which are filtered out toward the surface, leaving only larger topographic undulations on the surface.

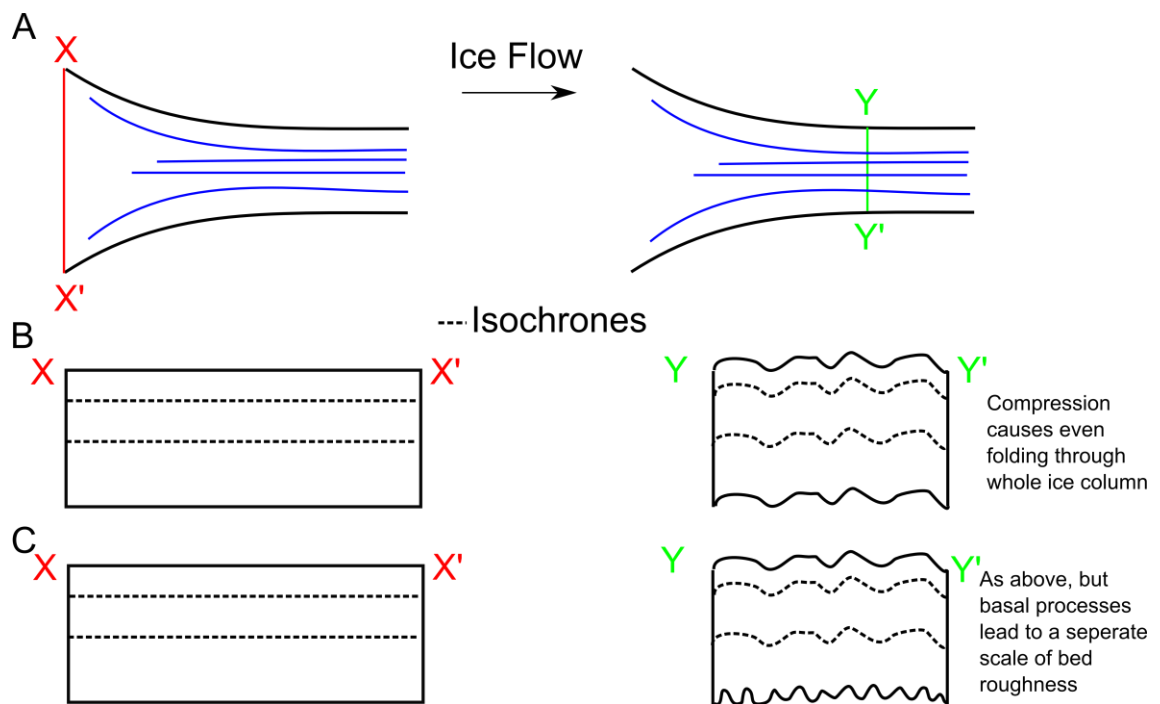
## 6.7 Discussion

There are several consistent findings that emerge from the multiple approaches, detailed above. Several lines of evidence show that subglacial lineations and LSSs are not linked. LSSs are generally much longer and spaced further apart than subglacial lineations (Figures 6.4 and 6.5). This difference in scale is highlighted in my analysis of the Rutford Ice Stream MSGL and LSSs (Figures 6.10 to 6.13). Also, features here do not co-evolve, suggesting a lack of communication between MSGL's and the surface (Figure 6.9). The disparity in scale between the bed and the surface is also apparent in my analysis of across-flow radar (Figures 6.15 to 6.20). Further modelling work is required to see if LSSs can be generated at all from flow-aligned bedforms.

Together, the above evidence suggests that subglacial lineations are not transmitted to the surface of an ice sheet, and that LSSs do not have an effect upon the formation of subglacial lineations (e.g. Figure 6.3). The apparent lack of transfer of subglacial lineations to the surface is perhaps expected given their small amplitude (7 m and 3 m average for drumlins and MSGL respectively (Spagnolo et al., 2011; 2014)). Thus, subglacial lineations are not a viable source for LSSs (e.g. Schoof, 2002). This supports my hybrid model of LSS formation (Figure 4.30), whereby the majority of LSSs are created by convergent flow and longitudinal extension of the ice (e.g. Hambrey and Dowdeswell, 1994), with only rare LSSs created by flow over basal perturbations (e.g. Gudmundsson et al., 1998). These exceptional, basally induced, LSSs are more likely a consequence of flow over a much larger amplitude bed bump than provided by subglacial lineations. If LSSs are formed by lateral compression and longitudinal extension (e.g. Hambrey and Lawson, 2000, p.70), then one might expect the base of the ice to also fold in a similar manner to the surface, creating 3-D foliation-like features (e.g. Figure 6.31A). If such folding does occur throughout the entirety of a glacier or ice sheet, basal processes must alter their wavelength at the bed (e.g. Figure 6.31B; Knight, 1997), potentially by enhanced melting and basal friction eroding some fold structures.

The lack of correspondence between subglacial lineations and LSSs also provides further evidence against the groove ploughing hypothesis of MSGL formation (Clark et

al., 2003; See Section 6.2), which requires LSSs to be the same wavelength as MSGL in order to preserve basal keels (Figure 6.2).



6.31. Hypothetical arrangement of the bed and internal isochrones under lateral compression and longitudinal extension. For more details see text. A) Plan view geometry. X-X' occurs before lateral compression. Y-Y' occurs after lateral compression. B) If the entire ice mass reacted to compression in the same way, one would expect undulations of the basal ice to be the same wavelength as LSS. Clearly this is not the case (see text). C) The majority of the ice mass may have similar undulations throughout, indicated by isochrones. Yet basal processes and friction may remove their influence and the bed.

Transverse undulations in a bed profile seem to be more readily transmitted to the ice surface creating corresponding TSSs (Figures 6.22 to 6.28). Morphometrically, TSSs are reasonably similar in terms of scale and spacing to subglacial mega-ribs (Figures 6.6 and 6.7). This makes them a potential candidate as a source for TSSs, as suggested by Sergienko and Hindmarsh (2013) and Sergienko et al. (2014). However, modelling shows that the cumulative effect of multiple smaller subglacial ribs can also result in TSSs (Figures 6.29 and 6.30). This highlights how much of the information transferred from the bed of an ice sheet to the surface can be lost, especially at smaller scales such as that of subglacial bedforms (Gudmundsson and Raymond, 2008). Therefore, attempts to resolve subglacial bedform scale features from surface data may be flawed (e.g. Sergienko and Hindmarsh, 2013 and Sergienko et al., 2014). Subglacial ribs, of multiple scales, are therefore a likely source for TSSs (Figure 6.32A and B).

However, TSSs may also form from flow over a bedrock bump (Gudmundsson, 2003; Figure 6.32C), as is observed at the Rutford Ice Stream (Figure 6.10 and 6.11), or by flow over a sticky spot (Ashmore et al., 2014; Whillans and Johnsen 1983; Figure 6.32D), as possibly occurs across my radar profiles where the bed appears near flat (e.g. Figures 6.22 and 6.24). Therefore, a hybrid model of TSS formation is required, as is conceptualised in Figure 6.32E.

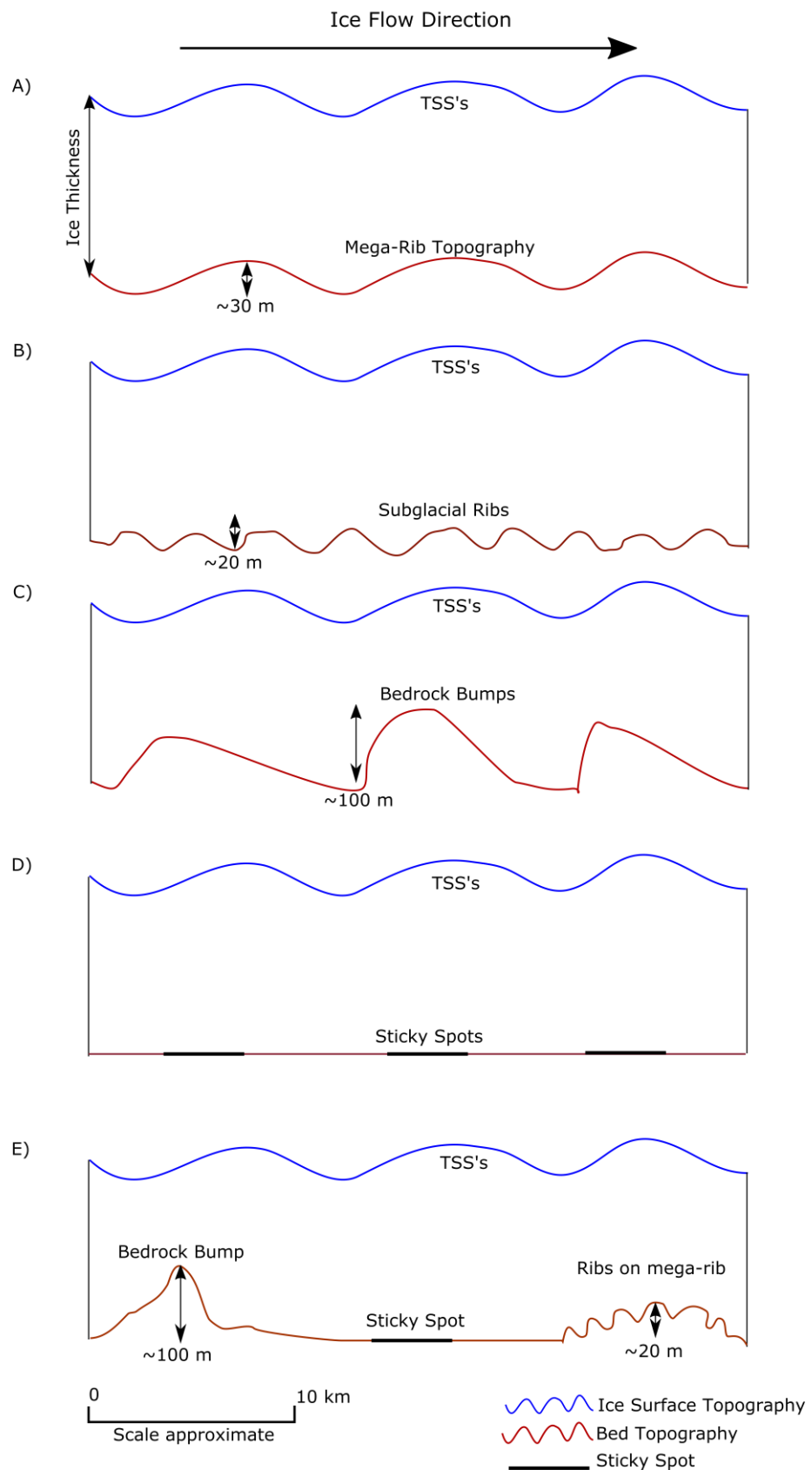


Figure 6.32. Proposed hybrid model of TSS formation. Note scales are approximate, especially in the vertical dimension. TSSs are formed by ice flow over A) mega-ribs, B) lots of smaller subglacial ribs, C) bedrock bumps, D) sticky spots and E) a combination of the above.

## 6.8 Summary and Conclusions

The flow of ice produces patterns in both the surface and the bed of the ice. Previous work has suggested that these two sets of flow signatures may be linked. Through multiple methods, here I examined whether basal and surficial flow signatures of the same alignment were linked. For features aligned with flow direction, I found that LSSs are typically much longer and spaced further apart than subglacial lineations. This was observed in the general morphometrics of the two features (Figures 6.4 and 6.5), and also when the bed and the surface of the Rutford Ice Stream were compared (Figure 6.10). LSSs often bare little observable correspondence to undulations of the bed, especially those at the scale of subglacial bedforms (Figure 6.15 to 6.20). I therefore find that LSSs and subglacial lineations are not linked. This supports my previously proposed hybrid model of LSS formation (Figure 4.30), and provides evidence against the groove-ploughing hypothesis as a universal explanation for MSGL formation (Clark et al., 2003).

TSSs also have a different morphology to their flow transverse basal counterparts, subglacial ribs. TSSs generally have a longer crestline length and are spaced further apart than subglacial bedforms (Figures 6.6 and 6.7). Limited spatial coverage of geophysical data means that only a single TSS could be studied at the Rutford Ice Stream. This corresponds to a bedrock undulation (Figure 6.10). However, analysis of airborne radar data suggests that TSSs are not always located over a bed undulation (Figures 6.22-6.27). Whilst the morphometry of subglacial mega-ribs is closer to that of TSSs, making them a more likely candidate for linking to TSSs, modelling shows that the flow of ice over multiple “normal-scale” subglacial bedforms results in TSSs (Figures 6.29 and 6.30). This loss of information from the bed to the surface means that caution is required when interpreting inversions for basal conditions at the scale of subglacial mega-ribs (e.g. Sergienko and Hindmarsh, 2013; Sergienko et al., 2014). I propose a hybrid model for TSS formation, whereby flow over bedrock bumps, sticky spots and subglacial bedforms of all scales can cause TSSs to form (Figure 6.32).

Based upon my analysis of flow signature morphometrics compiled from previous chapters (Section 6.3), my case study of the Rutford Ice Stream (Section 6.4), analysis of airborne radar (Section 6.5) and modelling of the flow of ice over subglacial bedforms (Section 6.6), it is apparent that:

- Surficial flow signatures are generally larger and spaced further apart than subglacial flow signatures;

- LSSs are often unrelated to bed undulations;
- Transverse bed undulations are more likely to be transmitted to the surface, but are not a prerequisite for TSS formation.

Therefore, I conclude that, despite previous suggestions in the literature (Section 6.2) there are few connections between surficial and basal flow signatures.

# Chapter 7 Summary and Conclusions

## 7.1 Aims and Objectives

As ice flows it produces sets of morphological features, both at the ice-bed interface and on the ice surface. At the bed, ice flow produces a suite of landforms referred to as subglacial bedforms. On the surface, longitudinal and transverse surface structures (LSSs and TSSs respectively) are observed. These ‘flow signatures’ were the focus of this thesis. The overall aim of this thesis was to further our understanding of ice flow by elucidating the characteristics of, and possible links between, ice sheet flow signatures. To achieve this aim, three objectives were set. These are listed below, with a statement of how they were addressed.

*Objective 1: Examine the morphological and spatial properties of subglacial bedforms, in order to shed light onto their genesis.*

Two pertinent questions regarding the formation of subglacial bedforms were identified and addressed. Firstly, Chapter 2 asked ‘do subglacial bedforms display characteristics of patterning?’ Analysis was limited to drumlins, as these are the most common variant of subglacial bedforms and the variety for which the question of patterning seemed most relevant. Although subglacial bedforms occur in fields, the principles of patterning that have developed through observing other natural patterns have rarely been applied to them. Drawing on examples from other natural systems, two characteristics of patterns were identified: i) regularity in the spatial positioning of constituent components, and ii) interaction between these components.

Frequency histograms of the spacing of ribbed moraine, drumlins and MSGs display prominent peaks, suggesting a preferred spacing. However, previous literature and statistical testing has painted a mixed picture, disagreeing on whether drumlins are placed in the landscape regularly, randomly or within clusters (Table 2). This is partially due to the application of immature or inappropriate methods. After using a range of approaches, the inhomogeneous pair-correlation function was found to be the most appropriate for drumlin fields. For the first time, drumlins were considered to be part of a spatially inhomogeneous pattern. That is, the inherent ‘patchiness’ found in drumlin fields was accounted for in my statistical analysis, so that clustering introduced by factors such as post-formational erosion and sediment availability did not bias the result.



The results show that the vast majority of drumlins are regularly placed. Therefore, drumlins conform to my first characteristic of patterned phenomena.

Chapter 2 went on to analyse whether the patterning interactions which occur for other patterned phenomena can be detected in drumlin fields. Specifically, these are drumlin growth (or lack of), stabilisation of the drumlin pattern, drumlin migration and drumlin-pattern coarsening. In order to tackle this, the size, shape and spacing metrics of drumlins were analysed. Spacing metrics suggested that drumlins initiate a specific distance apart. After initialisation, probability functions of drumlin size indicate that they grow (but may also shrink) over time. Whether drumlins migrate and collide as they grow is unresolved. Therefore drumlins, and by extension other subglacial bedforms, are likely formed by a patterning process, and future work should consider them within a patterning framework.

The second question regarding subglacial bedform morphological and spatial properties was addressed in Chapter 3: ‘Do subglacial bedforms form a size and shape continuum?’ The hypothesis that all subglacial bedforms conform to a size and shape continuum is longstanding within the literature. To address this question, a dataset of  $\approx$  100,000 measurements of subglacial bedform size and shape was collated. Refuting or confirming the continuum hypothesis relied upon whether clusters existed within the dataset. In order to overcome the difficulties of nomenclature-biasing (i.e., ‘I call this a drumlin you call it an MSGL’), several approaches to cluster detection were adopted; a visual assessment, a clustering algorithm (DBSCAN) ignoring nomenclature, and an assessment of the overlap of specifically-named populations.

Analysis and interpretation of the variation in the size and shape of subglacial bedforms, searching for the presence or absence of clusters, revealed several continua. Flutes formed a statistically distinct population of narrow bedforms. Drumlins and MSGL merged to form a continuum of subglacial lineations. Similarly, there were no natural breaks in the data to suggest separate populations of subglacial ribs. Between ribs and lineations, quasi-circular forms were noted. These mostly occur in spatial transitions between ribs and lineations, and potentially merge these two continua to form a larger continuum of ribs-circles to lineations.

Drawing on previous observations, it was argued that the main control upon subglacial bedform size and shape is ice velocity, with subglacial ribs progressively elongating through circular to lineated bedforms as ice velocity increases. Furthermore,

it was argued that flutes require a separate set of boundary conditions for their formation. Using the morphology of subglacial bedforms to derive unequivocal statements about subglacial processes is of course challenging. However, in Chapter 3 I argue that the specific scale of flutes means that a process different to that which forms the other bedforms is responsible for flute formation. Furthermore, it is argued that the continuity of form displayed by all other subglacial bedforms is difficult to reconcile with equifinite hypotheses for their formation. Instead, ‘unifying’ formation hypotheses that aim to explain the formation of either the separate continua of lineations and ribs, or the much larger continuum of ribs-circles-lineations may be more promising. The major caveat of this approach is that all subglacial bedform hypotheses should also be able to explain the composition of bedforms, as well as their morphology.

*Objective 2: Examine the morphological, spatial and glaciological properties of ice sheet surface flow signatures.*

Surface flow signatures were divided into two classes, longitudinal (LSSs) and transverse (TSSs), based upon their orientation to flow. The morphological, spatial and glaciological properties of LSSs were examined in Chapter 4. These metrics were studied in order to test the competing hypotheses of LSS formation suggested in previous work. Mapping was conducted upon satellite imagery of the Antarctic Ice Sheet, to produce an Antarctic-wide map of LSSs comprising over 42,000 lines. LSSs spacing was generally between 850 m and 1250 m, and spacing had a strong positive correlation with the width of the flow unit (e.g. ice stream). LSSs were found to form in both thick (3949 m) and thin (51 m) ice. Surprisingly, they also occurred in regions of the ice sheet flowing at less than 10 m/a, demonstrating that rapid basal sliding is not a prerequisite for their formation and preservation. Instead, LSSs often start forming upstream of ice streams. LSSs also form as ice flows over a basal bump or ice rumple and between flow unit boundaries.

The data collected, and observations made in Chapter 4 did not support a single hypothesis of LSS formation. Instead, a hybrid model of LSS formation was proposed. Here, the vast majority of LSSs are thought to form by lateral compression and longitudinal extension. These are added to by LSSs formed at other situations of high shear strain; at the onset of fast ice flow, where two or more flow units meet, and as ice flows over a sticky spot.

TSSs were studied in Chapter 5. These features make up the surface texture of an ice stream, but are less frequently studied than their longitudinal counterparts. Three hypotheses had previously been put forward to explain their formation, viewing them as either i) variations in bed topography transmitted to the surface; ii) variations in basal slipperiness transmitted to the surface; or iii) variations in ice strength. Furthermore, it was unclear whether TSSs migrate or remain stationary on the ice surface. 4,234 TSSs were mapped across West Antarctica, and their morphological, spatial and glaciological properties were defined. Furthermore, multi-temporal maps of three case studies of TSSs were created in order to ascertain whether or not they migrate.

In contrast to longitudinal forms, TSSs were found to be limited to the grounded portion of the ice sheet, and only occurred on ice streams, outlet glaciers and their tributaries. The multi-temporal mapping showed that on the Evans, Slessor and MacAyeal Ice streams, TSSs were static for approximately 50 years. Morphologically, TSSs are typically 12 km long and spaced 9 km apart, metrics that vary little between ice streams. The majority occur where ice is flowing above 27.5 m/a. Across the wavelength of 1 TSS, velocity fluctuates by 7 m/a on average. TSSs showed little correspondence toward a certain ice thickness, occurring in ice between 500 and 3500 m thick, but had a preference for an ice thickness to spacing ratio of 4.5. Based upon this, Chapter 5 concluded by suggesting that the ice strength hypothesis is incompatible with the vast majority of TSSs. TSSs are interpreted as the consequence of flow over varying basal topography and resistance, and exist as ‘standing waves’ rather than migratory features

***Objective 3:** Compare and contrast the properties of basal and surficial ice sheet flow signatures, in order to determine the extent to which they are linked.*

Multiple approaches were conducted in Chapter 6 in order to compare and contrast basal and surficial flow signatures. Morphologically, LSSs were compared to subglacial lineations and TSSs were compared to subglacial ribs. To compliment this, a study of flow signatures of the Rutford Ice Stream, and analysis of ice penetrating radar were conducted. Furthermore, modelling of ice flow was examined, and supplemented by preliminary modelling, to see if surficial flow signatures could be created in controlled numerical experiments.

LSSs are typically spaced further apart and are much longer than subglacial lineations. At the Rutford Ice Stream, LSSs had little to no correspondence with the

imaged subglacial bedforms. Furthermore, radar data of structures in the ice column showed there to be little correspondence between basal bumps and LSSs, especially basal bumps the scale of subglacial bedforms. Chapter 6 therefore concluded that LSSs and subglacial lineations are unlikely to be linked phenomena.

TSSs are also spaced further apart and have a larger crestline length than their basal counterparts, subglacial ribs. Only one TSS is apparent for the region of the Rutford Ice Stream where there is sufficient geophysical data to reveal subglacial bedforms. This corresponds to a bedrock undulation. Airborne radar data of the beds of Support Force, Academy, Slessor and Thwaites glaciers revealed that this situation is not always the case, with some TSSs occurring where there is no undulation apparent in the bed topography. In the comparison between subglacial and surficial transverse features, subglacial mega-ribs have the closest match in scale with TSSs (Figure 6.6). However, modelling of the flow of ice over ‘normal-scale’ subglacial bedforms also results in TSSs. Therefore, despite limited empirical support for connections between subglacial ribs and TSSs, modelling shows that the flow of ice over smaller scales of subglacial ribs produces TSSs. This confirms that information is lost from the bed before it reaches the ice surface. This, and Chapter 5, led to a hybrid model of TSS formation, whereby flow over bedrock bumps, sticky spots and subglacial bedforms leads to the formation TSSs. Given the lack of correspondence between basal topography and LSSs, the latter explanation for TSSs is the only link found in this thesis between subglacial and ice sheet surface flow signatures, suggesting that the majority are separate entities.

## **7.2 Future Work**

The work conducted in this thesis prompts several further questions and lines of further enquiry. The investigation on patterning interactions (Chapter 2) is necessarily inferential because I used relict forms, but draws from understanding of other natural systems, such as sand dunes, where the patterned system can be observed to evolve. Repeat surveys of contemporary ice sheet beds may reveal whether bedforms grow or shrink in time, migrate, or even collide. More observations of subglacial bedforms under contemporary ice masses may also help solve questions raised by the continuum hypothesis. Although some evidence exists from previous surveys that MSGL are associated with fast ice flow (King et al., 2009), and ribbed moraine with slower ice flow (King et al., 2007), further contemporary evidence is required to support the

hypothesis that ice flow velocity controls bedform size and shape. Furthermore, geophysical surveys may help elucidate how other factors such as ice thickness affect subglacial bedform morphology. An ideal situation for studying subglacial bedforms (in terms of both patterning interactions and a continuum) would be to observe the evolution of a flat surface into one of undulating subglacial bedforms, whilst also measuring the physical properties of the bed and ice flow. Such a circumstance is likely to be difficult to achieve for some time, and nor would it be easy to replicate this in a laboratory experiment for reasons of scale. In the meantime, progress is likely to be achieved by observations of relict bedforms and by modelling.

The work presented in this thesis provides observations and findings that might inspire modelling approaches of subglacial bedform creation, or be used as tests of existing or new models. Can process-models explain the full continuum of subglacial bedform sizes and shapes? If so, can these models simulate any patterning interactions that may occur in subglacial bedform fields? Can they make subglacial bedforms grow and evolve, perhaps in response to changes in subglacial ice velocity? Tantalisingly, if models of subglacial bedform production ever reach a maturity that can be considered to sufficiently explain the phenomenon, then perhaps models could then be inverted to predict some ice sheet properties (effective pressure, ice velocity, thickness, etc.) from subglacial bedform morphology. Such an approach would revolutionise the field of palaeoglaciology.

As highlighted in Chapter 3, further work is required on quasi-circular bedforms and bedform transition zones. Do these bedforms require two phases of ice flow, two separate processes, or are they the result of a transitory state of a single overlying process? Sedimentological studies, of numerous bedforms in transition zones may be able to help solve this. Indeed, there is a growing need for sedimentological studies which represent entire bedform fields, instead of individual sections. Geophysical techniques, such as ground penetrating radar, have proved promising in this respect for some cases (Spagnolo et al., 2014b; Spagnolo et al., 2016).

Future work on LSSs is also required. Can different ‘types’ of LSS be distinguished (i.e. those from basal bumps or those from lateral compression)? Radar surveys over sticky spots where LSSs emerge may reveal any large basal topographic controls upon LSS genesis. Furthermore, high resolution DEMs, which were unavailable for this project, could reveal whether such different types have different

amplitudes, explaining why some may be more prominent on satellite imagery than others. Studies of LSSs on the Greenland ice sheet are also lacking, and may provide further insight into their formation.

Extensive radar surveying of the ice column may also be useful for furthering our understanding of TSSs. The prevalence of TSSs that are a consequence of basal topography, compared to TSSs caused by variation in basal resistance is unknown, and may vary between ice streams. Topographic TSSs are likely more permanent than those corresponding to changes in basal resistance, which may alter with subglacial hydrological or thermal changes. As these two types of sticky spot reduce the rate of ice flow toward the ocean, knowing which is predominate on different ice streams may help us understand under which ice streams the basal force budget is susceptible to change.

Modelling studies, of which only preliminary attempts were made in this thesis, would also be useful for studying the formation of TSSs and potentially LSSs, as well as the links they may have to subglacial bedforms. The following questions should be addressed. Do TSSs emerge if the bed is flat? Do TSSs form over a drumlin field, or do linear bedforms produce LSS? Can bedforms create both TSSs and LSSs?

### **7.3 Concluding remark**

This thesis started with the following quote: “Nature uses only the longest threads to weave her patterns, so that each small piece of her fabric reveals the organisation of the entire tapestry” (Feynman et al., 1965). Here, Feynman was referring to the patterns in the orbit of planets which originate from the law of gravity, and how these can be scaled to smaller objects due to the gravitational constant. When viewed from above, the flow signatures studied in this thesis have an apparent order, appearing to be patterns weaved onto the beds and the surfaces of ice sheets. Multiple variables changing over space and time have influenced the formation of these patterns. Therefore, rather than study a small piece of the fabric, it has been necessary to study a large portion of these tapestries in order to quantify these patterns and shed light on their genesis.

## Bibliography

- Aario, R. (1977). Classification and terminology of morainic landforms in Finland. *Boreas*, 6(2), 87-100.
- Aario, R. (1987). Drumlins of Kuusmo and Rogen ridges of Ranua, northeast Finland. In Menzies, J. and Rose, J. (eds.) *Drumlin Symposium*, Balkema, Rotterdam, 87-101.
- Aario, R. and Peuraniemi, V. (1992). Glacial dispersal of till constituents in morainic landforms of different types. *Geomorphology*, 6(1), 9-25.
- Allen, C. R., Kamb, W. B., Meier, M. F. and Sharp, R. P. (1960) Structure of the lower Blue Glacier, Washington, *Journal of Glaciology*, 68, 601-625.
- Allen, J. R. L. (1968). The nature and origin of bed-form hierarchies. *Sedimentology*, 10(3), 161-182.
- Alley, R. B. (1989). Water-pressure coupling of sliding and bed deformation: I. Water system. *Journal of Glaciology*, 35(119), 108-118.
- Alley, R.B. (1993). In search of ice stream sticky spots. *Journal of Glaciology*, 19, 447-454.
- Alley, R. B., Blankenship, D. D., Bentley, C. R., and Rooney, S. (1986). Deformation of till beneath ice stream B, West Antarctica. *Nature*, 322, 57-59.
- Alley, R. B., Blankenship, D. D., Rooney, S. T., and Bentley, C. R. (1989). Sedimentation beneath ice shelves—the view from ice stream B. *Marine Geology*, 85(2), 101-120.
- Alley, R. B., Clark, P. U., Huybrechts, P., and Joughin, I. (2005). Ice-sheet and sea-level changes. *Science*, 310(5747), 456-460
- Åmark, M. (1980). Glacial flutes at Isfallsglaciären, Tarfala, Swedish Lapland. *GFF*, 102(3), 251-259.
- Amos, C. L. and King, E. L. (1984). Bedforms of the Canadian eastern seaboard: a comparison with global occurrences. *Marine Geology*, 57(1), 167-208.
- Anandakrishnan, S., Alley, R. B., Jacobel, R. W. and Conway, H. (2001). The flow regime of Ice Stream C and hypotheses concerning its recent stagnation. *The West Antarctic Ice Sheet: Behavior and Environment, AGU Antarctic Research Series*, 77, 283-296.
- Andreassen, K., Laberg, J. S. and Vorren, T. O. (2008). Seafloor geomorphology of the SW Barents Sea and its glaci-dynamic implications. *Geomorphology*, 97(1), 157-177.

- Appleby, J. R., Brook, M. S., Vale, S. S., and Macdonald-Creevy, A. M. (2010). Structural glaciology of a temperate maritime glacier: Lower Fox Glacier, New Zealand. *Geografiska Annaler: Series A, Physical Geography*, 92(4), 451-467.
- Ashley, G. M. (1990). Classification of large-scale subaqueous bedforms: a new look at an old problem-SEPM bedforms and bedding structures. *Journal of Sedimentary Research*, 60(1), 160-172.
- Ashmore, D. W., Bingham, R. G., Hindmarsh, R. C., Corr, H. F. and Joughin, I. R. (2014). The relationship between sticky spots and radar reflectivity beneath an active West Antarctic ice stream. *Annals of Glaciology*, 55(67), 29-38.
- Aylesworth, J. M. and Shilts, W. W. (1989). Bedforms of the Keewatin Ice Sheet, Canada. *Sedimentary Geology*, 62, 407-428.
- Baas, A. C. (2007). Complex systems in aeolian geomorphology. *Geomorphology*, 91(3), 311-331.
- Baddeley, A. and Turner, R. (2000). Practical maximum pseudolikelihood for spatial point patterns. *Australian and New Zealand Journal of Statistics*, 42(3), 283-322.
- Ball, P. and Borley, N. R. (1999). *The self-made tapestry: pattern formation in nature* (Vol. 198). Oxford: Oxford University Press.
- Baranowski, S. (1969). Some remarks on the origin of drumlins. In: *Geographia Polonica*, 17, 197-208.
- Baranowski, S. (1970). The origin of fluted moraine at the fronts of contemporary glaciers. *Geografiska Annaler. Series A. Physical Geography*, 68-75.
- Baranowski, S. (1977). Regularity of drumlin distribution and the origin of their formation. *Studia Geologica Polonica* 52, 53-68.
- Bartholdy, J., Bartholomae, A., and Flemming, B. W. (2002). Grain-size control of large compound flow-transverse bedforms in a tidal inlet of the Danish Wadden Sea. *Marine Geology*, 188(3), 391-413.
- Benn, D. and Evans, D. J. (2014). *Glaciers and glaciation*. Routledge.
- Bennett, M. R. (2003). Ice streams as the arteries of an ice sheet: their mechanics, stability and significance. *Earth-Science Reviews*, 61(3), 309-339.
- Bindschadler, R. and Scambos, T.A. (1991). Satellite-Image-Derived Velocity Field of an Antarctic Ice Stream, *Science*, 252, 242--246.
- Bindschadler, R., Vornberger, P., Blankenship, D., Scambos, T., and Jacobel, R. (1996). Surface velocity and mass balance of Ice Streams D and E, West Antarctica. *Journal of Glaciology*, 42(142), 461-475.



- Bingham, R. G. and Siegert, M. J. (2007). Radar-derived bed roughness characterization of Institute and Möller ice streams, West Antarctica, and comparison with Siple Coast ice streams. *Geophysical Research Letters*, 34(21).
- Bingham, R. G. and Siegert, M. J. (2009). Quantifying subglacial bed roughness in Antarctica: implications for ice-sheet dynamics and history. *Quaternary Science Reviews*, 28(3), 223-236.
- Boots, B. N. and Burns, R. K. (1984). Analyzing the spatial distribution of drumlins: a two-phase mosaic approach. *Journal of Glaciology*, 30, 302-307.
- Bouchard, M. A. (1989). Subglacial landforms and deposits in central and northern Quebec, Canada, with emphasis on Rogen moraines. *Sedimentary Geology*, 62(2), 293-308.
- Boulton, G. S. (1976). The origin of glacially fluted surfaces--observations and theory. *Journal of Glaciology*, 17, 287-309.
- Boulton, G.S. (1987). A theory of drumlin formation by subglacial sediment deformation. In Menzies, J. and Rose, J. (eds.) *Drumlin Symposium*, Balkema, Rotterdam, 25-80.
- Boulton, G. S. and Jones, A. S. (1979). Stability of temperate ice caps and ice sheets resting on beds of deformable sediment. *Journal of Glaciology*, 24, 29-43.
- Boulton, G. S. and Hindmarsh, R. C. A. (1987). Sediment deformation beneath glaciers: rheology and geological consequences. *Journal of Geophysical Research: Solid Earth (1978–2012)*, 92(B9), 9059-9082.
- Boulton, G. S. and Clark, C. D. (1990a). A highly mobile Laurentide ice sheet revealed by satellite images of glacial lineations. *Nature*, 346(6287), 813-817.
- Boulton, G. S. and Clark, C. D. (1990b). The Laurentide ice sheet through the last glacial cycle: the topology of drift lineations as a key to the dynamic behaviour of former ice sheets. *Transactions of the Royal Society of Edinburgh: Earth Sciences*, 81(04), 327-347.
- Boyce, J. I. and Eyles, N. (1991). Drumlins carved by deforming till streams below the Laurentide ice sheet. *Geology*, 19(8), 787-790.
- Briner, J. P. (2007). Supporting evidence from the New York drumlin field that elongate subglacial bedforms indicate fast ice flow. *Boreas*, 36(2), 143-147.
- Brown, V. H., Stokes, C. R. and O'Cofaigh, C. (2011). The glacial geomorphology of the north-west sector of the Laurentide Ice Sheet. *Journal of Maps*, 7(1), 409-428.
- Budd, W. F. (1970), Ice flow over bedrock perturbations, *Journal of Glaciology*, 9(55), 29-48.

- Callens, D., Matsuoka, K., Steinhage, D., Smith, B., Witrant, E. and Pattyn, F. (2014). Transition of flow regime along a marine-terminating outlet glacier in East Antarctica. *The Cryosphere*, 8(3), 867-875.
- Campbell, I., Jacobel, R., Welch, B., and Pettersson, R. (2008). The evolution of surface flow stripes and stratigraphic folds within Kamb Ice Stream: why don't they match?. *Journal of Glaciology*, 54(186), 421-427.
- Canals, M., Urgeles, R. and Calafat, A. M. (2000). Deep sea-floor evidence of past ice streams off the Antarctic Peninsula. *Geology*, 28(1), 31-34.
- Carl, J. D. (1978). Ribbed moraine–drumlin transition belt, St. Lawrence Valley, New York. *Geology*, 6(9), 562-566.
- Carling, P. A. (1999). Subaqueous gravel dunes. *Journal of Sedimentary Research*, 69(3).
- Casassa, G., Jezek, K. C., Turner, J. and Whillans, I. M. (1991). Relict flow stripes on the Ross Ice Shelf. *Annals of Glaciology*, 15, 132-138.
- Casassa, G. and Brecher, H. H. (1993). Relief and decay of flow stripes on Byrd Glacier, Antarctica. *Annals of Glaciology*, 17, 255-255.
- Casassa, G. and Whillans, I. M. (1994). Decay of surface topography on the Ross Ice Shelf, Antarctica. *Annals of Glaciology*, 20(1), 249-253.
- Catania, G., Hulbe, C., Conway, H., Scambos, T. A. and Raymond, C. F. (2012). Variability in the mass flux of the Ross ice streams, West Antarctica, over the last millennium. *Journal of Glaciology*, 58(210), 741-752.
- Chamberlin, T.C. (1883). Terminal moraines of the second glacial epoch, *United States Geological Survey, 3<sup>rd</sup> Annual Report*, 291-402.
- Chapwanya, M., Clark, C. D. and Fowler, A. C. (2011). Numerical computations of a theoretical model of ribbed moraine formation. *Earth Surface Processes and Landforms*, 36(8), 1105-1112.
- Church, J. A., Gregory, J. M., Huybrechts, P., Kuhn, M., Lambeck, K., Nhuan, M. T., Qin, D. and Woodworth, P. L. (2001). Changes in sea level. , in: *JT Houghton, Y. Ding, DJ Griggs, M. Noguer, PJ Van der Linden, X. Dai, K. Maskell, and CA Johnson (eds.): Climate Change 2001: The Scientific Basis: Contribution of Working Group I to the Third Assessment Report of the Intergovernmental Panel*, 639-694.
- Clark, C. D. (1993). Mega-scale glacial lineations and cross-cutting ice-flow landforms. *Earth Surface Processes and Landforms*, 18(1), 1-29.
- Clark, C. D. (1994). Large-scale ice-moulding: a discussion of genesis and glaciological significance. *Sedimentary Geology*, 91(1), 253-268.

- Clark, C. D. (1997). Reconstructing the evolutionary dynamics of former ice sheets using multi-temporal evidence, remote sensing and GIS. *Quaternary Science Reviews*, 16(9), 1067-1092.
- Clark, C. D. (2010). Emergent drumlins and their clones: from till dilatancy to flow instabilities. *Journal of Glaciology*, 56(200), 1011-1025.
- Clark, C. D. and Meehan, R. T. (2001). Subglacial bedform geomorphology of the Irish Ice Sheet reveals major configuration changes during growth and decay. *Journal of Quaternary Science*, 16(5), 483-496.
- Clark, C. D., Tulaczyk, S. M., Stokes, C. R. and Canals, M. (2003). A groove-ploughing theory for the production of mega-scale glacial lineations, and implications for ice-stream mechanics. *Journal of Glaciology*, 49(165), 240-256.
- Clark, C. D., Hughes, A. L., Greenwood, S. L., Spagnolo, M. and Ng, F. S. (2009). Size and shape characteristics of drumlins, derived from a large sample, and associated scaling laws. *Quaternary Science Reviews*, 28(7), 677-692.
- Clark, P. J. and Evans, F. C. (1954). Distance to nearest neighbor as a measure of spatial relationships in populations. *Ecology*, 445-453.
- Clarke, G. K., Leverington, D. W., Teller, J. T., Dyke, A. S. and Marshall, S. J. (2005). Fresh arguments against the Shaw megaflood hypothesis. A reply to comments by David Sharpe on "Paleohydraulics of the last outburst flood from glacial Lake Agassiz and the 8200 BP cold event". *Quaternary Science Reviews*, 24(12), 1533-1541.
- Colgan, P. M. and Mickelson, D. M. (1997). Genesis of streamlined landforms and flow history of the Green Bay Lobe, Wisconsin, USA. *Sedimentary Geology*, 111(1), 7-25.
- Concise Oxford English Dictionary: Luxury Edition* (2011), 12<sup>th</sup> Edition, Stevenson, A. and Waite, M. Eds., Oxford University Press, 309.
- Condit, R., Ashton, P. S., Baker, P., Bunyavejchewin, S., Gunatilleke, S., Gunatilleke, N., Hubbell, S. P., Foster, R. B., Itoh, A., LaFrankie, J.V., Lee, H.S., Losos, E., Manokaran, N., Sukumar, R. and Yamakura, T. (2000). Spatial patterns in the distribution of tropical tree species. *Science*, 288(5470), 1414-1418.
- Conway, H., Catania, G., Raymond, C. F., Gades, A. M., Scambos, T. A. and Engelhardt, H. (2002). Switch of flow direction in an Antarctic ice stream. *Nature*, 419(6906), 465-467.
- Costello, W. R. and Southard, J. B. (1981). Flume experiments on lower-flow-regime bed forms in coarse sand. *Journal of Sedimentary Research*, 51(3).

- Couteron, P., Seghier, J. and Chadœuf, J. (2003). A test for spatial relationships between neighbouring plants in plots of heterogeneous plant density. *Journal of vegetation science*, 14(2), 163-172.
- Crabtree, R. D. and Doake, C. S. M. (1980). Flow lines on Antarctic ice shelves. *Polar Rec*, 20(124), 31-37.
- Creys, T. T. and Schoof, C. G. (2009). Drainage through subglacial water sheets. *Journal of Geophysical Research: Earth Surface (2003–2012)*, 114(F4).
- Cross, M. C. and Hohenberg, P. C. (1993). Pattern formation outside of equilibrium. *Reviews of modern physics*, 65(3), 851.
- Cutts, J. A. and Smith, R. S. U. (1973). Eolian deposits and dunes on Mars. *Journal of Geophysical Research*, 78(20), 4139-4154.
- Dardis, G. F., McCabe, A. M. and Mitchell, W. I. (1984). Characteristics and origins of lee-side stratification sequences in late pleistocene drumlins, northern Ireland. *Earth Surface Processes and Landforms*, 9(5), 409-424.
- Davis, W. M. (1884). The distribution and origin of drumlins. *American Journal of Science*, (168), 407-416.
- De Rydt, J., Gudmundsson, G. H., Corr, H. F. J. and Christoffersen, P. (2013). Surface undulations of Antarctic ice streams tightly controlled by bedrock topography. *The Cryosphere*, 7(2), 407-417.
- Diggle P (2003). *Statistical Analysis of Spatial Point Patterns*. Arnold, second edition, Arnold.
- Dixon, P. M. (2006). Nearest neighbor methods. *Encyclopedia of environmetrics*.
- Dixon, P. M. (2012). Ripley's K function. *Encyclopedia of environmetrics*.
- Dowdeswell, J. A. and McIntyre, N. F. (1987). The surface topography of large ice masses from Landsat imagery. *Journal of Glaciology*, 33(113), 16-23.
- Dowling, T. P., Spagnolo, M. and Möller, P. (2015). Morphometry and core type of streamlined bedforms in southern Sweden from high resolution LiDAR. *Geomorphology*, 236, 54-63.
- Dunlop, P. and Clark, C. D. (2006a). Distribution of ribbed moraine in the Lac Naococane region, central Québec, Canada. *Journal of Maps*, 2(1), 59-70.
- Dunlop, P. and Clark, C. D. (2006b). The morphological characteristics of ribbed moraine. *Quaternary Science Reviews*, 25(13), 1668-1691.
- Dunlop, P., Clark, C. D. and Hindmarsh, R. C. (2008). Bed ribbing instability explanation: testing a numerical model of ribbed moraine formation arising from

- coupled flow of ice and subglacial sediment. *Journal of Geophysical Research: Earth Surface* (2003–2012), 113(F3).
- Dyke, A.S., Morris, T. F., Green, D. E. and England, J. (1992). Quaternary geology of Prince of Wales island, arctic Canada. *Geological survey of Canada Memoir 433*, 108 pages.
- Eastwood, E., Nield, J., Baas, A. and Kocurek, G. (2011). Modelling controls on aeolian dune-field pattern evolution. *Sedimentology*, 58(6), 1391-1406.
- Ehlers, J. and Gibbard, P. L. (2004). *Quaternary Glaciations-Extent and Chronology: Part I: Europe* (Vol. 2). Elsevier.
- Eklund, A. and Hart, J. K. (1996). Glaciotectonic deformation within a flute from the Isfallsglaciären, Sweden. *Journal of Quaternary Science*, 11(4), 299-310.
- Ellwood, J. M., Evans, P. D. and Wilson, I. G. (1975). Small scale aeolian bedforms. *Journal of Sedimentary Research*, 45(2).
- Ely, J.C. and Clark, C.D., 2016. Flow-stripes and foliations of the Antarctic ice sheet. *Journal of Maps*, 12(2) pp.249-259.
- Ely, J.C., Clark, C.D., Spagnolo, M., Stokes, C.R., Greenwood, S.L., Hughes, A.L., Dunlop, P. and Hess, D., 2016. Do subglacial bedforms comprise a size and shape continuum?. *Geomorphology*, 257, pp.108-119.
- Engelhardt, H. and Kamb, B. (1998). Basal sliding of ice stream B, West Antarctica. *Journal of Glaciology*, 44(147), 223-230.
- Ester, M., Kriegel, H. P., Sander, J. and Xu, X. (1996, August). A density-based algorithm for discovering clusters in large spatial databases with noise. *Kdd*, 96(34), 226-231.
- Evans, D. J. (2000). Quaternary geology and geomorphology of the Dinosaur Provincial Park area and surrounding plains, Alberta, Canada: the identification of former glacial lobes, drainage diversions and meltwater flood tracks. *Quaternary Science Reviews*, 19(10), 931-958.
- Evans, D. J. and Twigg, D. R. (2002). The active temperate glacial landsystem: a model based on Breiðamerkurjökull and Fjallsjökull, Iceland. *Quaternary Science Reviews*, 21(20), 2143-2177.
- Evans, D. J., Clark, C. D. and Mitchell, W. A. (2005). The last British Ice Sheet: A review of the evidence utilised in the compilation of the Glacial Map of Britain. *Earth-Science Reviews*, 70(3), 253-312.
- Evans, D. J., Rea, B. R., Hiemstra, J. F. and Cofaigh, C. Ó. (2006). A critical assessment of subglacial mega-floods: a case study of glacial sediments and

- landforms in south-central Alberta, Canada. *Quaternary Science Reviews*, 25(13), 1638-1667.
- Evans, I. S. (2003). Scale-specific landforms and aspects of the land surface. *Concepts and Modelling in Geomorphology: International Perspectives*. Terrapub, Tokyo, 61-84.
- Ewing, R. C., Kocurek, G. and Lake, L. W. (2006). Pattern analysis of dune-field parameters. *Earth Surface Processes and Landforms*, 31(9), 1176-1191.
- Ewing, R. C. and Kocurek, G. (2010). Aeolian dune-field pattern boundary conditions. *Geomorphology*, 114(3), 175-187.
- Fahnestock, M. A., Scambos, T. A., Bindschadler, R. A. and Kvaran, G. (2000). A millennium of variable ice flow recorded by the Ross Ice Shelf, Antarctica. *Journal of Glaciology*, 46(155), 652-664.
- Favier, L., Gagliardini, O., Durand, G. and Zwinger, T. (2012). A three-dimensional full Stokes model of the grounding line dynamics: effect of a pinning point beneath the ice shelf. *The Cryosphere*, 6(1), 101-112.
- Ferrigno, J. G., Mullins, J. L., Stapleton, J. A., Bindschadler, R. A., Scambos, T. A., Bellisime, L. B., Powell, J.A. and Acosta, A. V. (1994). Landsat TM image maps of the Shirase and Siple Coast ice streams, West Antarctica. *Annals of Glaciology*, 20(1), 407-412.
- Feynman, R. P., Leighton, R. B., Sands, M. and Hafner, E. M. (1965). The feynman lectures on physics; vol. i. *American Journal of Physics*, 33(9), 750-752.
- Finlayson, A. (2013). Digital surface models are not always representative of former glacier beds: palaeoglaciological and geomorphological implications. *Geomorphology*, 194, 25-33.
- Fisher, T. G. and Taylor, L. D. (2002). Sedimentary and stratigraphic evidence for subglacial flooding, south-central Michigan, USA. *Quaternary International*, 90(1), 87-115.
- Fourriere, A., Claudin, P. and Andreotti, B. (2010). Bedforms in a turbulent stream: formation of ripples by primary linear instability and of dunes by nonlinear pattern coarsening. *Journal of Fluid Mechanics*, 649, 287-328.
- Fowler, A. C. (2000). An instability mechanism for drumlin formation. *Geological Society, London, Special Publications*, 176(1), 307-319.
- Fowler, A. C. (2009). Instability modelling of drumlin formation incorporating lee-side cavity growth. In *Proceedings of the Royal Society of London A: Mathematical, Physical and Engineering Sciences*, 465, 2109, 2681-2702.



- Fowler, A. C. (2010). The instability theory of drumlin formation applied to Newtonian viscous ice of finite depth. In *Proceedings of the Royal Society of London A: Mathematical, Physical and Engineering Sciences*, 466, 2121, 2673-2694.
- Fowler, A. C. (2010). The formation of subglacial streams and mega-scale glacial lineations. In *Proceedings of the Royal Society of London A: Mathematical, Physical and Engineering Sciences*, 466, 2123, 3181-3201
- Fowler, A. C., Spagnolo, M., Clark, C. D., Stokes, C. R., Hughes, A. L. C., and Dunlop, P. (2013). On the size and shape of drumlins. *GEM-International Journal on Geomathematics*, 4(2), 155-165.
- Fowler, A. C. and Chapwanya, M. (2014). An instability theory for the formation of ribbed moraine, drumlins and mega-scale glacial lineations. In *Proceedings of the Royal Society of London A: Mathematical, Physical and Engineering Sciences*, 470, No. 2171, 20140185.
- Fretwell, P., Pritchard, H. D., Vaughan, D. G., Bamber, J. L., Barrand, N. E., Bell, R., Bianchi, C., Bingham, R.G., Blankenship, D. D., Casassa, G., Catania, G., Callens, D., Conway, H., Cook, A. J., Corr, H. F. J., Damaske, D., Damm, V., Ferraccioli, F., Forsberg, R., Fujita, S., Gim, Y., Gogineni, P., Griggs, J. A., Hindmarsh, R. C. A., Holmlund, P., Holt, J. W., Jacobel, R. W., Jenkins, A., Jokat, W., Jordan, T., King, E. C., Kohler, J., Krabill, W., Riger-Kusk, M., Langley, K. A., Leitchenkov, G., Leuschen, C., Luyendyk, B. P., Matsuoka, K., Mouginot, J., Nitsche, F. O., Nogi, Y., Nost, O.A., Popov, S. V., Rignot, E., Rippin, D. M., Rivera, A., Roberts, J., Ross, N., Siegert, M. J., Smith, A. M., Steinhage, D., Studinger, M., Sun, B., Tinto, B. K., Welch, B. C., Wilson, D., Young, D. A., Xiangbin, C. and Zirizzotti, A. (2013). Bedmap2: improved ice bed, surface and thickness datasets for Antarctica. *The Cryosphere*, 7(1).
- Fricker, H. A., Hyland, G., Coleman, R. and Young, N. W. (2000). Digital elevation models for the Lambert Glacier–Amery Ice Shelf system, East Antarctica, from ERS-1 satellite radar altimetry. *Journal of Glaciology*, 46(155), 553-560.
- Fuller, S. and Murray, T. (2000). Evidence against pervasive bed deformation during the surge of an Icelandic glacier. *Geological Society, London, Special Publications*, 176(1), 203-216.
- Glasser, N. F. and Gudmundsson, G. H. (2012). Longitudinal surface structures (flowstrips) on Antarctic glaciers. *The Cryosphere*, 6(2), 383-391.
- Glasser, N. F. and Scambos, T. A. (2008). A structural glaciological analysis of the 2002 Larsen B ice-shelf collapse. *Journal of Glaciology*, 54(184), 3-16.
- Glasser, N. F., Jennings, S. J. A., Hambrey, M. J. and Hubbard, B. (2015). Origin and dynamic significance of longitudinal structures (“flow stripes”) in the Antarctic Ice Sheet. *Earth Surface Dynamics*, 3, 239-249.

- Gordon, J. E., Whalley, W. B., Gellatly, A. F. and Vere, D. M. (1992). The formation of glacial flutes: assessment of models with evidence from Lyngsdalen, North Norway. *Quaternary Science Reviews*, 11(7), 709-731.
- Graham, A. G., Larter, R. D., Gohl, K., Hillenbrand, C. D., Smith, J. A. and Kuhn, G. (2009). Bedform signature of a West Antarctic palaeo-ice stream reveals a multi-temporal record of flow and substrate control. *Quaternary Science Reviews*, 28(25), 2774-2793.
- Greenwood, S. L. and Clark, C. D. (2008). Subglacial bedforms of the Irish ice sheet. *Journal of Maps*, 4(1), 332-357.
- Greenwood, S. L. and Clark, C. D. (2009). Reconstructing the last Irish Ice Sheet 1: changing flow geometries and ice flow dynamics deciphered from the glacial landform record. *Quaternary Science Reviews*, 28(27), 3085-3100.
- Greenwood, S. L. and Clark, C. D. (2010). The sensitivity of subglacial bedform size and distribution to substrate lithological control. *Sedimentary Geology*, 232(3), 130-144.
- Greenwood, S. L. and Kleman, J. (2010). Glacial landforms of extreme size in the Keewatin sector of the Laurentide Ice Sheet. *Quaternary Science Reviews*, 29(15), 1894-1910.
- Gray, L., Conway, H., King, E. C. and Smith, B. (2008). Flow stripes, GPR stratigraphy and RADARSAT imagery. *Journal of Glaciology*, 54(188), 936-938.
- Gudmundsson, G. H., Raymond, C. F. and Bindschadler, R. (1998). The origin and longevity of flow-stripes on Antarctic ice streams. *Annals of Glaciology*, 27, 145-152.
- Gudmundsson, G. H. (2003). Transmission of basal variability to a glacier surface. *Journal of Geophysical Research: Solid Earth (1978–2012)*, 108(B5).
- Gudmundsson, G. H. and Raymond, M. (2008). On the limit to resolution and information on basal properties obtainable from surface data on ice streams. *The Cryosphere Discussions*, 2(3), 413-445.
- Hallet, B. (1990). Spatial self-organization in geomorphology: from periodic bedforms and patterned ground to scale-invariant topography. *Earth-Science Reviews*, 29(1), 57-75.
- Hambrey, M. J. (1975). The origin of foliation in glaciers: evidence from some Norwegian examples. *Journal of Glaciology*, 14, 181-185.
- Hambrey, M. J. (1977). Foliation, minor folds and strain in glacier ice. *Tectonophysics*, 39(1), 397-416.



- Hambrey, M. J. and Milnes, A. G. (1977). Structural geology of an Alpine glacier (Griesgletscher, Valais, Switzerland). *Eclogae Geologicae Helvetiae*, 70(3), 667-684.
- Hambrey, M. J. and Müller, F. (1978). Structures and ice deformation in the white glacier, Axel Heiberg Island, Northwest Territories, Canada. *Journal of glaciology*, 20, 41-66.
- Hambrey, M. J. and Dowdeswell, J. A. (1994). Flow regime of the Lambert Glacier-Amery Ice Shelf system, Antarctica: structural evidence from Landsat imagery. *Annals of Glaciology*, 20(1), 401-406.
- Hambrey, M. J. and Lawson, W. (2000). Structural styles and deformation fields in glaciers: a review. *Geological Society, London, Special Publications*, 176(1), 59-83.
- Hambrey, M. J. and Glasser, N. F. (2003). The role of folding and foliation development in the genesis of medial moraines: examples from Svalbard glaciers. *The Journal of geology*, 111(4), 471-485.
- Hambrey, M. J., Murray, T., Glasser, N. F., Hubbard, A., Hubbard, B., Stuart, G., Hansen, S. and Kohler, J. (2005). Structure and changing dynamics of a polythermal valley glacier on a centennial timescale: Midre Lovénbreen, Svalbard. *Journal of Geophysical Research: Earth Surface* (2003–2012), 110(F1).
- Hansen, J. L., van Hecke, M., Haaning, A., Ellegaard, C., Andersen, K. H., Bohr, T. and Sams, T. (2001). Pattern formation: Instabilities in sand ripples. *Nature*, 410(6826), 324-324.
- Hart, J. K. (1995). Drumlin formation in southern Anglesey and Arvon, northwest Wales. *Journal of Quaternary Science*, 10(1), 3-14.
- Hart, J. K. (1997). The relationship between drumlins and other forms of subglacial glaciotectionic deformation. *Quaternary Science Reviews*, 16(1), 93-107.
- Hart, J. K. (1999). Identifying fast ice flow from landform assemblages in the geological record: a discussion. *Annals of Glaciology*, 28(1), 59-66.
- Hättestrand, C. and Kleman, J. (1999). Ribbed moraine formation. *Quaternary Science Reviews*, 18(1), 43-61.
- Hättestrand, C., Goodwillie, D. and Kleman, J. (1999). Size distribution of two cross-cutting drumlin systems in northern Sweden: a measure of selective erosion and formation time length. *Annals of Glaciology*, 28(1), 146-152.
- Hättestrand, C., Götz, S., Näslund, J. O., Fabel, D. and Stroeven, A. P. (2004). Drumlin formation time: evidence from northern and central Sweden. *Geografiska Annaler: Series A, Physical Geography*, 86(2), 155-167.

- Heroy, D. C. and Anderson, J. B. (2005). Ice-sheet extent of the Antarctic Peninsula region during the Last Glacial Maximum (LGM)—Insights from glacial geomorphology. *Geological Society of America Bulletin*, 117(11-12), 1497-1512.
- Hess, D. P. and Briner, J. P. (2009). Geospatial analysis of controls on subglacial bedform morphometry in the New York Drumlin Field—implications for Laurentide Ice Sheet dynamics. *Earth Surface Processes and Landforms*, 34(8), 1126-1135.
- Hill, A. R. (1973). The distribution of drumlins in County Down, Ireland. *Annals of the Association of American Geographers*, 63(2), 226-240.
- Hillier, J. K., Smith, M. J., Clark, C. D., Stokes, C. R. and Spagnolo, M. (2013). Subglacial bedforms reveal an exponential size–frequency distribution. *Geomorphology*, 190, 82-91.
- Hindmarsh, R. C. A. (1996). Sliding of till over bedrock: scratching, polishing, comminution and kinematic-wave theory. *Annals of Glaciology*, 22, 41-47.
- Hindmarsh, R. C. (1998a). The stability of a viscous till sheet coupled with ice flow, considered at wavelengths less than the ice thickness. *Journal of Glaciology*, 44(147), 285-292.
- Hindmarsh, R. C. (1998b). Drumlinization and drumlin-forming instabilities: viscous till mechanisms. *Journal of Glaciology*, 44(147), 293-314.
- Hindmarsh, R. C. (1998c). The stability of a viscous till sheet coupled with ice flow, considered at wavelengths less than the ice thickness. *Journal of Glaciology*, 44(147), 285-292.
- Holt, T., Glasser, N. and Quincey, D. (2013a). The structural glaciology of southwest Antarctic Peninsula Ice Shelves (ca. 2010). *Journal of Maps*, 9(4), 523-531.
- Holt, T. O., Glasser, N. F., Quincey, D. J. and Siegfried, M. R. (2013b). Speedup and fracturing of George VI Ice Shelf, Antarctic Peninsula. *The Cryosphere*, 7(3), 797-816.
- Hooke, R. L. and Hudleston, P. J. (1978). Origin of foliation in glaciers. *Journal of Glaciology*, 20, 285-299.
- Hooke, R. L. and Medford, A. (2013). Are drumlins a product of a thermo-mechanical instability? *Quaternary Research*, 79(3), 458-464.
- Hoppe, G. and Schytt, V. (1953). Some observations on fluted moraine surfaces. *Geografiska Annaler*, 105-115.
- Hudleston, P. J. and Hooke, R. L. (1980). Cumulative deformation in the Barnes Ice Cap and implications for the development of foliation. *Tectonophysics*, 66(1), 127-146.

- Hughes, A. L., Clark, C. D. and Jordan, C. J. (2010). Subglacial bedforms of the last British Ice Sheet. *Journal of Maps*, 6(1), 543-563.
- Hughes, A. L., Clark, C. D. and Jordan, C. J. (2014). Flow-pattern evolution of the last British Ice Sheet. *Quaternary Science Reviews*, 89, 148-168.
- Hulbe, C. L. and Whillans, I. M. (1994). Evaluation of strain rates on Ice Stream B, Antarctica, obtained using GPS phase measurements. *Annals of Glaciology*, 20(1), 254-262.
- Hulbe, C. L. and Whillans, I. M. (1997). Weak bands within Ice Stream B, West Antarctica. *Journal of Glaciology*, 43 (145), 377-386.
- Jacobel, R. W. and Gades, A. M. (1995). Radar observations of a relict ice-stream margin traversing Siple Dome, Antarctica. *Antarctic Journal of the United States*, 30(5), 89-90.
- Jacobel, R. W., Scambos, T. A., Nereson, N. A. and Raymond, C. F. (2000). Changes in the margin of Ice Stream C, Antarctica. *Journal of Glaciology*, 46(152), 102-110.
- Jackson, R. G. (1975). Hierarchical attributes and a unifying model of bed forms composed of cohesionless material and produced by shearing flow. *Geological Society of America Bulletin*, 86(11), 1523-1533.
- Jain, A. K. (2010). Data clustering: 50 years beyond K-means. *Pattern recognition letters*, 31(8), 651-666.
- Jansson, K. N. and Glasser, N. F. (2005). Using Landsat 7 ETM+ imagery and Digital Terrain Models for mapping glacial lineaments on former ice sheet beds. *International Journal of Remote Sensing*, 26(18), 3931-3941.
- Jauhianen, F. (1975). Morphometric analysis of drumlin fields in northern Central Europe. *Boreas*, 4(4), 219-230.
- Jennings, S. J., Hambrey, M. J. and Glasser, N. F. (2014). Ice flow-unit influence on glacier structure, debris entrainment and transport. *Earth Surface Processes and Landforms*, 39(10), 1279-1292.
- Johnson, M. D., Schomacker, A., Benediktsson, Í. Ö., Geiger, A. J., Ferguson, A. and Ingólfsson, Ó. (2010). Active drumlin field revealed at the margin of Múlajökull, Iceland: a surge-type glacier. *Geology*, 38(10), 943-946.
- Jørgensen, F. and Piotrowski, J. A. (2003). Signature of the Baltic ice stream on Funen Island, Denmark during the Weichselian glaciation. *Boreas*, 32(1), 242-255.
- Joughin, I., MacAyeal, D. R. and Tulaczyk, S. (2004). Basal shear stress of the Ross ice streams from control method inversions. *Journal of Geophysical Research: Solid Earth (1978–2012)*, 109(B9).

- Joughin, I., Bamber, J. L., Scambos, T., Tulaczyk, S., Fahnestock, M. and MacAyeal, D. R. (2006). Integrating satellite observations with modelling: basal shear stress of the Filcher-Ronne ice streams, Antarctica. *Philosophical Transactions of the Royal Society of London A: Mathematical, Physical and Engineering Sciences*, 364(1844), 1795-1814.
- Joughin, I., Tulaczyk, S., Bamber, J. L., Blankenship, D., Holt, J. W., Scambos, T. and Vaughan, D. G. (2009). Basal conditions for Pine Island and Thwaites Glaciers, West Antarctica, determined using satellite and airborne data. *Journal of Glaciology*, 55(190), 245-257.
- Kamb, B. (2001). Basal zone of the West Antarctic ice streams and its role in lubrication of their rapid motion. *The West Antarctic ice sheet: behavior and environment*, 157-199.
- Kargel, J. S. and Strom, R. G. (1992). Ancient glaciation on Mars. *Geology*, 20(1), 3-7.
- Kennedy, J. F. (1969). The formation of sediment ripples, dunes, and antidunes. *Annual Review of Fluid Mechanics*, 1(1), 147-168.
- Kessler, M. A. and Werner, B. T. (2003). Self-organization of sorted patterned ground. *Science*, 299(5605), 380-383.
- King, E. C. (2011). Ice stream or not? Radio-echo sounding of Carlson Inlet, West Antarctica. *The Cryosphere*, 5(4), 907-916.
- King, E. C., Woodward, J. and Smith, A. M. (2007). Seismic and radar observations of subglacial bed forms beneath the onset zone of Rutford Ice Stream, Antarctica. *Journal of Glaciology*, 53(183), 665-672.
- King, E. C., Hindmarsh, R. C. and Stokes, C. R. (2009). Formation of mega-scale glacial lineations observed beneath a West Antarctic ice stream. *Nature Geoscience*, 2(8), 585-588.
- Kjær, K. H., Larsen, E., van der Meer, J., Ingólfsson, Ó., Krüger, J., Benediktsson, Í. Ö., Knudsen, C.G. and Schomacker, A. (2006). Subglacial decoupling at the sediment/bedrock interface: a new mechanism for rapid flowing ice. *Quaternary Science Reviews*, 25(21), 2704-2712.
- Klages, J. P., Kuhn, G., Hillenbrand, C. D., Graham, A. G. C., Smith, J. A., Larter, R. D. and Gohl, K. (2013). First geomorphological record and glacial history of an inter-ice stream ridge on the West Antarctic continental shelf. *Quaternary Science Reviews*, 61, 47-61.
- Kleman, J. and Borgström, I. (1996). Reconstruction of palaeo-ice sheets: the use of geomorphological data. *Earth surface processes and landforms*, 21(10), 893-909.
- Kleman, J., Hättstrand, C., Stroeven, A. P., Jansson, K. N., De Angelis, H. and Borgström, I. (2006). Reconstruction of Palaeo-Ice Sheets-Inversion of their

- Glacial Geomorphological Record. *Glacier science and environmental change*, 192-198.
- Kleman, J. and Glasser, N. F. (2007). The subglacial thermal organisation (STO) of ice sheets. *Quaternary Science Reviews*, 26(5), 585-597.
- Knight, J., McCarron, S. G. and McCabe, A. M. (1999). Landform modification by palaeo-ice streams in east-central Ireland. *Annals of Glaciology*, 28(1), 161-167.
- Kocurek, G. and Ewing, R. C. (2005). Aeolian dune field self-organization—implications for the formation of simple versus complex dune-field patterns. *Geomorphology*, 72(1), 94-105.
- Kocurek, G., Ewing, R. C., and Mohrig, D. (2010). How do bedform patterns arise? New views on the role of bedform interactions within a set of boundary conditions. *Earth Surface Processes and Landforms*, 35(1), 51-63.
- Kurimo, H. (1980). Depositional deglaciation forms as indicators of different glacial and glaciomarginal environments. *Boreas*, 9(3), 179-192.
- Lancaster, N. (1988). Controls of eolian dune size and spacing. *Geology*, 16(11), 972-975.
- Lancaster, N. (2013). *Geomorphology of desert dunes*. Routledge. P.159.
- Lawson, W. J., Sharp, M. J. and Hambrey, M. J. (1994). The structural geology of a surge-type glacier. *Journal of Structural Geology*, 16(10), 1447-1462.
- Limpert, E., Stahel, W. A. and Abbt, M. (2001). Log-normal Distributions across the Sciences: Keys and Clues On the charms of statistics, and how mechanical models resembling gambling machines offer a link to a handy way to characterize log-normal distributions, which can provide deeper insight into variability and probability—normal or log-normal: That is the question. *BioScience*, 51(5), 341-352.
- Lindén, M., Möller, P. and Adrielsson, L. (2008). Ribbed moraine formed by subglacial folding, thrust stacking and lee-side cavity infill. *Boreas*, 37(1), 102-131.
- Livingstone, S. J., Clark, C. D. and Tarasov, L. (2013). Modelling North American palaeo-subglacial lakes and their meltwater drainage pathways. *Earth and Planetary Science Letters*, 375, 13-33.
- Lundqvist, J. (1969). Problems of the so-called Rogen moraine. *Sveriges Geologiske Undersogelse Series C*, 648, 32.
- Lundqvist, J. (1989). Rogen (ribbed) moraine—identification and possible origin. *Sedimentary Geology*, 62(2), 281-292.
- Lundqvist, J. (1997). Rogen moraine—an example of two-step formation of glacial landscapes. *Sedimentary Geology*, 111(1), 27-40.

- MacAyeal, D. (1992). The basal stress distribution of Ice Stream E, Antarctica, inferred by control methods. *Journal of Geophysical Research*, 97(B1), 595-603.
- MacAyeal D.R., Bindschadler, R.A. and Scambos, T.A. Basal friction of ice stream E, West Antarctica. *Journal of Glaciology*, 41, (138), 247-262.
- Maclachlan, J. C. and Eyles, C. H. (2013). Quantitative geomorphological analysis of drumlins in the Peterborough drumlin field, Ontario, Canada. *Geografiska Annaler: Series A, Physical Geography*, 95(2), 125-144.
- Margold, M., Stokes, C. R., and Clark, C. D. (2015). Ice streams in the Laurentide Ice Sheet: Identification, characteristics and comparison to modern ice sheets. *Earth-Science Reviews*, 143, 117-146.
- Markgren, M. and Lassila, M. (1980). Problems of moraine morphology: Rogén moraine and Blattnick moraine. *Boreas*, 9(4), 271-274.
- McCabe, A. M. and Dardis, G. F. (1989). A geological view of drumlins in Ireland. *Quaternary Science Reviews*, 8(2), 169-177.
- McCabe, A. M., Knight, J. and McCarron, S. G. (1999). Ice-flow stages and glacial bedforms in north central Ireland: a record of rapid environmental change during the last glacial termination. *Journal of the Geological Society*, 156(1), 63-72.
- McIntyre, N. F. (1986). The Antarctic ice sheet topography and surface bedrock relationship. *Annals of Glaciology*, 8, 124-128.
- Meier, M. F. (1958). Vertical profiles of velocity and the flow of glacier ice. In *Int. association of scientific hydrology publication 47, Symp. of Chamonix 1958—Physics of the Movement of the Ice* (pp. 169-170).
- Menzies, J. (1979). A review of the literature on the formation and location of drumlins. *Earth-Science Reviews*, 14(4), 315-359.
- Menzies, J., and Rose, J. (1987). Drumlin symposium. In *Drumlin Symposium (1985: Manchester, England)*. AA Balkema.
- Menzies, J. and Brand, U. (2007). The internal sediment architecture of a drumlin, Port Byron, New York State, USA. *Quaternary Science Reviews*, 26(3), 322-335.
- Merry, C. J. and Whillans, I. M. (1993). Ice-flow features on Ice Stream B, Antarctica, revealed by SPOT HRV imagery. *Journal of Glaciology*, 39, 515-527.
- Mitchell, W. A. (1994). Drumlins in ice sheet reconstructions, with reference to the western Pennines, northern England. *Sedimentary Geology*, 91(1), 313-331.
- Möller, P. (1987). Moraine morphology, till genesis, and deglaciation pattern in the Asnen area, south-central Smaland. *Sweden: Lundqua thesis, Lund University, Lund, Sweden*, 20.



- Möller, P. (2006). Rogen moraine: an example of glacial reshaping of pre-existing landforms. *Quaternary Science Reviews*, 25(3), 362-389.
- Möller, P. (2010). Melt-out till and ribbed moraine formation, a case study from south Sweden. *Sedimentary Geology*, 232(3), 161-180.
- Morris, E. M. and Morland, L. W. (1976). A theoretical analysis of the formation of glacial flutes. *Journal of Glaciology*, 17, 311-323.
- Munro-Stasiuk, M. J. and Shaw, J. (2002). The Blackspring Ridge Flute Field, south-central Alberta, Canada:: evidence for subglacial sheetflow erosion. *Quaternary International*, 90(1), 75-86.
- Murray, A. B., Goldstein, E. B. and Coco, G. (2014). The shape of patterns to come: from initial formation to long-term evolution. *Earth Surface Processes and Landforms*, 39(1), 62-70.
- Myllymäki, M., Mrkvicka, T., Seijo, H. and Grabarnik, P. (2013). Global envelope tests for spatial processes. *arXiv preprint arXiv:1307.0239*.
- Napieralski, J. and Nalepa, N. (2010). The application of control charts to determine the effect of grid cell size on landform morphometry. *Computers and geosciences*, 36(2), 222-230.
- Newman, W. A., Berg, R. C., Rosen, P. S. and Glass, H. D. (1990). Pleistocene stratigraphy of the Boston Harbor drumlins, Massachusetts. *Quaternary Research*, 34(2), 148-159.
- Newman, W.A. and Mickelson, D.M., 1994. Genesis of Boston Harbor drumlins, Massachusetts. *Sedimentary Geology*, 91(1), pp.333-343.
- Newton, I. (1730), *Opticks: Or a treatise of the reflections, refractions, inflections and colours of light*. Fourth Edition. Project Gutenberg EBook of Opticks. P. 293
- Ó Cofaigh, C., Pudsey, C. J., Dowdeswell, J. A. and Morris, P. (2002). Evolution of subglacial bedforms along a paleo-ice stream, Antarctic Peninsula continental shelf. *Geophysical Research Letters*, 29(8), 41-1.
- Ó Cofaigh, C., Dowdeswell, J. A., King, E. C., Anderson, J. B., Clark, C. D., Evans, D. J., Evans, J., Hindmarsh, R.C.A., Larter, R.D. and Stokes, C. R. (2009). Comment on Shaw J., Pugin, A. and Young, R.(2008):“A meltwater origin for Antarctic shelf bedforms with special attention to megalineations”, *Geomorphology* 102, 364–375. *Geomorphology*, 117(1), 195-198.
- Ó Cofaigh, C., Evans, D. J., and Smith, I. R. (2010). Large-scale reorganization and sedimentation of terrestrial ice streams during late Wisconsinan Laurentide Ice Sheet deglaciation. *Geological Society of America Bulletin*, 122(5-6), 743-756.

- Cofaigh, C.Ó., Stokes, C.R., Lian, O.B., Clark, C.D. and Tulaczyk, S., 2013. Formation of mega-scale glacial lineations on the Dubawnt Lake Ice Stream bed: 2. Sedimentology and stratigraphy. *Quaternary science reviews*, 77, pp.210-227.
- O'Sullivan, D. and Unwin, D. J. (2010). Geographic Information Analysis and Spatial Data. *Geographic Information Analysis, Second Edition, John Wiley and Sons, Inc., Hoboken, NJ, USA*.
- Ottesen, D., Dowdeswell, J. A. and Rise, L. (2005). Submarine landforms and the reconstruction of fast-flowing ice streams within a large Quaternary ice sheet: The 2500-km-long Norwegian-Svalbard margin (57–80 N). *Geological Society of America Bulletin*, 117(7-8), 1033-1050.
- Patterson, C. J. and Hooke, R. L. (1995). Physical environment of drumlin formation. *Journal of Glaciology*, 41(137), 30-38.
- Pattyn, F., Perichon, L., Durand, G., Favier, L., Gagliardini, O., Hindmarsh, R. C., Zwinger, T., Albrecht, T., Cornford, S., Docquier, D., Fürst, J. J., Goldberg, D., Gudmundsson, G. H., Humbert, A., Hütten, M., Huybrechts, P., Jouvét, G., Kleiner, T., Larour, E., Martin, D., Morlighem, M., Payne, A. J., Pollard, D., Rückamp, M., Rybck, O., Seroussi, H., Thoma, M. and Wilkens, N. (2013). Grounding-line migration in plan-view marine ice-sheet models: results of the ice2sea MISMIP3d intercomparison. *Journal of Glaciology*, 59(215), 410-422.
- Perry, G. L., Miller, B. P. and Enright, N. J. (2006). A comparison of methods for the statistical analysis of spatial point patterns in plant ecology. *Plant ecology*, 187(1), 59-82.
- Phillips, J. D. (2003). Sources of nonlinearity and complexity in geomorphic systems. *Progress in Physical Geography*, 27(1), 1-23.
- Piotrowski, J. A. and Tulaczyk, S. (1999). Subglacial conditions under the last ice sheet in northwest Germany: ice-bed separation and enhanced basal sliding?. *Quaternary Science Reviews*, 18(6), 737-751.
- Piotrowski, J. A., Larsen, N. K. and Junge, F. W. (2004). Reflections on soft subglacial beds as a mosaic of deforming and stable spots. *Quaternary Science Reviews*, 23(9), 993-1000.
- Pollard, D., and DeConto, R. M. (2009). Modelling West Antarctic ice sheet growth and collapse through the past five million years. *Nature*, 458(7236), 329-332.
- Pralong, A. and Funk, M. (2005). Dynamic damage model of crevasse opening and application to glacier calving. *Journal of Geophysical Research: Solid Earth (1978–2012)*, 110(B1).
- Price, S. F. and Whillans, I. M. (2001). Crevasse patterns at the onset to Ice Stream B, West Antarctica. *Journal of Glaciology*, 47(156), 29-36.



- Price, S. F., Bindschadler, R. A., Hulbe, C. L., and Joughin, I. R. (2001). Post-stagnation behavior in the upstream regions of Ice Stream C, West Antarctica. *Journal of Glaciology*, 47(157), 283-294.
- Punkari, M. (1984). The relations between glacial dynamics and tills in the eastern part of the Baltic Shield. *Striae*, 20, 49-54.
- Radebaugh, J., Lorenz, R. D., Lunine, J. I., Wall, S. D., Boubin, G., Reffet, E., Kirk, R.L., Lopes, R.M., Stofan, E.R., Soderblom, L., Allison, M., Janssen, M., Paillou, P., Callahan, P., Spencer, C. and the Cassini Radar Team (2008). Dunes on Titan observed by Cassini RADAR. *Icarus*, 194(2), 690-703.
- Rattas, M. and Piotrowski, J. A. (2003). Influence of bedrock permeability and till grain size on the formation of the Saadjärve drumlin field, Estonia, under an east-Baltic Weichselian ice stream. *Boreas*, 32(1), 167-177.
- Raukas, A. and Tavast, E. (1994). Drumlin location as a response to bedrock topography on the southeastern slope of the Fennoscandian Shield. *Sedimentary geology*, 91(1), 373-382.
- Raup, B. H., Scambos, T. and Haran, T. (2005). Topography of streaklines on an Antarctic ice shelf from photogrammetry applied to a single Advanced Land Imager (ALI) image. *Geoscience and Remote Sensing, IEEE Transactions on*, 43(4), 736-742.
- Raymond, C. (1996). Shear margins in glaciers and ice sheets. *Journal of Glaciology*, 42(140), 90-102.
- Reed, B., Galvin, C. J. and Miller, J. P. (1962). Some aspects of drumlin geometry. *American Journal of Science*, 260(3), 200-210.
- Reffet, E., du Pont, S. C., Hersen, P. and Douady, S. (2010). Formation and stability of transverse and longitudinal sand dunes. *Geology*, 38(6), 491-494.
- Reusch, D. and Hughes, T. (2003). Surface “waves” on Byrd Glacier, Antarctica. *Antarctic Science*, 15(04), 547-555.
- Reynolds, J. M. and Hambrey, M. J. (1988). The structural glaciology of George VI Ice Shelf, Antarctic Peninsula. *British Antarctic Survey Bulletin*, 79, 79-95.
- Rignot, E., Mouginot, J. and Scheuchl, B. (2011). Ice flow of the Antarctic ice sheet. *Science*, 333(6048), 1427-1430.
- Ripley, B. (1981) *Spatial statistics*. Wiley, New York.
- Ripley B (1988). *Statistical Inference for Spatial Processes*. Cambridge University Press.

- Rippin, D. M., Siegert, M. J., Bamber, J. L., Vaughan, D. G. and Corr, H. F. (2006). Switch-off of a major enhanced ice flow unit in East Antarctica. *Geophysical research letters*, 33(15).
- Rippin, D. M., Vaughan, D. G. and Corr, H. F. (2011). The basal roughness of Pine Island Glacier, West Antarctica. *Journal of Glaciology*, 57(201), 67-76.
- Rippin, D. M., Bingham, R. G., Jordan, T. A., Wright, A. P., Ross, N., Corr, H. F. J., Ferraccioli, F., Le Brocq, A. M., Rose, K. C. and Siegert, M. J. (2014). Basal roughness of the Institute and Möller Ice Streams, West Antarctica: Process determination and landscape interpretation. *Geomorphology*, 214, 139-147.
- Roberson, S., Hubbard, B., Coulson, H. R., and Boomer, I. (2011). Physical Properties and Formation of Flutes at a Polythermal Valley Glacier: Midre Lovénbreen, Svalbard. *Geografiska Annaler: Series A, Physical Geography*, 93(2), 71-88.
- Rose, J. (1987). Drumlins as part of glacier bedform continuum. In Menzies, J. and Rose, J. (eds.) *Drumlin Symposium*, Balkema, Rotterdam, 103-118.
- Rose, J. (1989). Glacier stress patterns and sediment transfer associated with the formation of superimposed flutes. *Sedimentary Geology*, 62(2), 151-176.
- Rose, J. and Letzer, J. M. (1977). Superimposed drumlins. *Journal of Glaciology*, 18(80), 471-480.
- Rose, J. and Menzies, J. (1987). Introduction. In Menzies, J. and Rose, J. (eds.) *Drumlin Symposium*, Balkema, Rotterdam, 103-118.
- Ross, M., Campbell, J. E., Parent, M. and Adams, R. S. (2009). Palaeo-ice streams and the subglacial landscape mosaic of the North American mid-continental prairies. *Boreas*, 38(3), 421-439.
- Rubin, D. M. and Hunter, R. E. (1987). Bedform alignment in directionally varying flows. *Science*, 237(4812), 276-278.
- Rubin, D. M. and Ikeda, H. (1990). Flume experiments on the alignment of transverse, oblique, and longitudinal dunes in directionally varying flows. *Sedimentology*, 37(4), 673-684.
- Saha, K., Wells, N. A. and Munro-Stasiuk, M. (2011). An object-oriented approach to automated landform mapping: A case study of drumlins. *Computers and Geosciences*, 37(9), 1324-1336.
- Sarala, P. (2006). Ribbed moraine stratigraphy and formation in southern Finnish Lapland. *Journal of Quaternary Science*, 21(4), 387-398.
- Scambos, T. A. and Nereson, N. A. (1995). Satellite image and global positioning system study of the morphology of Siple Dome, Antarctica. *Antarctic Journal of the United States*, 30, 87-88.

- Scambos, T. A., Haran, T. M., Fahnestock, M. A., Painter, T. H. and Bohlander, J. (2007). MODIS-based Mosaic of Antarctica (MOA) data sets: Continent-wide surface morphology and snow grain size. *Remote Sensing of Environment*, 111(2), 242-257.
- Schomacker, A., Krüger, J. and Kjær, K. H. (2006). Ice-cored drumlins at the surge-type glacier Brúarjökull, Iceland: a transitional-state landform. *Journal of Quaternary Science*, 21(1), 85-93.
- Schoof, C. (2002). Basal perturbations under ice streams: form drag and surface expression. *Journal of Glaciology*, 48(162), 407-416.
- Schoof, C. (2004). Bed topography and surges in ice streams. *Geophysical research letters*, 31(6).
- Schoof, C. (2007). Pressure-dependent viscosity and interfacial instability in coupled ice–sediment flow. *Journal of Fluid Mechanics*, 570, 227-252.
- Schoof, C. (2012). Thermally driven migration of ice-stream shear margins. *Journal of Fluid Mechanics*, 712, 552-578.
- Schoof, C. G. and Clarke, G. K. (2008). A model for spiral flows in basal ice and the formation of subglacial flutes based on a Reiner-Rivlin rheology for glacial ice. *Journal of Geophysical Research: Solid Earth (1978–2012)*, 113(B5).
- Sergienko, O. V. (2012). The effects of transverse bed topography variations in ice-flow models. *Journal of Geophysical Research: Earth Surface (2003–2012)*, 117(F3).
- Sergienko, O. V. and Hulbe, C. L. (2011). 'Sticky spots' and subglacial lakes under ice streams of the Siple Coast, Antarctica. *Annals of Glaciology*, 52(58), 18-22.
- Sergienko, O. V. and Hindmarsh, R. C. (2013). Regular patterns in frictional resistance of ice-stream beds seen by surface data inversion. *Science*, 342(6162), 1086-1089.
- Sergienko, O. V., Creyts, T. T. and Hindmarsh, R. C. A. (2014). Similarity of organized patterns in driving and basal stresses of Antarctic and Greenland ice sheets beneath extensive areas of basal sliding. *Geophysical Research Letters*, 41(11), 3925-3932.
- Shabtaie, S., Whillans, I. M. and Bentley, C. R. (1987). The morphology of Ice Streams A, B, and C, West Antarctica, and their environs. *Journal of Geophysical Research: Solid Earth (1978–2012)*, 92(B9), 8865-8883.
- Shackleton, N. J. (1987). Oxygen isotopes, ice volume and sea level. *Quaternary Science Reviews*, 6(3), 183-190.
- Shaw, J. (1979). Genesis of the Sveg tills and Rogen moraines of central Sweden: a model of basal melt out. *Boreas*, 8(4), 409-426.

- Shaw, J. (1983, p. 476). Drumlin formation related to inverted melt-water erosional marks. *Journal of Glaciology*, 29, 461-479.
- Shaw, J. (1994). Hairpin erosional marks, horseshoe vortices and subglacial erosion. *Sedimentary Geology*, 91(1), 269-283.
- Shaw, J. (2002). The meltwater hypothesis for subglacial bedforms. *Quaternary International*, 90(1), 5-22.
- Shaw, J. (2010). In defence of the meltwater (megaflood) hypothesis for the formation of subglacial bedform fields. *Journal of Quaternary Science*, 25(3), 249-260.
- Shaw, J. and Sharpe, D. R. (1987). Drumlin formation by subglacial meltwater erosion. *Canadian Journal of Earth Sciences*, 24(11), 2316-2322.
- Shaw, J., Kvill, D. and Rains, B. (1989). Drumlins and catastrophic subglacial floods. *Sedimentary Geology*, 62(2), 177-202.
- Shaw, J., Pugin, A. and Young, R. R. (2008). A meltwater origin for Antarctic shelf bedforms with special attention to megalineations. *Geomorphology*, 102(3), 364-375.
- Siegert, M. J., Taylor, J., Payne, A. J. and Hubbard, B. (2004). Macro-scale bed roughness of the Siple Coast ice streams in West Antarctica. *Earth Surface Processes and Landforms*, 29(13), 1591-1596.
- Siegert, M., Ross, N., Corr, H., Kingslake, J. and Hindmarsh, R. (2013). Late Holocene ice-flow reconfiguration in the Weddell Sea sector of West Antarctica. *Quaternary Science Reviews*, 78, 98-107.
- Sivashinsky, G. I. (1983). Instabilities, pattern formation, and turbulence in flames. *Annual Review of Fluid Mechanics*, 15(1), 179-199.
- Smalley, I. J. and Unwin, D. J. (1968). The formation and shape of drumlins and their distribution and orientation in drumlin fields. *Journal of Glaciology*, 7, 377-390.
- Smalley, I. J., and Piotrowski, J. A. (1987). Critical strength/stress ratios at the ice-bed interface in the drumlin forming process: from dilatancy to cross-over. In *Drumlin symposium*, Balkema, Rotterdam, 81-86.
- Smalley, I. and Warburton, J. (1994). The shape of drumlins, their distribution in drumlin fields, and the nature of the sub-ice shaping forces. *Sedimentary geology*, 91(1), 241-252.
- Smith, B. E., Lord, N. E. and Bentley, C. R. (2002). Crevasse ages on the northern margin of Ice Stream C, West Antarctica. *Annals of Glaciology*, 34(1), 209-216.
- Smith, A. M., Murray, T., Nicholls, K. W., Makinson, K., Adalgeirsdóttir, G., Behar, A. E. and Vaughan, D. G. (2007). Rapid erosion, drumlin formation, and changing hydrology beneath an Antarctic ice stream. *Geology*, 35(2), 127-130.

- Smith, M. J. and Clark, C. D. (2005). Methods for the visualization of digital elevation models for landform mapping. *Earth Surface Processes and Landforms*, 30(7), 885-900.
- Smith, M. J. and Wise, S. M. (2007). Problems of bias in mapping linear landforms from satellite imagery. *International Journal of Applied Earth Observation and Geoinformation*, 9(1), 65-78.
- Smith, M. J., Rose, J. and Gousie, M. B. (2009). The Cookie Cutter: a method for obtaining a quantitative 3D description of glacial bedforms. *Geomorphology*, 108(3), 209-218.
- Spagnolo, M., Clark, C. D., Hughes, A. L., Dunlop, P. and Stokes, C. R. (2010). The planar shape of drumlins. *Sedimentary Geology*, 232(3), 119-129.
- Spagnolo, M., Clark, C. D. and Hughes, A. L. (2012). Drumlin relief. *Geomorphology*, 153, 179-191.
- Spagnolo, M., Clark, C. D., Ely, J. C., Stokes, C. R., Anderson, J. B., Andreassen, K., Graham, A. G. C. and King, E. C. (2014a). Size, shape and spatial arrangement of mega-scale glacial lineations from a large and diverse dataset. *Earth Surface Processes and Landforms*, 39(11), 1432-1448.
- Spagnolo, M., King, E. C., Ashmore, D. W., Rea, B. R., Ely, J. C. and Clark, C. D. (2014b). Looking through drumlins: testing the application of ground-penetrating radar. *Journal of Glaciology*, 60(224), 1126-1134.
- Spagnolo, M., Phillips, E., Piotrowski, J.A., Rea, B.R., Clark, C.D., Stokes, C.R., Carr, S.J., Ely, J.C., Ribolini, A., Wysota, W. and Szuman, I., 2016. Ice stream motion facilitated by a shallow-deforming and accreting bed. *Nature Communications*, 7.
- Stephenson, S. N. and Bindshadler, R. A. (1990). Is ice-stream evolution revealed by satellite imagery. *Annals of Glaciology*, 14, 273-277.
- Stokes, C. R. and Clark, C. D. (1999). Geomorphological criteria for identifying Pleistocene ice streams. *Annals of Glaciology*, 28(1), 67-74.
- Stokes, C. R. and Clark, C. D. (2001). Palaeo-ice streams. *Quaternary Science Reviews*, 20(13), 1437-1457.
- Stokes, C. R. and Clark, C. D. (2002). Are long subglacial bedforms indicative of fast ice flow?. *Boreas*, 31(3), 239-249.
- Stokes, C. R. and Clark, C. D. (2003). The Dubawnt Lake palaeo-ice stream: evidence for dynamic ice sheet behaviour on the Canadian Shield and insights regarding the controls on ice-stream location and vigour. *Boreas*, 32(1), 263-279.

- Stokes, C. R., Clark, C. D., Lian, O. B. and Tulaczyk, S. (2007). Ice stream sticky spots: a review of their identification and influence beneath contemporary and palaeo-ice streams. *Earth-Science Reviews*, 81(3), 217-249.
- Stokes, C. R., Spagnolo, M. and Clark, C. D. (2011). The composition and internal structure of drumlins: Complexity, commonality, and implications for a unifying theory of their formation. *Earth-Science Reviews*, 107(3), 398-422.
- Stokes, C. R., Fowler, A. C., Clark, C. D., Hindmarsh, R. C. and Spagnolo, M. (2013a). The instability theory of drumlin formation and its explanation of their varied composition and internal structure. *Quaternary Science Reviews*, 62, 77-96.
- Stokes, C. R., Spagnolo, M., Clark, C. D., Cofaigh, C. Ó., Lian, O. B. and Dunstone, R. B. (2013b). Formation of mega-scale glacial lineations on the Dubawnt Lake Ice Stream bed: 1. size, shape and spacing from a large remote sensing dataset. *Quaternary Science Reviews*, 77, 190-209.
- Storrar, R. and Stokes, C. R. (2007). A glacial geomorphological map of Victoria Island, Canadian Arctic. *Journal of Maps*, 3(1), 191-210.
- Stoyan, D., and Stoyan, H. (1985). On One of Matérn's Hard-core Point Process Models. *Mathematische Nachrichten*, 122(1), 205-214.
- Sutinen, R., Middleton, M., Liwata, P., Piekkari, M. and Hyvönen, E. (2009). Sediment anisotropy coincides with moraine ridge trend in south-central Finnish Lapland. *Boreas*, 38(3), 638-646.
- Sutinen, R., Jakonen, M., Piekkari, M., Haavikko, P., Närhi, P. and Middleton, M. (2010). Electrical-sedimentary anisotropy of Rogen moraine, Lake Rogen area, Sweden. *Sedimentary Geology*, 232(3), 181-189.
- Swithinbank, C. W. M. (1954). Ice streams. *Polar Record*, 7(48), 185-186.
- Swithinbank, C., Brunk, K. and Sievers, J. (1988). A glaciological map of Filchner-Ronne ice shelf, Antarctica. *Annals of Glaciology*, 11, 150-155.
- Tarr, R. S. (1894). The Origin of Lake Basins. *Nature*, 49, 315-316.
- Thorsteinsson, T., Raymond, C. F., Gudmundsson, G. H., Bindschadler, R. A., Vornberger, P., and Joughin, I. (2003). Bed topography and lubrication inferred from surface measurements on fast-flowing ice streams. *Journal of Glaciology*, 49(167), 481-490.
- Trenhaile, A. S. (1971). Drumlins: Their distribution, orientation, and morphology. *The Canadian Geographer/Le Géographe canadien*, 15(2), 113-126.
- Tulaczyk, S., Kamb, W. B. and Engelhardt, H. F. (2000). Basal mechanics of ice stream B, West Antarctica: 1. Till mechanics. *Journal of Geophysical Research* B, 105(B1), 463-481.



- Tulaczyk, S. M., Scherer, R. P. and Clark, C. D. (2001). A ploughing model for the origin of weak tills beneath ice streams: a qualitative treatment. *Quaternary International*, 86(1), 59-70.
- Unwin, D.J. (1996). GIS, spatial analysis and spatial statistics. *Progress in Human Geography*, 20(4), 540–551.
- Upham, W. (1894). The Madison type of drumlins. *American Geology*, 14, 69-83.
- Van der Meer, J. J. M. (1983). A recent drumlin with fluted surface in the Swiss Alps. *Tills and Related Deposits: Genesis, Petrology, Application, Stratigraphy*. AA Balkema Publishers. Rotterdam, 105-110.
- Vaughan, D. G. (1993). Implications of the break-up of Wordie Ice Shelf, Antarctica for sea level. *Antarctic Science*, 5(04), 403-408.
- Vernon, P. (1966). Drumlins and Pleistocene Ards Peninsula, Strangford Down, Ireland. *Journal of Glaciology*, 6(45).
- Vornberger, P. L., and Whillans, I. M. (1990). Crevasse deformation and examples from Ice Stream B, Antarctica. *Journal of Glaciology*, 36, 3-10.
- Waller, R. I., Van, D., Thaienne, A., and Knudsen, Ó. (2008). Subglacial bedforms and conditions associated with the 1991 surge of Skeiðarárjökull, Iceland. *Boreas*, 37(2), 179-194.
- Walker, R. T., Parizek, B. R., Alley, R. B., Anandakrishnan, S., Riverman, K. L. and Christianson, K. (2013). Ice-shelf tidal flexure and subglacial pressure variations. *Earth and Planetary Science Letters*, 361, 422-428.
- Wasson, R. J., Fitchett, K., Mackey, B. and Hyde, R. (1988). Large-scale patterns of dune type, spacing and orientation in the Australian continental dunefield. *The Australian Geographer*, 19(1), 89-104.
- Werner, B. T. (1995). Eolian dunes: computer simulations and attractor interpretation. *Geology*, 23(12), 1107-1110.
- Werner, B. T. (1999). Complexity in natural landform patterns. *Science*, 284(5411), 102-104.
- Werner, B. T. and Kocurek, G. (1999). Bedform spacing from defect dynamics. *Geology*, 27(8), 727-730.
- Werth E. (1909) Eine Drumlinlandschaft und Rirmenseen SE von Posen, *Zitschr.d.d. Geol. Ges.*, 61.
- Whillans, I. M. and Johnsen, S. J. (1983). Longitudinal variations in glacial flow: theory and test using data from the Byrd Station strain network, Antarctica. *Journal of Glaciology*, 29(101), 78-97.

- Whillans, I. M. and van der Veen, C. J. (1993). New and improved determinations of velocity of Ice Streams B and C, West Antarctica. *Journal of Glaciology*, 39(133), 483-490.
- Whillans, I. M. and Van Der Veen, C. J. (1997). The role of lateral drag in the dynamics of Ice Stream B, Antarctica. *Journal of Glaciology*, 43(144), 211-217.
- Whittecar, G. R. and Mickelson, D. M. (1979). Composition, internal structures, and an hypothesis of formation for drumlins, Waukesha County, Wisconsin, USA. *Journal of Glaciology*, 22, 357-371.
- Wiegand, T. and A Moloney, K. (2004). Rings, circles, and null-models for point pattern analysis in ecology. *Oikos*, 104(2), 209-229.
- Wilson, I. G. (1972). Aeolian bedforms—their development and origins. *Sedimentology*, 19(3-4), 173-210.
- Wingham, D. J., Shepherd, A., Muir, A. and Marshall, G. J. (2006). Mass balance of the Antarctic ice sheet. *Philosophical Transactions of the Royal Society of London A: Mathematical, Physical and Engineering Sciences*, 364(1844), 1627-1635.
- Winsborrow, M., Clark, C. D., and Stokes, C. R. (2004). Ice streams of the Laurentide ice sheet. *Géographie physique et Quaternaire*, 58(2-3), 269-280.
- Worman, S. L., Murray, A. B., Littlewood, R., Andreotti, B. and Claudin, P. (2013). Modeling emergent large-scale structures of barchan dune fields. *Geology*, 41(10), 1059-1062.
- Wuite, J. and Jezek, K. C. (2009). Evidence of past fluctuations on Stancomb-Wills Ice Tongue, Antarctica, preserved by relict flow stripes. *Journal of Glaciology*, 55(190), 239-244.
- Zelcs, V. and Dreimanis, A. (1997). Morphology, internal structure and genesis of the Burtnieks drumlin field, Northern Vidzeme, Latvia. *Sedimentary Geology*, 111(1), 73-90.